

H24/3599

MONASH UNIVERSITY
THESIS ACCEPTED IN SATISFACTION OF THE
REQUIREMENTS FOR THE DEGREE OF
DOCTOR OF PHILOSOPHY

ON..... 24 June 2003

.....
Sec Sec. Research Graduate School Committee

Under the Copyright Act 1968, this thesis must be used only under the normal conditions of scholarly fair dealing for the purposes of research, criticism or review. In particular no results or conclusions should be extracted from it, nor should it be copied or closely paraphrased in whole or in part without the written consent of the author. Proper written acknowledgement should be made for any assistance obtained from this thesis.

BROADBAND WIRELESS COMMUNICATIONS:
ISSUES IN OFDM AND MULTI-CODE CDMA

BY

K. SATHANANTHAN
B.Sc.ENG. (HONOURS I), M.ENG

A THESIS SUBMITTED IN FULFILLMENT OF THE
REQUIREMENTS FOR THE DEGREE OF
DOCTOR OF PHILOSOPHY

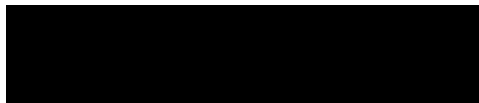
SCHOOL OF COMPUTER SCIENCE AND SOFTWARE ENGINEERING



JUNE 11, 2003

DECLARATION

I, K. Sathananthan, hereby declare that this thesis contains no material which has been accepted for the award of any other degree or diploma in any university. Further to the best of my knowledge and belief, this thesis contains no material previously published or written by another person except where due reference is made in the text of the thesis.



K. Sathananthan

12/06/2003

date

Contents

List of Tables	v
List of Figures	vi
Abstract	ix
Acknowledgements	xi
Author's Publications	xii
List of Abbreviations	xv
List of Symbols	xix
1 Introduction	1
1.1 Motivations	2
1.2 Thesis Outline	2
1.3 Research Contributions	4
2 Orthogonal Frequency Division Multiplexing (OFDM)	6
2.1 Introduction	6
2.1.1 OFDM Background	6
2.1.2 OFDM Signalling	10
2.1.3 Discrete-time Representation of OFDM Signals	12
2.1.4 Receiver Structure	13
2.2 Intercarrier Interference (ICI)	14
2.3 Frequency Offset Errors	15
2.3.1 Carrier Frequency Offset Problem Formulation	17

2.3.2	Frequency Offset Estimation Methods	23
2.3.3	Frequency Offset Sensitivity Reduction Methods	26
2.4	Phase Noise	29
2.5	Time Variations of the Channel	31
2.6	Peak-to-Average Power Ratio	33
2.6.1	PAR Bounds and Statistics	37
2.6.2	Memoryless Nonlinearities	40
2.6.3	Effects of Nonlinearities	44
2.6.4	PAR Reduction Schemes	47
2.7	Extension of OFDM Principles	55
2.7.1	Multicarrier-Code Division Multiple Access (MC-CDMA)	55
2.7.2	Multi Input Multi Output (MIMO) OFDM	56
2.8	Conclusions	58
3	Exact Error Rate Calculations	59
3.1	Introduction	59
3.2	Error Rate Calculations	60
3.2.1	Precise Calculations	60
3.2.2	Gaussian Approximation	65
3.2.3	Numerical Results	66
3.3	Error Performance of Rate-half Repetition Codes	67
3.4	Exact Error Rate Calculations with Phase Noise	69
3.5	Conclusions	71
4	ICI Reduction by Coding	73
4.1	Introduction	73
4.2	Code Design for a Channel with Frequency Offset	74
4.3	Rate $\frac{2}{3}$ and $\frac{3}{4}$ ICI-reduction Codes	75
4.3.1	Simulation Results	77
4.4	Reducing ICI by using Error Correction Codes	81
4.4.1	Error Performance of RCPC codes	83
4.4.2	Simulation Results	83
4.5	Conclusions	86

5	Peak Interference-to-Carrier Ratio (PICR)	88
5.1	Introduction	89
5.2	PICR Problem Formulation	90
5.2.1	Average Interference-to-Carrier Ratio (ICR)	90
5.2.2	PICR Definition	90
5.2.3	Complementary Cumulative Density Function (CCDF) of PICR	92
5.2.4	PICR and BER Relationship	94
5.3	PICR Reduction by Coding	95
5.3.1	Independence in PICR Performance on Frequency Offset	96
5.3.2	PICR Reduction by Block Coding	97
5.3.3	Construction of PICR-reduction Codes	99
5.4	PICR Reduction by Tone Reservation	101
5.4.1	Least Square Error Optimization	102
5.4.2	Standard Linear Programming Approach	102
5.4.3	Simulation Results	103
5.5	PICR Reduction by SLM and PTS Schemes	105
5.5.1	Selected Mapping (SLM)	105
5.5.2	Partial Transmit Sequences (PTS)	107
5.6	Both PAR and PICR Reduction by Coding	110
5.6.1	Block Coding for both PAR and PICR Reduction	111
5.6.2	Golay Complementary Repetition Codes	112
5.6.3	Simulation Results	113
5.7	Conclusions	114
6	Adaptive Zero-padded PSK for both PAR and ICI Reduction	117
6.1	Introduction	117
6.2	PAR Reduction by Adaptive Mapping	118
6.2.1	M-ZPSK Modulation Scheme	118
6.2.2	Adaptive Approach for PAR Reduction	119
6.2.3	Selected Mapping (SLM)	122
6.2.4	BER Analysis	123
6.3	ICI Reduction	129
6.4	Out-of-band Radiation	133

6.5	Side Information (SI)	135
6.5.1	Explicit SI	135
6.5.2	Implicit SI	136
6.6	Conclusions	139
7	PAR Reduction for Multi-Code CDMA	140
7.1	Introduction	140
7.2	Multi-code CDMA Systems	142
7.3	PAR Analysis	143
7.3.1	PAR Definition	145
7.3.2	CCDF of the PAR	146
7.3.3	Achievable Coding Rate	148
7.4	Reducing PAR Using Multiple Signal Generation	148
7.4.1	Partial Transmit Sequences (PTS)	149
7.4.2	Selected Mapping (SLM)	151
7.4.3	Impairments in the Presence of Nonlinearities	153
7.5	Conclusions	155
8	Conclusions and Future Work	157
8.1	Thesis Conclusions	157
8.2	Recommendations for Future Work	158

List of Tables

3.1	QPSK OFDM error probabilities for $\sigma^2 = 0.4$ and $\varepsilon = 0.05$	66
5.1	PICR for $N = 4$ and BPSK modulation	99
5.2	PICR and PAR for $N = 4$ and BPSK modulation	112
6.1	Comparison of the complexity	122

List of Figures

2.1	Multicarrier transmission concept.	7
2.2	Typical OFDM system.	10
2.3	Typical OFDM windowing function $g(t)$	11
2.4	Illustration of frequency offset effect.	16
2.5	Block diagram of an OFDM system with frequency offset.	17
2.6	QPSK signal constellation.	20
2.7	BER performance of an OFDM system with $N = 128$	21
2.8	Average CIR of an OFDM system with $N = 128$	22
2.9	Typical OFDM signal.	34
2.10	Variation of PAR characteristics with oversampling factor.	35
2.11	CCDF of PAR of an OFDM signal.	39
2.12	Typical HPA characteristics.	42
2.13	Normalized AM/AM characteristics of a SSPA.	44
2.14	Spectrum of an OFDM signal after passing through a SSPA.	45
2.15	BER performance of an OFDM signal after passing through a SSPA.	46
3.1	Probability of symbol error for BPSK and QPSK with $\epsilon = 0.1$	67
3.2	Probability of symbol error with normalized frequency offset ($E_b/N_o = 8$ dB for BPSK and $E_b/N_o = 10$ dB for QPSK.)	68
3.3	Probability of symbol error for 16QAM with $\epsilon = 0.05$	69
3.4	Probability of symbol error for BPSK, $\epsilon = 0.1$	70
3.5	Probability of symbol error for BPSK and QPSK, $\gamma = 0.1$	71
3.6	Probability of symbol error with γ and $SNR = 8dB$	72
4.1	A schematic diagram for different code rates: (a) Uncoded, (b) Rate-half, (c) Rate $\frac{2}{3}$ and (d) Rate $\frac{3}{4}$	76
4.2	Variation of average CIR of rate $\frac{2}{3}$ and $\frac{3}{4}$ codes with subcarrier index.	78
4.3	Variation of average CIR of rate $\frac{2}{3}$ and $\frac{3}{4}$ codes with ϵ	79
4.4	QPSK signal constellations for $\epsilon = 0.1$	80
4.5	BER performance of rate $\frac{2}{3}$ and $\frac{3}{4}$ codes in AWGN channel and $\epsilon = 0.1$	80
4.6	BER performance of rate $\frac{2}{3}$ and $\frac{3}{4}$ codes in multipath fading channel and $\epsilon = 0.1$	81

4.7	BER performance for BPSK with $\varepsilon = 0.1$ (upper bound).	84
4.8	Variation of BER of BPSK with ε and $E_b/N_o = 8$ dB (upper bound).	85
4.9	BER performance for QPSK with $\varepsilon = 0.1$.	86
4.10	Variation of BER of QPSK with ε and $E_b/N_o = 8$ dB.	87
5.1	CCDF of PICR of an OFDM system as a function of N .	93
5.2	CCDF of PICR for an OFDM system with N and ε .	94
5.3	Upper bound for the BER of BPSK OFDM system with $N = 128$ and $\varepsilon = 0.1$.	95
5.4	Variation of BER with average PICR for an OFDM system with $N = 128$.	96
5.5	Variation of code rate with $PICR_0$.	98
5.6	CCDF of PICR for a coded OFDM system with $N = 16$ and $\varepsilon = 0.1$.	100
5.7	CCDF of PICR for rate rate $\frac{2}{3}$ and $\frac{3}{4}$ codes with $N = 128$ and $\varepsilon = 0.1$.	101
5.8	CCDF of PICR for an OFDM System with $N = 128$ and $\varepsilon = 0.1$.	104
5.9	CCDF of PICR for an OFDM system with $N = 128$; a: Conventional OFDM ($\varepsilon = 0.05$), b: $\varepsilon = 0.05$ and $\varepsilon_{wc} = 0.05$, c: $\varepsilon = 0.05$ and $\varepsilon_{wc} = 0.05$.	104
5.10	Simplified block diagram of SLM for PICR reduction.	106
5.11	CCDF of PICR of SLM OFDM system with $\varepsilon = 0.1$.	107
5.12	BER Performance of SLM OFDM system in AWGN channel with $\varepsilon = 0.1$.	108
5.13	Simplified block diagram of PTS for PICR reduction.	109
5.14	CCDF of PICR of PTS OFDM system with $\varepsilon = 0.1$.	110
5.15	CCDF of PICR of an OFDM system with a: ($\varepsilon = 0.08, \varepsilon_{wc} = 0.08$) and b: ($\varepsilon = 0.08, \varepsilon_{wc} = 0.1$).	111
5.16	Variation of code rate with PAR and PICR for $N = 16$ and $\varepsilon = 0.1$.	114
5.17	CCDF of PAR of an OFDM System.	115
5.18	CCDF of PICR of an OFDM system with $\varepsilon = 0.1$.	116
6.1	Signal constellation for M-ZPSK modulation scheme.	119
6.2	Block diagram for an adaptive OFDM scheme.	120
6.3	Mapping signal constellation for an adaptive OFDM system for $M = 4$.	121
6.4	CCDF of the PAR of a conventional and adaptive OFDM signal for $M = 4$.	121
6.5	CCDF of the PAR of an adaptive OFDM and SLM scheme.	123
6.6	Typical 4-ZPSK signal constellation and approximate decision boundaries.	124
6.7	BER of an adaptive OFDM scheme in AWGN channel for $M = 4$.	128
6.8	BER of an adaptive OFDM scheme in multipath fading channel for $M = 4$.	130
6.9	Variation of average CIR of non zero symbol with ε .	131
6.10	BER Performance in AWGN channel for $M = 4$.	132
6.11	Variation of BER with ε in AWGN channel for $M = 4$ and $E_b/N_o = 10dB$.	132
6.12	Spectrum of an OFDM signal after passing through a SL.	134
6.13	Spectrum of an OFDM signal after passing through a SSPA.	134

6.14	CCDF of the PAR of an adaptive OFDM for $M = 4$ with embedded SI.	135
6.15	BER of an adaptive OFDM in AWGN channel for $M = 4$ with embedded SI.	136
6.16	Receiver block diagram for an adaptive OFDM with implicit SI.	137
6.17	CCDF of the PAR of an adaptive coded OFDM for $M = 4$	138
6.18	BER of an adaptive coded OFDM in AWGN channel for $M = 4$	138
7.1	Simplified block diagram of the transmitter in multi-code CDMA system.	142
7.2	Simplified block diagram of the receiver in multi-code CDMA system. .	143
7.3	CCDF of PAR of conventional multi-code CDMA system.	147
7.4	Variation of code rate with PAR.	149
7.5	CCDF of PAR of multiple signal generated multi-code CDMA system for $n = 32$	150
7.6	Simplified block diagram for the PTS scheme.	151
7.7	CCDF of PAR of PTS multi-code CDMA system with $n = 32$	152
7.8	Simplified block diagram for the SLM scheme.	153
7.9	CCDF of PAR of SLM multi-code CDMA system with $n = 32$	154
7.10	BER of multi-code CDMA signal passed through SL ($n = 32$ and $M = 8$).	154
7.11	BER of multi-code CDMA signal passed through SSPA ($n = 32$ and $M = 8$).	155
7.12	BER of multi-code CDMA signal passed through SSPA ($n = 32$, $M = 8$, IBO=1 dB).	156

Abstract

For many broadband wireless communications systems, Orthogonal Frequency Division Multiplexing (OFDM) is the technology of choice because of its simple equalization process for high data rate transmission in a multipath fading channel. However, OFDM suffers from its high peak-to-average power ratio (PAR) and high sensitivity to frequency offset errors. The OFDM signal has a large dynamic signal range (high PAR) due to linear processing of large number of subcarriers by discrete Fourier transformation. These high signal peaks can lead to in-band distortion and spectral spreading in the presence of non-linear devices, resulting in performance degradation and inefficiency. On the other hand, the mismatch in carrier frequencies or Doppler shift introduces intercarrier interference (ICI) among the orthogonal subcarriers. This loss in orthogonality degrades error performance and causes error floor. This thesis mainly deals with these two drawbacks by developing new schemes to reduce their effects.

A precise numerical technique is developed to evaluate the error performance of an OFDM system with ICI. Since a highly effective self-ICI cancellation or polynomial coded cancellation scheme halves the data throughput, high rate ICI-reduction codes are investigated. To this end, an optimal design rule for ICI-reduction codes and rate $2/3$ and $3/4$ ICI-reduction codes are developed. These two new codes offer significant performance over normal OFDM. Moreover, rate-compatible punctured convolutional (RCPC) codes with high code rate are studied analytically, and by simulation, to illustrate the applicability of high rate error correction codes for ICI reduction.

A new measure, peak interference-to-carrier ratio (PICR), is introduced to quantify ICI resulting from carrier frequency offset. The definition of PICR translates the ICI problem in parallel with the PAR issue. Analytical expressions and simulation results are used to show an improvement in error performance by PICR reduction. Block coding and an algebraic construction of PICR-reduction codes are discussed. Tone reservation, selected mapping (SLM) and partial transmit sequences (PTS) approaches,

which were originally proposed for PAR reductions, are investigated as a means of reducing PICR. Performances of these schemes are evaluated by simulation. Moreover, the concept of PAR-PICR-reduction codes are introduced to reduce both PAR and PICR simultaneously. This coding is based on selecting only those messages with both low PAR and PICR as valid codewords. As an example of an explicit construction of such codes, Golay complementary repetition codes are studied.

A simple adaptive modulation scheme is also proposed to reduce both PAR and ICI simultaneously. This is achieved by using M-point zero-padded phase shift keying (M-ZPSK), which includes a signal point of zero amplitude. Analytical expressions for the error rates of M-ZPSK on additive white Gaussian noise (AWGN), Rayleigh, Nakagami-m and Ricean fading channels are derived. The performance of this scheme and the issue of side information (SI) are addressed.

The other attractive scheme proposed for broadband wireless applications is the multi-code code division multiple access (multi-code CDMA). However, this multi-code CDMA signal also experiences PAR problem. This thesis also analyzes this problem and derives analytical expressions for the statistical distribution of PAR. PTS and SLM methods are also investigated to reduce the PAR of the multi-code CDMA signal.

Acknowledgements

I would like to express my sincere gratitude and appreciation to my thesis supervisor, Associate Prof. Chintha Tellambura, for his thoughtful guidance, helpful discussions, continual encouragement and kind support throughout my candidature at Monash University.

I am also grateful to my present supervisor, Associate Prof. Bin Qui, for his valuable advice and continued encouragement of my research.

I would also like to extend my sincere thanks to Associate Prof. R. M. A. P. Rajatheva, Asian Institute of Technology, Thailand, and Associate Prof. Ben Slimane, Royal Institute of Technology, Sweden, for introducing me to research on wireless communications and sharing their great knowledge on this subject with me.

I would also like to thank my colleagues for their help and interesting discussions. Special thanks are also due to all administrative and technical staff members for their prompt help and support in numerous ways.

Grateful acknowledgement is also made to Monash University for offering me scholarships, without which this study would have been impossible.

My special thanks go to my lovely wife, Vijitha, and my sweet son, Thivyesh, for their love, cheer and support throughout my graduate studies. Finally, I would like to thank my parents for their continued love, support, encouragement and sacrifice throughout the years. I wish to dedicate this work to them.

Author's Publications

Much of the research work in this thesis has been published or has been submitted for publications. The details of these publications are listed below. Publications that are not directly related to this thesis has also been included.

Refereed Journal Articles

1. K. Sathananthan, R. M. A. P. Rajatheva, and S. B. Slimane, "Cancellation technique to reduce intercarrier interference in OFDM," *IEE Elect. Lett.*, vol. 36, pp. 2078 -2079, Dec. 2000.
2. K. Sathananthan and C. Tellambura, "Probability of error calculation of OFDM systems with frequency offset," *IEEE Trans. Commun.*, vol. 49, pp. 1884-1888, Nov. 2001.
3. K. Sathananthan and C. Tellambura, "Partial transmit sequence and selected mapping schemes to reduce ICI in OFDM systems," *IEEE Commun. Lett.*, vol. 6, pp. 313-315, Aug. 2002.
4. K. Sathananthan and C. Tellambura, "Coding to reduce both PAR and PICR of an OFDM signal," *IEEE Commun. Lett.*, vol. 6, pp. 316-318, Aug. 2002.
5. K. Sathananthan and C. Tellambura, "New adaptive modulation scheme to reduce both PAR and ICI of an OFDM signal," *IEEE Trans. Veh. Technol.*, Under first revision.
6. K. Sathananthan and C. Tellambura, "Partial transmit sequence and selected mapping schemes to reduce PAPR in multicode CDMA," *IEICE Trans. Commun.*, Under first revision.

7. **K. Sathananthan** and C. Tellambura, "Peak Interference-to-Carrier Ratio (PICR): New approach to Carrier Frequency Offset problem in OFDM", In preparation.

Book Chapter

1. **K. Sathananthan**, and C. Tellambura, "Reducing PAR and PICR of an OFDM Signal," *Advanced Signal Processing for Communications Systems.*, Kluwer Academic Publishers Group, Dordrecht, Nertherlands, 2002.

Refereed Conference Papers

1. **K. Sathananthan** and C. Tellambura, "Carrier frequency offset effect on OFDM systems: analysis and solutions," in *International Symposium on Wireless Personal Multimedia Communications*, vol. 2, (Bangkok, Thailand), pp. 688-692, Nov. 2000.
2. **K. Sathananthan**, R. M. A. P. Rajatheva, and K. M. Ahmed, "Reduction of peak to average power ratio by limiting the dynamic range of an OFDM signal," in *International Symposium on Wireless Personal Multimedia Communications*, vol. 1, (Bangkok, Thailand), pp. 33-34, Nov. 2000.
3. **K. Sathananthan**, R. M. A. P. Rajatheva, and S. B. Slimane, "Analysis of OFDM in the presence of frequency offset and a method to reduce performance degradation," in *IEEE GLOBECOM*, vol. 1, (San Francisco, USA), pp. 72 - 76, IEEE, Nov. 2000.
4. A. D. S. Jayalath, **K. Sathananthan**, and C. Tellambura, "OFDM with Reduced Peak-to-Average Power Ratio by Interleaving," in *IEEE Pacific-Rim Conference on Multimedia*, vol. 1, (Sydney, Australia), pp. 120 - 123, IEEE, Dec. 2000.
5. **K. Sathananthan** and C. Tellambura, "Forward error correction codes to reduce intercarrier interference in OFDM," in *IEEE ISCAS 2001*, (Sydney, Australia), IEEE, 2001.

6. **K. Sathananthan** and C. Tellambura, "New ICI reduction schemes for OFDM system," in *IEEE Vehicular Technology Conference*, (Atlantic City, USA), pp. 834-838, IEEE, Oct. 2001.
7. **K. Sathananthan** and C. Tellambura, "Performance analysis of an OFDM system with carrier frequency offset and phase noise," in *IEEE Vehicular Technology Conference*, (Atlantic City, USA), pp. 2329-2332, IEEE, Oct. 2001.
8. **K. Sathananthan** and C. Tellambura, "Novel adaptive modulation scheme to reduce both PAR and ICI of an OFDM signal," in *6th International Symposium on DSP for Communication Systems*, (Sydney, Australia), pp. 229-233, Jan. 2002.
9. **K. Sathananthan** and C. Tellambura, "Reducing intercarrier interference in OFDM systems by partial transmit sequence and selected mapping," in *6th International Symposium on DSP for Communication Systems*, (Sydney, Australia), pp. 234-238, Jan. 2002.
10. **K. Sathananthan** and C. Tellambura, "On the existence of codes to reduce both PAR and PICR of an OFDM signal," in *3rd Australian Communication Theory Workshop*, (Canberra, Australia), pp. 28-32, Feb. 2002.
11. **K. Sathananthan** and C. Tellambura, "Peak-to-average power ratio analysis in multicode CDMA," in *IEEE Vehicular Technology Conference*, (Vancouver, Canada), pp. 1686-1690, IEEE, Sept. 2002.

List of Abbreviations

2-D/2D	Two dimensional
3G	Third Generation
4G	Fourth Generation
A&P	Amplitude and Phase
ADC	Analog to Digital Converter
ADSL	Asymmetric Digital Subscriber Line
AM	Amplitude Modulation
AWGN	Additive White Gaussian Noise
BCH	Bose Chaudhuri and Hocquenghem
BCM	Block Code Modulation
BER	Bit Error Rate
BPF	Band Pass Filter
BPSK	Binary Phase Shift Keying
CBEP	Conditional Bit Error Probability
CCDF	Complementary Cumulative Density Function
CDF	Cumulative Density Function
CDMA	Code Division Multiple Access
CF	Crest Factor
CFO	Carrier Frequency Offset
CHF	Characteristic Function
CIR	Carrier-to-Interference Ratio
CP	Cyclic Prefix
CRB	Cramer-Rao Bound
DA	Data Aided
DAB	Digital Audio Broadcasting

DAC	Digital to Analog Converter
DFE	Decision Feedback Equalization
DFT	Discrete Fourier Transform
DMT	Discrete Multi Tone
DSP	Digital Signal Processing
DVB	Digital Video Broadcasting
DVB-T	Digital Video Broadcasting-Terrestrial
FDM	Frequency Division Multiplexing
FEC	Forward Error Correction
FEQ	Frequency Domain Equalization
FFT	Fast Fourier Transform
FM	Frequency Modulation
GSM	Global System for Mobile
HDSL	High-speed Digital Subscriber Lines
HIPERLAN	High Performance Local Area Network
HPA	High Power Amplifier
IBO	Input Back-Off
ICI	Intercarrier Interference
ICR	Interference-to-Carrier Ratio
IDFT	Inverse Discrete Fourier Transform
IEEE	Institute of Electrical and Electronic Engineers
IFFT	Inverse Fast Fourier Transform
IMT-2000	International Mobile Telecommunications - 2000
ISI	Intersymbol Interference
IWHT	Inverse Walsh-Hadamard Transform
LAN	Local Area Network
LP	Linear Programming
LPF	Low Pass Filter
LSE	Least Square Error
MC	Multicarrier or Multicode
MC-CDMA	Multicarrier CDMA
MIMO	Multi-Input Multi-Output

ML	Maximum Likelihood
MLE	Maximum Likelihood Estimation
MMSE	Minimum Mean Square Error
M-PSK	M-point Phase Shift Keying
M-QAM	M-point Quadrature Amplitude Modulation
M-ZPSK	M-point Zero-padded Phase Shift Keying
NDA	Non-Data Aided
OBO	Output Back-Off
OFDM	Orthogonal Frequency Division Multiplexing
P/S	Parallel to Serial
PAP	Peak-to-Average Power ratio
PAPR	Peak-to-Average Power Ratio
PAR	Peak-to-Average power Ratio
PCC	Polynomial Coded Cancellation
PD	Phase Distortion/Predistortor
PDF	Probability Density Function
PICR	Peak Interference-to-Carrier Ratio
PLL	Phase Locked Loop
PM	Phase Modulation
PMEPR	Peak-to-Mean Envelope Power Ratio
PN	Pseudo Noise
PRC	Peak Reduction Carriers
PSD	Power Spectral Density
PSK	Phase Shift Keying
PTS	Partial Transmit Sequence
QAM	Quadrature Amplitude Modulation
QoS	Quality of Service
QPSK	Quadrature Phase Shift Keying
RCPC	Rate Compatible Punctured Convolutional
RF	Radio Frequency
RM	Reed Muller

RS	Reed Solomon
RV	Random Variable
S/P	Serial to Parallel
SDMA	Space Division Multiplexing Access
SEP	Symbol Error Probability
SER	Symbol Error Rate
SI	Side Information
SISO	Single-Input Single-Output
SL	Soft Limiter
SLM	Selected Mapping
SNR	Signal to Noise Ratio
SSPA	Solid State Power Amplifier
TCM	Trellis Coded Modulation
TEQ	Time domain Equalization
VHDSL	Very High-speed Digital Subscriber Lines
VLSI	Very Large Scale Intergared
WCDMA	Wideband Code Division Multiplexing Accesss
WHT	Walsh-Hadamard Transform
WLAN	Wireless Local Area Network

List of Symbols

α_l	fading coefficient of the l -th path
β	two sided 3-dB line width of Lorentzian power density spectrum
β_k	intercarrier interference on k -th subcarrier due to time selectivity of the channel
\mathcal{C}	Code
δf	frequency offset error
Δf	subcarrier spacing
Δt	sampling interval
ϵ	error term
γ_{eff}	effective signal-to-noise ratio
γ_s	ideal signal-to-noise ratio
$\Im\{.\}$	imaginary value of a complex number
λ_k	interference coefficient caused by phase noise
\mathbf{I}	intercarrier interference matrix of $N \times N$
ω	angular frequency
ϕ	characteristic function
$\Re\{.\}$	real value of a complex number
$\rho(k)$	aperiodic autocorrelation function
σ^2	variance of noise
σ_{ICI}^2	variance of ICI
τ_l	time delay of the l -th path
\mathbf{c}	codeword or data frame
\mathbf{S}	ICI coefficient matrix of $N \times N$
$\theta(t)$	time varying phase
ϵ	normalized frequency offset
$.\ $	denotes the magnitude

A	saturated output of the amplifier
A_{ct}	clipping threshold
c_k	data symbol on the k -th subcarrier
$c_{l,k}$	data symbol on the k -th subcarrier of l -th OFDM symbol
D	degradation in SNR
d	free distance
$d_*(.)$	minimum Hamming distance
d_H	Hamming weight
$E[.]$	denotes the average
E_b	bit energy
E_b/N_0	bit energy to noise ratio
E_S	symbol energy
f_c	carrier frequency
f_d	Doppler spread
F_M	signal constellation of the M -ary modulation
f_{off}	frequency offset error
$g(t)$	impulse response of the filter in the transmitter
$h(t)$	impulse response of the channel
H_k	Fourier transform of the impulse response of the k -th subchannel
$h_{n,l}$	fading coefficient of the n -th subcarrier from l -th path
I_k	intercarrier interference at k -th subcarrier
J	oversampling factor
L	number of resolvable paths in multipath fading channel
n	number of parallel channels in multi-code CDMA
N	Number of subcarriers
$n(t)$	additive white Gaussian noise
N_0	one sided noise spectral density
n_k	additive white Gaussian noise sample on k -th subcarrier
N_z	number of zero amplitude symbols in an OFDM block
P_b	probability of bit error
R	code rate
$r(t)$	received signal

r_k	received signal sample on k -th subcarrier
S_k	ICI coefficient
T_c	channel coherence time
T_g	guard interval
T_o	OFDM symbol duration
T_s	symbol duration
T_u	useful OFDM symbol duration
v_l	velocity of light
v_r	relative velocity of the receiver
$x(t)$	continuous time-domain baseband OFDM signal at transmitter
$x[n]$	discrete time-domain baseband OFDM signal at transmitter
$x_I(t)$	in-phase component of $x(t)$
$x_l(t)$	base band signal for the l -th OFDM symbol
x_n	baseband OFDM signal sample at transmitter
$x_{PB}(t)$	time-domain bandpass OFDM signal at the transmitter
$x_Q(t)$	quadrature component of $x(t)$
y_k	received signal sample on the k -th subcarrier after the DFT process

Chapter 1

Introduction

Mobile communications services are now being used in all fields of human activities and the demand for high data rate services with a high quality of service (QoS) is likely to increase in the near future. Many new applications, such as wireless multimedia services and wireless Internet access now require high data rate wireless communications systems. But, the physical limitations and impairments on radio channels, including bandwidth constraints, multipath fading, noise and interference, present a technical challenge to reliable high data rate communication.

Mobile communication services, on the other hand, are still in a state of flux. For example, second generation mobile systems are limited to basic services such as voice and low bit-rate data applications. Third generation (3G) wireless systems, called IMT-2000, are still being designed to support such wideband services and to provide universal access and global roaming, but are not yet fully deployed. At the same time, the concept of fourth generation (4G) systems has been emerging, motivating the design of new techniques.

A promising transmission technique for the support of such large data rates, and one which has sufficient robustness to handle radio channel impairments, is orthogonal frequency division multiplexing (OFDM). It has been accepted in several wireless local area network (WLAN) standards, as well as a number of mobile multimedia applications such as digital audio broadcasting (DAB), asynchronous digital subscriber lines (ADSL), digital video broadcasting (DVB) and IEEE 802.11a wireless local area network (WLAN). However, two major drawbacks of OFDM are its potentially large peak-to-average power ratio (PAR) and intercarrier interference (ICI) due to frequency offset

errors. These impairments degrade the performance and efficiency that the OFDM systems are designed to provide.

Multi-code code division multiple access (multi-code CDMA) has been recently introduced to provide high speed and flexible data rate transmission over wireless channels. This scheme has already been included in wideband CDMA (WCDMA) standards. However, the multi-code signal also exhibits high PAR and its performance degrades in the presence of nonlinearities. This PAR problem is similar to the PAR issue in OFDM, although PAR arises due to two different orthogonal transforms.

1.1 Motivations

Despite the many advantages of OFDM and its standardization in many applications, its high PAR and the frequency offset errors are considered as limiting factors for efficient implementation of OFDM systems. These limitations have already motivated several studies to find solutions. As a result, several techniques have been developed but with some sacrifice in other factors such as bandwidth efficiency, complexity, performance, power consumption and cost. Therefore, the limitations noted above still remain as open research problems. On the other hand, all of the above studies consider high PAR and frequency offset errors as two separate problems. Therefore, a technique developed for one problem results in poor performance with another problem. For instance, the self-ICI cancellation or the polynomial coded cancellation scheme is effective in reducing ICI but its PAR characteristics are worse than those in conventional OFDM. This observation has motivated the attempt to find a single method to solve both problems. Moreover, such a cancellation scheme, which can be considered as involving rate-half repetition codes, would halve the data throughput. Therefore, it is highly desirable to find an ICI-reduction scheme with high data throughput. These observations motivate the research in this thesis.

1.2 Thesis Outline

Chapter 2 presents the analysis of an OFDM system and its impairments, specifically PAR and ICI. The causes of ICI, frequency offset errors, phase noise and time variations of the channel are discussed in detail and, more specifically, carrier frequency offset.

Proposed methods for dealing with the frequency offset issue are described. The PAR problem and the proposed schemes to reduce PAR are reviewed. For completeness, the multicarrier CDMA (MC-CDMA) and multi-input multi-output OFDM (MIMO OFDM) systems are both briefly described.

Chapter 3 describes a precise numerical technique for calculating the effect of the carrier frequency offset (CFO) on the symbol error rate (SER) in an OFDM system. The common modulation formats, binary phase shift keying (BPSK), quadrature phase shift keying (QPSK) and 16-point quadrature amplitude modulation (16QAM), are considered. Previously proposed methods are compared with this new technique. Moreover, the bit error rate (BER) performance of rate-half repetition codes are evaluated precisely. The proposed technique is extended to analyze error performance of an OFDM system with phase noise.

Chapter 4 describes higher-rate ICI-reduction codes. An optimal design rule for ICI-reduction codes is derived. Since algebraic construction of higher-rate ICI-reduction codes are rather difficult, two new codes that map data onto three and four adjacent subcarriers are proposed. The performance of the proposed codes is justified by its average carrier-to-interference ratio (CIR) and BER results. This chapter also investigates rate-compatible punctured convolutional (RCPC) codes to reduce ICI.

Chapter 5 introduces a measure, peak interference-to-carrier ratio (PICR), to quantify ICI due to carrier frequency offset. Analysis of PICR statistics, PICR and BER relationships and the algebraic construction of PICR-reduction codes are discussed. The block coding approach for PICR reductions is explored. Chapter 5 also introduces the use of tone reservation, selected mapping (SLM) and partial transmit sequence (PTS) approaches to reduce PICR. This chapter also demonstrates the existence of codes to reduce both the PAR and PICR simultaneously. The block coding scheme, which is based on selecting only those messages with both low PAR and PICR as valid codewords, is described. The performance of Golay complementary repetition codes is discussed to show an example of an explicit construction for PAR-PICR-reduction codes.

Chapter 6 proposes a simple adaptive mapping scheme to reduce both PAR and ICI simultaneously by using M-point zero-padded phase shift keying (M-ZPSK), which includes a signal point of zero amplitude. Analytical expressions for the error rates

of M-ZPSK on additive white Gaussian noise (AWGN), Rayleigh, Nakagami-m and Ricean fading channels are derived. Performance in wide band fading channels is also evaluated. Explicit and implicit methods for reliable transmission of side information (SI) are discussed.

Chapter 7 briefly describes the multi-code CDMA system and its PAR problem. Analytical expressions for the statistical distribution of PAR are derived. Achievable PAR reduction for a given code rate and the multiple signal representation schemes for PAR reduction are also analytically justified. Chapter 7 also discusses the SLM and PTS schemes for PAR reduction in multi-code CDMA systems.

Chapter 8 summarizes the thesis and discusses possible future work. This thesis has proposed a single approach for reducing both PAR and ICI in OFDM systems simultaneously. While coding seems to be an attractive solution in this context, more research on algebraic construction of such codes is necessary.

1.3 Research Contributions

The main contributions of this thesis are a rigorous analysis of ICI caused by frequency offset errors, and the development of several ICI-reduction schemes. This thesis also introduces the concept of developing a single scheme to deal with both PAR and ICI issues. Another contribution of this thesis is the derivation of a statistical distribution of PAR in multi-code CDMA. The details of these contributions are listed by chapter below.

- Chapter 3 derives exact analytical expressions for the probability of symbol error of an OFDM system with carrier frequency offset errors. These precise expressions are likely to be very useful in evaluating the performance of an OFDM system since previous methods have been approximations only. This technique is used to evaluate the performance of rate-half repetition codes. The proposed technique is also applied to analyze the error performance with phase noise.
- Chapter 4 introduces a code design rule for ICI-reduction. High-rate ICI reduction codes based on symbol mapping are proposed and their performances evaluated. High code rate RCPC codes are studied analytically, and by simulation, as a means of overcoming ICI effects.

- Chapter 5 introduces a new measure, PICR, to quantify ICI effects as an alternative to average CIR. This new parameter formulates the ICI problem parallel to PAR issues and is used to devise several PICR reduction schemes. Chapter 5 also presents an analysis of PICR statistics, the PICR-BER relationship and algebraic construction of PICR reduction codes. Chapter 5 also proposes a new concept of PAR-PICR-reduction codes to reduce both PAR and PICR simultaneously. This chapter demonstrates the existence of such codes analytically and by simulation.
- Chapter 6 proposes a new adaptive mapping scheme to reduce both PAR and ICI based on M-ZPSK modulation. Analytical expressions for bit error rates in various channel models are derived.
- Chapter 7 derives analytical expressions for PAR statistics in multi-code CDMA systems and introduces the PTS and SLM schemes for PAR reduction.

Chapter 2

Orthogonal Frequency Division Multiplexing (OFDM)

This chapter presents the general concept of OFDM systems, their background, applications and mathematical descriptions. Despite the many inherent advantages of OFDM, its performance is limited by a high peak-to-average power ratio (PAR) and high sensitivity to carrier frequency offset (CFO) errors. Since this thesis mostly deals with these two problems, they are discussed in detail in this chapter. We briefly outline the solutions proposed in the open literature to overcome these problems. We also present a brief introduction to emerging OFDM-based technologies, namely multi-carrier code division multiple access (MC-CDMA) and multiple-input multiple-output OFDM (MIMO OFDM).

2.1 Introduction

2.1.1 OFDM Background

The concept of the parallel data transmission scheme was introduced in the 1960s and was first used in Collins Kineplex system [1]. In this classical parallel data system, which is also called a conventional multicarrier system, the data is divided into several bit streams to modulate several carriers. This idea is analogous to frequency division multiplexing (FDM) in analog systems. The total signal band is divided into N nonoverlapping frequency subchannels. Each subchannel is modulated separately and then all N subchannels are frequency multiplexed. A guard band between the subchannels is used to correctly separate the subchannels at the receiver using conventional filters. The main problem with this conventional approach is the inefficient

use of the spectrum. Chang [2] proposed the idea of overlapping subchannels which are orthogonal to each other. Hence, this is referred to as Orthogonal Frequency Division Multiplexing (OFDM). Figure 2.1 shows the spectral efficiency which results from overlapping subchannels over a conventional multicarrier scheme.

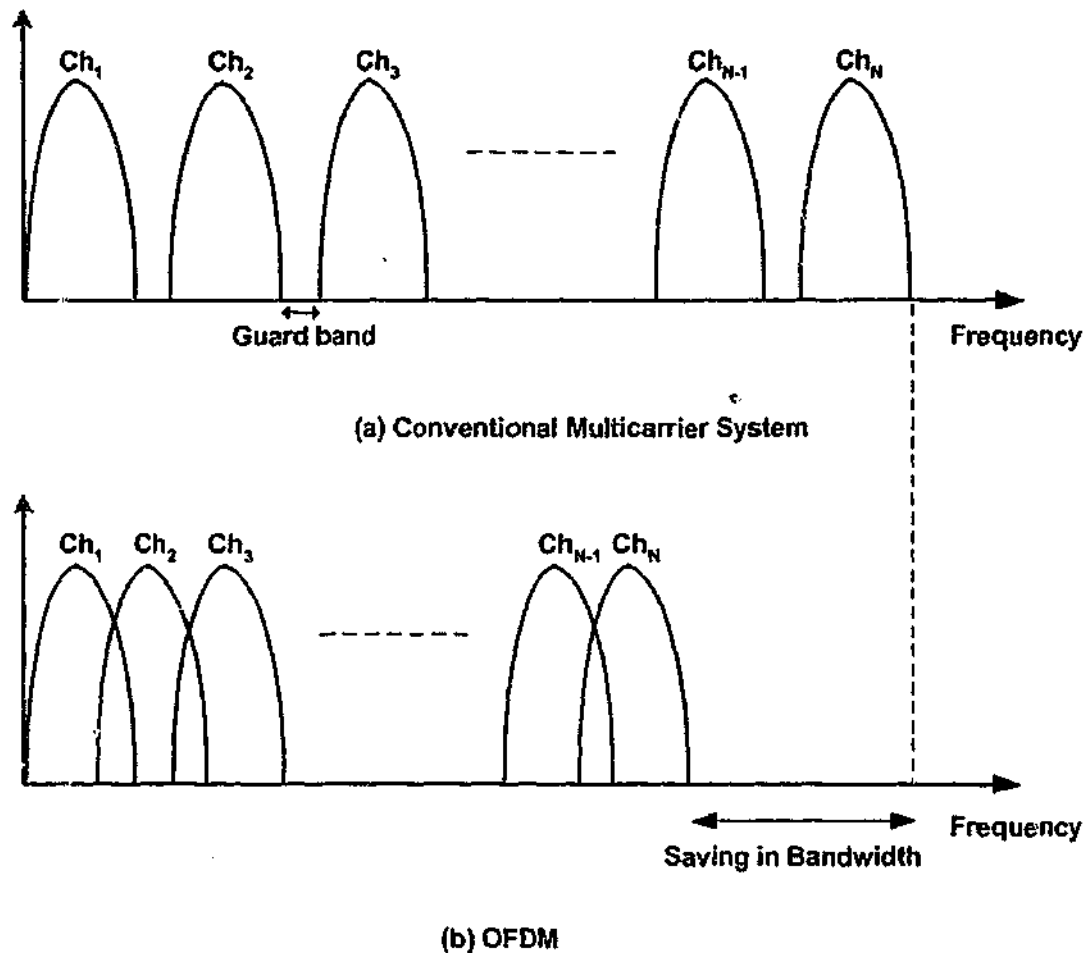


Figure 2.1: Multicarrier transmission concept.

Another advantage in overlapping subchannels is the avoidance of steep band filters. The conventional multicarrier scheme requires steep band filters to separate subchannels. These filters are expensive and complex. Moreover, the arrays of sinusoidal generators and coherent demodulators required in multicarrier systems are unreasonably expensive and complex, particularly for large N . Weinstein [3] proposed that the concept of OFDM could be efficiently realized by using the discrete-time Fourier transform (DFT) in transmitters and receivers. This reduces the complexity of the OFDM system significantly. The inverse DFT (IDFT) in the transmitter performs modulation and multiplexing and the DFT in the receiver performs the demodulation and demultiplexing. The computational complexity has since been further reduced by the use of

fast Fourier transform (FFT) algorithms. Recent advances in digital signal processing (DSP) and very large scale integrated (VLSI) circuit technologies have also simplified its implementation and opened the doors to many applications [4,5]. In the literature, OFDM is also called discrete multitone (DMT) which is used with cable transmission. Thus, in general practice, a multicarrier system refers both to OFDM and DMT.

An OFDM transmission system offers possibilities for alleviating many of the problems encountered with single carrier systems. It has the advantage of spreading out a frequency selective fade over many symbols. This effectively randomizes burst errors caused by fading or impulse interference so that, instead of several adjacent symbols being completely destroyed, many symbols are only slightly distorted. This allows successful reconstruction of the majority of them even without the use of forward error correction codes [4-6]. The frequency response over an individual subchannel is also relatively flat since subchannels are smaller than the coherence bandwidth of the channel. Thus, equalization is potentially simpler than in a single carrier system [4-6]. Moreover, equalization may be avoided altogether if differential encoding is implemented [4, 5, 7].

The orthogonality of subchannel in OFDM can be maintained and individual subchannels completely separated by DFT at the receiver, if there is no intersymbol interference (ISI) or intercarrier interference (ICI) introduced by the transmission channel. However, as multipath propagation causes each subchannel to spread energy into the adjacent channels, consequently this can lead to ISI. To prevent ISI, Peled and Ruiz [8] proposed a cyclically extended guard interval, where each OFDM symbol is preceded by a periodic extension of the signal itself. When the guard interval is longer than the channel impulse response or multipath delay, the ISI can be completely eliminated [4, 5, 8-10].

By using time and frequency diversity, OFDM provides a means of transmitting data in a frequency selective channel. However, it does not suppress fading itself. Depending on their position in the frequency domain, individual subchannels could be affected by fading. This requires the use of channel coding to further protect transmitted data. Coded OFDM combined with frequency and time interleaving is considered the most effective means to a frequency selective fading channel [4, 5, 11].

Drawbacks in OFDM Systems

Two major drawbacks in OFDM systems are:

- high peak-to-average power ratio (PAR)

The OFDM signal has a large dynamic signal range (high peaks) due to the large number of subcarriers. These high signal peaks can lead to in-band distortion and spectral spreading in the presence of non-linear devices. Consequently, performance degradation and/or inefficiency occur.

- high sensitivity to frequency offset errors

The OFDM system is very sensitive to inaccurate frequency references or frequency dispersion due to carrier frequency drifts and other environmental variations. A frequency offset at the receiver can cause loss of subcarrier orthogonality and thus introduce ICI, severely degrading system performance.

Applications of OFDM

The OFDM technique was initially used in several high-frequency military systems [1,4-6]. With the introduction of DFT processing and the advancement of DSP technologies, it has been exploited for wideband communication over radio FM channels, asymmetric digital subscriber lines (ADSL), high-speed digital subscriber lines (HDSL), very high-speed digital subscriber lines (VDSL), digital audio broadcasting (DAB), digital video broadcasting (DVB) and wireless local area networks (WLAN) [12,13]. It has already been selected for the standards of ADSL, DAB, DVB and WLANs, namely IEEE 802.11a and HIPERLAN/2.

Typical OFDM Systems

Figure 2.2 shows a typical OFDM system. The input bit stream is fed into a channel encoder and then followed by a modulator. The modulated symbols are split into N frequency subbands or subchannels by a serial-to-parallel (S/P) converter. This parallel stream undergoes an N -point IFFT to obtain a time-domain signal for transmission. However, this signal is not sufficient for reliable transmission, since channel distortion may cause interference between neighboring blocks. To alleviate this, a guard interval of length, ν , is inserted in the form of a cyclic prefix, which takes the last ν time-domain samples and inserts them into the beginning of the block. This time-domain signal is then converted to an analog signal by a digital-to-analog converter (DAC), filtered, and finally modulated into the carrier frequency to be sent across the channel. At the

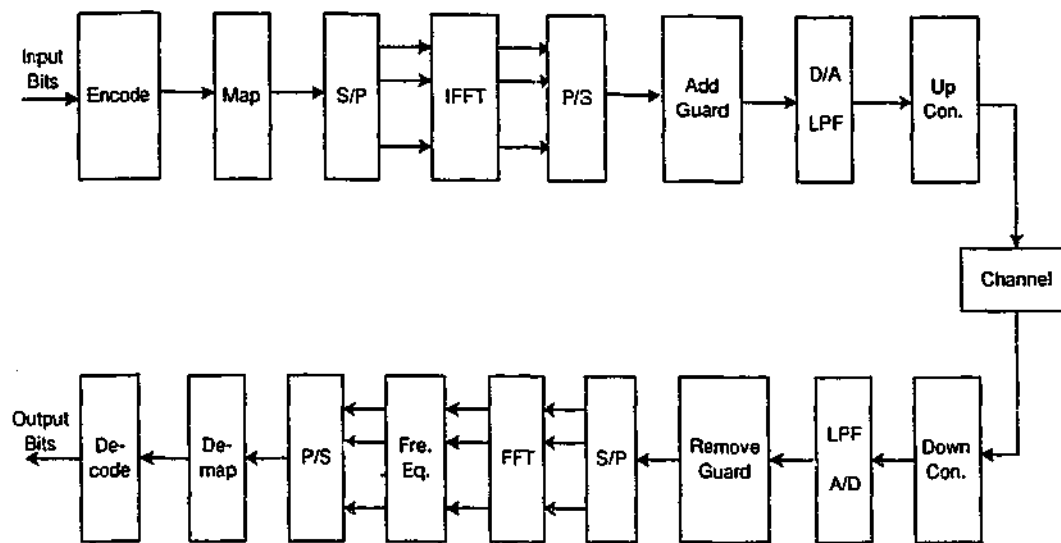


Figure 2.2: Typical OFDM system.

receiver (also shown in Figure 2.2), the received signal is downconverted to baseband, filtered and sampled. The cyclic-prefix portion of the received block is then stripped off, and the resulting signal is then converted back to discrete-frequency domain by an N -point FFT. A frequency-domain equalizer (FEQ), consisting of N single-tap complex equalizers, is applied. The output is passed through the demodulator and then through the channel decoder in order to obtain the received bit stream.

2.1.2 OFDM Signalling

The l -th complex baseband OFDM signal may be represented as

$$x_l(t) = \frac{1}{\sqrt{N}} \sum_{k=0}^{N-1} c_{l,k} e^{j2\pi k \Delta f t} \quad (2.1)$$

where $j^2 = -1$, N is the total number of subcarriers, and $c_{l,k}$ is the data symbol for the k -th subcarrier of the l -th OFDM symbol. Note that the N subcarrier OFDM system transmits a block of N data symbols per OFDM symbol and all these subcarriers are mutually orthogonal. Each modulated symbol $c_{l,k}$ is chosen from the set $F_M = \{\lambda_1, \lambda_2, \dots, \lambda_M\}$ of M distinct elements. The set F_M is called the *signal constellation* of the M -ary modulation scheme. While several modulation schemes are commonly in use, we are mostly concerned with phase shift keying (PSK) constellations in which

$$F_M = \left\{ 1, \exp j \frac{2\pi}{M}, \exp j \frac{4\pi}{M}, \dots, \exp j \frac{(M-1)2\pi}{M} \right\} \quad (2.2)$$

and quadrature amplitude modulation (QAM) constellations in which

$$F_M = \{\pm(2b_1 + 1) \pm j(2b_2 + 1)\} \quad (2.3)$$

where $b_1, b_2 \in \{0, 1, \dots, \log_2 M - 2\}$.

The frequency separation Δf , between any two adjacent subcarriers, is given by

$$\Delta f = \frac{1}{T_u} \quad (2.4)$$

where T_u is the useful interval of the OFDM symbol period.

To avoid ISI due to multipath fading, a guard interval of T_g is added to each OFDM block. Thus, the total OFDM symbol period is $T_o = T_u + T_g$. Since $x_l(t)$ is a periodic-like function with period T_o , the baseband signal $x(t)$ can be expressed as

$$x(t) = \sum_{l=-\infty}^{\infty} x_l(t)g(t - lT_o) \quad (2.5)$$

where $g(t)$ is the windowing function that controls the spectral spread due to the abrupt transition of successive OFDM symbols. Figure 2.3 shows an example of a window, $g(t)$, in which the parameter Δ controls the smoothness of the window [14].

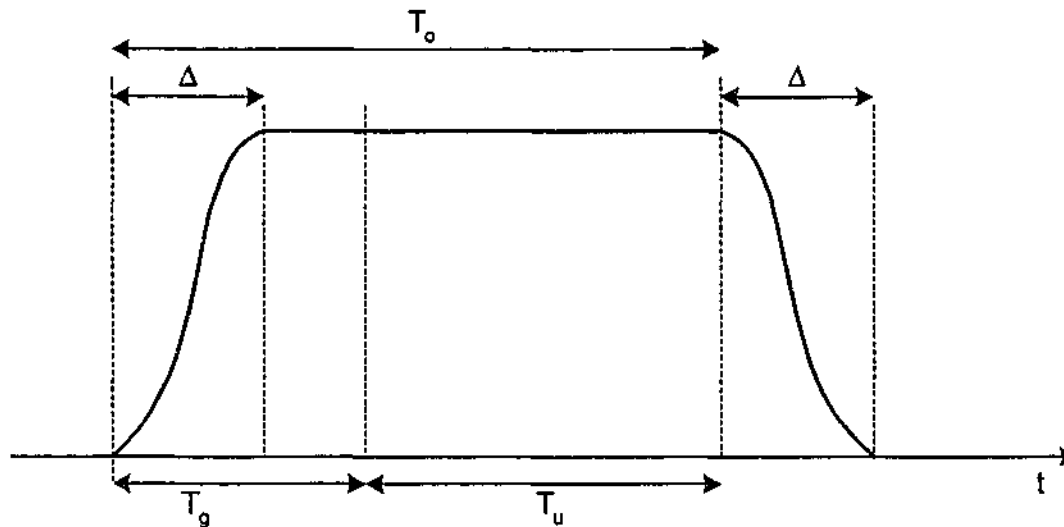


Figure 2.3: Typical OFDM windowing function $g(t)$.

The windowing of the OFDM signal does not change the maximum amplitude of the OFDM signal. Moreover, it does not influence the frequency offset errors realized at the receiver. Also, the guard interval does not change the peak power property of the OFDM signals and the frequency offset errors at the receiver. Therefore, we assume that $g(t)$ is an unit rectangular pulse and $\Delta = T_g = 0$. To be more specific, we assume

the OFDM signal consists of successive OFDM symbols without any overlap in time. Thus, the complex baseband signal may be represented as

$$x(t) = \sum_{l=-\infty}^{\infty} x_l(t - lT_u) \quad (2.6)$$

and the bandpass OFDM signal may be represented as

$$x_{BP}(t) = \Re\{x(t)e^{j2\pi f_c t}\} \quad (2.7)$$

where f_c is the carrier frequency of the bandpass signal.

Because there is no overlap between different OFDM symbols, it is sufficient to consider a single OFDM symbol ($l = 0$). In practice, filtering can cause some degree of intersymbol interference and peak regrowth, which will be neglected here. Therefore, the complex baseband signal may be represented as

$$x(t) = \frac{1}{\sqrt{N}} \sum_{k=0}^{N-1} c_k e^{j2\pi k \Delta f t} \quad (2.8)$$

2.1.3 Discrete-time Representation of OFDM Signals

The OFDM signal sampled at time instant $t = n\Delta t$ (for $n = 0, \dots, JN - 1$) can be expressed as

$$x_n = x(n\Delta t) = x[n] = \frac{1}{\sqrt{N}} \sum_{k=0}^{N-1} c_k e^{j2\pi k \Delta f n \Delta t} \quad (2.9)$$

where Δt is the sampling interval given by

$$\Delta t = T_u / JN \quad (2.10)$$

and J is an integer that determines the number of samples per OFDM symbol. Equation (2.9) can be restated as

$$x_n = \frac{\sqrt{J}}{\sqrt{JN}} \sum_{k=0}^{N-1} c_k e^{j2\pi k \frac{n}{JN}} \quad (2.11)$$

Equation (2.11) indicates that the continuous OFDM signal (2.8) can be approximated by using a JN -point IDFT of the zero-padded sequence of length JN . That is denoted as

$$x_n = \sqrt{J} \times \text{IDFT}(\mathbf{c}, JN)_n \quad (2.12)$$

where

$$\mathbf{c} = \{c_0, c_1, \dots, c_{N-1}, \underbrace{0, 0, \dots, 0}_{JN-N}\}. \quad (2.13)$$

In order to reconstruct the continuous OFDM signal from its samples, N samples are sufficient. Since the baseband OFDM signal with N successive subcarriers is completely determined by the N complex samples, the band-limited signal can be reconstructed without distortion if the sampling interval satisfies

$$\Delta t = \frac{T_u}{JN} \leq \frac{T_u}{N}. \quad (2.14)$$

Therefore, $J = 1$ is enough and ideal low-pass filtering of the samples may reconstruct the continuous complex waveform from the N -point complex samples. This is called the Nyquist-rate sampling. The parameter J is thus referred to as the oversampling factor. Therefore, the Nyquist-rate sampled signal is expressed as

$$x_n = \frac{1}{\sqrt{N}} \sum_{k=0}^{N-1} c_k e^{j2\pi k \frac{n}{N}}. \quad (2.15)$$

2.1.4 Receiver Structure

The received signal through a multipath channel can be expressed as

$$r(t) = x(t) * h(t) + n(t) \quad (2.16)$$

where $*$ denotes convolution. Further, $n(t)$ is the additive white Gaussian noise (AWGN) and $h(t)$ is the impulse response of the multipath channel given by [15]

$$h(t) = \sum_{l=0}^{L-1} \alpha_l \delta(t - \tau_l) \quad (2.17)$$

where α_l is the fading coefficient of the l -th path and L is the total number of resolvable paths. We assume that the delays τ_l are uniformly and independently distributed over the guard length of the OFDM symbol. The DFT demodulated received signal can be expressed as

$$y_k = H_k c_k + n_k \quad \text{for } k = 0, 1, \dots, N-1, \quad (2.18)$$

where H_k is the attenuation on each tone given by [15]

$$H_k = H \left(\frac{2\pi k}{N} \right) = \sum_{n=0}^{N-1} h_n e^{-j \frac{2\pi n k}{N}} \quad (2.19)$$

and $H(\cdot)$ is the frequency response of the channel.

Eq. (2.18) shows that c_k can be recovered by multiplying y_k by the reciprocal of the channel DFT coefficients, $1/H_k$. This operation is termed as single tap equalization. In order to have this single tap equalization, the receiver needs to perceive perfect cyclic convolution with the channel. The requirement for this is that the cyclic prefix length should be equal to or greater than the channel length. However, the addition of a cyclic prefix reduces the data throughput of the OFDM system.

2.2 Intercarrier Interference (ICI)

An OFDM system uses a set of orthogonal subcarriers. This orthogonality allows the receiver to separate the data symbol on the subcarriers, which are overlapped at the transmitter to achieve spectral efficiency. The loss of orthogonality results in ICI. This ICI deteriorates the bit error rate of the system and introduces an error floor. This error floor cannot be removed by just increasing the transmit power. Thus, ICI is considered as a serious problem in OFDM system. Generally, the cause for ICI can be grouped into three categories:

- frequency offset errors,
- phase noise,
- time variations of the channel.

However, these causes are independent and their statistical characteristics are different. These are treated in the literature as independent problems and several studies have been reported for each case. They are discussed in detail in this chapter.

In addition to those listed factors, the ISI also causes interference among the subcarriers. The different time delays in a multipath channel causes the OFDM symbols to overlap at the receiver, resulting in ISI. This ISI introduces interference among the subcarriers within an OFDM block and adjacent OFDM blocks. This ISI can be effectively controlled by using cyclically extended guard interval longer than the channel impulse response or multipath delay spread [4, 5, 8–10]. Therefore, interference caused by this ISI is not very problematic, unlike others.

2.3 Frequency Offset Errors

Frequency offset errors are the main cause of ICI in OFDM systems. Thus, most of the ICI studies in OFDM systems deal with frequency offset errors. The frequency offset errors are caused by the mismatch of oscillators' frequencies between the transmitter and the receiver and/or by Doppler shifts, which are due to the movement of the receiver [16–18]. The Doppler shift is defined as [15]

$$f_d = \frac{f_c v_r}{v_l \cos \theta} \quad (2.20)$$

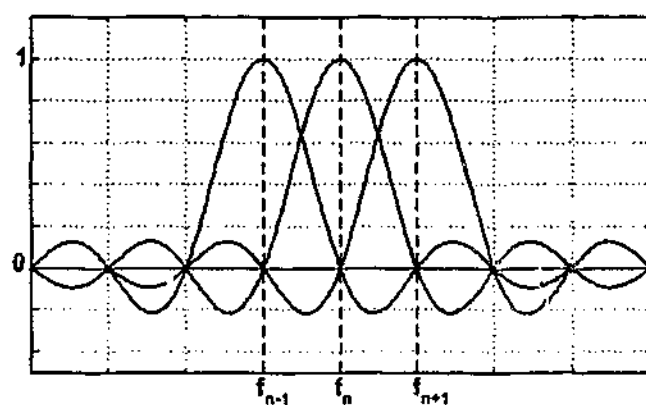
where f_c is the transmitted carrier frequency, v_l is the velocity of light, v_r is the velocity of the receiver and θ is the relative angle between the direction of the movement of the receiver and the direction of the transmitter. We define normalized frequency offset as

$$\varepsilon = \frac{\delta f}{\Delta f} \quad (2.21)$$

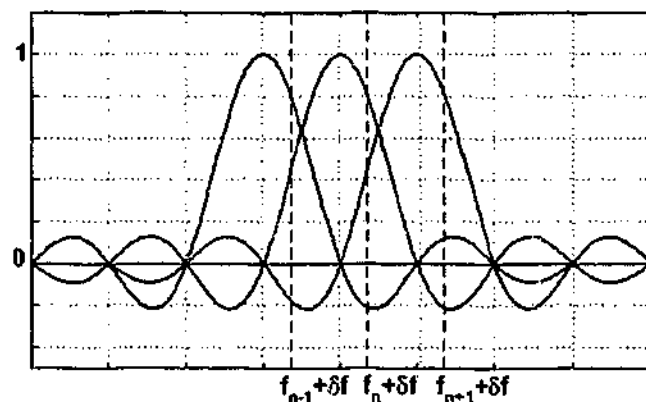
where δf is the frequency offset error and Δf is the subcarrier separation. This thesis mostly deals with frequency offset errors caused by oscillator's carrier frequency mismatch. Thus, CFO, frequency offset errors and frequency errors are used interchangeably.

Frequency offset errors result in a shift of the received signal's spectrum in the frequency domain [13]. These errors can be considered as consisting of two parts, one is the integer part and the other is the fractional part. If the frequency error is an integer multiple n ($n = \pm 1, \pm 2, \dots$) of the subcarrier spacing Δf , then the received frequency subcarriers are shifted by $n\Delta f$. The subcarriers are still mutually orthogonal, but the spectrum of the demodulated signal will be in the wrong position in the frequency domain. That means the demodulated data symbols will be in the wrong position in the spectrum, causing BER degradation. If the frequency error is a fraction of the subcarrier spacing Δf , then the received frequency subcarriers are shifted by $\varepsilon\Delta f$ ($= \delta f$), where $|\varepsilon| \leq 0.5$. This fractional frequency error causes energy to spill over all other subcarriers, resulting in a loss of mutual orthogonality. The loss of orthogonality introduces interference among the subcarriers, which deteriorates the bit error rate of the system. Figure 2.4 shows these interference effects in the frequency domain. When there is no frequency error, subchannels are orthogonal at the sampling instant. That means the zero crossing of the subchannels occurs at the sampling instant. But with

frequency offset, zero crossing does not occur at the sampling instant and thus, each sample is influenced by all other subchannels. This results in ICI. As seen in this figure, the interference effects also increase with increasing frequency errors.



(a) No frequency error



(b) Frequency error

Figure 2.4: Illustration of frequency offset effect.

Therefore, an accurate frequency reference must be achieved at the receiver to correctly demodulate the data symbols. Several frequency synchronization algorithms have been reported in the open literature. The integer part of the frequency error is estimated and corrected by using coarse frequency synchronization and the fractional part is by fine frequency synchronization. These synchronizations are achieved at the beginning of the transmission. However, the receiver needs to maintain an accurate frequency reference throughout the transmission since it may be susceptible to small frequency drift. This is achieved by tracking part of the synchronization algorithm.

2.3.1 Carrier Frequency Offset Problem Formulation

In order to simplify the problem and emphasize the analysis of the frequency offset error, we assume that the channel is an additive white Gaussian noise (AWGN) but with a frequency offset error. A simplified model for frequency offset analysis is shown in Figure 2.5.

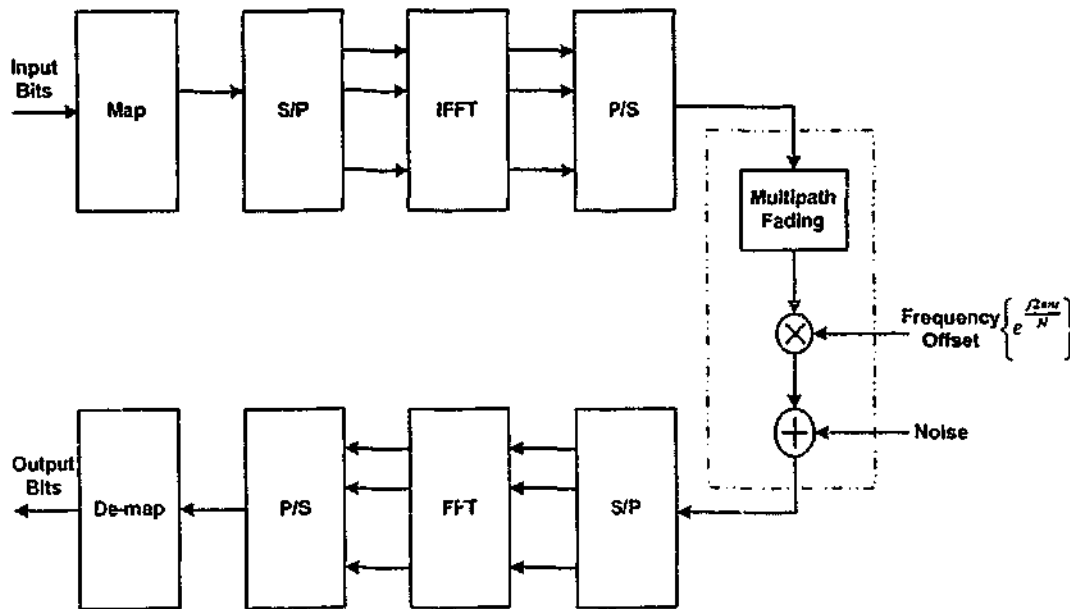


Figure 2.5: Block diagram of an OFDM system with frequency offset.

The received signal after the frequency down conversion can be expressed as

$$r(t) = x(t) \cdot e^{j2\pi\delta ft} + z(t) \quad (2.22)$$

where $z(t)$ is the Gaussian noise. Sampling the received signal at the Nyquist rate results in

$$r(k\Delta t) = x(k\Delta t) \cdot e^{j2\pi\delta f k\Delta t} + z(k\Delta t) \quad (2.23)$$

where $\Delta t = T_u/N$ and $k = 0, \dots, N-1$. This received signal (2.23) can also be denoted as

$$r_k = x_k e^{j2\pi\epsilon k} + z_k \quad (2.24)$$

The received signal for the k -th subcarrier after the DFT processing can be written

as

$$\begin{aligned}
 y_k &= \frac{1}{\sqrt{N}} \sum_{m=0}^{N-1} r_m e^{-j\frac{2\pi}{N}km} \\
 &= \frac{1}{N} \sum_{m=0}^{N-1} e^{j\frac{2\pi\epsilon m}{N}} \sum_{l=0}^{N-1} c_l e^{j\frac{2\pi}{N}(l-k)m} + n_k \\
 &= \frac{1}{N} \sum_{l=0}^{N-1} c_l \sum_{m=0}^{N-1} e^{j\frac{2\pi\epsilon m}{N}} e^{j\frac{2\pi}{N}(l-k)m} + n_k \\
 &= \sum_{l=0}^{N-1} c_l S_{l-k} + n_k
 \end{aligned} \tag{2.25}$$

where n_k is the DFT output of z_k . However, n_k is also a complex Gaussian noise sample (with its real and imaginary components being independent and identically distributed with the variance σ^2). The sequence S_k s are called ICI coefficients and given by

$$\begin{aligned}
 S_k &= \frac{1}{N} \sum_{m=0}^{N-1} e^{j\frac{2\pi\epsilon m}{N}} e^{j\frac{2\pi}{N}km} \\
 &= \frac{\sin \pi(k + \epsilon)}{N \sin \frac{\pi}{N}(k + \epsilon)} \exp[j\pi(1 - \frac{1}{N})(k + \epsilon)].
 \end{aligned} \tag{2.26}$$

In matrix notation, the demodulated signal can be expressed as

$$\mathbf{y} = \mathbf{S}\mathbf{c} + \mathbf{n} \tag{2.27}$$

where \mathbf{S} is defined as

$$\mathbf{S} = \begin{pmatrix} S_0 & S_1 & S_2 & \dots & S_{N-1} \\ S_{-1} & S_0 & S_1 & \dots & S_{N-2} \\ \vdots & & & & \vdots \\ S_{-(N-1)} & S_{-(N-2)} & S_{-(N-3)} & \dots & S_0 \end{pmatrix} \tag{2.28}$$

where the (m, n) th element of the \mathbf{S} matrix is S_{n-m} , as defined earlier. When $\epsilon = 0$, \mathbf{S} becomes an identity matrix.

In order to show the effects of the frequency offset errors more clearly, the received signal (2.25) is rewritten as

$$y_k = c_k S_0 + \underbrace{\sum_{l=0, l \neq k}^{N-1} S_{l-k} c_l}_{\text{ICI}} + n_k \text{ for } k = 0, 1, \dots, N-1. \tag{2.29}$$

where the first term is the distorted signal of the desired subcarriers and the second right is the ICI term attributable to frequency offset errors. The ICI term can be expressed as

$$I_k = \sum_{l=0, l \neq k}^{N-1} S_{l-k} c_l, \text{ for } 0 \leq k \leq N-1. \quad (2.30)$$

This can be denoted in a vector form as

$$\mathbf{I} = \mathbf{S}_I \mathbf{c} \quad (2.31)$$

where \mathbf{S}_I is defined as

$$\mathbf{S}_I = \begin{pmatrix} 0 & S_1 & S_2 & \dots & S_{N-1} \\ S_{-1} & 0 & S_1 & \dots & S_{N-2} \\ \vdots & & & & \vdots \\ S_{-(N-1)} & S_{-(N-2)} & S_{-(N-3)} & \dots & 0 \end{pmatrix}. \quad (2.32)$$

Note that I_k is a function of both c_k and ϵ . When there is no frequency error in the channel, S_k reduces to the unit impulse sequence and the received signal will then reduce to

$$y_k = c_k + n_k \text{ for } k = 0, 1, \dots, N-1. \quad (2.33)$$

Therefore, the frequency offset error causes two types of impairments. One is the attenuation and rotation of desired signal components and the other is the ICI. The latter introduces an error floor and cannot be reduced by just increasing the transmitted power. As a result, the bit error rate degrades. Figure 2.6 illustrates the effects of the frequency offset on the performance of the OFDM system. Shown in Figure 2.6 are the ideal QPSK constellation and the received constellations in different conditions. In this figure, $N = 128$, $E_b/N_0 = 6\text{dB}$ and $\epsilon = 0.1$ are assumed. Figure 2.6 clearly shows the attenuation, rotation and ICI effects when there is no noise. The combined effect of the noise and the frequency errors further degrades the error performance of the system.

Figure 2.7 shows the BER performance of an OFDM system for various ϵ . An AWGN channel and 128 subcarriers are assumed in the simulation. For $\epsilon = 0.1$, there is a 10 dB degradation in SNR at 10^{-4} over conventional OFDM. The error floor increases with large ϵ .

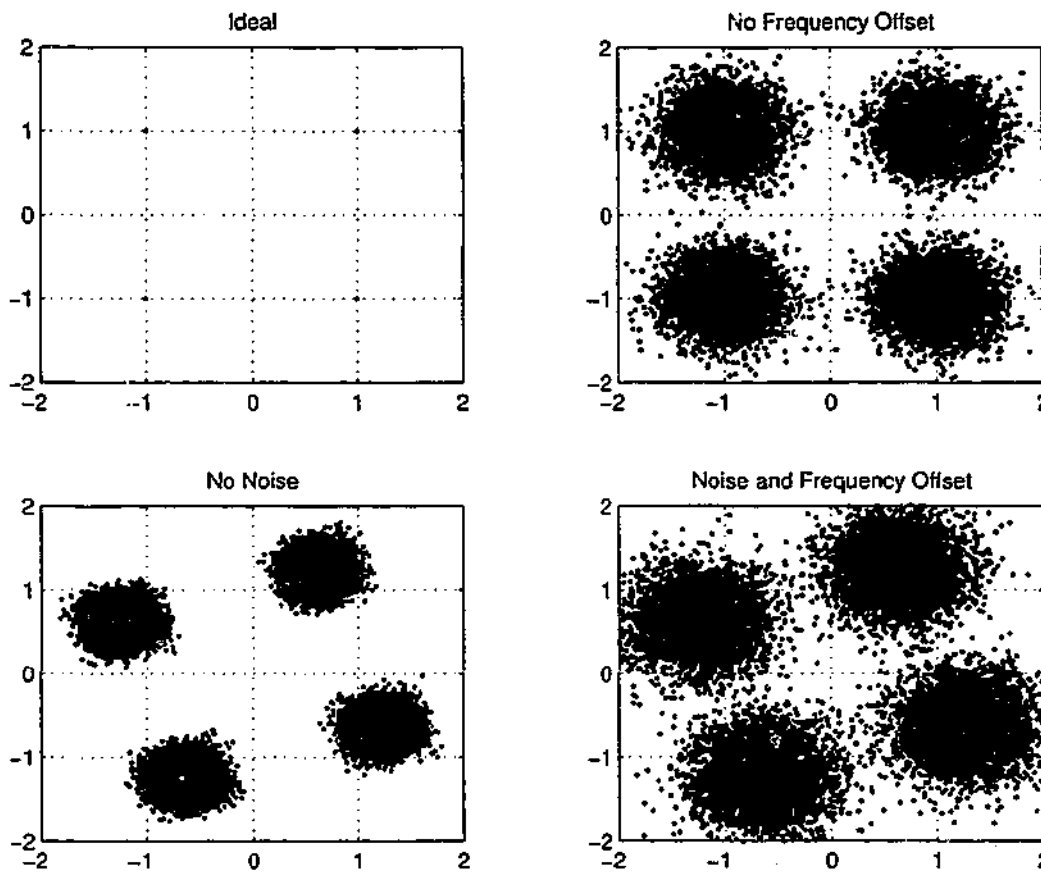


Figure 2.6: QPSK signal constellation.

In the literature, the average carrier-to-interference ratio (CIR) is widely used to quantify the ICI effects. The average CIR for subcarrier k can be expressed as

$$\text{CIR}(k) = \frac{|c_k S_0|^2}{E\left\{\left|\sum_{l=0, l \neq k}^{N-1} S_{l-k} c_l\right|^2\right\}} = \frac{|S_0|^2}{\sum_{l=0, l \neq k}^{N-1} |S_{l-k}|^2} \quad (2.34)$$

where $E\{\cdot\}$ denotes the expected value over the distribution of data, $|c_k|^2 = 1$ for a unit amplitude constellation such as PSK. Further, $\sum_{l=0}^{N-1} |S_{l-k}|^2 \approx 1$ for large N . We thus have

$$\text{CIR}(k) = \frac{|S_0|^2}{1 - |S_0|^2} \quad (2.35)$$

where $|S_0| = \frac{\sin \pi \epsilon}{N \sin \pi \epsilon / N}$. Hence, $\text{CIR}(k)$ varies very little with k and does not depend on the data frame. For small ϵ and large N , $|S_0| \approx \text{sinc} \epsilon$. By neglecting the higher order terms in the expansion of sinc function, $|S_0|^2$ is approximately equal to $(1 - \frac{(\pi \epsilon)^2}{3})$. Thus, (2.35) reduces to

$$\text{CIR} \approx \frac{3}{(\pi \epsilon)^2}. \quad (2.36)$$

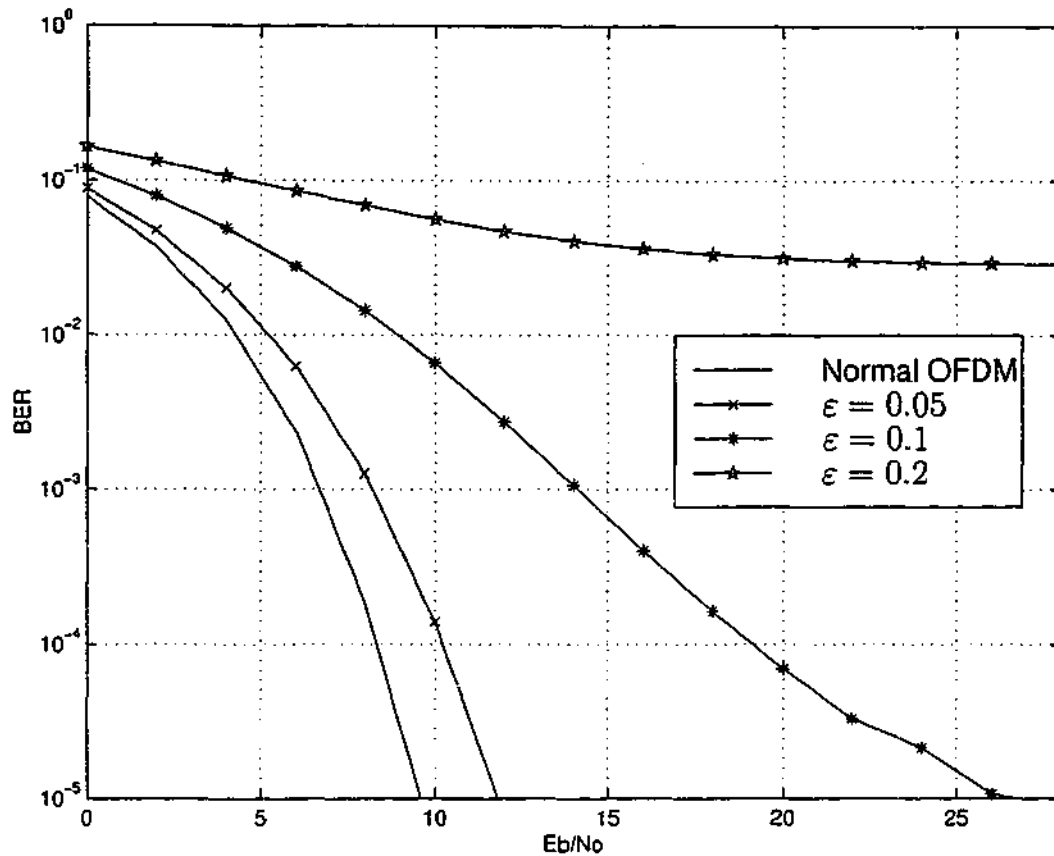


Figure 2.7: BER performance of an OFDM system with $N = 128$.

Figure 2.8 shows the average CIR of an OFDM system for $N = 128$. The theoretical results agree with simulation results for small ϵ . Further, the average CIR decreases with increasing ϵ , as one expects.

It is worthwhile to discuss the effects of carrier frequency offset in multipath fading channel. The received signal for the k -th subcarrier in a multipath fading channel, after the DFT processing can be written as

$$y_k = H_k S_0 c_k + \underbrace{\sum_{l=0, l \neq k}^{N-1} H_l S_{l-k} c_l}_{\text{ICI}} + n_k \quad (2.37)$$

where H_k is the channel frequency response. In matrix notation, the received signal can be expressed as

$$\mathbf{r} = \mathbf{H}\mathbf{S}\mathbf{c} + \mathbf{n} \quad (2.38)$$

where \mathbf{H} is a diagonal matrix of the channel frequency response. Because of this ICI, a single tap equalizer in the frequency domain will not be effective in removing channel fading impairments. This results in a complicated equalization if the frequency

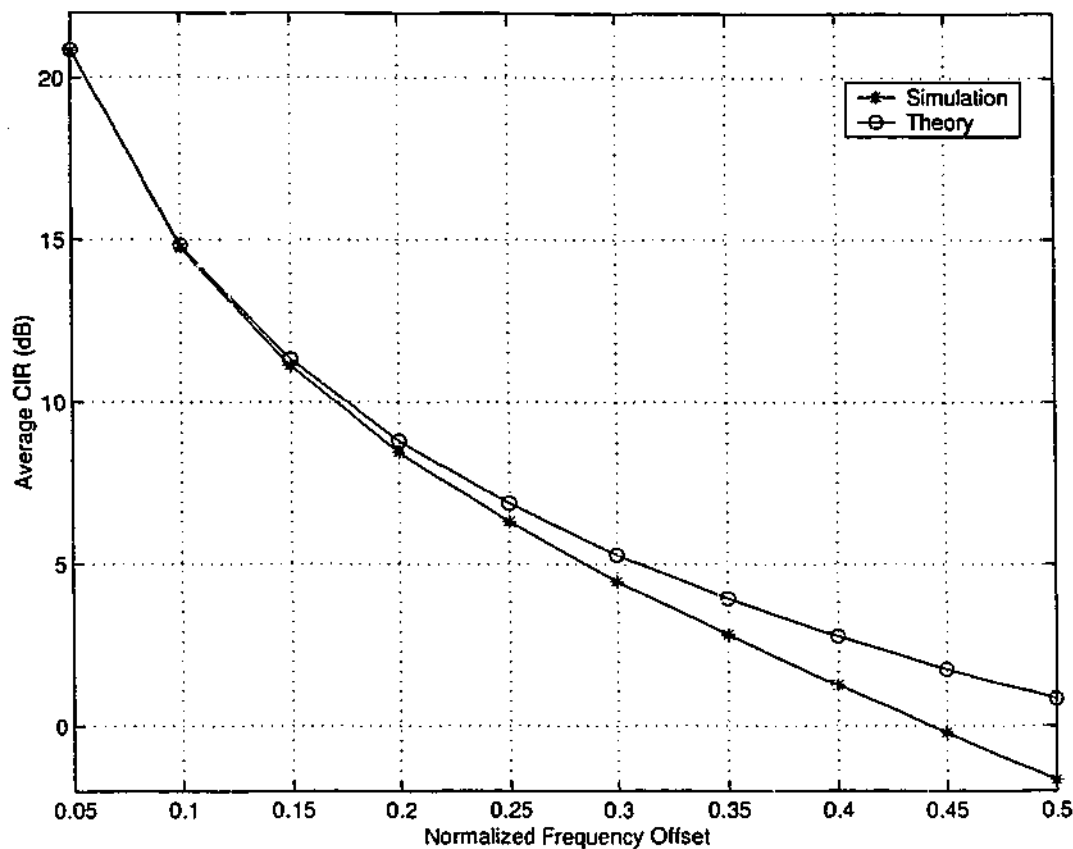


Figure 2.8: Average CIR of an OFDM system with $N = 128$.

offset effects are not removed. Therefore, the advantage of using OFDM in a frequency-selective fading channel will not be realized unless the channel is ICI free. Moreover, the frequency offset effects influence the performance of the channel estimation algorithms [19].

The frequency offset error issue is considered as a limiting factor in the commercial application of OFDM for high-rate mobile communications. Especially, when the number of subchannels is several hundreds or thousands, which is a common case, the tolerable frequency offset range is very small due to the closely spaced subcarriers. Several techniques have been reported in the open literature to overcome this frequency offset problem. These techniques can be grouped into two broad categories as:

- estimation and correction methods,
- sensitivity reduction methods.

2.3.2 Frequency Offset Estimation Methods

A simple approach to a frequency offset problem is to estimate the frequency errors at the receiver and correct them before demodulating the data. The estimation algorithms include pilot symbol assisted estimation [16, 20–33] and blind estimation using the redundancy in the OFDM signal [34–54]. The pilot symbol assisted estimation approach causes loss in data throughput and power due to pilot symbols. Moreover, this estimation approach involves complex computations at the receiver. Thus, this approach is not suitable where low-cost mobile handsets are used that cannot employ very accurate frequency estimators because of the cost involved. Generally, it is preferred that frequency offset estimation methods have the following features [55]:

- high estimation accuracy,
- large estimation range,
- small threshold (that is the critical SNR below which large estimation errors begin to occur),
- low implementation complexity.

A simple and efficient algorithm was first proposed by Moose [16]. In Moose's algorithm, a repeated OFDM symbol was used to estimate the frequency offset error by using the maximum likelihood (ML) estimate. If the channel impairments are neglected, the received DFT output of the first and second symbols are altered in exactly the same way, by a phase shift proportional to a frequency offset. Thus, the maximum likelihood estimate of the normalized frequency offset ϵ is expressed as [16],

$$\hat{\epsilon} = \frac{1}{2\pi} \left\{ \frac{\sum_{k=0}^{N-1} \Im\{Y_{2k}Y_{1k}^*\}}{\sum_{k=0}^{N-1} \Re\{Y_{2k}Y_{1k}^*\}} \right\} \quad (2.39)$$

where Y_{1k} and Y_{2k} are the received DFT outputs for the first and second OFDM symbols respectively. This algorithm generates extremely accurate results for a large range of frequency offset errors since the interference energy and signal energy both contribute coherently to the estimate. Moreover, the estimation error depends only on

total symbol energy, so it is not sensitive to channel spreading and frequency selective fading. However, the impulse response of the channel should be constant for a period of two symbols. The other disadvantage of this approach is the loss in data throughput. If the frequency offset error needs to be continuously monitored and estimated, then this approach will halve the data throughput because of symbol repetition.

Classen and Meyr [20] proposed a data-aided algorithm to cope with the frequency offset in the order of multiples of subchannel spacing. However, this method requires a significant number of test trials in the acquisition mode and its algorithm is very complicated to implement. Nogami and Nagashima [21] introduced a frequency and timing offset acquisition technique by using only one pilot symbol with a suitable frequency assignment. The frequencies of the pilot symbols are assigned by a pseudo noise (PN) sequence to widen the acquisition range [21].

Schmidl and Cox [22] proposed an estimation algorithm based on one unique symbol which has a repetition within half a symbol period. This scheme provides robust and rapid estimation of timing and frequency offset with a very wide acquisition range. This is further improved in [23] by considering a training symbol composed of more than two identical parts. A fast, simple and accurate algorithm for the integer part of the frequency offset is reported in [24] by using a null in a center carrier. This integer part of the frequency offset is estimated in [26] by considering two consecutive OFDM symbols. Integer part estimation is achieved in [25] by adjusting the power of the transmitted reference symbol and utilizing a guard-band power detection method in the receiver. A coarse frequency offset algorithm in the presence of timing offset is proposed in [27] based on dividing the total system bandwidth into a number of smaller blocks. The estimate is calculated by averaging correlation values of individual block [27]. Ghogho et al. [28] proposed an optimum null-subcarrier selection algorithm using a deterministic maximum likelihood approach for the CFO estimate. They [28] also proved that nulling every other subcarrier generates an OFDM symbol with two repeated half-symbols. The Cramer-Rao bound (CRB) for the CFO and the optimal placement of null subcarriers for minimum CRB are derived in [28]. A recent study by Keller et al. [29] reports various issues in frequency estimation problems. A reference symbol and various correlation methods are also studied by these authors [29] for frequency synchronization in frequency-selective fading channels. Patel et al. [30] reports

a study of comparison of frequency offset estimation techniques.

Interestingly, a pilot based frequency offset estimation approach has been adapted for IEEE 802.11a WLAN and HIPERLAN2. A packet preamble information is used for these estimates. A cyclic structure of a training sequence is exploited in [31, 32] to estimate frequency offsets in HIPERLAN. Li et al. [33] further exploited the packet preamble information by using a high performance nonlinear least squares fitting approach for OFDM-based WLANs.

An OFDM signal contains some redundancy due to cyclic prefix. This redundancy is exploited in many blind estimation algorithms. Interestingly, most of these schemes estimate both timing and frequency offset errors. Daffara and Adami [34] derived a characteristic function by using the redundancy of a guard interval and designed a frequency detector based on it. However, this detector [34] cannot correct the offset if the offset is larger than half of the intercarrier spacing. Oh et al. [35] introduced a new correlation algorithm with a wide acquisition range and fast convergence property. In this method, the received OFDM signals are oversampled and divided into even and odd numbered sample sets and the correlations between these two sets are exploited to derive the acquisition and the tracking algorithms. A sign pattern technique using a look-up table is used for the acquisition process. By maximizing the correlation function of the received samples, the reduced frequency offset is brought to zero in the tracking process.

Beek et al. [36] proposed a joint ML estimator for timing and frequency offset by exploiting the excess cyclic prefix. This scheme is further improved in [37] by globally optimizing the estimate. New likelihood functions for the ML estimator to achieve a global optimum estimate are also reported in [38, 39]. Tureli et al. [40] introduced a subspace-based algorithm, without using an extra cyclic prefix, to improve the estimate in [36]. This is further discussed in [41] by comparing it with experimental results. The inherent orthogonality among OFDM subchannels is exploited in [42] to derive an efficient estimator. A blind method based on the correlation of data samples and an adaptive approach for tracking time-variant frequency offset has been developed in [43]. McNair et al. [44] proposed time and frequency offset schemes using the centroid properties of the modulated symbols. However, this approach can only be used for M-PSK systems.

Hwang et al. [45] proposed a frequency domain estimator for time and carrier frequency offset based on linear least squares (LLS) fitting. However, this approach assumes that the channel attenuation is the same for all subcarriers, thus neglecting the channel frequency selectivity. This frequency domain estimator is improved in [46] by using a ML algorithm and taking into account the channel frequency selectivity. A pre-coder based blind channel and carrier frequency offset estimation is reported in [47]. The intrinsic phase shift between neighboring samples due to frequency offset is exploited in [48] to estimate the frequency offset. In fact, this algorithm turns out to be a ML estimate in a noisy channel [48]. Chen and Wang [49, 50] introduced a ML estimate method for frequency offset in the presence of virtual carriers and revealed how this scheme becomes equivalent to the blind estimation method in [40, 41].

Exploiting the cyclostationarity of the OFDM signal, a blind estimation method without using cyclic prefix is proposed in [51]. Ma et al. [52] investigated the identifiability of non-data-aided schemes based on null subcarriers, paying special attention to the possibility of channel nulls. They [52] demonstrate that the approaches in [40, 41] suffer from channel nulls and propose a new approach, where the null subcarriers are placed with distinct spacings. Blind frequency offset estimation methods for OFDM systems with pulse shaping are investigated in [53, 54]

2.3.3 Frequency Offset Sensitivity Reduction Methods

The key idea of the Sensitivity Reduction Methods is to make the OFDM signal robust to very small frequency errors or reduce the frequency offset effects. The following techniques are in these categories:

- windowing,
- coding,
- other methods.

Windowing

Muschallik [56] first proposed an adaptive Nyquist windowing approach to improve the reception of an OFDM signal, which is subject to frequency offset and phase noise impairments. In this scheme, the OFDM transmitter remains unchanged and the

received signal is windowed. This windowing uses the part of the guard interval which is not disturbed by the ISI. It adapts to channel conditions since the undisturbed part of the guard interval varies with channel conditions. In [56], a raised-cosine windowing is used. This windowing approach is further improved by using a near-optimum Nyquist window [57] and an optimum Nyquist window [58, 59]. By minimizing the joint noise and ICI using minimum mean square error (MMSE) criterion, the time-domain window is derived in [58, 59]. However, a matrix inversion is required to derive the optimum Nyquist window [58, 59]. General optimization [58, 59] shows that all optimum rolloff regions exhibit an approximately linear course. Incorporating this a priori linear course into a simpler optimization and determining its optimum slope, the authors [57] derive a near-optimum window, which requires no matrix inversion.

Coding

The ICI caused by frequency offset degrades the BER performance. The simplest approach to improve the BER performance is to use coding to correct the errors caused by ICI. This approach was first used in [60] to correct errors caused by ICI. However, the ICI is due to time variations of the channel. In this study [60], trellis coding and antenna diversity schemes are examined to reduce the error floor caused by ICI. The use of forward error correction codes to reduce ICI effects due to carrier frequency offset is studied in [61–63]. In [61], trellis coded modulation is used to correct errors caused by channel time variation and carrier frequency offset. The use of rate-compatible punctured convolutional codes to correct errors caused by carrier frequency offset is investigated in [63]. These approaches are discussed in detail in Chapter 3.

Zhao et al. [64] proposed a correlative coding approach to reduce ICI caused by frequency offset. In fact, correlative coding was used in conventional single carrier systems to reduce intersymbol interference (ISI) caused by timing errors. Here, time-domain correlative coding or partial response signalling was employed. Since an OFDM system can be viewed as a dual system in the frequency domain of a conventional single carrier system, the correlative coding is performed in the frequency domain. If the data sequence is c_k ($k = 0, 1, \dots, N - 1$), then the correlated sequence b_k is expressed as

$$b_k = c_k - c_{k-1}, \text{ for } k = 0, 1, \dots, N - 1. \quad (2.40)$$

This means that the correlated sequence is generated using the correlation polynomial

$F(D) = 1 - D$, where D denotes the delay of the subcarrier index k . To avoid error propagation, a precoding is performed before modulation, in a similar way to the duobinary signalling in single carrier communication systems. This correlative coding approach does not reduce bandwidth efficiency and its complexity is minimal. This scheme improves the average CIR by 3.5 dB over conventional OFDM.

The other popular scheme for reducing carrier frequency offset effects is the self-ICI cancellation [65,66] or polynomial coded cancellation [67,68]. This cancellation scheme has received much attention due to its simplicity and its high robustness to frequency offset errors. In this technique, each data symbol is transmitted on two adjacent subcarriers with opposite polarity in order to cancel ICI. The data throughput of this scheme will therefore be half of that of ordinary OFDM. Thus, this cancellation scheme is also referred to as rate-half repetition coding. Throughout the thesis, the cancellation scheme and the rate-half repetition coding will be used interchangeably.

Sathananthan et al. [69,70] improved the cancellation scheme by transmitting the data symbols on k -th and $(N - 1 - k)$ -th subcarriers, instead of adjacent subcarriers. This approach offers a frequency diversity because of the frequency separation between the same data symbols. Therefore, [69,70] outperforms the adjacent subcarrier case in a time variant channel. The cancellation scheme is further extended to reduce more ICI by mapping data symbols onto a larger group of subcarriers [66,68,71]. For the general case of mapping onto a group of k subcarriers, the relative weighting of the subgroup is given by the coefficients of the polynomial expansion of $(1 - D)^{k-1}$ [66,68,71]. However, this further reduces the data throughput, despite more ICI reductions.

Doubling the signal constellation is proposed as a means to recover the data throughput loss in the cancellation scheme [66,69]. For example, QPSK with cancellation scheme can be used if BPSK is used in the conventional OFDM. Armstrong et al. [72,73] proposed a symbol overlapping approach to the cancellation scheme to avoid data throughput loss. In this overlapping scheme [72,73], intersymbol interference is deliberately introduced at the transmitter to increase the data rate. The transmitted signal at any instant is the sum of components due to two different symbols. Two-dimensional equalizers are required at the receiver to recover the information from the received signal. Interference occurs in the time domain between symbols and in the frequency domain between subchannels within a symbol. However, the complexity of

the equalizers are low because of the repetitive structure [72, 73]. Moreover, the overlapping scheme exhibits good bandwidth efficiency over conventional OFDM since it does not require cyclic prefix/guard band [72, 73].

Other methods

Remvik et al. [74, 75] proposed the use of different pulse shaping filters to reduce the frequency offset effects. An OFDM scheme using M-offset QAM and pulses of finite duration with minimized excess band-width power is shown to be more robust to frequency errors than a conventional OFDM scheme using M-QAM and square pulses [74, 75]. Chang and Powers [76] studied the use of nonlinear adaptive filter to reduce ICI effects. The linear adaptive filter can only relate to second-order statistics of the input data while the nonlinear filter uses higher-order statistics. Thus, the nonlinear filter is superior to the conventional linear filter in removing ICI. An equalization scheme using simple linear predictions for tuning the equalizer has been proposed in [77] to improve performance in multipath channels with frequency offset and phase noise. This scheme requires no extra pilot tones for equalization.

2.4 Phase Noise

Phase noise has been considered as a major performance limiting factor in a number of communication systems. These include optical coherent or weakly coherent systems, coherent analog amplitude-modulated wide-band rectifier, narrow-band optical links and multicarrier systems [78]. These phase noises are introduced by the local oscillator in a transmitter and/or receiver. Ideally, the oscillator's signal would be a unique carrier with constant amplitude, frequency and phase. The variation of this carrier phase introduces the phase noise. One difficulty in phase noise analysis is accurate prediction and modelling, which enables the system and RF designers to relax specifications based on tolerable phase noise. Several authors have addressed this phase noise problem. In the context of multicarrier systems, phase noise is widely assumed to be a continuous path Brownian motion (or Wiener process) [79–81]. In the open literature, analysis of OFDM system performance in the presence of phase noise and several techniques to overcome this problem have been reported by many authors. Here, we will briefly summarize the phase noise effects and proposed solutions for this problem.

Consider a transmitted signal $x(t)$ (Eq. 2.8) on an additive white Gaussian noise channel, and assume that the received signal is only affected by phase noise. Then, the received signal is expressed as

$$r(t) = x(t) \cdot e^{j\theta(t)} + z(t) \quad (2.41)$$

where $z(t)$ is the Gaussian noise and $\theta(t)$ is the time varying phase caused by phase noise. $\theta(t)$ is modelled as a Wiener process with zero mean and variance of $2\pi\beta|t|$, where β represents the two sided 3-dB line width of the Lorentzian power density spectrum of the oscillator [79-81].

The sampled signal for the k -th subcarrier after the receiver DFT processing can be written as

$$\begin{aligned} y_k &= \sum_{m=0}^{N-1} r[m] \cdot e^{-j\frac{2\pi}{N}km} + n_k \\ &= \sum_{m=0}^{N-1} e^{j\theta[m]} \sum_{l=0}^{N-1} c_l e^{j\frac{2\pi}{N}(l-k)m} + n_k \\ &= \sum_{l=0}^{N-1} c_l \sum_{m=0}^{N-1} e^{j\theta[m]} e^{j\frac{2\pi}{N}(l-k)m} + n_k \\ &= \sum_{l=0}^{N-1} c_l \lambda_{l-k} + n_k \end{aligned} \quad (2.42)$$

where n_k is a complex Gaussian noise sample (with its real and imaginary components being independent and identically distributed with variance σ^2). The sequence for the interference coefficient λ_k is given by

$$\lambda_k = \sum_{m=0}^{N-1} e^{j\theta[m]} e^{j\frac{2\pi}{N}km}. \quad (2.43)$$

Equation (2.43) can be rearranged as

$$y_k = c_k \lambda_0 + \underbrace{\sum_{l=0, l \neq k}^{N-1} \lambda_{l-k} c_l}_{\text{ICI}} + n_k \text{ for } k = 0, 1, \dots, N-1. \quad (2.44)$$

The second term from the right in (2.44) is the ICI term attributable to phase noise. When there is no phase noise in the channel, λ_k reduces to the unit impulse sequence. Since $\theta(t)$ is modelled as a Wiener process, λ_k 's are random. The statistical properties

of phase noise have been studied by several authors [78, 82, 83]. It is a complex problem and different approaches such as simulation techniques, characterization through moments and recursive methods are reported in these studies.

The impact of phase noise effects on OFDM systems and the resulting error performance are analytically derived in [80, 81, 84–86]. In [87], the phase noise effects on OFDM based digital television terrestrial broadcasting systems are investigated. Armada and Calvo [88] studied the influence of subcarrier spacing on phase noise effects. To reduce phase noise effects, subcarrier spacing needs to be increased, resulting in a small number of subcarriers N . However, large N can offer a better protection against multipath delay spread.

Robertson and Kaiser [89] proposed a simple feed-forward correction technique based on pilot cells to reduce the degradation due to phase noise. Benvenuto et al. [90] introduced a phase noise suppression scheme by estimating the phase noise using the guard interval. Construction of a low phase noise local oscillator using double conversion architecture using GaAs mixer ICs is discussed in [91]. Interestingly, the pilot-based channel estimation methods correct the phase noise effects under some circumstances [88, 92].

2.5 Time Variations of the Channel

In mobile radio communication, the fading channels generally exhibit both frequency selectivity and time selectivity. OFDM has been proposed to combat the frequency selectivity, but its performance might be affected by the time selectivity. In most studies in the literature, OFDM performance is evaluated for time invariant channels. It is valid if the channel coherence time T_c , defined as the time over which the channel can be assumed to be constant, is large compared to the symbol duration T_s .

The coherence time is inversely proportional to the Doppler spread f_d . A frequency nonselective channel is slowly fading if the time duration of the transmitted symbol T_s is much smaller than the coherence time of the channel (i.e., $T_s \ll T_c$). Equivalently, $T_s \ll 1/f_d$ or $f_d \ll 1/T_s$. A slowly fading, frequency-nonselective channel is normally under spread. A rapidly fading channel is defined by the condition $T_s \geq T_c$. The resulting time selective fading causes a loss of subcarrier orthogonality, thus resulting in ICI. Hence, the system performance degrades drastically. This performance degradation in terms of

error rate is investigated by many authors in various channel conditions [60,61,93–99].

The received sequence, in a frequency selective and time selective channel, after the DFT modulation can be expressed as

$$y_k = \sum_{m=0}^{N-1} \sum_{l=0}^{L-1} c_m H_l^{(k-m)} e^{-\frac{j2\pi lm}{N}} + n_k, \text{ for } k = 0, 1, \dots, N-1 \quad (2.45)$$

where

$$H_l^{(k-m)} = \frac{1}{N} \sum_{n=0}^{N-1} h_{n,l} e^{-\frac{j2\pi n}{N}(k-m)} \quad (2.46)$$

where $h_{n,l}$ is the fading coefficient of the n -th subcarrier from l -th path, L is the number of paths and n_k is the Gaussian noise. Eq. (2.45) can be restated as

$$y_k = \alpha_k c_k + \underbrace{\beta_k}_{\text{ICI}} + n_k, \text{ for } k = 0, 1, \dots, N-1 \quad (2.47)$$

where

$$\alpha_k = \frac{1}{N} \sum_{n=0}^{N-1} \sum_{l=0}^{L-1} h_{n,l} e^{-\frac{j2\pi nk}{N}}, \text{ for } k = 0, 1, \dots, N-1 \quad (2.48)$$

and

$$\beta_k = \sum_{m=0, m \neq k}^{N-1} \left\{ \sum_{l=0}^{L-1} \left(\frac{1}{N} \sum_{n=0}^{N-1} h_{n,l} e^{-\frac{j2\pi n}{N}(m-k)} \right) e^{-\frac{j2\pi km}{N}} \right\} c_k, \text{ for } k = 0, 1, \dots, N-1. \quad (2.49)$$

Thus, Eq. (2.47) reveals that frequency selective and time selective channels introduce ICI. Even if the channel is frequency nonselective, the time variant nature of the channel will yield ICI. For this frequency nonselective and time selective channels, α_k and β_k can be expressed as where

$$\alpha_k = \frac{1}{N} \sum_{n=0}^{N-1} h_n, \text{ for } k = 0, 1, \dots, N-1 \quad (2.50)$$

and

$$\beta_k = \frac{1}{N} \sum_{m=0, m \neq k}^{N-1} \sum_{n=0}^{N-1} h_n e^{-\frac{j2\pi n}{N}(m-k)} c_k, \text{ for } k = 0, 1, \dots, N-1. \quad (2.51)$$

Several techniques have been developed to overcome this ICI problem. A pilot tone-assisted estimation and linear equalization before DFT demodulation was proposed in [6]. However, the correction of fading distortion in the time domain introduces a problem of noise enhancement and/or irreducible error floor. To overcome this, a frequency domain equalization approach was proposed in [100]. In this approach, linear

equalizers and decision feedback equalizers are used and their coefficients are calculated by inserting frequency domain pilot symbols. In [101], this frequency-domain equalization technique is investigated by using the assumption that the channel impulse response varies in a linear fashion during a block period. Russell and Stuber [60] investigated trellis coded modulation (TCM) and antenna diversity schemes to improve the error performance of the OFDM system in a time variant channel. The studies of Reed-Solomon (RS) codes as a means to time-varying channel effects are reported in [94, 102]. The effects of ICI caused by both channel time variant and carrier frequency offset are investigated in [61] and a trellis coded modulation scheme is considered to mitigate these effects. Toeltsch and Molisch [103] proposed parallel and serial interference cancellation techniques based on the co-channel interference suppression techniques developed for CDMA. In this scheme [103], the decisions of the symbols on the subcarriers are improved iteratively. These improvements are due to the determination and subtraction of the interference of all the other subcarriers, based on the decisions of the previous iteration.

2.6 Peak-to-Average Power Ratio

The OFDM signal has a large dynamic range since large numbers of independently modulated symbols are linearly processed by an IDFT operation. The IDFT operation is simply an operation forming N time-domain samples from a linear combination of the N frequency-domain samples. According to the central limit theorem in probability theory, the time-domain sample magnitudes $|x_n|$ can be approximately modelled as Gaussian random variables for large values of N . This means that most magnitudes will be very close to average while a very small percentage of them will have a very large magnitude. This large magnitude can also be realized when all modulated symbols with the same phases are added up. Thus, the large dynamic range of an OFDM signal is inherent in its nature. This introduces the PAR problem that OFDM systems must deal with. A magnitude variation of an OFDM signal for one OFDM symbol duration is shown in Figure 2.9 for $N = 128$. This signal is oversampled at eight times the Nyquist rate. Figure 2.9 shows that the magnitude of most samples is around the average value while a few samples have a high peak.

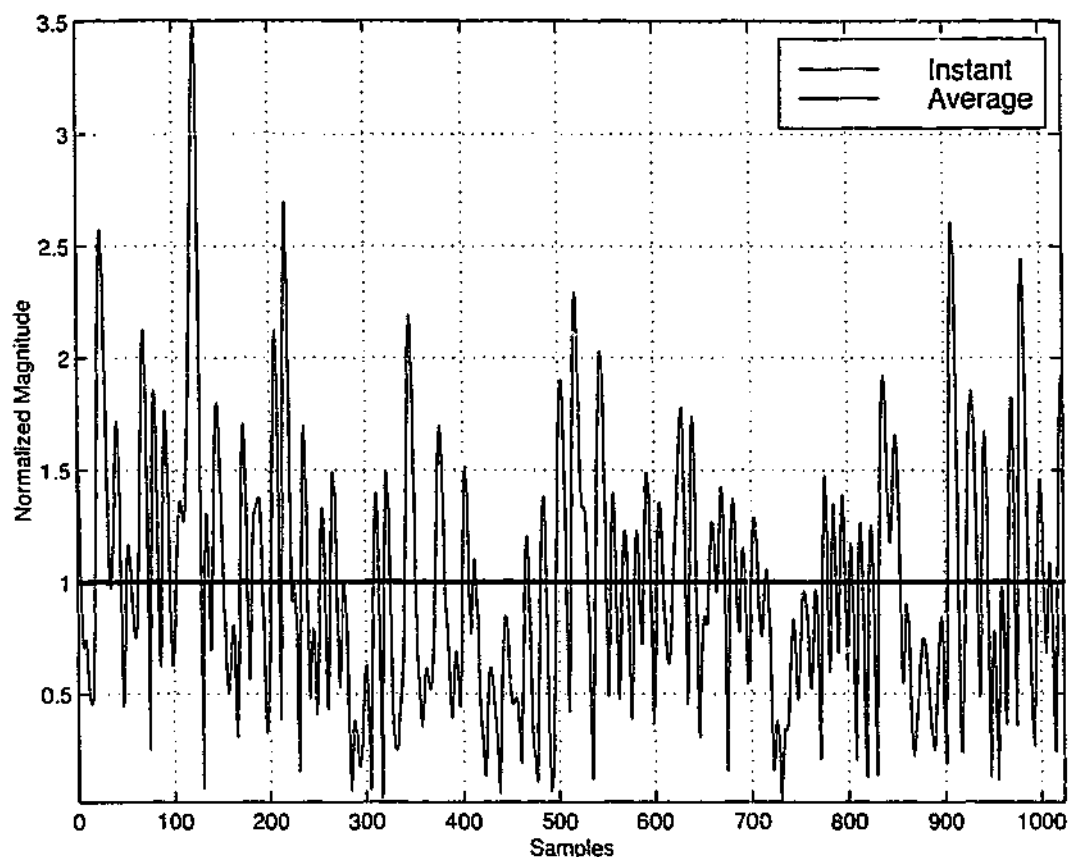


Figure 2.9: Typical OFDM signal.

These high signal peaks can lead to nonlinear distortion in the presence of nonlinear devices at the transmitter; more specifically, at the high power amplifier (HPA). In order to pass the OFDM signal through HPA linearly (without distortion), HPA must be able to handle occasional large peaks. However, such a HPA can be very power consuming and very expensive. To alleviate this problem, one can simply lower the average power, which in turn lowers the peaks that a HPA needs to handle. However, this reduces the entire SNR of the system and the power efficiency of the transmitter, and is thus not a practical solution. Another approach is to simply use the HPA which cannot handle large peaks, and let it introduce nonlinear distortion (typically some sort of clipping). These nonlinear distortion effects can be tolerated under certain specifications since the large peaks rarely occur. Consequently, performance degradation and/or inefficiency can occur. Therefore, reducing the PAR of the signal is highly desirable.

The PAR of a continuous time-domain signal $x(t)$ over $t \in T$ is defined as

$$\text{PAR}(x(t)) = \frac{\max |x(t)|^2}{E \left[\frac{1}{T} \int_{t \in T} |x(t)|^2 dt \right]} \quad (2.52)$$

and the PAR of a discrete time-domain signal $x[n]$ is defined as

$$\text{PAR}(x[n]) = \frac{\max |x_i|^2}{E[|x[n]|^2]} \quad (2.53)$$

where x_i denotes the instantaneous sample value of $x(t)$, $|\cdot|$ denotes the magnitude and $E[\cdot]$ denotes the average. This defines the PAR for the baseband OFDM signal. Several related terms and definitions are used in the literature to specify peak power problem. The above definition is also termed as PAPR, PAP and peak-to-mean envelope power ratio (PMEPR). Another widely-used term in the literature is the crest factor (CF), which is the square root of the PAR ($CF = \sqrt{\text{PAR}}$). Throughout this thesis the term PAR will be used to denote the peak power problem.

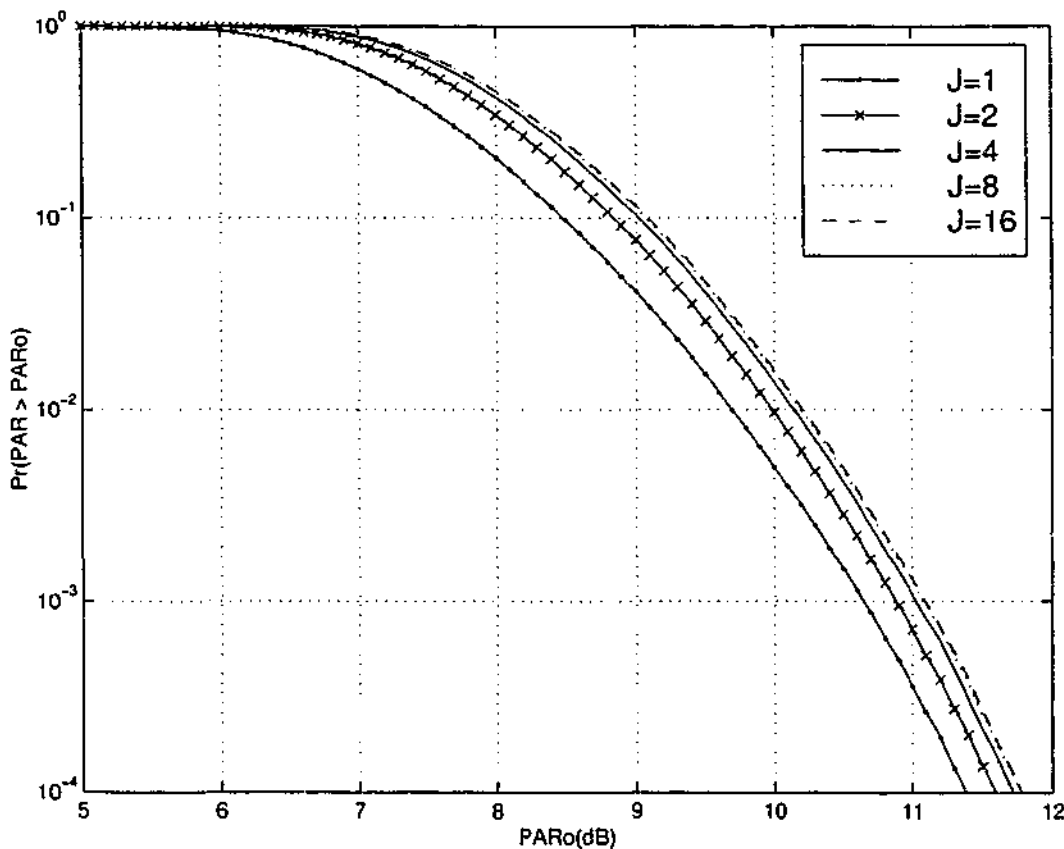


Figure 2.10: Variation of PAR characteristics with oversampling factor.

We assume in this thesis that no filtering for power spectrum shaping is performed and that $x(t)$ is an ideal analog construction of $x[n]$. Generally, $\text{PAR}(x(t)) \geq \text{PAR}(x[n])$ since discrete time samples might miss some of the peaks of the analog signal. Note that analog PAR measurement is important since the actual signal passing through HPA or nonlinear device is analog. However, $\text{PAR}(x(t))$ can be approximated by using a sufficiently oversampled version of $x[n]$ [104]. That is $\text{PAR}(x(t)) \approx \text{PAR}(x[n/J])$ for

sufficiently large J , where J is the oversampling factor. Figure 2.10 shows the complementary cumulative density function (CCDF) of PAR of an OFDM signal for $N = 128$, as a function of oversampling factor, J . Note that PAR_0 denotes a threshold value for the PAR statistics. The PAR of the oversampled signal is higher than that of Nyquist sampled ($J = 1$) signal. However, the PAR statistics do not change significantly beyond the oversampling factor of four. Thus, $J = 4$ appears sufficient to estimate the actual PAR and this is used throughout the thesis unless otherwise specified.

If $x(t)$ is a complex-baseband signal, the transmitted signal is expressed as

$$\begin{aligned} x_{PB}(t) &= \Re \{ x(t) e^{j2\pi f_c t} \} \\ &= \Re \{ x(t) \} \cos 2\pi f_c t - \Im \{ x(t) \} \sin 2\pi f_c t \\ &= x_I(t) \cos 2\pi f_c t - x_Q(t) \sin 2\pi f_c t \end{aligned} \quad (2.54)$$

where f_c is the carrier frequency, $x_I(t)$ and $x_Q(t)$ represents the in-phase and quadrature components of $x(t)$. Generally, the carrier frequency is much greater than the signal bandwidth (i.e., $f_c \gg \frac{N}{T_s}$). Hence, the peak magnitudes of the complex-baseband and passband signals are approximately the same. That is

$$\max |x_{PB}(t)| \approx \max |x(t)|. \quad (2.55)$$

The average power of $x_{PB}(t)$ is written as

$$E[|x_{PB}(t)|^2] = \frac{1}{2} E[|x_I(t)|^2] + \frac{1}{2} E[|x_Q(t)|^2]. \quad (2.56)$$

Assuming equal average power in the in-phase and quadrature phase components of $x(t)$ (as in M-QAM and M-PSK constellations),

$$E[|x_I(t)|^2] = E[|x_Q(t)|^2] = \frac{1}{2} E[|x(t)|^2], \quad (2.57)$$

and so the average power relationship is expressed as

$$E[|x_{PB}(t)|^2] = \frac{1}{2} E[|x(t)|^2]. \quad (2.58)$$

Using (2.58) and the definition of PAR, the resulting PAR relationship between complex-baseband and passband signals is

$$\text{PAR}(x_{PB}(t)) \approx 2\text{PAR}(x(t)). \quad (2.59)$$

Thus, the PAR of the passband signal is approximately 3 dB higher than that of the complex-baseband signal. Therefore, we can simply measure the PAR of the passband signal by analyzing it in the complex-baseband domain. Moreover, the cyclic prefix does not change the average or peak power of the signal since it is just a replica of the last v samples of $x[n]$. Therefore, the cyclic prefix will not be considered in the PAR calculations.

2.6.1 PAR Bounds and Statistics

The PAR is defined on a block-by-block basis. Therefore, it is worthwhile to find the maximum PAR of an OFDM signal. Consider the OFDM signal defined in (2.8)

$$x(t) = \frac{1}{\sqrt{N}} \sum_{k=0}^{N-1} c_k e^{j2\pi k \Delta f t}. \quad (2.60)$$

Without loss of generality, we can assume power normalized data symbols. Thus, $E[|c_k|^2] = 1$ and the PAR can be bounded as,

$$\begin{aligned} \text{PAR}(x(t)) &= \max |x(t)|^2 \\ &= \max \left| \frac{1}{\sqrt{N}} \sum_{k=0}^{N-1} c_k e^{j2\pi k \Delta f t} \right|^2 \\ &\leq \frac{1}{N} \left[\sum_{k=0}^{N-1} |c_k e^{j2\pi k \Delta f t}| \right]^2 \\ &\leq N. \end{aligned} \quad (2.61)$$

Therefore, the maximum PAR of a complex baseband signal of an N subcarrier OFDM system is

$$\max \text{PAR}(x(t)) = N. \quad (2.62)$$

Thus, the maximum PAR grows linearly with the number of subcarriers. It is shown in [14] that there are only M^2 sequences with maximum PAR of N for M-PSK modulated OFDM signal, where M is the signal constellation size. Therefore, the probability of this occurrence is extremely small and equal to M^{2-N} . This is negligible for large N , as is the case in practice. Thus, this bound does not provide any much useful information about PAR. Moreover, PAR reduction by reducing N is not an effective solution since N is restricted by other parameters, such as data throughput and delay

spread. Another bound in terms of aperiodic auto-correlation is reported in [105], and is expressed as

$$\text{PAR}(x(t)) \leq 1 + \frac{2}{N} \sum_{k=1}^{N-1} |\rho(k)| \quad (2.63)$$

where $\rho(k)$ is the aperiodic autocorrelation function of the data sequence given by

$$\rho(k) = \sum_{n=1}^{N-k} c_{n+k} c_n, \quad k = 0, 1, \dots, N-1. \quad (2.64)$$

This bound shows that PAR is greatly influenced by the correlation properties of the transmitted sequence. The peak value of the autocorrelation is the average power of the input sequence and the sidelobe of the autocorrelation indicates the correlation of the input sequence [105, 106]. If the sidelobe of the autocorrelation has a larger value, then the input sequence is highly correlated and its PAR is high. The high correlation in the input sequence causes the IDFT output to be aligned in phase. Thus, summing these in-phase functions results in a large magnitude. However, the above bound is not very useful from a system design point of view.

Since the worst case PAR occurs rarely, qualifying the PAR problem according to this figure does not give the whole picture but rather the worst case picture. From a system design point of view, it may be more important to know the PAR on a block-by-block basis. That is the probability that the PAR of the l -th symbol block, $\text{PAR}(x_l(t))$, is worse than a certain specified level, PAR_0 . This measure is represented by the CCDF of the random variable PAR and defined as

$$\text{CCDF}(\text{PAR}(x_l(t))) = \text{Pr}\{\text{PAR} > \text{PAR}_0\}. \quad (2.65)$$

This CCDF and cumulative distribution function (CDF) are widely used in the literature to quantify PAR problem and evaluate the performance of PAR reduction schemes.

Figure 2.11 shows the CCDF of PAR of QPSK modulated OFDM signal for $N = 16, 32, 64, 128$ and 256 . For $N = 128$, the maximum PAR is 21 dB and this occurs with a probability of 2.21×10^{-75} (4^{2-128}). In practice, this is negligible. In fact, PAR exceeds 12 dB for 1 in 10^4 of all the possible transmitted OFDM symbols. Therefore, improving the statistics of the PAR is more important rather than the maximum PAR. A lot of attention has been given in deriving the expression for PAR statistics.

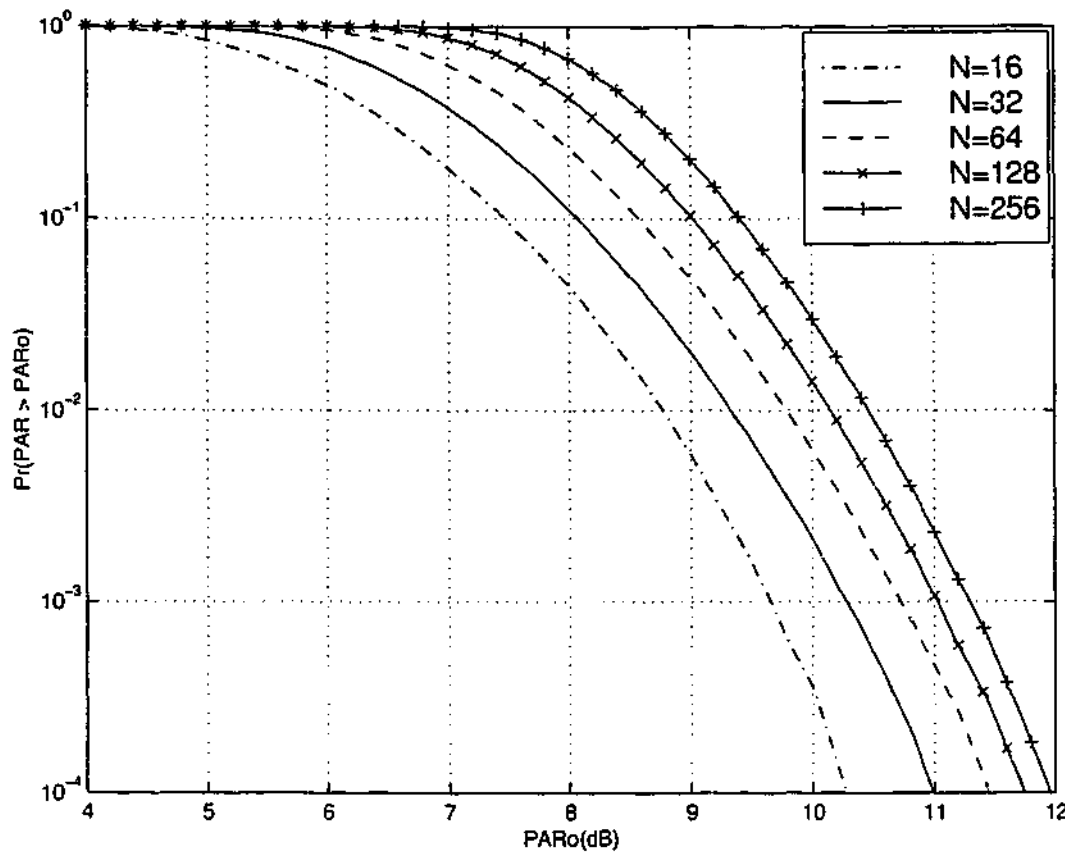


Figure 2.11: CCDF of PAR of an OFDM signal.

A simple analytical expression for the distribution of PAR has been described in [107,108]. Consider the complex baseband OFDM signal sampled at the Nyquist rate

$$x_n = \frac{1}{\sqrt{N}} \sum_{k=0}^{N-1} c_k e^{j2\pi k \frac{n}{N}}. \quad (2.66)$$

Since each real and imaginary part of x_n is a sum of independent and uncorrelated random variables, both approach a Gaussian distribution with mean zero and variance of half for large N , according to the central limit theorem. Consequently, the amplitude $r_k = |x_k|$ of the OFDM signal becomes Raleigh distributed with a probability density function (pdf) given by

$$f_{r_k}(r) = 2re^{-r^2}, \quad r \geq 0 \quad (2.67)$$

and the power $p_k = r_k^2$ approaches a chi-squared distribution with two degrees of freedom and its cumulative distribution function (CDF) is given by

$$\Pr(p_k \leq p) = 1 - e^{-p}. \quad (2.68)$$

Assuming the samples are mutually independent and uncorrelated, the CDF of $\max(p_k)$

can be expressed as

$$\Pr(\max(p_k) \leq p) = (1 - e^{-p})^N. \quad (2.69)$$

By changing the variable, the CCDF of PAR of an OFDM signal can then be expressed as

$$\Pr(\text{PAR} \geq \text{PAR}_0) = 1 - (1 - \exp(-\text{PAR}_0))^N. \quad (2.70)$$

However, the independent assumption in deriving (2.70) is not strictly true and does not hold for the oversampling case. Van Nee and Wild [108] approximated the effect of oversampling by the addition of a certain number of extra independent samples. By considering αN subcarriers ($\alpha > 1$), the CCDF of the PAR of an oversampled OFDM signal is expressed as

$$\Pr(\text{PAR} \geq \text{PAR}_0) = 1 - (1 - \exp(-\text{PAR}_0))^{\alpha N}. \quad (2.71)$$

α can be found iteratively and $\alpha = 2.8$ seems to be a good approximation for the oversampled OFDM signal in general [108]. This approximation results in non-integer value for αN , which is considered as total samples/subcarriers to include oversampling effect. Moreover, the above distributions are not exact, particularly for small N . Several analytical expressions have been derived for the distribution of the PAR. Friese [109] derived an exact distribution of PAR of nonoversampled signals without assuming an independent relationship among the samples. An exact distribution of PAR of oversampled signals are also derived in [14, 110, 111]. Since they involve many numeric computations, simple closed form solutions are also reported in [14, 110, 111] based on level-crossing rate analysis. The distribution of PAR for continuous time signals are reported in [112, 113]. The approximate CCDF of the PAR of an oversampled signal reported in [14, 110] is used in this thesis to justify the simulation results and it is expressed as

$$\Pr\{\text{PAR} > \text{PAR}_0\} \approx 1 - \exp\left[-\sqrt{\frac{\pi}{3}}N\sqrt{\text{PAR}_0}\exp(-\text{PAR}_0)\right]. \quad (2.72)$$

2.6.2 Memoryless Nonlinearities

An OFDM signal is subject to various hardware non-linearities in both the transmitter and receiver. Examples of these non-linearities are signal clipping in the analog to digital converter (ADC), digital to analog converter (DAC), signal clipping in the IFFT

and FFT processors with a limited word length and distortion in high power amplifiers (HPA). It is worthwhile here to describe some nonlinear models that are commonly used in the literature to represent commonly used nonlinear physical devices. The degradation effects of these nonlinearities are highly dependent on the characteristics of the nonlinear devices. Further, these nonlinearities are commonly assumed in the literature as memoryless. This simplified assumption is quite reasonable since many commonly used nonlinear devices, such as limiters and high-power amplifiers, can be accurately modelled as memoryless devices.

If the memoryless nonlinear operation is performed on the discrete -time samples, the output can be expressed as

$$x_g[n] = g(x[n]). \quad (2.73)$$

Similarly, for the continuous-time signal, the output can be expressed as

$$x_g(t) = g(x(t)) \quad (2.74)$$

where $g(\cdot)$ denotes the nonlinear operation.

The transceiver components with nonlinear behavior operate either on discrete time-domain samples or continuous time-domain signals. The most common sources of nonlinear behavior in the discrete time-domain are the DAC and ADC. The main source of distortion for both DAC and ADC is the quantizer. However, these type of distortions are beyond the scope of this thesis and will not be considered further.

Generally, the most common source of nonlinear behavior in the continuous time-domain is HPA. The HPA plays an important role in current wireless personal communications. Power efficiency is of crucial importance in battery-oriented applications such as handheld cellular phones or WLAN cards used in laptops. In these applications, power consumption translates into battery size, weight and recharging intervals. In fact, these features are even more important to the mobile user. Power efficiency becomes increasingly important as customers become accustomed to the convenience of small handheld communication devices. The main purpose of the HPA is to deliver a specific (usually high) amount of power to the antenna for transmission. The radiated signal power translates directly into signal coverage. As shown in Figure 2.12, a typical HPA exhibits saturation effects, where the output power does not change with an increase in input power. The HPA operates more efficiently when operating near

its saturation region. However, amplifier saturation introduces nonlinear effects, which will significantly distort the original signal. The occasional peaks in the input signal, as in the OFDM signal, also drives the amplifier into a nonlinear/saturation region. In fact, the optimum operating point of the HPA is very important for power efficiency and undistorted amplification. This section will describe some commonly used HPA models.

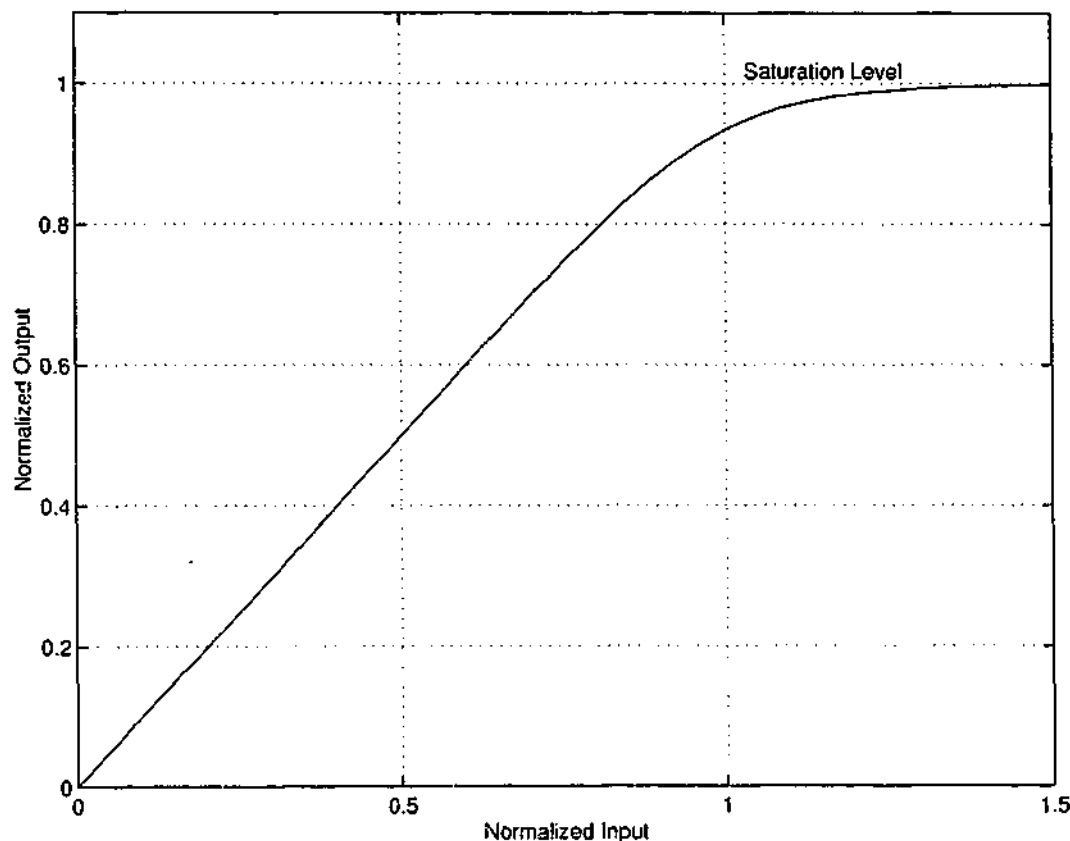


Figure 2.12: Typical HPA characteristics.

For most nonlinear memoryless HPA operations, it is convenient to represent the input signal in polar coordinates as

$$x = |x|e^{j\arg(x)} = \rho e^{j\phi}. \quad (2.75)$$

Hence, the output signal can be expressed as [114–116]

$$g(x) = F[\rho]e^{j(\phi+\Phi[\rho])} \quad (2.76)$$

where $F[\rho]$ and $\Phi[\rho]$ represent the AM/AM and AM/PM conversion characteristics of the memoryless nonlinearity respectively. Here, AM and PM stand for amplitude modulation and phase modulation respectively. Common nonlinear devices found in practice are soft limiter (SL) and solid-state power amplifier (SSPA) [116].

Soft Limiter (SL)

The AM/AM and AM/PM characteristics of a Soft Limiter (SL) can be written as

$$F[\rho] = \begin{cases} \rho & |\rho| \leq A, \\ A & |\rho| > A \end{cases} \quad (2.77)$$

$$\Phi[\rho] = 0.$$

Therefore, nonlinear characteristics of SL can be written as

$$g(x) = \begin{cases} x & |x| \leq A, \\ Ae^{j\phi} & |x| > A \end{cases} \quad (2.78)$$

where A is the saturated output. Although most physical components will not exhibit this piecewise linear behavior, the SL can be a good model if the nonlinear element is linearized by a suitable pre-distorter.

Solid-State Power Amplifiers (SSPA)

The input output relationship of many solid-state power amplifiers (SSPA) can be modelled as

$$F[\rho] = \frac{\rho}{[1 + (\frac{\rho}{A})^{2p}]^{\frac{1}{2p}}} \quad (2.79)$$

$$\Phi[\rho] = 0.$$

where the parameter p controls the smoothness of the transition from the linear region to the limiting or saturation region. Normalized AM/AM characteristics of a SSPA with varying values of p is shown in Figure 2.13. When, $p \rightarrow \infty$, the SSPA model approximates the SL characteristics.

All these models satisfy the non-expansive property and give a maximum output signal amplitude of A .

The amount of distortion introduced by the nonlinearity mostly depends on the maximum power output from the nonlinear device and the average power of the input signal to the nonlinearity. In other words, the distortion depends on the operating point of the amplifier. To characterize this amplifier operation, a parameter called input back-off (IBO) is defined as

$$\text{IBO} = 10 \log_{10} \left(\frac{A^2}{E\{|x|^2\}} \right) \quad (2.80)$$

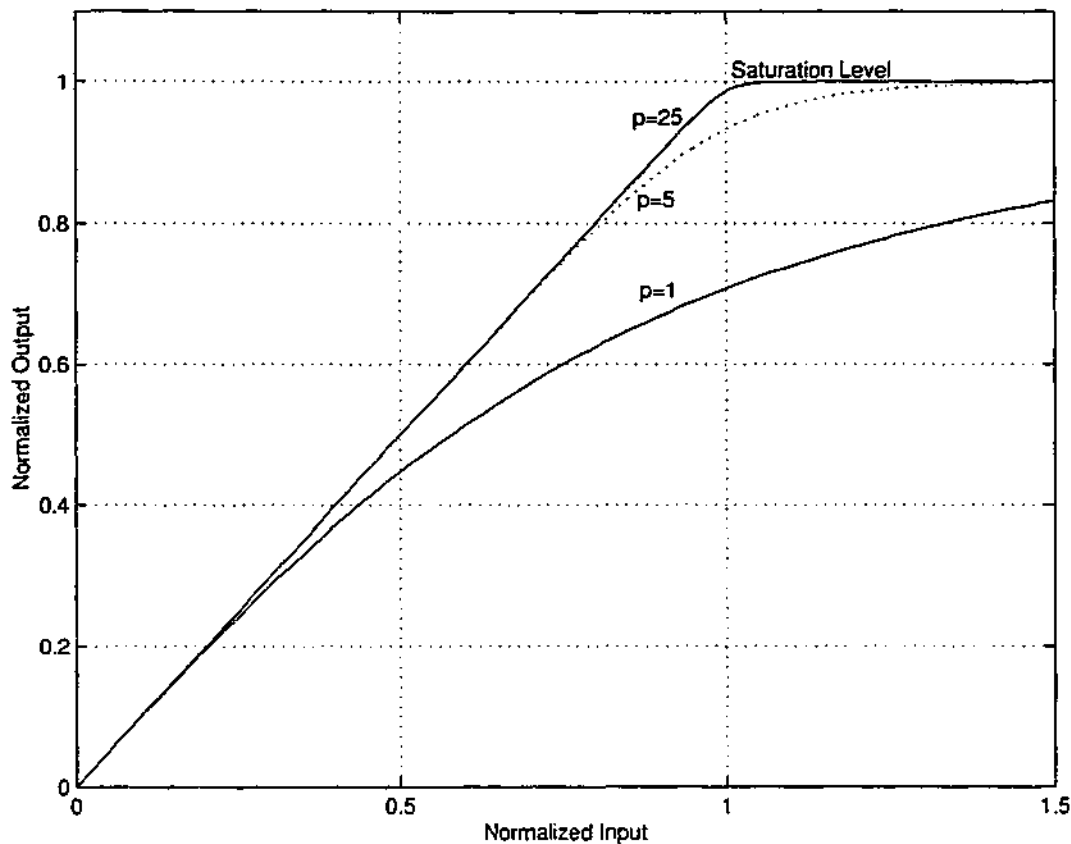


Figure 2.13: Normalized AM/AM characteristics of a SSPA.

where A^2 is the maximum power output from the nonlinear device and $E\{|x|^2\}$ is the average energy of the input signal to the nonlinear device. This same measure is sometimes referred in the literature as the "Clip Level".

Similar to IBO, the term output back-Off (OBO) is defined as

$$\text{OBO} = 10 \log_{10} \left(\frac{A^2}{E\{|g(x)|^2\}} \right) \quad (2.81)$$

where $E\{|g(x)|^2\}$ is the average output power of the nonlinear device. Generally, the output power is smaller than the input power for any non-expansive nonlinearity. However, if the signal operates in the linear region of the device most of the time, then these two powers are very similar and the $\text{IBO} \approx \text{OBO}$.

2.6.3 Effects of Nonlinearities

Hardware nonlinearities not only affect the performance of an OFDM system, but also may affect the system performance of an adjacent channel because of generated side lobes. Several studies on the effects of hardware nonlinearities on OFDM systems are reported in the open literature [115–125]. Analytical expressions for the symbol

error rate of an OFDM signal subject to nonlinear distortion are derived in [121, 122]. Explicit analytical expression for output power spectral density is derived in [123]. In [124], effects of HPA nonlinearity on DVB-T systems are investigated. The joint effects of amplifier nonlinearity and phase noise are reported in [125].

The nonlinear distortion due to a high PAR causes two effects. One is the increased BER at the receiver, also known as in-band distortion. The other is the development of higher-order harmonics that spill over adjacent bands, known as out-of-band radiation. As there are usually rather strict limits on this spectral leakage, the PAR of the signal and the presence of nonlinear devices at the transmitter limit the system capacity and performance. To reduce these effects to a acceptable level, the HPA needs to be operated at a certain back-off level. The reduction in distortion increases with the back-off of HPA. However, the cost and inefficiency of the transmitter will increase with increasing back-off of the HPA. Therefore, a PAR reduction technique may help to overcome this bottleneck.

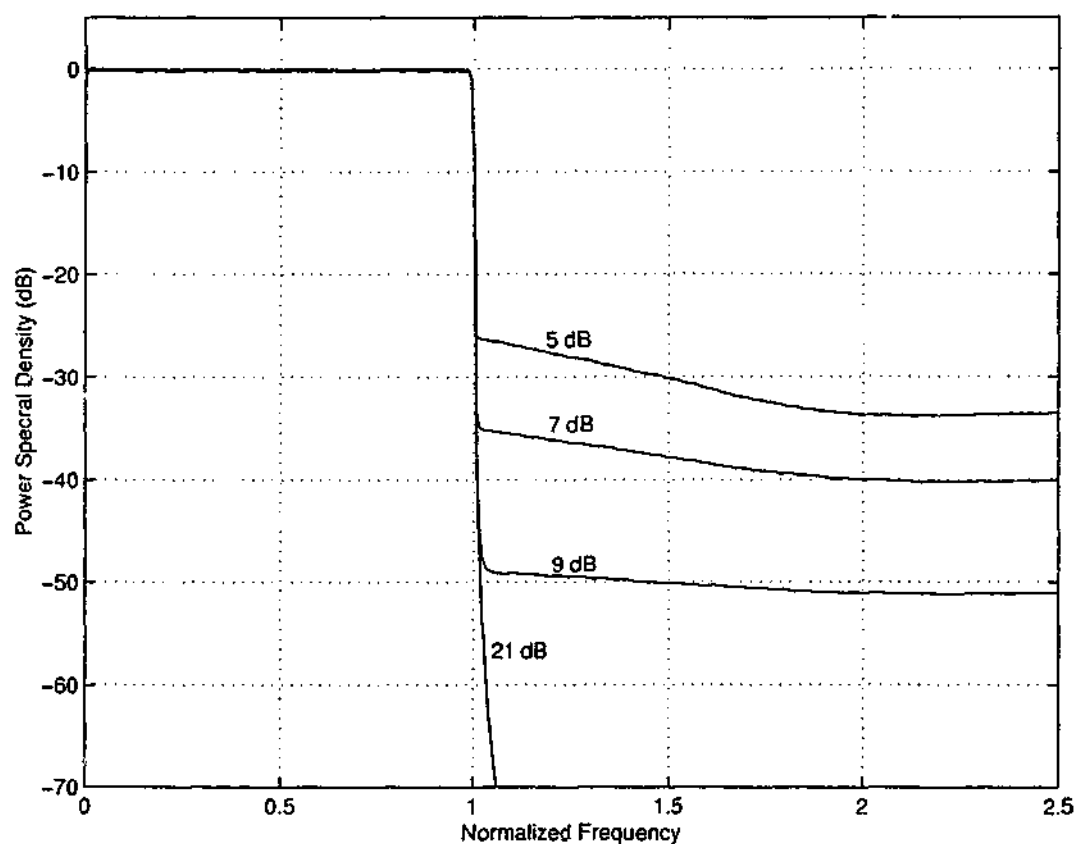


Figure 2.14: Spectrum of an OFDM signal after passing through a SSPA.

For power spectral density (PSD) analysis, it is convenient to define the normalized frequency $B = fT_u$, where T_u is the OFDM symbol duration. Figure 2.14 depicts the

PSD of the OFDM signal in the presence of a SSPA nonlinear device for $N = 128$ and QPSK. The PSD is estimated by simulation using Welch's averaged periodogram method with a Hanning window. An oversampling factor of 8 is used. Curves 1 to 4 represent the different back-off values of the amplifier. The out of band radiation level increases when the back-off of the amplifier is decreased. For example, the minimum value of normalized frequencies for the out of band radiation below -40 dB are approximately 2 and 1 for the back-off of 7 dB and 9 dB respectively. Thus, for a back-off of 7 dB, to provide -40 dB adjacent channel separation requires a channel spacing of about two times the symbol rate for conventional OFDM. Figure 2.14 also reveals that depending on the permissible out of band radiation level, the amplifier back-off can be reduced.

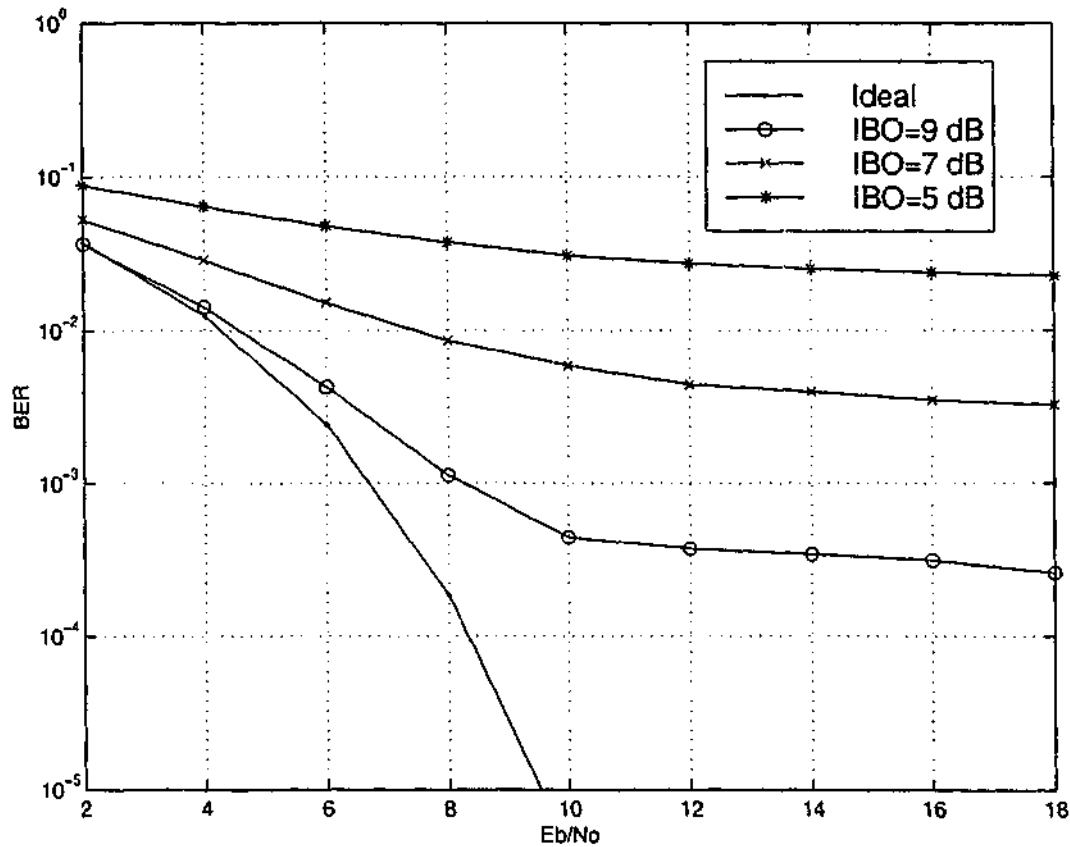


Figure 2.15: BER performance of an OFDM signal after passing through a SSPA.

Figure 2.15 shows the BER performance of an OFDM signal in the presence of SSPA nonlinear device. An AWGN channel is assumed. As one expects, the BER performance improves when the back-off of the amplifier is increased.

2.6.4 PAR Reduction Schemes

An increased interest in OFDM for many wireless applications and the detrimental effects of PAR have motivated the search for PAR reduction techniques. In the open literature, several techniques have been proposed to reduce PAR. These techniques can be grouped into two major categories;

- signal distortion techniques,
- signal distortionless techniques.

In the first method, the transmitted signals are distorted by clipping or pre-distortion techniques. Thus, these methods degrade the error performance and cause spectral leakage. The distortionless techniques reduce the data rate and/or introduce more complexity. All these PAR reduction techniques are briefly described below.

Signal Distortion Techniques

The simplest approach to reduce PAR is to deliberately clip the OFDM signal before amplification [126–129]. Since large peaks occur with very low probability, clipping could be an effective technique for PAR reduction. However, clipping is a nonlinear process and may cause in-band distortion and out-of-band radiation. This degrades the BER performance and reduces spectral efficiency. These degradations and PAR reductions depend on the severity of the clipping. Several techniques based on clipping and the related issues are reported in the literature. In these studies, clipping is performed when the signal amplitude exceeds a predefined clipping threshold. When a signal $x(t)$ is passed through a clipper, the resulting signal $x_c(t)$ will be described as

$$x_c(t) = \begin{cases} x(t) & \text{if } |x(t)| \leq A_{ct} \\ A_{ct}e^{j\angle x(t)} & \text{if } |x(t)| > A_{ct} \end{cases} \quad (2.82)$$

where A_{ct} is the clipping threshold.

Clipping oversampled signals causes out-of-band radiation from the clipped power, and a bandpass filter is required to suppress the out-of-band radiation. However, bandpass filtering results in significant PAR regrowth [128–130]. If the clipping is performed on the signal sampled at the Nyquist rate, all the distortion noise falls in-band, thus avoiding the out-of-band radiation significantly [128–130]. Therefore, in

the Nyquist sampling case, the bandpass filter for removal of out of band radiation is not required. However, ideal low pass filtering after clipping is necessary for strictly band-limited communications systems, which is the case normally. This filtering causes peak regrowth and results in large PAR again. Therefore, several factors determine whether clipping the oversampled signal or Nyquist-rate sampled signal is better. This tradeoff depends on whether out-of-band leakage or in-band distortion is finally going to be tolerated. Generally, the oversampled signal should be clipped for efficient PAR reduction [131].

In [132], deliberate clipping is performed followed by the bandpass filter, and the resulting BER performance degradation is compensated by the BCH codes. This coding and clipping idea is further extended with adaptive symbol selection method in [130] to further improve the PAR reduction. The use of powerful turbo codes to remove in-band distortion is reported in [130]. In [133], the degradation is compensated by the iterative decision-aided reconstruction of the original OFDM signals. Saeedi and Maevasti [134] proposed a least square method with bandwidth expansion to reconstruct the clipped signal. In this approach, an oversampled signal is clipped to avoid peak regrowth. An effective form of clipping and filtering is also reported in [135]. The effect of filtering on the performance of OFDM systems and the influence of filtering on guard band are discussed in [136]. The asymptotic behavior of clipped higher-order OFDM signals and the relationship between the PAR and the probability of error in clipped OFDM systems are reported in [111].

An alternative approach to clipping is peak windowing. In this approach, large signal peaks are multiplied with a certain window [108, 137]. In [137], a Gaussian shape window is used. Since the OFDM signal is multiplied with several of these windows, the resulting spectrum is a convolution of the original OFDM spectrum with the spectrum of the applied window. Therefore, the window should be as narrow as possible to reduce out-of-band radiation. A window that is too long in time domain affects more signal samples and results in an increased bit error rate. Therefore, the window should be optimum such as a Kaiser, cosine and Hamming [108]. Van Nee and Wild [108] claimed that windowing causes less out-of-band radiation than clipping. A rate-half convolutional code with constraint length 7 is also used in [108] to improve the error performance. This windowing technique is further extended in [138] to reduce

the dynamic range of the OFDM signal and consequently reduce the PAR.

Recently, Wang et al. [139] introduced a companding technique to reduce the PAR of the OFDM signal. This idea is based on companding in speech processing. An OFDM signal is similar to a speech signal in the sense that large signal peaks only occur very infrequently. Therefore, the same companding technique, that is μ -law, can be used to improve PAR. The samples of the OFDM signal are companded before they are converted into the analog waveform. In companding, small samples are enlarged while the large samples remain unchanged. Therefore, the average power of the OFDM signal is increased, thus resulting in low PAR. Unlike the clipping technique, PAR is reduced without introducing clipping noise. The nonlinear distortion introduced by the compressor at the transmitter is corrected after reconstruction by a complementary expander at the receiver [139]. Further results and comments on this technique are reported in [140, 141]. Optimal companding coefficients and symbol error rate of the companding technique are derived in [142]. A transform-based companding method is proposed in [143, 144] by combining the advantages of both clipping and companding. In this scheme, large samples are compressed while small samples are enhanced. This reduces the dynamic range of the OFDM signal and, consequently, PAR is reduced. By properly choosing the transformation parameters, this method keeps the average power unchanged. It is claimed that the companding technique outperforms the clipping-filtering approach [143, 144]. However, their performance will be severely degraded in fading channels because of distortion introduced to the companded signal. The expander at the receiver will not be able to completely remove the companding effects.

An alternative approach, suited to enhance the system power efficiency, is to apply a linearization technique to the HPA. A predistorter (PD), whose input-output response compensates for the intrinsic nonlinearity of the HPA, is inserted just before the HPA. Therefore, the combined characteristic of the PD and HPA becomes linear. Predistortion techniques have been extensively treated in the literature for single carrier transmission schemes employing multilevel amplitude and phase modulation schemes and they are now being considered for multicarrier systems. Minimum mean square error (MMSE) predistortion is applied to an OFDM system in [145]. The input-output response is modelled as a third-order polynomial. The coefficients are selected so as to minimize the mean square distance between the output of the actual PD and that

of the ideal PD providing an exact linearization of the HPA [146]. In [147], an analytical predistortion technique is investigated exhibiting good accuracy at the cost of considerable implementation complexity. An adaptive predistortion scheme based on MMSE criterion is reported in [148]. This adaptive scheme is further improved in [149]. D'Andrea et al. [150] proposed an amplitude and phase (A&P) predistortion technique and compared its performance and complexity with the MMSE schemes.

Signal distortionless techniques

These techniques can be further grouped into the following categories.

- coding: block codes, Reed Muller codes and Golay complementary sequences
- multiple signal representation: partial transmit sequence (PTS), selected mapping (SLM), interleaving and adaptive mapping
- modified signal constellations: tone injection, orthogonal transformation
- pilot tone methods: tone reservation
- other methods: trellis shaping, pulse shaping

These methods are summarized below.

Coding

Coding is considered as an effective way to reduce PAR since it does not introduce distortion and not require any side information. It also offers error correction capability while reducing PAR. However, designing a good coding scheme with low PAR, good error correction capability and higher code rates is still an open problem. Jones et al. [151] first proposed the block coding principle to reduce PAR. As few data frames result in large signal peaks, block codes can be designed so that such data frames are never used [151]. This block coding principle offers the flexibility to trade code rate against PAR reduction. For $N = 4$, PAR can be reduced from 6.02 dB to 2.48 dB with a code rate of $3/4$ [151]. This scheme needs a look-up table since encoding and decoding rules are non linear. This block coding principle is further enhanced in [152] by combining PAR reduction and error control. Shepherd et al. [153] proposed a half-rate coding scheme based on Rudin-Shapiro polynomials to reduce the PAR

for large N . Fragiaco [154] introduced a simple added bit block code to reduce the maximum PAR. The block coding principle in [151] is further extended in [155] to large N by dividing the data frame into several sub-blocks and encoding each sub-block as in [151]. Fan and Xia [156] introduced a block coded modulation (BCM) technique based on [151]. In this approach, binary blocks are mapped to M -ary blocks and M -ary blocks of small sizes with low PAR are selected. Large size M -ary blocks with low PAR are constructed by using the selected small size M -ary blocks.

Li and Ritcey [157] proposed the use of maximum-length shift-register sequences (m -sequences) for block coding the data to achieve PAR reduction and error correction. In this approach, a block of m input bits are mapped to an m -sequence of length $2^m - 1$. This results in a code rate of $\frac{m}{2^m - 1}$. The main drawback in this method is the extremely low code rates, particularly for large N . They [157] claimed that the PAR can be limited to 0.58, 0.28, 0.14, 0.07 and 0.03 dB for $m = 3, 4, 5, 6$ and 7 respectively. However, these results are incorrect since PAR cannot be established solely on the basis of N samples of the OFDM signal [104, 158]. Thus, PAR should be estimated based on oversampled signals. Tellambura [104] illustrated that the m -sequence for $3 \leq m \leq 10$ yields PAR of 5.4 to 7.3 dB.

Van Nee [159] proposed the use of complementary codes for PAR reduction and error correction. Davis and Jedwab [160] identified the connection between pairs of Golay complementary sequences and second-order Reed-Muller codes. The PAR of such codes is less than or equal to 3 dB. However, their code rate is low, particularly for large N and decreases rapidly with increasing N . In fact, several studies on complementary sequences for PAR reduction are reported in the open literature. A maximum likelihood decoding method for complementary codes is discussed in [161]. Davis and Jedwab [162] also proposed simple encoding and decoding rules for Golay complementary sequences. Paterson [163] developed generalized Reed-Muller codes and derived the bounds for PAR of these codes. The existence of PAR reduced codes and their bounds are mathematically proved in [164]. Minimum-distance decoding of PAR reduction codes are analyzed in [165]. The performance of complementary codes over frequency selective Rayleigh fading channels is evaluated in [166, 167]. Chong and Tarokh [168] proposed a coding scheme for QPSK-OFDM by exploiting QPSK as a

combination of BPSKs. This code construction provides simple encoding and decoding and the PAR is also limited to 6 dB. This approach is extended to 16-QAM case in [169]. Recently, Henkel [170] proposed the use of analog codes to reduce PAR.

Multiple signal representation

The main cause of large PAR is the phase alignment of the symbols in each subchannels. This results in peak when added constructively. So, PAR can be reduced by breaking the phase alignment of the symbols. In other words, PAR can be reduced by reducing the correlation of the data symbols. However, optimizing the phase to reduce PAR for any data frame is a difficult task. One simple solution is to generate several different sequences and then choose the sequence with the lowest PAR. This is the key idea for the approaches: Selected Mapping (SLM) [171–174], Partial Transmit Sequence (PTS) [172–175], interleaving [176, 177] or adaptive symbol selection [130] and adaptive mapping [178]. However, they all differ from each other in generating different sequences. Information about the generation process of the transmitted sequence should be sent to the receiver as side information. Since side information bits are critically important, they may be protected by channel coding, thus reducing the data throughput. These techniques also suffer from increased complexity due to the generation of several sequences and PAR calculations.

In SLM, the data symbols are multiplied by U different phase sequences and the resulting sequence with low PAR is selected for transmission. Breiling et al. [179, 180] proposed a scrambling technique for SLM without explicit side information. However, this approach [179, 180] still requires some redundancy to be introduced into the signal. A novel blind method based on minimum-distance decoding via the Viterbi algorithm is proposed in [181] to completely eliminate the transmission of side information in SLM. In PTS, the data block is partitioned into M disjoint blocks or clusters and they are separately transformed by N -point IFFT. These M different IFFT output sequences are called partial transmit sequences and they are weighted by phase factors and then summed up to generate a transmit sequence. PAR is reduced by optimizing the phase factors. Since finding the optimum phase factors is difficult, several phase factors are used to generate a sequence and the sequence with the lowest PAR is selected for transmission. To reduce an extensive search for the phase factors, Cimini and Sollenberger [182, 183] proposed a suboptimum approach by using the random,

iterative and Walsh sequences as phase factors. The computation of phase factors is further improved in [184, 185]. The PAR reduction in PTS is further improved in [186] by cyclically shifting the partial transmit sequences. Reference [187] reports a geometrical interpretation to the PTS approach and introduces a novel orthogonal projection-based PTS with improved performance. As in SLM, transmission of side information is necessary to correctly decode the data at the receiver. Cimini and Sollenberger [188] described a technique for embedding this side information within the transmitted data and reliably recovering it at the receiver without any overhead.

In [176, 177, 181], a simple interleaving approach is proposed to reduce the PAR. Interleaving of data sequences breaks the correlation among the data and thus reduces the PAR. Interleaving can be done either at bit or symbol level. Since finding the optimum interleaving is difficult, K fixed interleavers are used at the transmitter to produce K permuted data sequences. Then, the sequence with the minimum PAR is selected for transmission. Information about the interleaving process has to be sent to the receiver as side information. This interleaving is a simple operation and does not require complex multiplications as in SLM and PTS. Further, interleaving improves the error performance in a fading channel when employed with coding. This interleaving approach is independently reported in [130] and called "adaptive symbol selection".

Sathananthan and Tellambura [178] proposed an adaptive M -point Zero-padded Phase Shift Keying (M -ZPSK), which includes a signal point of zero amplitude, to reduce PAR. In this scheme, M bit patterns of $\log_2 M$ bits are mapped to a signal point of zero amplitude to generate M different data sequences representing the same information. Then, the sequence with the minimum PAR is selected for transmission. The mapping pattern used at the transmitter is sent to the receiver as side information. This scheme reduces the ICI as the signal point of zero amplitude does not contribute to overall ICI. This is a significant advantage over other multiple signal representation schemes. This scheme is discussed in detail in Chapter 6.

Modified signal constellations

Tellado and Coiffi [116, 189] introduced the tone injection method based on replicating the symbol constellation with known translating vectors. This expands the constellation and generates several points that represent the same information. Therefore, the points with the minimum PAR can be selected for transmission. The generalized

constellations can be easily mapped onto the original constellation with a modulo operation at the receiver. This scheme offers more than a 6 dB PAR reduction without data rate loss and with a negligible increase in average power. In [190], the QAM constellation size is enlarged at a number of tones to generate several signal points representing the same information. Then, the signal points with minimum PAR are selected for transmission. Kwok and Jones [191] proposed a constellation-shaping approach to reduce PAR. An active channel modification method is reported in [192]. In this approach, data carrying channels are dynamically moved to outer constellation points to minimize the peak magnitude by an iterative algorithm.

Another approach to change signal constellation is to transform the modulated symbols by an orthogonal transformation. Park et al. [106] investigated the use of Hadamard transformation for PAR reduction. In [193, 194], a pseudo-orthogonal carrier interferometry coding is proposed to reduce PAR. In fact, this pseudo-orthogonal carrier interferometry coding is equivalent to the Fourier transformation of data symbols. The orthogonal transformation reduces the correlation among the data symbols and thus results in low PAR. The inverse transformation at the receiver restores the data symbols to the original constellation.

Pilot tone methods

These methods are based on adding a symbol dependent time domain signal to the original signal to reduce its peaks. Some subcarriers are reserved for the insertion of pilot symbols that are optimized to reduce the peaks. In tone reservation [116, 189, 195], some subcarriers are reserved for pilot tones which are optimized to reduce the PAR. These tones are calculated at the transmitter and stripped off at the receiver. Since finding the optimum tones is a linear programming problem, a simple iterative gradient algorithm for faster calculation is proposed in [116, 189]. This tone reservation method is further improved in [196-198] by incorporating an active-set approach. Schmidt and Kammeyer [199] proposed the use of non-information carrying subcarriers to reduce PAR. These subcarriers are modulated iteratively depending on a threshold decision so that the resulting signal reduces the PAR. In [200], extra carriers referred to as peak reduction carriers (PRC) are added to reduce PAR. The phase and amplitude of the PRCs are varied to minimize the overall PAR. Information is not transmitted on PRCs and the receiver can disregard the PRCs, or they can be used for error detection.

The frequency of PRCs or the relative positioning of the PRCs are varied with respect to the information carriers. However, the optimal setting for PRCs was found using a computationally-intensive exhaustive search. In [201, 202], a two-dimensional pilot-symbol assisted modulation scheme to reduce PAR and estimate channel response is reported.

Other methods

Muta and Akaiwa [203, 204] proposed an adaptive power control scheme to reduce PAR. In this scheme, transmitted pulse power before filtering is decreased whenever the peak amplitude is above a given threshold. However, a small degradation in BER performance is tolerated. Henkel and Wagner [205, 206] proposed the use of trellis shaping to reduce the PAR of the multicarrier signal. The idea of trellis shaping was originally used in single carrier systems to minimize average transmit power. Slimane [207] proposed a new technique based on the selection of time-limited waveforms of the different subcarriers. These waveforms of the different subcarriers create an appropriate correlation to reduce PAR. This method can be considered as a precoding.

2.7 Extension of OFDM Principles

2.7.1 Multicarrier-Code Division Multiple Access (MC-CDMA)

Spread spectrum systems using code division multiple access (CDMA) have been widely used in many wireless communication systems. Recently, different combinations of OFDM and CDMA have been investigated in the context of high data rate communication over dispersive channels [208]. One of these systems is a multicarrier CDMA (MC-CDMA), which is considered as a promising candidate for future generation wireless communication systems. CDMA systems occupy a large bandwidth, resulting in frequency selective fading for single carrier implementations. MC-CDMA has been proposed to complement CDMA in mitigating this problem while maintaining bandwidth efficiency. In fact, MC-CDMA systems combine many aspects of these two (OFDM and CDMA) technologies to provide a better system having the advantages of both. This results in a finer partitioning of radio resources in time, frequency and code domains allowing effective resource-allocation schemes. This feature makes MC-CDMA more flexible in adapting to channel conditions and allows throughput optimization.

In MC-CDMA, each data bit is transmitted in parallel on multiple subcarriers with each subcarrier modulated by a single code chip. Therefore, MC-CDMA systems exhibit two levels of orthogonality. One is the orthogonality between subcarriers and the other is between users. For the same user, the subcarriers are orthogonal, which is similar to an OFDM system. For different users, multiple access is achieved by allocating different users different codes which are pseudo-orthogonal to each other. Thus, even though all the users are using the same set of subcarrier frequencies, they are orthogonal due to the orthogonal codes.

Because of the inherent nature of OFDM, MC-CDMA also suffers from high PAR and high sensitivity to frequency offset errors. Generally, the techniques proposed for OFDM can also be used in MC-CDMA to mitigate the effects of high PAR and frequency errors. Moreover, several studies are reported on these problems in the context of MC-CDMA's nature. A brief description of these studies is provided below.

Ho and Wei [209] proposed the use of Golay complementary sequences as spreading codes to bound the PAR below 6 dB. Orthogonal spreading codes are investigated in [210] for PAR reduction in MC-CDMA. Ochiai and Imai [211] also studied the use of Golay complementary spreading codes for an OFDM-CDMA system. In [212], carrier interferometry codes are used to reduce the PAR in MC-CDMA systems. A dynamic spreading code selection method for PAR reduction in OFDM-CDMA system is proposed in [213].

MC-CDMA is more sensitive to frequency offset errors than conventional OFDM. It is very sensitive even to a relatively small frequency offset [214]. The frequency offset causes to multiuser interference from the other users and carriers in addition to self-interference from other carriers [214]. These effects are investigated in detail in [80, 214–216]. Several frequency offset estimation algorithms are proposed in the open literature to correct frequency errors in MC-CDMA.

2.7.2 Multi Input Multi Output (MIMO) OFDM

Multiple-input multiple-output (MIMO) systems are today regarded as one of the most promising techniques to support the ever growing demand for high-data rate wireless access. This is due to its significant capacity gain over traditional single-input single-output (SISO) systems. A MIMO scheme offers a linear increase in spectral efficiency

for MIMO-OFDM systems using training symbols, that are directly modulateable orthogonal polyphase sequences.

2.8 Conclusions

This chapter has introduced the OFDM technology and its limitations, high PAR and ICI. The proposed techniques in the open literature to overcome these limitations have been discussed in detail. This chapter has shown that these impairments degrade the error performance and introduce an error floor. Therefore, an evaluation of error performance is important to correctly quantify these impairments. The next chapter presents this error performance analysis with ICI.

Chapter 3

Exact Error Rate Calculations

In this chapter, a precise numerical technique for calculating the effect of carrier frequency offset (CFO) on the symbol error rate (SER) in an OFDM system is proposed. We consider BPSK, QPSK and 16QAM, which are common modulation formats used in OFDM applications. The BPSK case is solved using a Beaulieu series. For the QPSK and 16QAM cases, we use an infinite series expression for the error function in order to express the average probability of error in terms of the two-dimensional (2D) characteristic function of the ICI. We use these precise error rate calculation methods to evaluate the error performance of the rate-half repetition codes. Moreover, the proposed technique is extended to compute the exact error performance of an OFDM system with phase noise.

3.1 Introduction

The effects of CFO on the performance of OFDM systems are calculated in various ways in the literature. It may be derived as a loss in the ratio between the signal power and the statistical average power of the ICI, called average carrier-to-interference ratio (CIR) [64, 66, 68, 70]. However, the average CIR does not readily indicate actual error performance of the system. In fact, the average CIR is loosely related to BER. However, the average CIR is useful in comparing the degree of ICI effects in various conditions. In [17, 18, 228, 229], the approximate degradation in signal-to-noise ratio (SNR) caused by the CFO is derived using simple algebraic manipulation.

Alternatively, computer simulations may be used to obtain the error performance of the system subject to ICI. The other simple approach is the approximate calculation of error rates. In this approach, ICI is assumed to be Gaussian distributed and is

added with channel noise [13,69,70]. ICI is a random process and its distribution by a Gaussian process is reasonable for large N , according to the central limit theorem. Zaho and Häggman [230] derived an upper bound and an exact method for the BER of BPSK scheme. However, this approach is difficult to extend to other modulation schemes such as QPSK and 16-QAM. Hasson and Bobrovsky [231] reported a BER calculation method for M-QAM schemes using the degradation in SNR, proposed in [18]. This [231] is again an approximation method since the calculation of degradation in SNR is not exact. Therefore, it is also both interesting and useful to know the precise correlation between the BER or SER and the CFO.

3.2 Error Rate Calculations

3.2.1 Precise Calculations

Assumptions and Problem Statement

We assume an ideal, additive white Gaussian noise channel. The CFO does not change during one OFDM symbol. Consider the sampled signal for the k -th subchannel after the receiver DFT processing and it is expressed as (2.29)

$$y_k = c_k S_0 + \sum_{l=0, l \neq k}^{N-1} S_{l-k} c_l + n_k \quad k = 0, 1, \dots, N-1 \quad (3.1)$$

where c_k denotes the transmitted symbol for the k -th subcarrier, n_k is a complex Gaussian noise sample (with its real and imaginary components being independent and identically distributed with variance σ^2) and N is the number of subcarriers. The sequence S_k depends on the CFO and is given by (2.26)

$$S_k = \frac{\sin \pi(k + \varepsilon)}{N \sin \frac{\pi}{N}(k + \varepsilon)} \exp \left[j\pi \left(1 - \frac{1}{N}\right)(k + \varepsilon) \right] \quad (3.2)$$

where ε is the normalized frequency offset.

We assume the data symbols c_k s are independent and identically distributed random variables (RV's). For M-ary signalling, c_k is equally likely to assume one out of M levels. Without any loss in generality, we will consider the error rate for the 0-th subcarrier (i.e. $k = 0$). So the problem at hand is to determine, for a given symbol sent on the 0-th subcarrier, the probability that an incorrect decision will be made.

BPSK Modulation

For BPSK modulation, $c_k \in \{1, -1\}$ and without incurring a loss in generality, it will be sufficient to consider the real part of (3.1). The characteristic function (CHF) of $\Re(y_k)$ can be expressed as

$$\phi(\omega) = e^{j\omega c_k \Re\{S_0\} - \frac{\omega^2 \sigma^2}{2}} \prod_{l=0, l \neq k}^{N-1} \cos(\omega \Re\{S_{l-k}\}) \quad (3.3)$$

where $\Re\{z\}$ denotes the real part of z . From the Beaulieu series [232, 233], the cumulative distribution function (CDF) of an RV can be expressed using its CHF, i.e.,

$$Pr(X < x) = \frac{1}{2} - \sum_{n \in N_0} \frac{2\Im\{e^{-jn\omega_0 x} \phi(n\omega_0)\}}{n\pi} + \epsilon(x, \omega_0) \quad (3.4)$$

where $\Im\{z\}$ denotes the imaginary part of z , $\omega_0 = 2\pi/T$, T is a parameter governing the sampling rate in the frequency domain, and $\epsilon(x, \omega_0)$ is an error term. Note that the error term depends on both x and T . For a given x , the error can be arbitrarily reduced by increasing T . In practice, once a suitable T is selected, it is used for all possible values of x . The index set $N_0 = \{1, 3, \dots\}$ is the set of all positive odd integers. Without loss of generality, we consider the first subcarrier and the transmitted symbol $c_0 = 1$. Now, a decision error occurs if the real part of y_0 (3.1) is less than zero. Thus, the probability of a bit error is

$$P_b = \frac{1}{2} - \sum_{n \in N_0} \frac{\sin[n\omega_0 \Re\{S_0\}] e^{-\frac{1}{2} \omega_0^2 \sigma^2}}{n\pi} \prod_{l=1}^{N-1} \cos(n\omega_0 \Re\{S_l\}) + \epsilon(0, \omega_0). \quad (3.5)$$

Here, the error term can be made negligibly small by selecting a sufficiently large T . The numerical evaluation of (3.5) gives the exact probability of a bit error.

It is worthwhile to explain how $\epsilon(x, \omega_0)$ originates. The CDF of an RV X may be written exactly as an infinite integral using the Gil-Plane theorem. In (3.4), this infinite integral is replaced by a series, which can be viewed as approximating the integral by a trapezoidal sum. Thus, $\epsilon(x, \omega_0)$ is the error introduced due to this discretization process. Reference [233] shows that $\epsilon(x, \omega_0) = \sum (-1)^{n+1} f(x + nT/2)$ where $f(x)$ is the probability density function (PDF). Most PDFs for physical applications have rapidly decaying tails. As a result, for the problem at hand, $\epsilon(x, \omega_0)$ can be made arbitrarily small provided T is large compared to the tails of $x = y_k$. Although y_k is not strictly bounded, the probability that real or imaginary part of y_k exceeding

$T_1 = \max_l |c_l \sum_k |S_k| + 3\sigma$ is very small. Thus, T can be chosen to be sufficiently larger than T_1 .

QPSK Modulation

For the QPSK case, the above approach cannot be applied directly because it deals with one dimensional signalling. Moreover, as can be seen below, the error probability is now a product involving the error function. Using an infinite series representation of the error function, we therefore transform the error probability into a form that is suitable for averaging.

Let us define the noise-free received signal point conditional on the ICI for the k -th subcarrier as

$$z = c_k S_0 + \sum_{l=0, l \neq k}^{N-1} S_{l-k} c_l \quad (3.6)$$

where $c_l \in \{\pm 1 \pm j\}$ for QPSK signalling. The variable z is simply the difference $y_k - n_k$ in (3.1) and the subscript k has been dropped for notational brevity. The two dimensional CHF of z is given by

$$\phi(\omega_I, \omega_Q) = \langle e^{j[\omega_I \Re\{z\} + \omega_Q \Im\{z\}]} \rangle \quad (3.7)$$

where $\langle \cdot \rangle$ denotes the average value over the distribution of z . Without loss of generality, we will assume that the transmitted symbol in the first subcarrier is $c_0 = (1 + j)$. Since c_l 's are independent and identically distributed RV's, the CHF becomes

$$\begin{aligned} \phi(\omega_I, \omega_Q) &= e^{j[\omega_I (\Re\{S_0\} - \Im\{S_0\}) + \omega_Q (\Im\{S_0\} + \Re\{S_0\})]} \\ &\times \prod_{l=1}^{N-1} (\cos(\omega_I \Re\{S_l\} + \omega_Q \Im\{S_l\}) \cos(\omega_I \Im\{S_l\} - \omega_Q \Re\{S_l\})). \end{aligned} \quad (3.8)$$

The probability of a correct decision is the probability that $z + n$ is inside the first quadrant in the complex plane. Since the real and imaginary components of the additive noise are independent and identically distributed with a variance of σ^2 , the correct decision probability is given by

$$\begin{aligned} P_c(z + n \in D_1 | c_0 = 1 + j, z) &= \int_0^\infty \frac{1}{\sqrt{2\pi\sigma}} e^{-\frac{(x - \Re\{z\})^2}{2\sigma^2}} dx \times \int_0^\infty \frac{1}{\sqrt{2\pi\sigma}} e^{-\frac{(y - \Im\{z\})^2}{2\sigma^2}} dy \\ &= Q\left(\frac{-\Re\{z\}}{\sigma}\right) Q\left(\frac{-\Im\{z\}}{\sigma}\right) \end{aligned} \quad (3.9)$$

where D_1 is the first quadrant in the complex plane and $Q(x) = \int_x^\infty \frac{e^{-t^2/2}}{\sqrt{2\pi}} dt$ denotes the Gaussian CDF and has the series representation [232, 234]

$$Q(x) = \frac{1}{2} - \frac{2}{\pi} \sum_{m \in N_0} \frac{\exp(-m^2 \omega_0^2 / 2) \sin(m \omega_0 x)}{m} + \epsilon(x, \omega_0) \quad (3.10)$$

where $\epsilon(x, \omega_0)$ is the approximation error. Neglecting it and substituting (3.10) in (3.9), we find

$$\begin{aligned} P_c(z + n \in D_1 | c_0 = 1 + j, z) &= \frac{1}{4} + \frac{1}{\pi} \sum_{m \in N_0} \frac{\exp(-m^2 \omega_0^2 / 2) \sin(m \omega_0 \Re\{z\} / \sigma)}{m} \\ &+ \frac{1}{\pi} \sum_{n \in N_0} \frac{\exp(-n^2 \omega_0^2 / 2) \sin(n \omega_0 \Im\{z\} / \sigma)}{n} \\ &+ \frac{4}{\pi^2} \sum_{m \in N_0} \sum_{n \in N_0} \left(\frac{\exp(-(n^2 + m^2) \omega_0^2 / 2)}{nm} \sin(m \omega_0 \Re\{z\} / \sigma) \sin(n \omega_0 \Im\{z\} / \sigma) \right). \end{aligned} \quad (3.11)$$

Next we need the average of this probability, $P_c(z + n \in D_1 | c_0 = 1 + j, z)$, over the distribution of z , which readily follows from the 2-D CHF in (3.7). Since $\sin \theta = \Im\{e^{j\theta}\}$, for instance, the average of $\sin(\omega \Re\{z\})$ can be given by $\Im\{\phi(\omega, 0)\}$. Consequently, the average of the first and second infinite series in (3.11) can be obtained using $\Im\{\phi(m \omega_0 / \sigma, 0)\}$ and $\Im\{\phi(0, m \omega_0 / \sigma)\}$. The sine product term in the double infinite series can be written as a sum of two cosine terms and (3.7) can again be used to get the average. Therefore, the average probability of correct decision may be expressed as

$$\begin{aligned} P_{c,av} &= \frac{1}{4} + \frac{1}{\pi} \sum_{m \in N_0} \frac{\exp(-m^2 \omega_0^2 / 2) \Im\{\phi(\frac{m \omega_0}{\sigma}, 0)\}}{m} + \frac{1}{\pi} \sum_{n \in N_0} \frac{\exp(-n^2 \omega_0^2 / 2) \Im\{\phi(0, \frac{n \omega_0}{\sigma})\}}{n} \\ &+ \frac{2}{\pi^2} \sum_{n \in N_0} \sum_{m \in N_0} \left(\frac{\exp(-(n^2 + m^2) \omega_0^2 / 2)}{nm} \Re\left\{ \phi\left(\frac{-m \omega_0}{\sigma}, \frac{n \omega_0}{\sigma}\right) - \phi\left(\frac{m \omega_0}{\sigma}, \frac{n \omega_0}{\sigma}\right) \right\} \right). \end{aligned} \quad (3.12)$$

Subsequently, the probability of symbol error is given by,

$$P_e = 1 - P_{c,av}. \quad (3.13)$$

16QAM Modulation

The 16QAM signal alphabet is the set $\Lambda_{16} = \{\pm 1 \pm j, \pm 3 \pm j, \pm 1 \pm 3j, \pm 3 \pm 3j\}$. Without loss of generality, we assume the transmitted symbol c_0 to be in the first

compared to a logarithmic increase in more traditional systems whether they utilize receiver diversity or not [217]. In a MIMO system, multiple antennas are used both in the transmitter and receiver. The incoming data stream is demultiplexed into sub-streams and then transmitted through a number of transmit antennas (say n_T). These signals are received by a number of receiving antennas (n_R). In a rich scattering environment, the signals from each individual transmitter appear highly uncorrelated at each of the receiving antennas. When the signals are conveyed through uncorrelated channels, the signals corresponding to each of the individual transmit antennas have attained different spatial signatures. The receiver can use these different spatial signatures to simultaneously and at the same frequency to separate the signals that originated from different transmit antennas [218].

The combination of OFDM and MIMO has recently gained much attention due to its benefits, gained from the advantages of both techniques. OFDM mitigates the ISI problem due to multipath propagation while MIMO improves the bandwidth efficiency. Several studies have been reported in the open literature on the MIMO-OFDM system. The concept of MIMO is also referred to in the literature as space division multiple access (SDMA) and consequently OFDM-SDMA [218-220] for MIMO-OFDM. In fact, several transmit antenna diversity schemes are proposed for OFDM to improve its performance [221, 222]. Transmitter diversity, combined with Reed-Solomon (RS) codes, has been investigated for clustered OFDM systems in [223]. Space-time codes are investigated in [224] to provide transmitter diversity for OFDM systems.

As in MC-CDMA, high PAR and high sensitivity for frequency errors are still the problem for MIMO-OFDM. However, the PAR problem in MIMO-OFDM is similar to conventional OFDM, whereas the frequency offset effects are severe and different from the conventional OFDM. Diggavi et al. [225] have developed a model for ICI in MIMO channels and proposed a time-domain filtering-based scheme for ICI reduction. Narasimhan [226] reported a study of bit error rate analysis for the OFDM system using transmit diversity and subject to frequency offset, phase noise and channel estimation errors. Mody and Stüber [227] claimed that frequency synchronization methods proposed for the conventional OFDM cannot be applied without major modifications to MIMO systems. This [227] reports a time and frequency synchronization

where D_1 is the first quadrant in the complex plane and $Q(x) = \int_x^\infty \frac{e^{-t^2/2}}{\sqrt{2\pi}} dt$ denotes the Gaussian CDF and has the series representation [232, 234]

$$Q(x) = \frac{1}{2} - \frac{2}{\pi} \sum_{m \in N_o} \frac{\exp(-m^2 \omega_0^2 / 2) \sin(m \omega_0 x)}{m} + \epsilon(x, \omega_0) \quad (3.10)$$

where $\epsilon(x, \omega_0)$ is the approximation error. Neglecting it and substituting (3.10) in (3.9), we find

$$\begin{aligned} P_c(z + n \in D_1 | c_0 = 1 + j, z) &= \frac{1}{4} + \frac{1}{\pi} \sum_{m \in N_o} \frac{\exp(-m^2 \omega_0^2 / 2) \sin(m \omega_0 \Re\{z\} / \sigma)}{m} \\ &+ \frac{1}{\pi} \sum_{n \in N_o} \frac{\exp(-n^2 \omega_0^2 / 2) \sin(n \omega_0 \Im\{z\} / \sigma)}{n} \\ &+ \frac{4}{\pi^2} \sum_{m \in N_o} \sum_{n \in N_o} \left(\frac{\exp(-(n^2 + m^2) \omega_0^2 / 2)}{nm} \sin(m \omega_0 \Re\{z\} / \sigma) \sin(n \omega_0 \Im\{z\} / \sigma) \right). \end{aligned} \quad (3.11)$$

Next we need the average of this probability, $P_c(z + n \in D_1 | c_0 = 1 + j, z)$, over the distribution of z , which readily follows from the 2-D CHF in (3.7). Since $\sin \theta = \Im\{e^{j\theta}\}$, for instance, the average of $\sin(\omega \Re\{z\})$ can be given by $\Im\{\phi(\omega, 0)\}$. Consequently, the average of the first and second infinite series in (3.11) can be obtained using $\Im\{\phi(m \omega_0 / \sigma, 0)\}$ and $\Im\{\phi(0, n \omega_0 / \sigma)\}$. The sine product term in the double infinite series can be written as a sum of two cosine terms and (3.7) can again be used to get the average. Therefore, the average probability of correct decision may be expressed as

$$\begin{aligned} P_{c,av} &= \frac{1}{4} + \frac{1}{\pi} \sum_{m \in N_o} \frac{\exp(-m^2 \omega_0^2 / 2) \Im\{\phi(\frac{m \omega_0}{\sigma}, 0)\}}{m} + \frac{1}{\pi} \sum_{n \in N_o} \frac{\exp(-n^2 \omega_0^2 / 2) \Im\{\phi(0, \frac{n \omega_0}{\sigma})\}}{n} \\ &+ \frac{2}{\pi^2} \sum_{n \in N_o} \sum_{m \in N_o} \left(\frac{\exp(-(n^2 + m^2) \omega_0^2 / 2)}{nm} \Re\left\{ \phi\left(\frac{-m \omega_0}{\sigma}, \frac{n \omega_0}{\sigma}\right) - \phi\left(\frac{m \omega_0}{\sigma}, \frac{n \omega_0}{\sigma}\right) \right\} \right). \end{aligned} \quad (3.12)$$

Subsequently, the probability of symbol error is given by,

$$P_e = 1 - P_{c,av}. \quad (3.13)$$

16QAM Modulation

The 16QAM signal alphabet is the set $\Lambda_{16} = \{\pm 1 \pm j, \pm 3 \pm j, \pm 1 \pm 3j, \pm 3 \pm 3j\}$. Without loss of generality, we assume the transmitted symbol c_0 to be in the first

quadrant; $c_0 \in \{1 + j, 3 + j, 1 + 3j, 3 + 3j\}$. Just as with the QPSK case, the correct decision probability can be written as a product of the error function. It is therefore convenient to define a function:

$$\Psi(\alpha, \beta) = Q\left(\frac{\alpha - \Re\{z\}}{\sigma}\right)Q\left(\frac{\beta - \Im\{z\}}{\sigma}\right) \quad (3.14)$$

where α and β represent the decision region boundaries. It will soon become evident that the required error probabilities can be expressed in terms of this function.

The CHF of z in this case is

$$\phi(\omega_I, \omega_Q) = e^{j[\omega_I \Re\{S_0 c_0\} + \omega_Q \Im\{S_0 c_0\}]} \prod_{l=1}^{N-1} \frac{1}{16} \sum_{X_l \in \Lambda_{16}} e^{j[\omega_I \Re\{S_l c_l\} + \omega_Q \Im\{S_l c_l\}]} \quad (3.15)$$

We can now evaluate the average value of (3.14) using this CHF. Substituting (3.10) in (3.14) and using the same approach as in (3.13), it can readily be shown that

$$\begin{aligned} \langle \Psi(\alpha, \beta) \rangle &= \frac{1}{4} - \sum_{m \in N_0} \frac{\exp(-m^2 \omega_0^2 / 2) \Im\{e^{j \frac{m \omega_0 \alpha}{\sigma}} \phi(\frac{-m \omega_0}{\sigma}, 0)\}}{m \pi} \\ &\quad - \sum_{n \in N_0} \frac{\exp(-n^2 \omega_0^2 / 2) \Re\{e^{j \frac{n \omega_0 \beta}{\sigma}} \phi(0, \frac{-n \omega_0}{\sigma})\}}{n \pi} \\ &\quad + \sum_{n \in N_0} \sum_{m \in N_0} \frac{2 \exp(-(n^2 + m^2) \omega_0^2 / 2)}{n m \pi^2} \Re \left\{ e^{j \frac{m \omega_0 \alpha - n \omega_0 \beta}{\sigma}} \phi\left(\frac{-m \omega_0}{\sigma}, \frac{n \omega_0}{\sigma}\right) \right. \\ &\quad \left. - e^{j \frac{m \omega_0 \alpha + n \omega_0 \beta}{\sigma}} \phi\left(\frac{-m \omega_0}{\sigma}, \frac{-n \omega_0}{\sigma}\right) \right\} \end{aligned} \quad (3.16)$$

Note that for $\alpha = \beta = 0$, this reduces to (3.12). This, (3.16), can be used to find the probability of a correct decision given the transmission of a particular signal constellation point.

For instance, consider $c_0 = 1 + j$. The correct decision region in the complex plane is now a square denoted by D_s with vertices at $(0, 0)$, $(0, 2)$, $(2, 0)$ and $(2, 2)$. Thus, we need the probability that $z + n$ lies inside this square. This conditional probability can be expressed as

$$\begin{aligned} P_c(z + n \in D_s | c_0 = 1 + j, z) &= \int_0^2 \frac{1}{\sqrt{2\pi}\sigma} e^{-\frac{(x - \Re\{z\})^2}{2\sigma^2}} dx \times \int_0^2 \frac{1}{\sqrt{2\pi}\sigma} e^{-\frac{(y - \Im\{z\})^2}{2\sigma^2}} dy \\ &= \left[Q\left(\frac{-\Re\{z\}}{\sigma}\right) - Q\left(\frac{2 - \Re\{z\}}{\sigma}\right) \right] \times \left[Q\left(\frac{-\Im\{z\}}{\sigma}\right) - Q\left(\frac{2 - \Im\{z\}}{\sigma}\right) \right] \\ &= \Psi(0, 0) - \Psi(0, 2) - \Psi(2, 0) + \Psi(2, 2). \end{aligned} \quad (3.17)$$

As a result, the average $P_{c,av}(c_0 = 1 + j)$ is readily obtained from (3.16). The same technique can be used to find the probability of a correct decision associated with the other three constellation points in the first quadrant. The total probability of a correct decision can then be given by

$$\begin{aligned} P_{c,av} &= \frac{1}{4} \{P_{c,av}(c_0 = 1 + j) + P_{c,av}(c_0 = 1 + 3j) + P_{c,av}(c_0 = 3 + j) + P_{c,av}(c_0 = 3 + 3j)\} \\ &= \frac{1}{4} \langle \Psi(0,0) \rangle. \end{aligned} \quad (3.18)$$

The probability of error can now be obtained using

$$P_e = 1 - P_{c,av}. \quad (3.19)$$

3.2.2 Gaussian Approximation

If the ICI is assumed to be a Gaussian distributed RV with a zero mean, both the BER and SER can readily be computed for various modulation formats. The approximate error rates then can be expressed in terms of the $Q(\cdot)$ function and the effective SNR for the k -th subcarrier is

$$\gamma_{eff} = \frac{|S_0|^2 \gamma_s}{(1 + \gamma_s \sigma_{ICI}^2)} \quad (3.20)$$

where $\gamma_s = E\{|c_k|^2\}/\sigma^2$ which is the SNR for the k -th subcarrier in the absence of a CFO. The variance of the signal constellation, $E\{|c_k|^2\}$, will be independent of k if all subcarriers use the same modulation format, which is the normal case. The variance of the ICI on the k -th subcarrier can be given by

$$\sigma_{ICI}^2 = \sum_{l=0, l \neq k}^{N-1} |S_{l-k}|^2 \quad (3.21)$$

This effective SNR (3.20) can be used directly to calculate the probability of error approximately. We will use our precise formulas to verify the accuracy of this approach.

Approximate SNR Degradation

In [18], the effect of the CFO is characterized as a loss of SNR. Using the approach of [18] and our notation, this SNR degradation in dB can be expressed as

$$D = \frac{10}{\ln 10} \frac{1}{3} (\pi \epsilon)^2 \gamma_s. \quad (3.22)$$

Note that this approximation is derived using $\ln(1+x) \approx x$ which holds for $x \ll 1$. Hence the above is accurate only for $(\pi\epsilon)^2 \ll 3$. Now $\gamma_{eff} = \gamma_s - D$ (all quantities in dB).

3.2.3 Numerical Results

Table 3.1 contains the QPSK error probabilities for small values of N . The error probability P_e is calculated using (3.12) and (3.13). The exact error probability P_{exact} is calculated by averaging (3.9) over all possible 4^{N-1} values of z . The relative error is defined as $|(P_e - P_{exact})/P_{exact}|$. It is evident that the solution (3.13) is extremely accurate (for 11 to 12 significant figures).

Table 3.1: QPSK OFDM error probabilities for $\sigma^2 = 0.4$ and $\epsilon = 0.05$

N	P_e ($\times 10^{-5}$)	P_{exact} ($\times 10^{-5}$)	Relative error ($\times 10^{-11}$)
2	0.7469366361	0.7469366361	0.3715921039
3	1.9927340483	1.9927340482	0.8357033586
4	2.9722979633	2.9722979633	0.6536660581
5	3.6800138543	3.6800138544	0.3016899035
6	4.2029145453	4.2029145453	1.3207775374
7	4.6024402437	4.6024402435	4.5229662114
8	4.9170074819	4.9170074819	1.0725140009

In Figure 3.1, error rates are shown for an OFDM system with $N = 128$ for BPSK, and QPSK modulation schemes. In the simulation results which follow, 10^7 random OFDM frames were generated to obtain each error rate point. The simulation results agree with those calculated using (3.5) and (3.13). While the Gaussian approximation yields optimistic estimates, it is acceptable for the BPSK case, since the difference in SNR between approximation and simulation is less than 0.4 dB. This difference increases for the QPSK modulation scheme. We may attribute this difference to the reduction of the minimum Euclidean distance between any two signal constellation points in QPSK.

The Gaussian approximation is acceptable for small values of CFO, though it does deviate from simulation results for increasing CFO (Figure 3.2). Furthermore, the approximation is accurate for small value of SNR. In fact, Gaussian approximation is acceptable when noise dominates the ICI in the system. The approximation [18] is

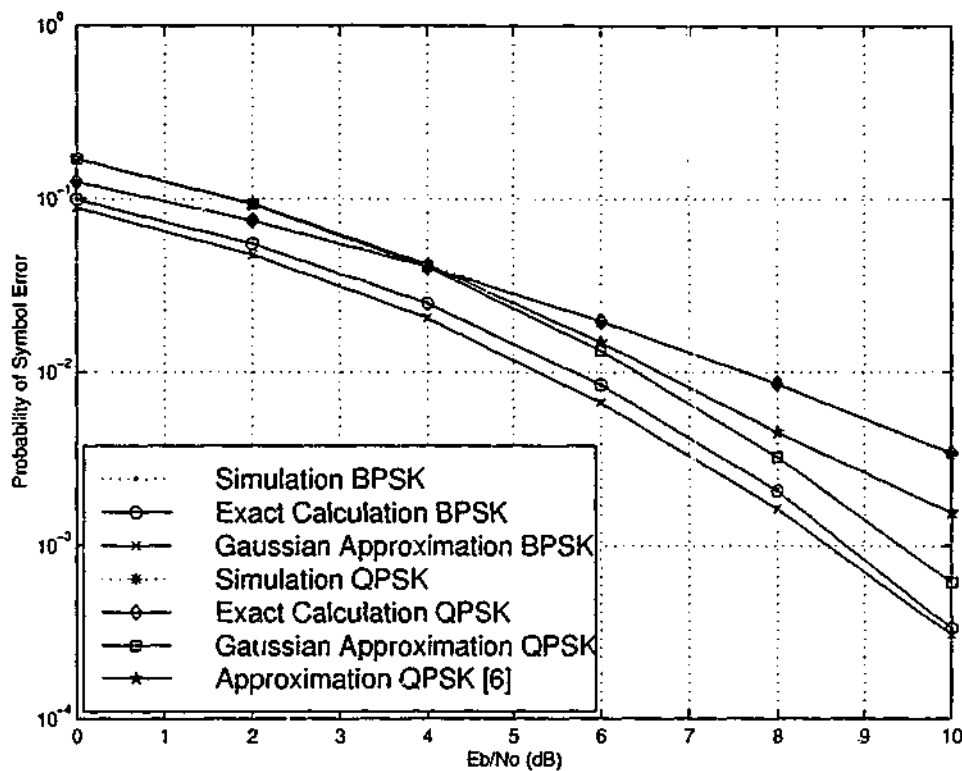


Figure 3.1: Probability of symbol error for BPSK and QPSK with $\epsilon = 0.1$.

fairly close to the Gaussian approximation for small SNR values.

Figure 3.3 shows results for 16QAM OFDM. Again, our technique is precise but the Gaussian approximation is much less accurate.

3.3 Error Performance of Rate-half Repetition Codes

It is worthwhile to briefly discuss the rate-half repetition coding scheme. It can be easily proved that $S_k \approx S_{k+1}$ for $0 < k \leq N - 1$. In other words, S_k slowly varies with k . As a result, if modulating symbols are repeated such that $c_1 = -c_0$, $c_3 = -c_2$ and so on, the total ICI term in (3.1) reduces. This slow varying nature of S_k is the key motivation for the rate-half repetition coding scheme. Since the same symbols are modulated on two subcarriers, they can be combined in the receiver to further improve the performance. Therefore, at the receiver the decision variable can be expressed as

$$d_k = y_{2k} - y_{2k+1} \quad \text{for } k = 0, 1, \dots, N/2 - 1 \quad (3.23)$$

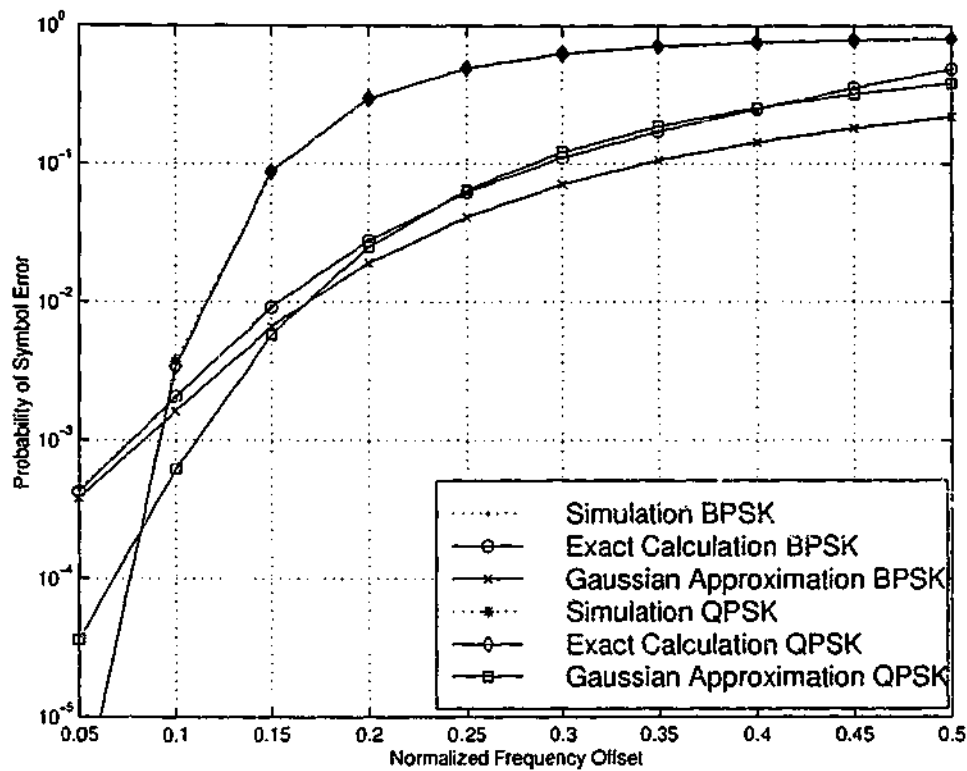


Figure 3.2: Probability of symbol error with normalized frequency offset ($E_b/N_0 = 8$ dB for BPSK and $E_b/N_0 = 10$ dB for QPSK.)

where y_k is the received sample on k -th subcarrier after the DFT processing. Therefore, (3.23) can be expressed as

$$d_k = (2S_0 - S_{-1} - S_1)c_{2k} + \sum_{l=0, 2l \neq 2k}^{N/2-1} (2S_{2l-2k} - S_{2l-1-2k} - S_{2l+1-2k})c_l + (n_{2k} - n_{2k+1}) \quad \text{for } k = 0, 1, \dots, N/2 - 1. \quad (3.24)$$

Therefore, the ICI in rate-half repetition codes (second term in (3.24)) is further reduced by this combining process at the receiver. This idea is further extended in [66, 68, 71] by mapping the weighted symbols on more than two subcarriers. At the receiver, the weighted y_k 's are combined to form the decision variable. This approach improves the ICI reduction significantly over that of rate-half repetition coding but with a further loss in data throughput.

The performance of rate-half repetition codes is measured by the average CIR gain [66, 68, 70] or BER performance by computer simulation or Gaussian approximation [65-67, 69, 70]. The proposed technique for precise calculation of BER or SER can be applied to rate-half repetition codes to evaluate its exact error performance. The decision variable (3.24) in the rate-half repetition codes is similar to conventional

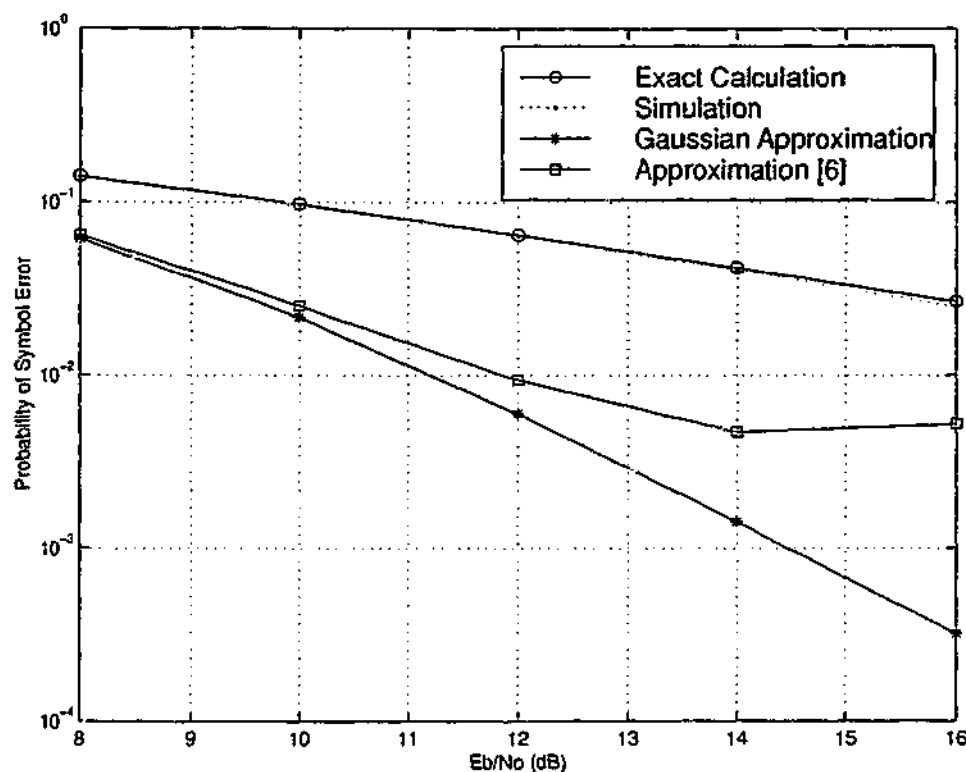


Figure 3.3: Probability of symbol error for 16QAM with $\varepsilon = 0.05$.

OFDM scheme, except the resulting ICI coefficients and the attenuation factor. These new effective ICI coefficients ($S_{k,\text{new}}$) and the attenuation factor ($S_{0,\text{new}}$) can be expressed as

$$S_{k,\text{new}} = 2S_{2k} - S_{2k-1} - S_{2k+1} \quad (3.25)$$

and

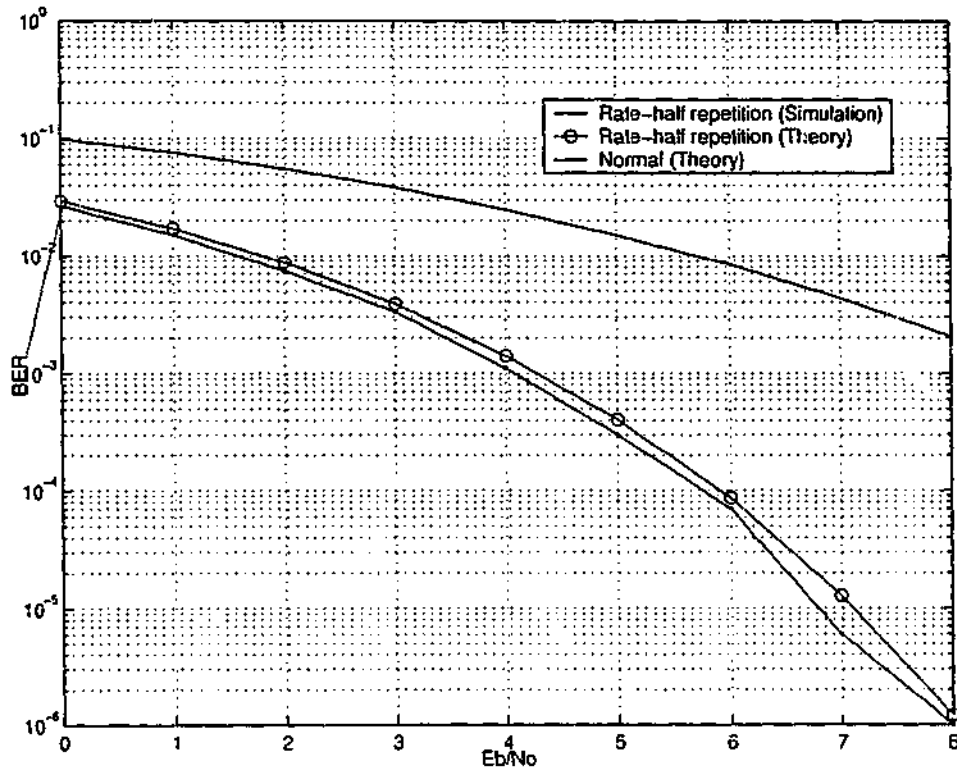
$$S_{0,\text{new}} = 2S_0 - S_{-1} - S_1. \quad (3.26)$$

Therefore, these coefficients (3.25) and (3.26) can be substituted in (3.4), (3.13) and (3.19) to compute BER or SER.

Figure 3.4 shows the BER performance of rate-half repetition codes for $N = 128$ and BPSK. The simulation results agree with theoretical calculations using (3.4). The difference in SNR between them is less than 0.2 dB.

3.4 Exact Error Rate Calculations with Phase Noise

We have seen in Chapter 2 that phase noise introduces ICI and attenuation and phase rotation of desired signal on each subcarrier. These are similar to frequency offset effects but with different statistics. Therefore, it is worthwhile to investigate the use of our precise error calculation techniques for phase noise.

Figure 3.4: Probability of symbol error for BPSK, $\varepsilon = 0.1$.

With phase noise, the sampled signal for the k -th subcarrier after the receiver DFT processing can be written as (2.44)

$$y_k = c_k \lambda_0 + \sum_{l=0, l \neq k}^{N-1} \lambda_{l-k} c_l + n_k \text{ for } k = 0, 1, \dots, N-1 \quad (3.27)$$

where n_k is a complex Gaussian noise sample. The sequence for the interference coefficient λ_k is given by (2.43)

$$\lambda_k = \sum_{m=0}^{N-1} e^{j\theta[m]} \cdot e^{j \frac{2\pi}{N} km}. \quad (3.28)$$

Since (3.27) is similar to (3.1), except the interference coefficients, the proposed technique can be extended to calculate precise error performance with phase noise. However, phase noise is modelled as a Wiener process, a continuous-path Brownian motion with zero mean and variance of $2\pi\beta t$. Therefore, the phase noise $\theta(t)$ is non-stationary. Consequently, λ_k 's are random and the calculation of SER based on (3.4), (3.13) and (3.19) are conditional probabilities of symbol error. Therefore, averaging (3.4), (3.13) and (3.19) over λ_k will give the exact SER. However, we need to derive the probability density function of λ_k , which is rather difficult.

We use a simple Monte Carlo method to calculate the exact SER. We generate λ_k randomly according to (3.28) and calculate the corresponding SER using (3.4) and

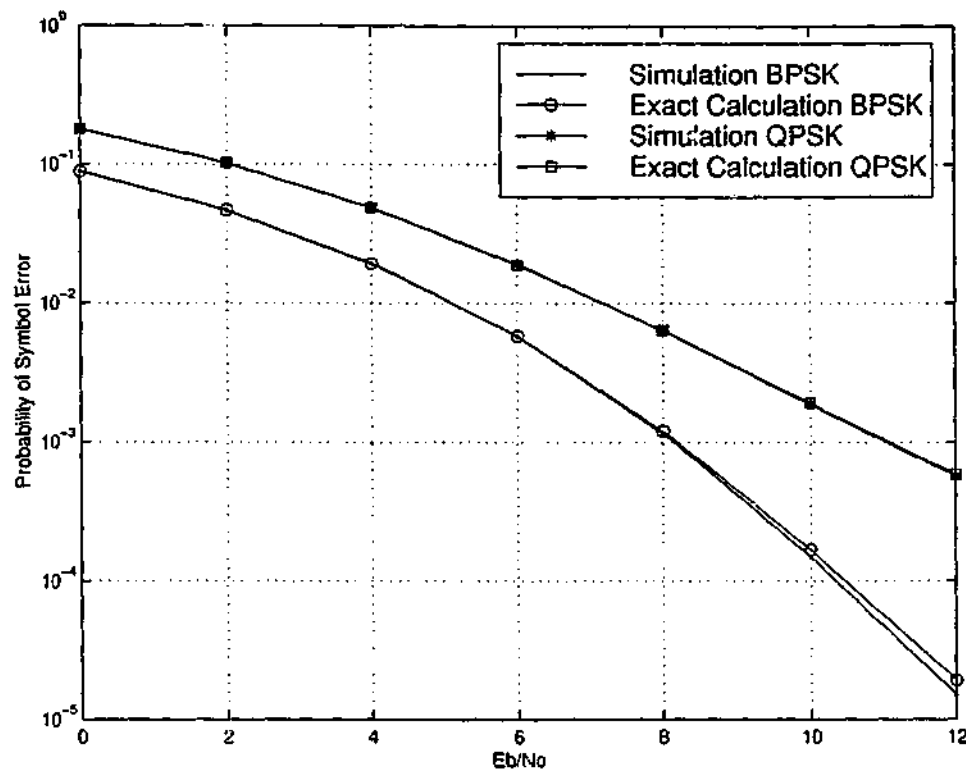


Figure 3.5: Probability of symbol error for BPSK and QPSK, $\gamma = 0.1$.

(3.13). These sample SER's are averaged to get the exact SER. These exact SERs are verified below by simulation. Note that we are interested in exact calculation of SER and thus, we avoid the use of probability density function of λ_k , which can be approximately calculated as in [78,82,83]. However, exact formulas in (3.4), (3.13) and (3.19) are not closed-form solutions in the case of phase noise.

Figure 3.5 shows the error rates of an OFDM system with $N = 128$ for BPSK, and QPSK modulation schemes for $\gamma = 0.1$ where $\gamma = 2\pi\beta T_u$ and T_u is the OFDM symbol duration. The simulation results agree with those calculated using (3.4) and (3.13). Figure 3.6 also confirms the agreement between the simulation and exact calculation results when γ varies.

3.5 Conclusions

In this chapter, we have developed a numerical technique to calculate precise SER or BER with CFO. We have considered BPSK, QPSK and 16QAM modulation schemes and their theoretical results agree with simulation results. We used this precise error rate calculation technique to evaluate the performance of rate-half repetition codes. We also used this technique to calculate the effect of phase noise on the BER or SER

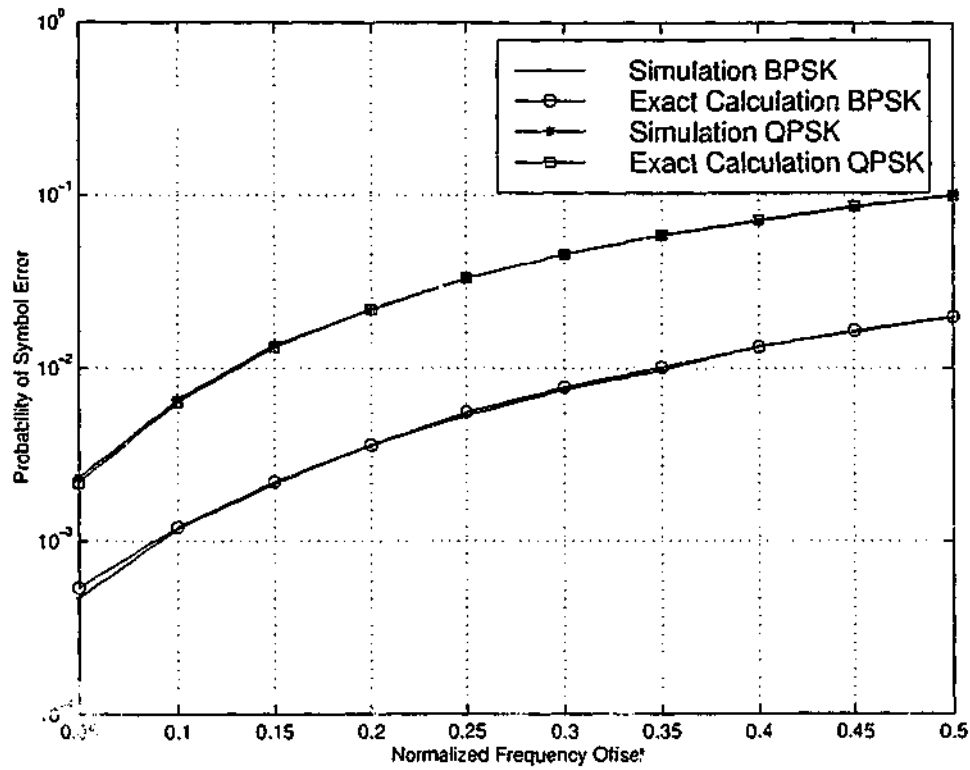


Figure 3.6: Probability of symbol error with γ and $SNR = 8dB$.

in an OFDM system. In fact, the proposed technique for the exact calculation of SER is independent of the statistics of interference coefficients (S_k). These interference coefficients become deterministic for CFO and become random for phase noise. In both cases, this technique readily achieves a high degree of accuracy. The accuracy does not depend on the amount of impairments or any other parameters.

Chapter 4

ICI Reduction by Coding

This chapter investigates the higher rate ICI-reduction codes. An optimal design rule for ICI-reduction codes is derived. However, algebraic construction of higher rate ICI-reduction codes are rather difficult. While explicit constructions of high rate ICI-reduction codes are much needed, we propose two new codes that map data onto three and four adjacent subcarriers. This idea is based on rate-half repetition coding. Since ICI degrades error performance, error correction codes can be used to reduce ICI effects. This motivates the use of high rate error codes for ICI reductions. We present a study of Rate-Compatible Punctured Convolutional (RCPC) codes to reduce ICI caused by CFO.

4.1 Introduction

The rate-half repetition coding technique is highly effective in cancelling ICI, albeit at a loss of 50% data throughput. This motivates the search for higher rate ICI-reduction codes. From an error correcting point of view, this rate-half repetition code has a rather limited capability. For instance, the minimum Hamming distance (d_{min}) of this code is 2. This raises an interesting question: can a more powerful error correction code with less redundancy be used for ICI cancellation just as effectively? Note that such a code would not have a direct ICI cancellation structure. Instead, a higher value of d_{min} would enable it to suppress more errors. To construct such codes, an optimal code design criterion needs to be established.

4.2 Code Design for a Channel with Frequency Offset

Suppose $\mathbf{c} = (c_0, c_1, \dots, c_{N-1})$ and $\hat{\mathbf{c}} = (\hat{c}_0, \hat{c}_1, \dots, \hat{c}_{N-1})$ are two codewords of a code \mathcal{C} . It is well known that for a fading channel, the optimal design goal is to maximize the minimum Hamming distance between any two $\mathbf{c}, \hat{\mathbf{c}} \in \mathcal{C}$. Similarly, for Gaussian channels, the optimum design rule is to maximize the minimum Euclidean distance between any two $\mathbf{c}, \hat{\mathbf{c}} \in \mathcal{C}$. To derive such a design rule for a frequency offset channel, we will consider optimal decoding of data on the assumption that S_k 's are known to the receiver.

Consider the decision variable for the k -th subchannel (2.29)

$$y_k = c_k S_0 + \sum_{l=0, l \neq k}^{N-1} S_{l-k} c_l + n_k \quad k = 0, 1, \dots, N-1. \quad (4.1)$$

The optimal decoding of data requires computing $|y_k - S_0 \hat{c}_k - \sum_l S_{l-k} \hat{c}_l|$ for all $\hat{\mathbf{c}} \in \mathcal{C}$ and choosing $\hat{\mathbf{c}}$ which minimizes the above. Substituting (2.29) for y_k , we see that in order to achieve performance approaching that of a Gaussian channel, we need to minimize

$$\Gamma(\varepsilon) = \max \left| \sum_{l=0, l \neq k}^{N-1} (c_l - \hat{c}_l) S_{l-k} \right|. \quad (4.2)$$

In other words, code design for a channel with frequency offset errors requires that for any two $\mathbf{c}, \hat{\mathbf{c}} \in \mathcal{C}$, $\Gamma(\varepsilon)$ should be minimized. Note that for uncoded modulation with BPSK type constellations, the worst case $(c_l - \hat{c}_l)$ is equal to 2 for all l . Thus, $\Gamma(\varepsilon)$ reduces to $2 \left| \sum_{l=0, l \neq k}^{N-1} S_{l-k} \right|$. In the rate-half repetition coding technique, $\Gamma(\varepsilon)$ approximately reduces to zero $\left(2 \left| \sum_{l=0, l \neq k}^{N-1} (-1)^l S_{l-k} \right| \right)$ since S_k 's are slowly varying and $c_{l+1} = -c_l$ for all l and \mathbf{c} . For example, $\Gamma(0.1)$ is 0.5803 for conventional OFDM whereas that of the rate-half repetition coding scheme is 0.0508, a 20 dB reduction.

Unfortunately, explicit construction rules for higher-rate codes based on $\Gamma(\varepsilon)$ appear to be difficult. However, $\Gamma(\varepsilon)$ explains the ICI-reduction capability of the codes. Therefore, search for good ICI-reduction codes with less redundancy is a challenging task.

Further, (4.2) requires ε to calculate the $\Gamma(\varepsilon)$ at the transmitter. $\Gamma(\varepsilon)$ is used as a design criteria to select the best ICI-reduction codes. Note that the ICI is a problem at the receiver and we need some parameter at the transmitter to choose the best

ICI-reduction codes. However, the relative performance of the codes are independent of the assumption of ϵ at the transmitter. For example, the rate-half repetition code reduces the ICI irrespective of the frequency offset present in the channel. This is further clarified analytically and by simulation in Chapter 5.

4.3 Rate $\frac{2}{3}$ and $\frac{3}{4}$ ICI-reduction Codes

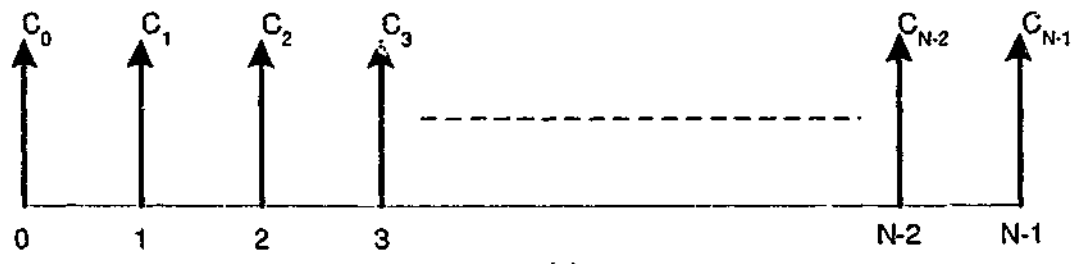
In rate half repetition codes, symbol repetition and combining of samples at the receiver achieve ICI reduction. Despite its ICI reduction capability and simplicity, the major drawback is low code rate ($= 0.5$). Naturally, one can use less redundancy for moderate ICI reduction so that code rate can be traded against ICI reduction. Note that such codes do not achieve the same performance as rate-half repetition codes. However, they will improve the data throughput.

For the new ICI-reduction schemes, modulated symbols (c_k) are repeated on the basis of expected code rate. For conventional OFDM, data are mapped to individual subcarriers, whereas for rate-half system data are mapped to pairs of adjacent subcarriers. Similarly, mapping two modulated symbols onto three adjacent subcarriers achieves a code rate of $\frac{2\lfloor \frac{N}{3} \rfloor + (N \bmod 3)}{N}$, which approximately reduces to $\frac{2}{3}$ for large value of N . In this case, the OFDM input block will be $\mathbf{c} = (c_0, c_1, -c_1, c_2, c_3, -c_3, \dots)$. Similarly, a rate $\frac{3}{4}$ code can be obtained by mapping three modulated symbols onto four adjacent subcarriers and the OFDM input block will be $\mathbf{c} = (c_0, c_1, c_2, -c_2, c_3, c_4, c_5, -c_5, \dots)$. Note that the OFDM input block for the rate-half code is $\mathbf{c} = (c_0, -c_0, c_1, -c_1, \dots)$. A schematic diagram for different code rate mapping is shown in Figure 4.1.

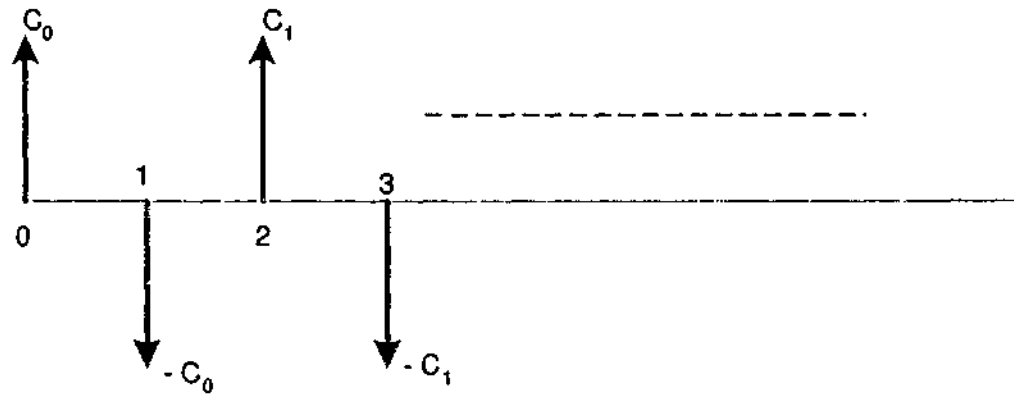
If same modulated symbols are repeated on subcarrier k and $(k + 1)$, then the receiver computes the difference between the received samples, $(y_k - y_{k+1})$, as a decision variable. Otherwise, the received sample y_k alone is the decision variable. Hence, ICI reduction in each subcarrier is not uniform and we can expect two level of ICI reduction among these subcarriers, one for repeated symbols and the other for non-repeated symbols.

For rate $\frac{2}{3}$ code, the decision variable d_k at the receiver can be expressed as

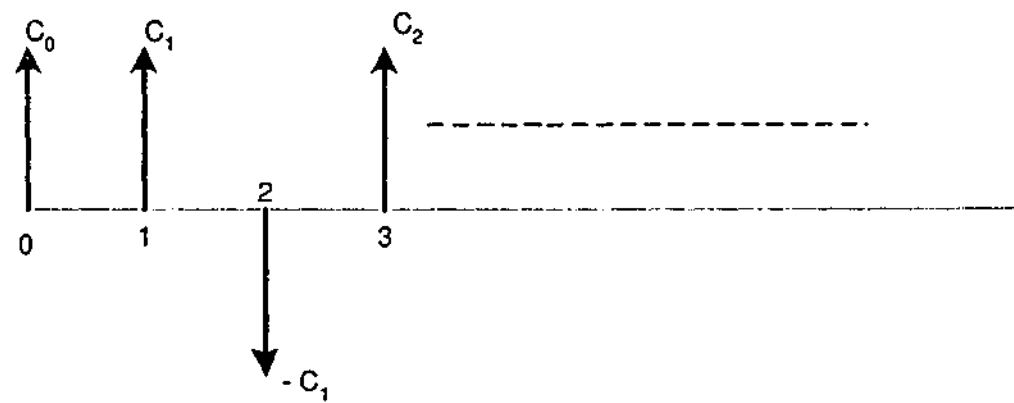
$$d_k = \begin{cases} y_k, & k = 0, 3, \dots \\ y_k - y_{k+1}, & k = 1, 4, \dots \end{cases} \quad (4.3)$$



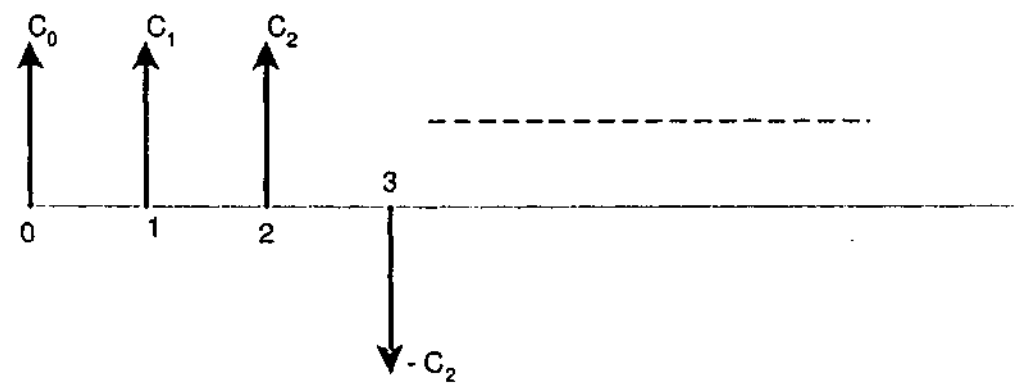
(a)



(b)



(c)



(d)

Figure 4.1: A schematic diagram for different code rates: (a) Uncoded, (b) Rate-half, (c) Rate $\frac{2}{3}$ and (d) Rate $\frac{3}{4}$.

and this reduces to

$$d_k = \begin{cases} S_0 c_k + I_k + n_k, & k = 0, 3, \dots \\ (2S_0 - S_{-1} - S_1) c_k + I_k + (n_k - n_{k+1}), & k = 1, 4, \dots \end{cases} \quad (4.4)$$

where

$$I_k = \begin{cases} \sum_{l=0,3,\dots,l \neq k}^{N-1} S_{l-k} c_l + \sum_{l=1,4,\dots,l \neq k}^{N-1} (S_{l-k} - S_{l+1-k}) c_l, & k = 0, 3, \dots \\ \sum_{l=0,3,\dots,l \neq k}^{N-1} (S_{l-k} - S_{l-k-1}) c_l + \sum_{l=1,4,\dots,l \neq k}^{N-1} (2S_{l-k} - S_{l+1-k} - S_{l-k-1}) c_l, & k = 1, 4, \dots \end{cases} \quad (4.5)$$

Therefore, the average carrier-to-interference ratio (CIR) on subcarrier k can be expressed as

$$\text{CIR}(k) = \begin{cases} \frac{|S_0|^2}{\sum_{l=0,3,\dots,l \neq k}^{N-1} |S_{l-k}|^2 + \sum_{l=1,4,\dots,l \neq k}^{N-1} |S_{l-k} - S_{l+1-k}|^2}, & k = 0, 3, \dots \\ \frac{|2S_0 - S_{-1} - S_1|^2}{\sum_{l=0,3,\dots,l \neq k}^{N-1} |S_{l-k} - S_{l-k-1}|^2 + \sum_{l=1,4,\dots,l \neq k}^{N-1} |2S_{l-k} - S_{l+1-k} - S_{l-k-1}|^2}, & k = 1, 4, \dots \end{cases} \quad (4.6)$$

A similar expression can be derived for rate $\frac{3}{4}$ code. Note that (4.6) consists of two summation terms, one for repeated symbols and the other for non-repeated symbols. For the rate half repetition code, the average CIR on subcarrier k can be expressed as

$$\text{CIR}(k) = \frac{|2S_0 - S_{-1} - S_1|^2}{\sum_{l=0,2l \neq k}^{N/2-1} |2S_{2l-k} - S_{2l+1-k} - S_{2l-1-k}|^2} \quad \text{for } k = 0, 2, \dots \quad (4.7)$$

Eq. (4.6) reveals how ICI is reduced in rate $\frac{2}{3}$ code. This ensures the ICI reduction capability of the proposed scheme. However, in code design point of view, the proposed technique is not an optimum but rather simple solution to improve data throughput.

4.3.1 Simulation Results

Figure 4.2 shows how the average CIR varies with the subcarrier index for $\epsilon = 0.1$. OFDM system with $N = 16$ and QPSK scheme in AWGN channel is assumed in this simulation. The proposed rate $\frac{2}{3}$ and $\frac{3}{4}$ codes perform better than conventional OFDM

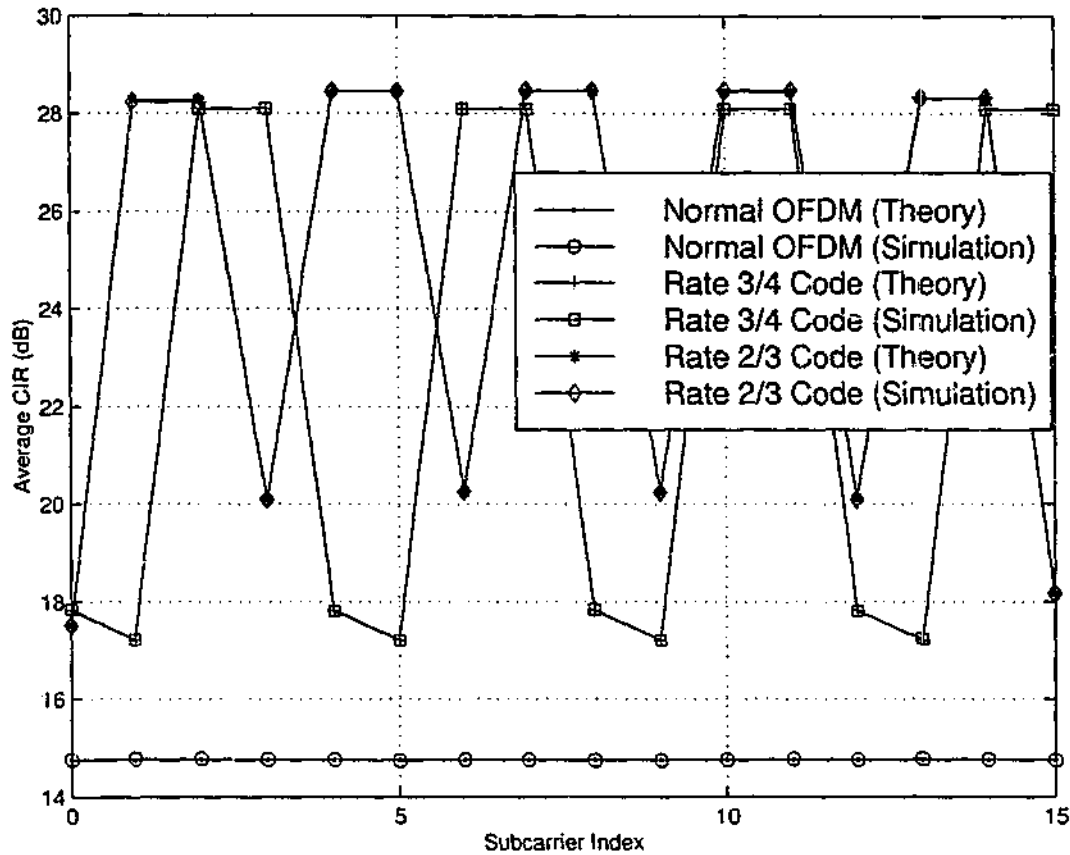


Figure 4.2: Variation of average CIR of rate $\frac{2}{3}$ and $\frac{3}{4}$ codes with subcarrier index.

and rate $\frac{2}{3}$ code performs better than rate $\frac{3}{4}$ code. Note that the average CIR of conventional OFDM does not depend on the subcarrier index. The proposed scheme is expected to have two average CIRs, one for non-repetition symbols and the other for repetition symbols. However, for the rate $\frac{2}{3}$ code, the subcarrier index 0 and $(N - 1)$ shows the lowest CIR comparing with other subcarrier indexes. This is due to non-symmetric structure in the OFDM input block as N is even and not divisible by 3. When N is large, these two values of CIRs are less effect on the overall performance of the system. The rate $\frac{3}{4}$ code shows three levels of CIRs but two of them are almost equal.

Figure 4.3 shows how CIR varies with the normalized frequency offset. Conventional OFDM and the rate-half repetition code are also compared with the new codes. The new codes have two average CIRs, one for non-repetition symbols and the other for repetition symbols. The rate-half repetition code performs better than others since every symbol is repeated to cancel ICI. However, the new codes show significant CIR gain over conventional OFDM with less data throughput loss. The rate $\frac{2}{3}$ code offers 5 to 13 dB gain in CIR over conventional OFDM and that of $\frac{3}{4}$ code is 2.5 to 13 dB.

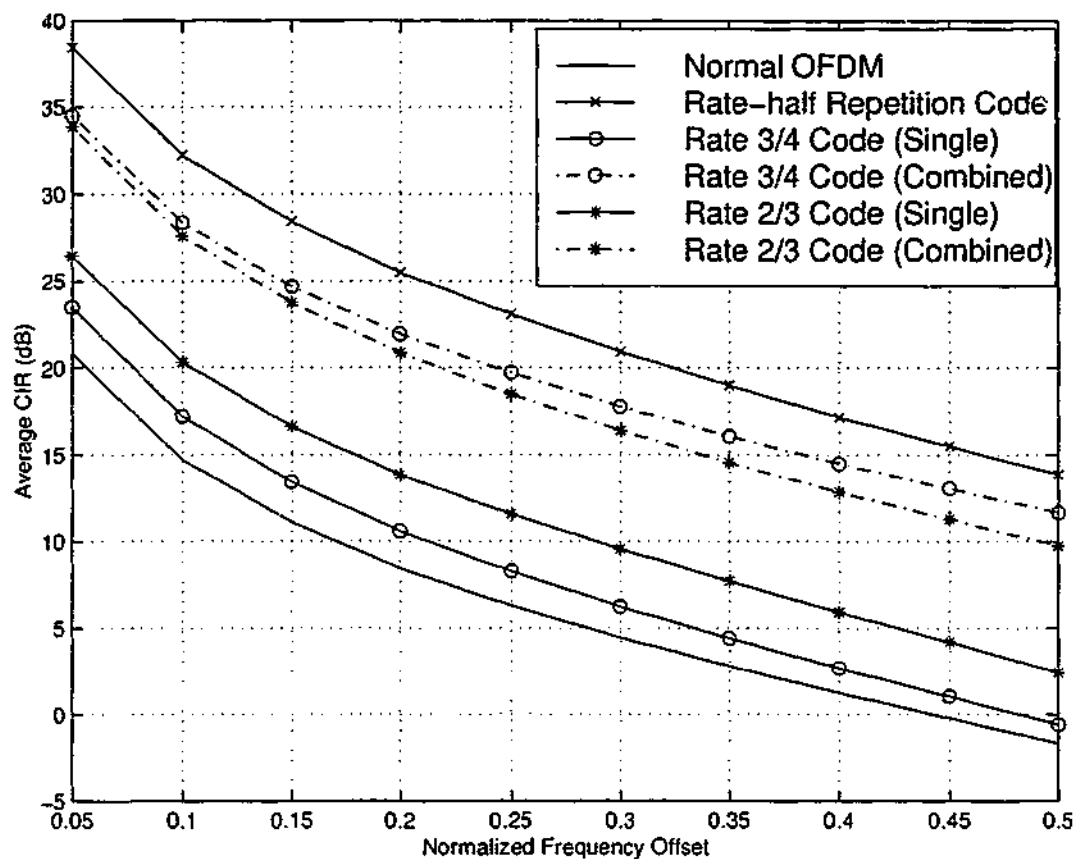


Figure 4.3: Variation of average CIR of rate $\frac{2}{3}$ and $\frac{3}{4}$ codes with ϵ .

Combining the repeated symbols at the receiver offers same CIR in rate $\frac{2}{3}$ and $\frac{3}{4}$ codes. However, $\frac{2}{3}$ code offers more CIR over rate $\frac{3}{4}$ code for the non-repeated symbols.

Figure 4.4 shows the received QPSK constellation for different code rates. Here, noise effect is ignored to visualize the ICI effects in each code. We can visualize how ICI effects are reduced in the coding scheme and they can be traded against code rate.

Figure 4.5 shows the BER performance of the proposed higher rate codes for QPSK with $N = 128$ in AWGN channel. The coding schemes remove the error floor. The SNR gain of coding schemes with code rates of $1/2$, $2/3$ and $3/4$, at a BER of 10^{-4} over conventional OFDM is 7 dB, 5 dB, and 4 dB respectively for a normalized frequency offset of 0.1. In fact, rate $2/3$ and $3/4$ codes decrease the SNR gain over rate-half repetition codes by 2 dB and 3 dB to gain 16% and 25% improvement in data throughput.

The BER performance of the proposed higher rate codes in a multipath fading channel is shown in Figure 4.5. We assume that the multipath fading channel consists of six taps (i.e., $L = 6$) and a rms delay spread of $1\mu\text{s}$ and exact knowledge of channel state information at the receiver. We also assume that the cyclic prefix (CP) eliminates the ISI between consecutive OFDM symbols. The coding schemes, particularly rate

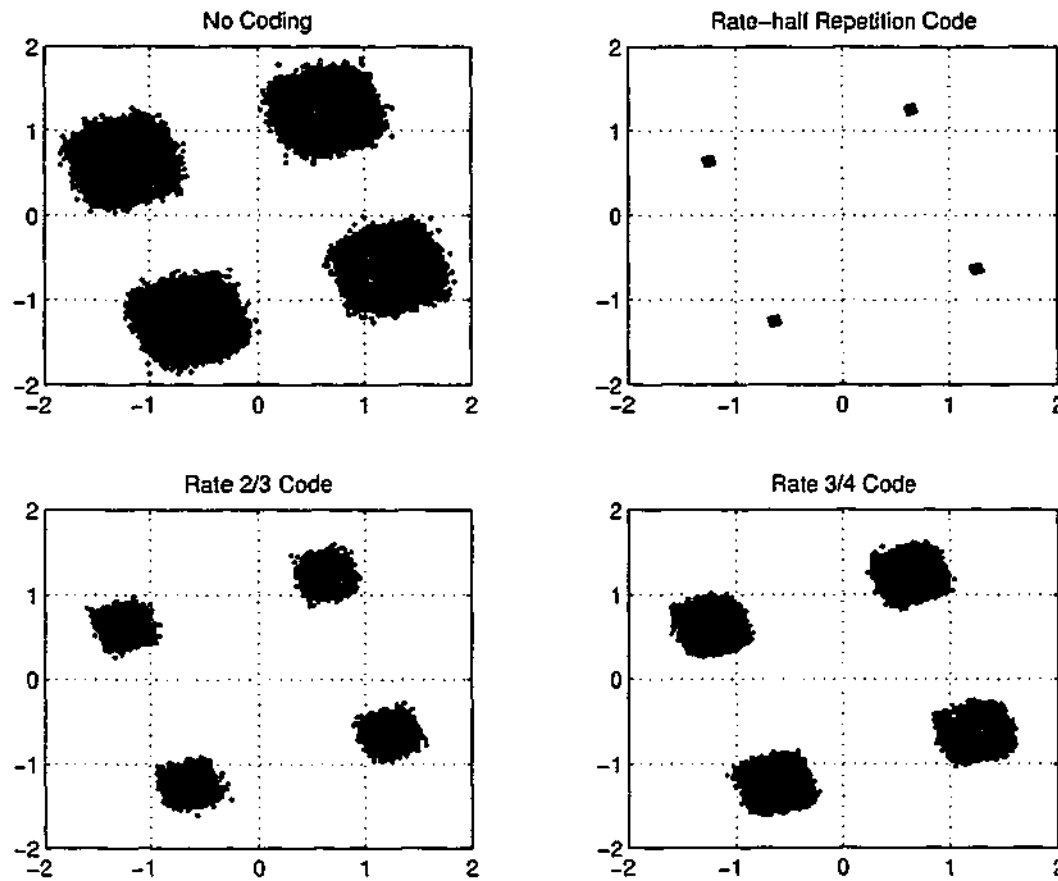


Figure 4.4: QPSK signal constellations for $\epsilon = 0.1$.

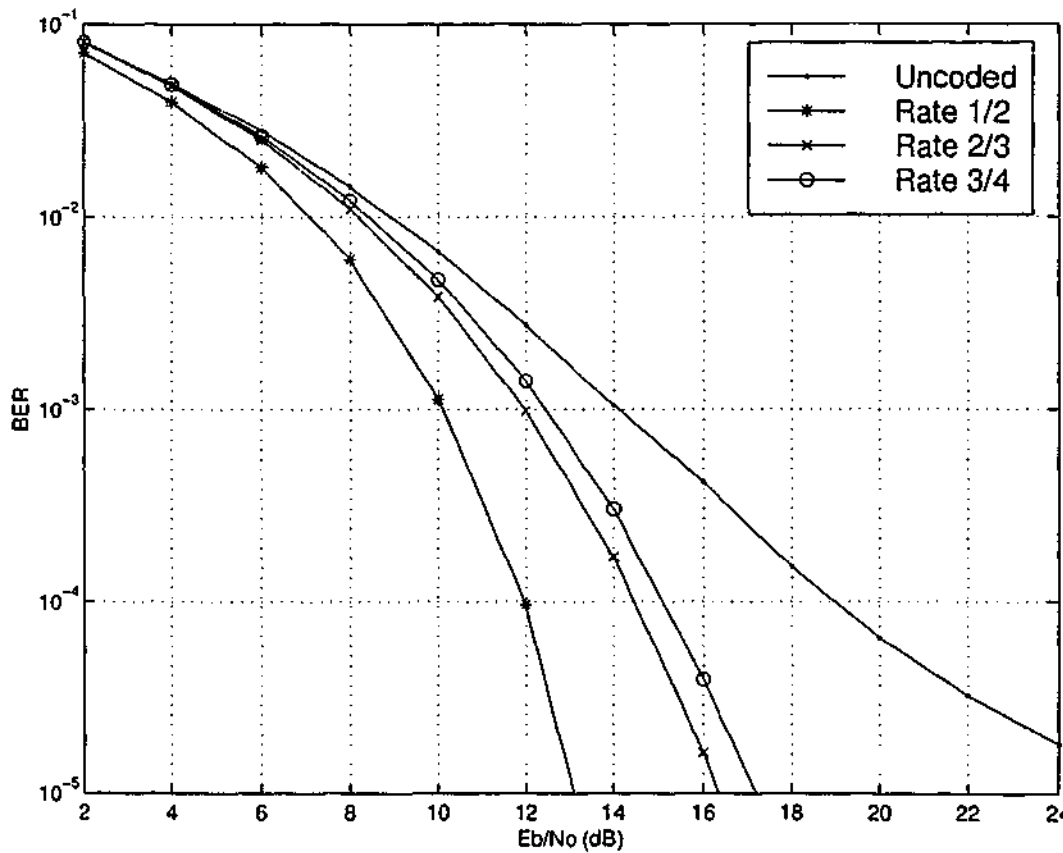


Figure 4.5: BER performance of rate $\frac{2}{3}$ and $\frac{3}{4}$ codes in AWGN channel and $\epsilon = 0.1$.

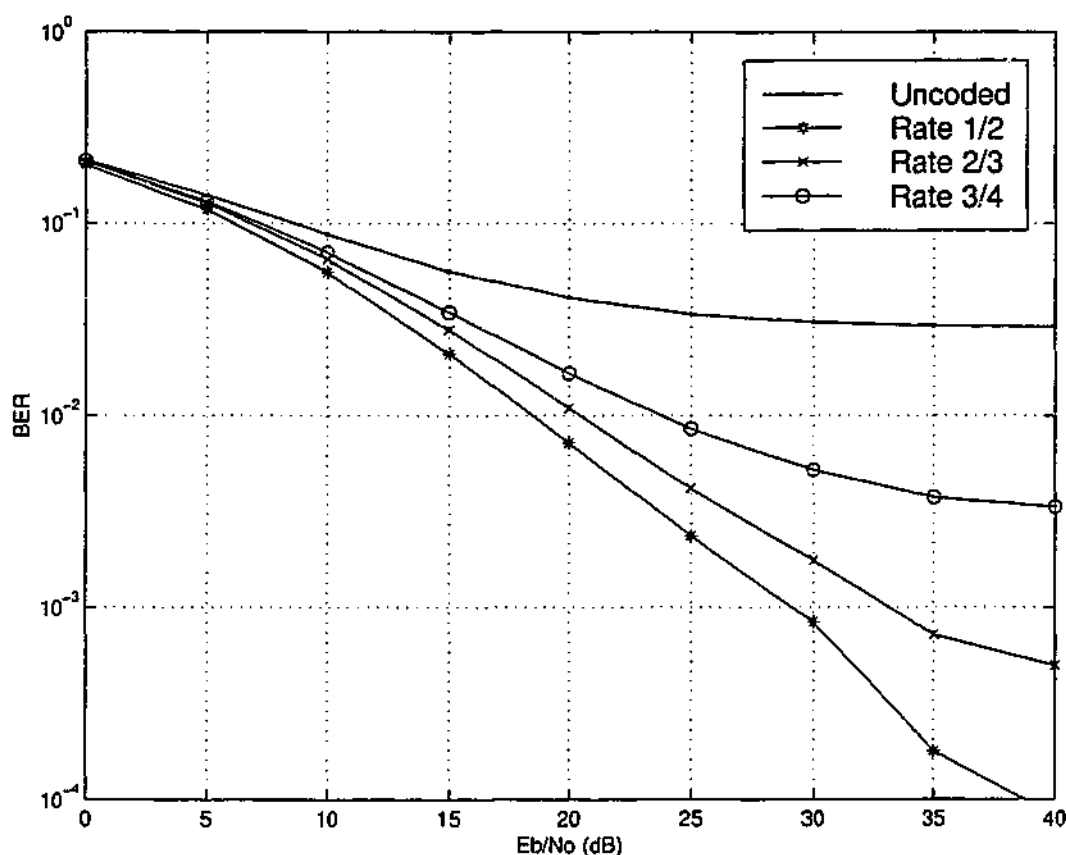


Figure 4.6: BER performance of rate $\frac{2}{3}$ and $\frac{3}{4}$ codes in multipath fading channel and $\varepsilon = 0.1$.

1/2 and 2/3, remove the error floor. Rate 2/3 code decreases the SNR gain over rate-half repetition codes by 3 dB at a BER of 10^{-3} to gain 16% improvement in data throughput.

In practice, the frequency offset caused by either Doppler shift or inaccuracies in the fine-tuning of oscillators will be very small. The proposed coding scheme also offers flexibility to choose different code rate depending on the ICI effects in the channel. The receiver only needs to know the position of the repeated symbols, as a side information, and padding zeros at the appropriate positions enables the same receiver to be used.

4.4 Reducing ICI by using Error Correction Codes

The other simple approach towards the construction of higher rate ICI reduction codes is to use the existing error correction codes. A more powerful error correction code with less redundancy can be used for ICI reduction just as effectively. Note that such a code would not have a direct ICI reduction structure as in rate-half repetition codes. Instead, a higher value of d_{min} would enable it to suppress more errors. It is obvious

that error correction codes will improve the performance of the ICI channel. However, it might be interesting and useful to analytically quantify them. It is also worthwhile to compare the performance of error correction codes with rate-half repetition codes. However, the complexity of error correcting code is higher than that of repetition coding. Given that hardware costs are currently decreasing rapidly, this may become less of an issue.

A rich collection of error correction codes is at our disposal for this application. For example, convolutional codes, Bose Chaudhuri and Hocquenghem (BCH) codes, Reed Soloman (RS) codes, trellis coded modulation and turbo codes are used in many applications. Convolutional codes are widely used in many practical applications such as space and satellite communications and GSM. For these applications, convolutional codes achieve the required performance at a desired information rate using a low complexity decoder [235]. Rate-compatible punctured convolutional (RCPC) codes offer simple Viterbi decoding for high rate convolutional codes, and furthermore, the code rate can be adjusted according to channel variation without changing the decoder [236]. Consequently, RCPC codes offer the flexibility to change the code rate for varying frequency offset values. This is a distinct advantage. For example, the code rate can be increased when there is no Doppler effect in the system.

We study the performance of 1/2, 2/3 and 4/5 rate convolutional codes as a function of the CFO and AWGN. Note that we are primarily interested in comparing the effectiveness of several coding schemes in the suppression of ICI. As such, we do not consider other channel impairments such as fading and shadowing etc. For this reason, performance in Gaussian noise channels with the CFO is evaluated by computer simulation. The NASA standard (2,1,6) convolutional code, with constraint length seven, is considered and 2/3 and 4/5 rate codes were obtained according to rate-compatible puncturing in [236]. We use soft decision Viterbi decoding to improve the coding gain. The Viterbi algorithm is a sequential trellis search for performing Maximum Likelihood sequence detection. The decoder selects the sequence that minimizes the Euclidean distance metric

$$D(y, c^{(m)}) = \sum_k |(y_k - c_k^{(m)})|^2. \quad (4.8)$$

4.4.1 Error Performance of RCPC codes

The Viterbi upper bound for the bit error probability of RCPC codes in AWGN channel is expressed as [236]

$$P_b \leq \frac{1}{P} \sum_{d=d_{free}}^{\infty} c_d P_d \quad (4.9)$$

where P is the puncturing period, d_{free} is the free distance of the code and $\{c_d\}$ is the distance spectra. P_d is the probability that wrong path at distance d is selected and is given by [236]

$$P_d = \frac{1}{2} \text{erfc}(\sqrt{dRE_b/N_o}) \quad (4.10)$$

where R is the code rate. This upper bound is only valid for Gaussian noise. If the ICI is approximated as Gaussian distributed, then the upper bound for bit error probability of RCPC codes with frequency offset can be expressed as

$$P_v \leq \frac{1}{2P} \sum_{d=d_{free}}^{\infty} c_d \text{erfc}(\sqrt{dR\gamma_{eff}}) \quad (4.11)$$

where γ_{eff} is effective SNR defined in (3.20). The Gaussian approximation of ICI is acceptable for BPSK as precise calculation of BER or SER yields almost same results as Gaussian approximation. This bound can be used to study the capability of RCPC codes to reduce ICI if the values of c_d are known.

Figure 4.7 and Figure 4.8 show the BER performance of RCPC codes [Table II(c) in [236]]. Rate-half repetition coding and conventional OFDM are shown for comparison. Note that the performance of the rate-half repetition coding and conventional OFDM are precise whereas that of RCPC is upper bounded. RCPC codes removes the error floor caused by ICI in conventional OFDM and they perform better than rate-half repetition coding for small values of CFOs with gain in data throughput. In fact, these upper bounds confirm that RCPC codes are capable of correcting ICI errors effectively over rate-half repetition coding for small values of CFOs and at high SNRs. Often, CFOs are small in practice. Further, actual BER performance of RCPC codes will offer more coding gain, as the upper bounds are not tight.

4.4.2 Simulation Results

Figure 4.9 shows the BER performance of a convolutionally coded OFDM system, for $N=128$ and QPSK with $\epsilon = 0.1$. The rate-half repetition coding approach is also shown

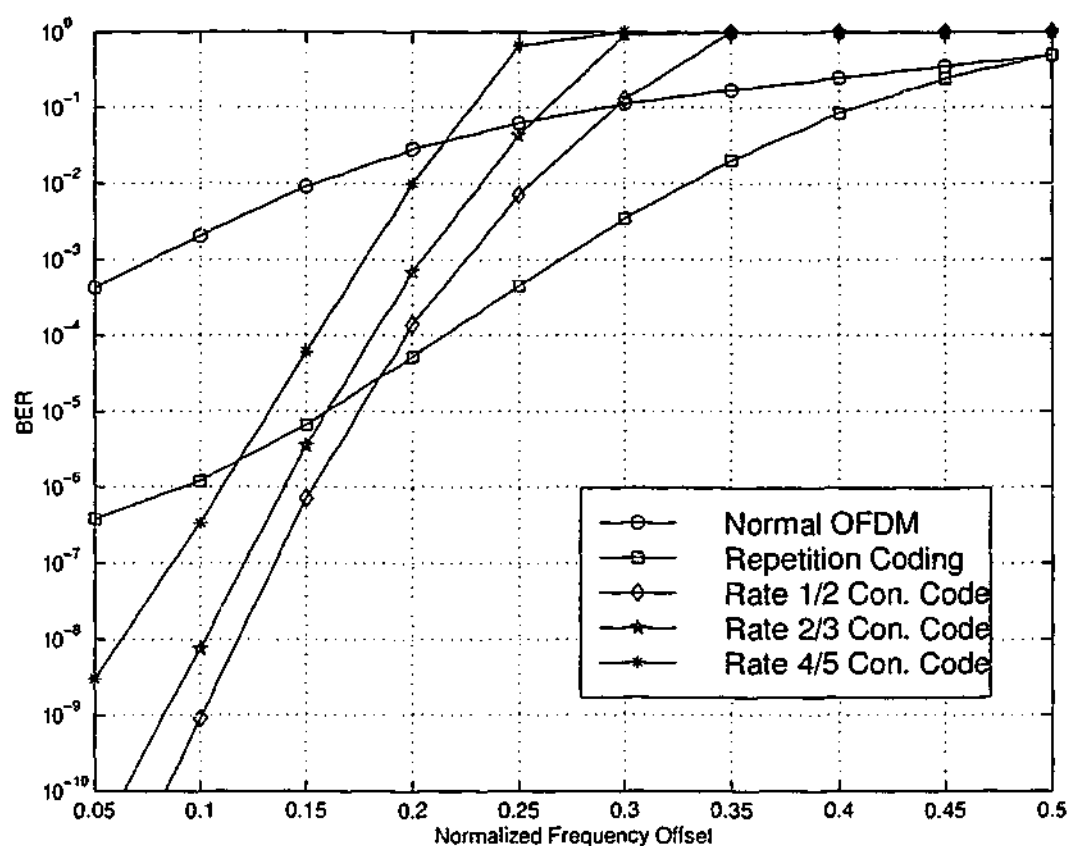


Figure 4.7: BER performance for BPSK with $\epsilon = 0.1$ (upper bound).

in Figure 4.9 for the purpose of comparison. Here, we used RCPC codes with code rates of 1/2, 2/3 and 4/5.

Covolutional codes perform worse than conventional OFDM for small values of SNR, whereas rate-half repetition coding always performs better than conventional OFDM. This is due to additive Gaussian noise dominating the ICI at low SNRs. Nevertheless, the coding scheme rapidly improves the BER performance at high SNR and convolutional codes perform better than the repetition coding and conventional OFDM. The performance gain is due to the increase in the minimum distance for the convolutional codes. The SNR gain of repetition coding and convolutional codes with code rates 1/2, 2/3 and 4/5, at a BER of 10^{-3} over conventional OFDM is 6.8 dB, 10 dB, 8.5 dB and 6.5 dB respectively for a normalized frequency offset of 0.1. At any BER less than 10^{-3} , the rate-half convolutional code offers an SNR gain of more than 3dB over rate-half repetition coding, but both have the same data throughput. In fact, all three convolutional codes perform better than the rate-half repetition coding for BER less than 10^{-3} . A similar phenomenon can be expected for a small frequency offset value.

Figure 4.10 shows the variation of the BER with the normalized frequency offset

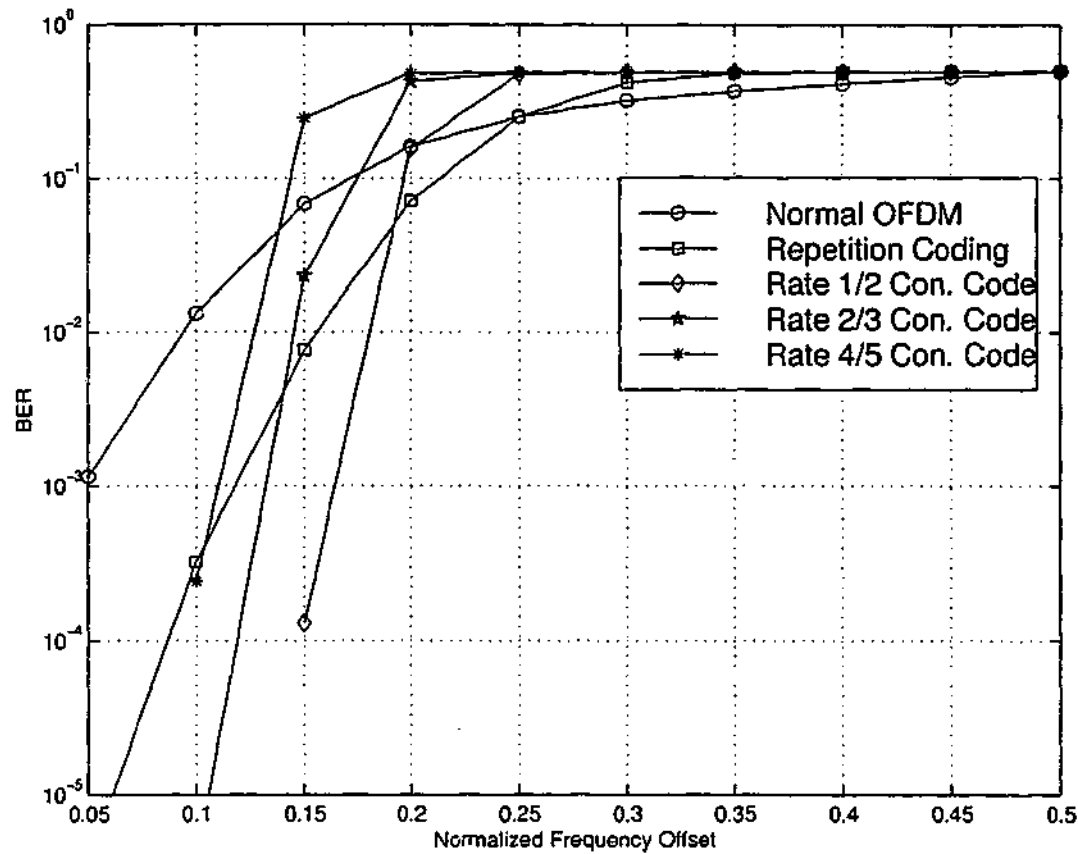


Figure 4.8: Variation of BER of BPSK with ϵ and $E_b/N_0 = 8$ dB (upper bound).

for an SNR of 8 dB. Convolutional codes perform better than the rate-half repetition coding and conventional OFDM for normalized frequency offsets less than 0.125. In practice, the frequency offset caused by either Doppler shift or inaccuracies in the fine-tuning of oscillators will be very small.

The 4/5 rate convolutional code offers a 0.5 dB SNR gain at a BER of 10^{-4} and a 30% gain in the data throughput over the repetition code. Nevertheless, the rate-half repetition coding technique may be preferable if the system is expected to deal with large frequency offsets. Using an RCPC code, we may adaptively vary the data throughput based on ICI effects. This can perhaps be realized in OFDM based automatic repeat request systems such as wireless LANs. The price for these benefits is decoding complexity. However, this may be acceptable, as Viterbi decoders are widely available and used in many communication systems. One can also surmise that in fading environments, the use of more sophisticated codes such as RCPC codes will be more advantageous than the use of repetition coding.

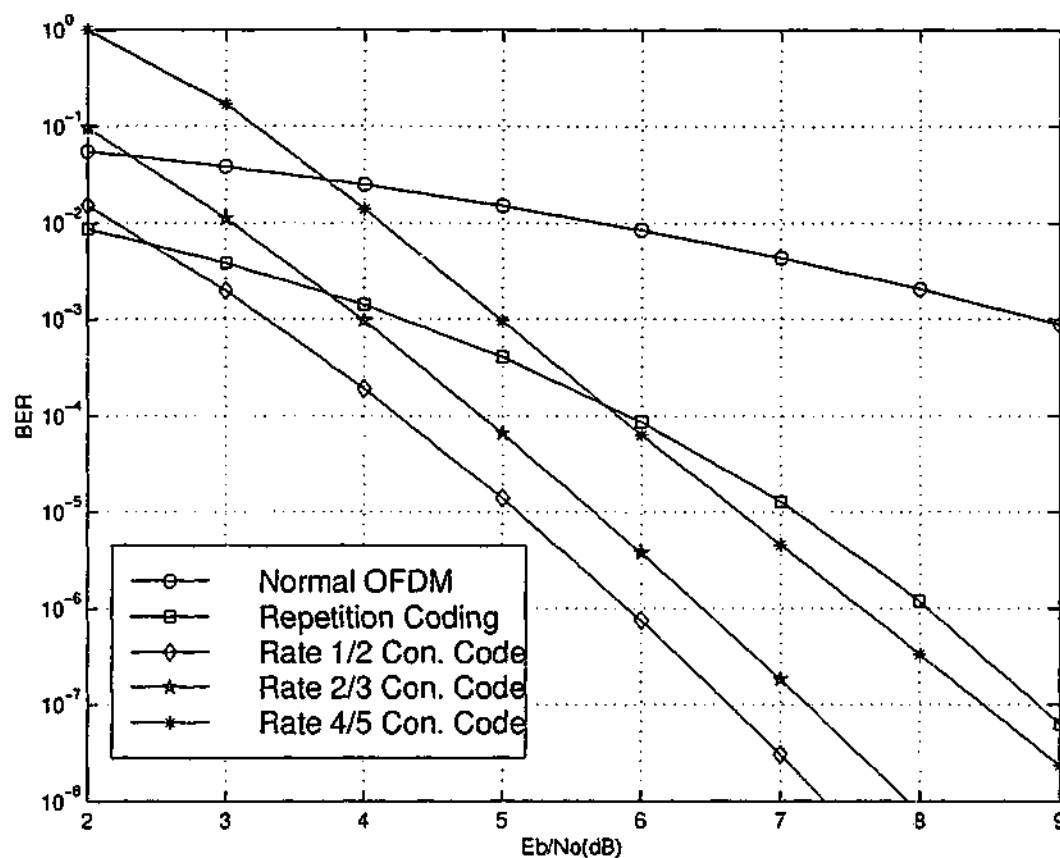


Figure 4.9: BER performance for QPSK with $\varepsilon = 0.1$.

4.5 Conclusions

This chapter has presented some high rate coding schemes to reduce ICI. One approach is based on a systematic way of symbol repetition and the other is the use of RCPC codes. The data throughput of these codes is higher than that of rate-half repetition codes and their error performance is comparable to rate-half repetition codes. However, the algebraic construction of codes for ICI reduction is still difficult. This is partially due to the nature of the ICI problem itself. To overcome this difficulty, we introduce a new measure for ICI in the next chapter.

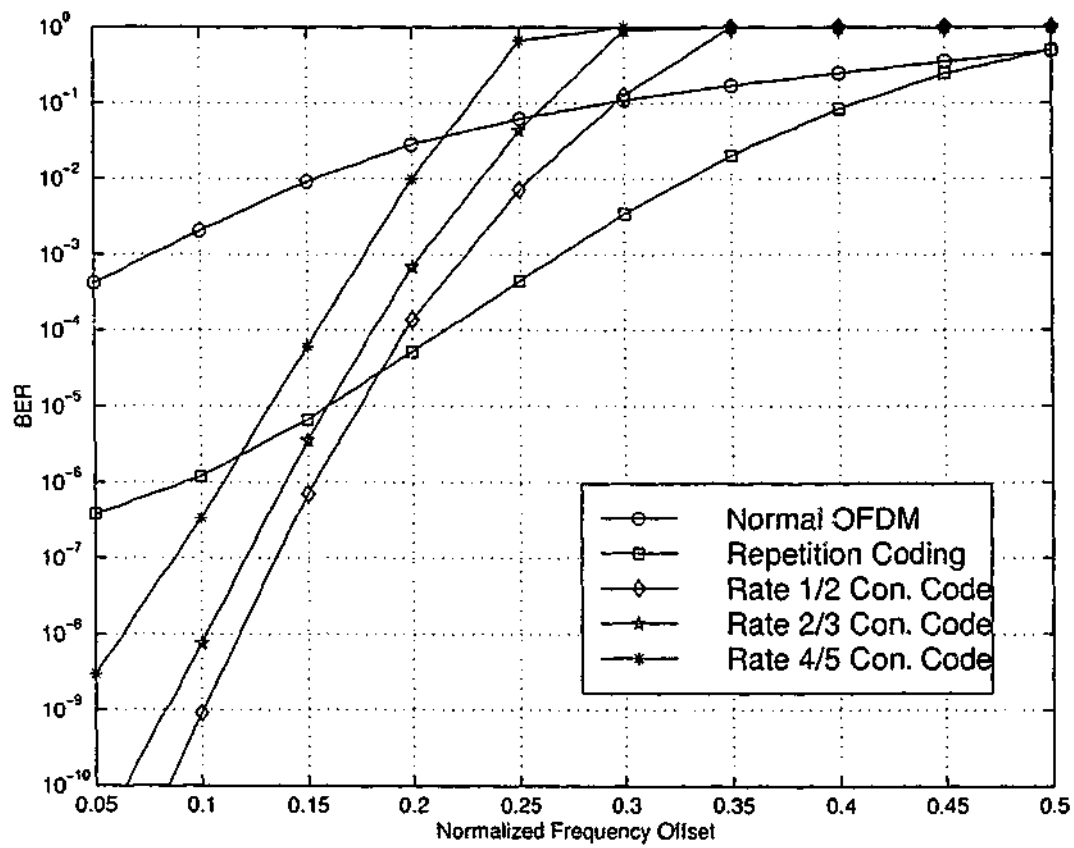


Figure 4.10: Variation of BER of QPSK with ϵ and $E_b/N_0 = 8$ dB.

Chapter 5

Peak Interference-to-Carrier Ratio (PICR)

This chapter introduces a measure, peak interference-to-carrier ratio (PICR), to quantify ICI due to CFO. This PICR can be calculated at the transmitter to predict the ICI effects at the receiver. The definition of PICR formulates the ICI problem in parallel with the PAR issue. An analytical expression is derived to show the relationship between PICR and the BER. We show that the PICR can be reduced by coding to select only those messages with a low PICR as valid codewords, via analytical and computer simulation results. Since the PICR problem is analogous to the PAR issue, we investigate some PAR reduction techniques for PICR reduction. One of them is the tone reservation, that inserts optimized pilot tones in the data frame. We also show that PICR can be reduced by SLM and PTS approaches. In SLM, several different OFDM symbols representing the same information are generated and the OFDM symbol with the lowest PICR is selected for transmission. In PTS, blocks of subcarriers are multiplied by a set of phase factors that are optimized to minimize the PICR. These schemes are analyzed theoretically and their performances are evaluated by simulation. We also show the existence of codes to reduce both the PAR and PICR simultaneously. The coding scheme is based on selecting only those messages with both low PAR and PICR as valid codewords. We identify those codes by computer search. As an example of an explicit construction for such codes, we construct Golay complementary repetition codes that can reduce both PAR and PICR simultaneously.

5.1 Introduction

Controlling the PAR of an OFDM signal has recently received much attention. The use of various coding strategies is a key idea to reduce the PAR (see [107, 151, 162, 164] for several examples of this nature). As few data frames result in large signal peaks, block codes can be designed so that such data frames are never used. Consequently, the PAR is reduced [151]. However, this block coding scheme requires a look-up table approach for encoding and decoding. The Reed-Muller codes and Golay complementary sequences are very attractive for PAR reductions as their encoding and decoding process are algebraically determined [107, 162, 164]. Despite their very low code rate, they limit the PAR below 3 dB for any value of N . On the other hand, several coding techniques have been proposed to reduce ICI effects caused by the carrier frequency offset. This includes error control codes [60–63], correlative coding [64] and rate-half repetition coding [65–70]. However, there is no parameter/measure available at the transmitter to specify or optimize when designing such codes. Despite this requirement, the proposed coding schemes are effective in reducing ICI. Moreover, several PAR reduction techniques are devised due to the availability of the measure (i.e., PAR) at the transmitter. Motivated by this observation, we introduce PICR and formulate the carrier frequency offset problem in parallel with the PAR issue in OFDM.

Consider the received signal sample for the k -th subcarrier after the DFT processing, expressed as (2.29)

$$y_k = c_k S_0 + \sum_{l=0, l \neq k}^{N-1} S_{l-k} c_l + n_k; k = 0, \dots, N-1 \quad (5.1)$$

where

$$S_k = \frac{\sin \pi(k + \varepsilon)}{N \sin \frac{\pi}{N}(k + \varepsilon)} \exp \left[j\pi \left(1 - \frac{1}{N}\right)(k + \varepsilon) \right] \quad (5.2)$$

and c_k denotes the transmitted symbol for the k -th subcarrier. We shall refer to $\mathbf{c} = (c_0, c_1, \dots, c_{N-1})$ as a data frame or codeword, as appropriate; also \mathbf{c} is a constellation symbol from an encoder. The ICI term can be expressed as (2.30)

$$I_k = \sum_{l=0, l \neq k}^{N-1} S_{l-k} c_l, \quad \text{for } 0 \leq k \leq N-1. \quad (5.3)$$

Note that I_k is a function of both \mathbf{c} and ε . In the sequel, we would be interested in reducing the peak magnitude of I_k .

and is equal to

$$\text{PICR}(\mathbf{c}) = \max_{0 \leq k \leq N-1} \left\{ \frac{\left| \sum_{l=0, l \neq k}^{N-1} S_{l-k} c_l \right|^2}{|S_0 c_k|^2} \right\}. \quad (5.8)$$

Therefore, the PICR is a function of both \mathbf{c} and ϵ . PICR is the maximum interference-to-signal ratio for any subcarrier. In other words, it specifies the worst-case ICI on any subcarrier.

To reduce ICI effects, (5.7) should be minimized and is zero for ICI-free channels. Interestingly, our definition (5.7) is similar to PAR issue in OFDM [164, 172, 180, 183, 185]. However, the PICR problem differs from the PAR issue in several ways:

- ICI occurs at the receiver side, whereas high PAR values affect the transmitter.
- Exact computation of PAR requires oversampling, whereas $\max |I_k|$ is obtained from N samples.
- As the transmitter does not know ϵ a priori, PICR can be computed only on the basis of a worst-case value, $\epsilon_{wc} > 0$. Therefore, the performance of a PICR reduction scheme should hold for any $|\epsilon| < \epsilon_{wc}$.

Bound for PICR

Using the Cauchy-Schwarz bound $|\sum a_k b_k|^2 \leq \sum |a_k|^2 \sum |b_k|^2$, we have

$$\text{PICR}(\mathbf{c}) \leq \frac{\max_{0 \leq k \leq N-1} (N-1) \sum_{l=0, l \neq k}^{N-1} |S_{l-k}|^2}{|S_0|^2} \quad (5.9)$$

which is a bound independent of \mathbf{c} . Like (5.6), (5.9) reduces to

$$\text{PICR}(\mathbf{c}) \leq \frac{N-1}{\frac{3}{(\pi\epsilon)^2} - 1}. \quad (5.10)$$

Despite being rather loose, this bound shows that the PICR increases with increasing N and ϵ . Note that (5.10) reduces to zero for $\epsilon = 0$. For a code \mathcal{C} , we define

$$\text{PICR}(\mathcal{C}) = \max_{\mathbf{c} \in \mathcal{C}} \text{PICR}(\mathbf{c}). \quad (5.11)$$

For $\mathcal{C}_{\frac{1}{2}}$, the PICR can be expressed as

$$\text{PICR}(\mathbf{c}) = \frac{\max_{0 \leq k \leq N-1} \left| \sum_{l=0, 2l \neq k}^{N/2-1} (S_{2l-k} - S_{2l+1-k}) c_l \right|^2}{|(S_0 - S_1) c_k|^2}. \quad (5.12)$$

Since S_k 's are varying slowly, we can assume $S_{k+1} \approx \alpha S_k$ where α is a constant. Thus, (5.12) reduces to

$$\text{PICR}(c) \leq \frac{\max_{0 \leq k \leq N-1} (N/2 - 1) \sum_{l=0, 2l \neq k}^{N/2-1} |S_{2l-k}|^2}{|S_0|^2}. \quad (5.13)$$

5.2.3 Complementary Cumulative Density Function (CCDF) of PICR

Figure 5.1 shows the Complementary Cumulative Distribution Function (CCDF) of PICR as a function of N for $\varepsilon = 0.1$. The subcarriers are modulated with binary phase shift keying (BPSK). This illustrates how PICR is dependent on the data frame and varies with N . From (5.6), the average ICR is approximately -14.6 dB for any value of N with $\varepsilon = 0.1$. For $N = 64$, the PICR exceeds -5 dB for only 1 out of 10^5 of all OFDM blocks and for 90% of all OFDM blocks, the PICR is below -8 dB. Therefore, the PICR can be considered as a random variable; for some data frames the PICR can be high and for others the PICR can be low. This PICR characteristic again shows the similarity with the PAR issue.

It is worthwhile to derive an analytical expression for the CCDF of PICR. However, finding an exact statistical distribution of I_k is difficult. Since I_k is the weighted summation of independent random variable, it can be approximated by a Gaussian distribution, according to the central limit theorem. This is particularly true for large N , which is the usual case. Note that this Gaussian approximation is widely used in the analysis of error rate performance with ICI.

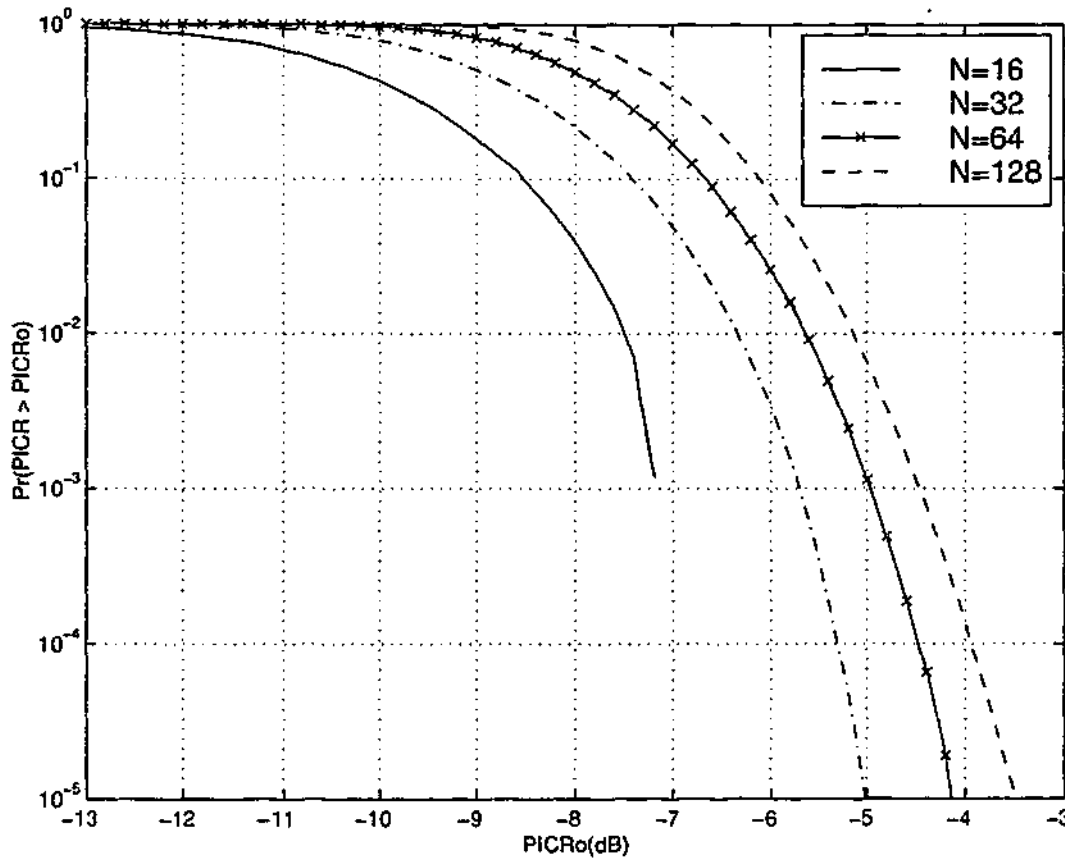
Consider the ICI on k -th subcarrier (2.29)

$$I_k = \sum_{l=0, l \neq k}^{N-1} S_{l-k} c_l, \quad \text{for } 0 \leq k \leq N-1 \quad (5.14)$$

and its variance is given by

$$\sigma_i^2 = \sum_{l=0, l \neq k}^{N-1} |S_{l-k}|^2. \quad (5.15)$$

We assume I_k is Gaussian distributed with zero mean and variance of σ_i^2 . Consequently, the ICI amplitude $r_k = |I_k|$ becomes Raleigh distributed with a probability density

Figure 5.1: CCDF of PICR of an OFDM system as a function of N .

function (pdf) given by

$$f_{r_k}(r) = \frac{2r}{\sigma_i^2} \exp\left(\frac{-r^2}{\sigma_i^2}\right), \quad r \geq 0 \quad (5.16)$$

and the power $p_k = r_k^2$ approaches a chi-squared distribution with two degrees of freedom and its cumulative distribution function (CDF) is given by

$$Pr(p_k \leq p) = 1 - \exp\left(\frac{-p}{\sigma_i^2}\right). \quad (5.17)$$

Assuming the samples are mutually independent and uncorrelated, we can approximate the CDF of $\max(p_0, p_1, \dots, p_{N-1})$ by

$$Pr(\max(p_k) \leq p) = \left[1 - \exp\left(\frac{-p}{\sigma_i^2}\right)\right]^N. \quad (5.18)$$

By changing the variable, the CCDF of PICR of an OFDM signal can then be expressed as

$$Pr(\text{PICR} \geq \text{PICR}_o) = 1 - \left[1 - \exp\left(\frac{-\text{PICR}_o}{\sigma_i^2}\right)\right]^N. \quad (5.19)$$

Figure 5.2 shows the approximate CCDF of PICR for $N = 16$ and $N = 512$ with $\epsilon = 0.1$. For large N , this approximation is very close to simulation results.

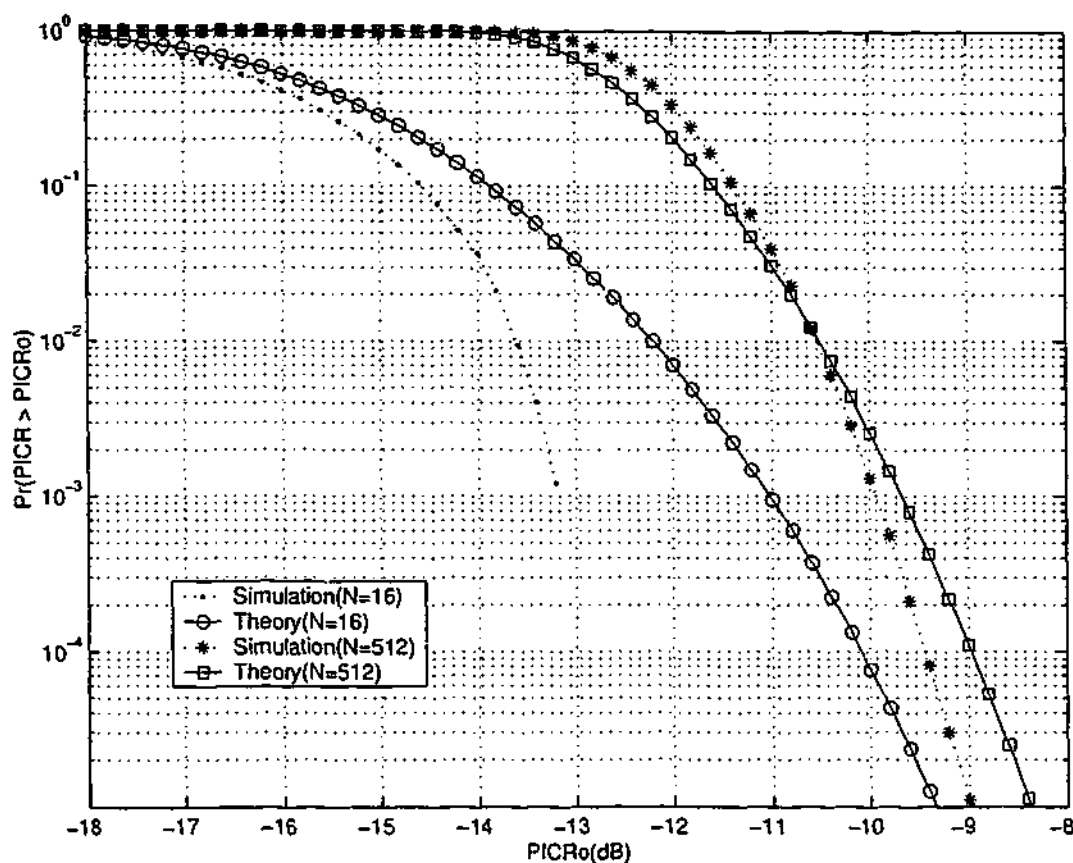


Figure 5.2: CCDF of PICR for an OFDM system with N and ϵ .

However, this approximation does not provide any proper upper bound for any N . This approximation seems to be an upper bound only for large PICR values. Despite the large variation between the simulation and this approximate results for small N , this approximation may be considered as an upper bound for small N .

5.2.4 PICR and BER Relationship

It would be desirable to find the relationship between BER and PICR. As the exact BER is a complicated function of ICI, the precise relationship between PICR and BER has eluded us. We are however able to present a weaker relationship. In [230], the upper bound for the BER is derived in terms of maximum ICI (I_{max}) for Binary Phase Shift Keying (BPSK). Using the approach of [230] and our definition of PICR, an upper bound for the BER of BPSK can be expressed as

$$\text{BER} \leq \frac{1}{4} \left[\text{erfc}\{\lambda(1 - \sqrt{\text{PICR}})\} + \text{erfc}\{\lambda(1 + \sqrt{\text{PICR}})\} \right] \quad (5.20)$$

where $\lambda = \frac{|S_0|}{\sqrt{2}\sigma}$ and $\text{erfc}(x) = 1 - \frac{2}{\sqrt{\pi}} \int_0^x e^{-t^2} dt$.

Figure 5.3 shows this upper bound as a function of PICR for $\epsilon = 0.1$. As expected,

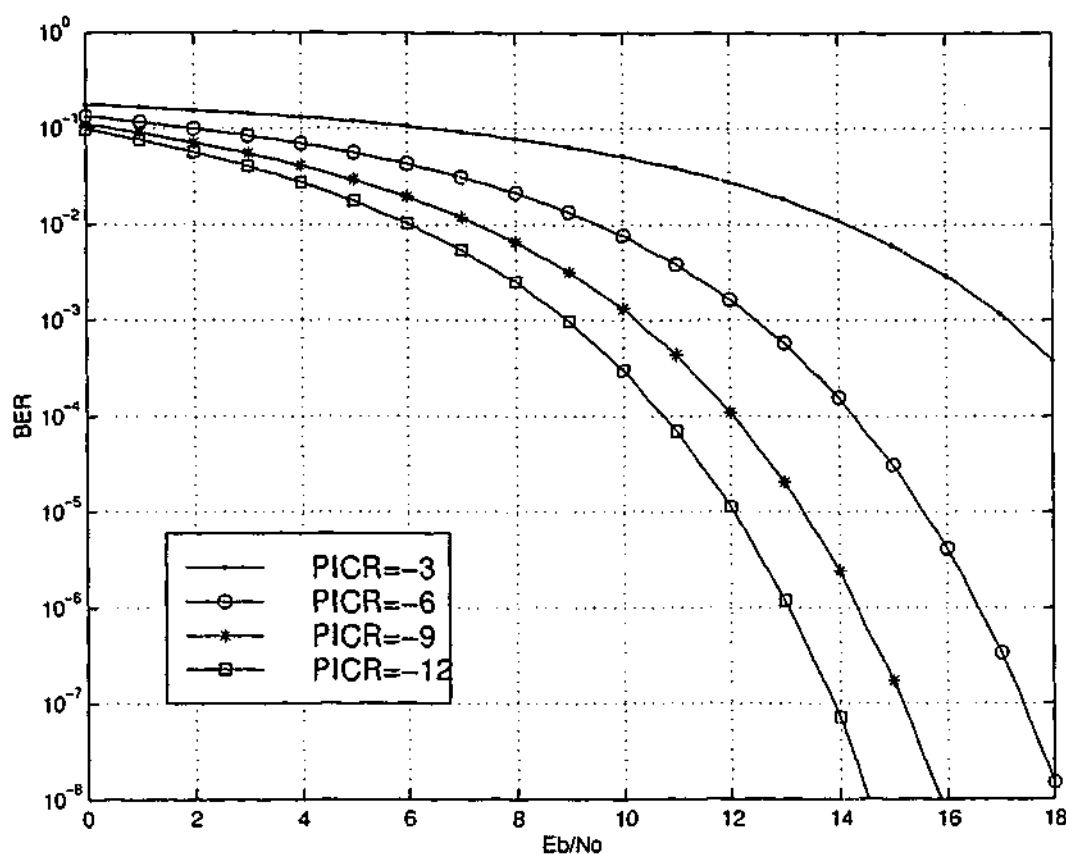


Figure 5.3: Upper bound for the BER of BPSK OFDM system with $N = 128$ and $\varepsilon = 0.1$.

the PICR reduction improves the error performance. Moreover, the improvement in error performance is not significant at low SNR. This is due to noise dominating the ICI effects.

The relationship between the average PICR and BER is interesting. Figure 5.4 shows the variation of BER with PICR as a function of N and ε . The subcarriers are modulated with BPSK and $N = 128$. For comparison, performance of $C_{\frac{1}{2}}$ is also shown in Figure 5.4. This illustrates that reducing PICR will effectively improve the BER performance of the system.

5.3 PICR Reduction by Coding

We next state the main problem arising from the PICR definitions. What is the achievable region of triplets $(R, d, \text{PICR}(C))$ for length N ?

So the problem at hand is to find out all the codewords in C that minimize the PICR for a fixed ε and have error correcting capability with high code rate. Moreover, the code should be independent of CFO. Once the code is designed for a worst case

The admissible sequences $\mathbf{c} \in F_q^N$ are called codewords, and the ensemble of all possible codewords is a code C of rate

$$R = \log_2 (|C|) / (N \log_2 (q)) \quad (5.4)$$

where $|C|$ is the number of codewords of C . We also denote by d the minimum Euclidean distance of C . We will denote the rate-half repetition codes by $C_{\frac{1}{2}}$. For any $\mathbf{c} \in C_{\frac{1}{2}}$, $\mathbf{c} = (c_0, -c_0, c_1, -c_1, \dots)$.

5.2 PICR Problem Formulation

5.2.1 Average Interference-to-Carrier Ratio (ICR)

A conventional measure of ICI is the average carrier-to-interference ratio (CIR). The CIR and its reciprocal, average interference-to-carrier ratio (ICR), have previously been used by many authors to study the effects of ICI [64,66,68]. The average ICR for subcarrier k can be expressed as

$$\text{ICR}(k) = \frac{E \left\{ \left| \sum_{l=0, l \neq k}^{N-1} S_{l-k} c_l \right|^2 \right\}}{|c_k S_0|^2} = \frac{\sum_{l=0, l \neq k}^{N-1} |S_{l-k}|^2}{|S_0|^2} \quad (5.5)$$

where $E\{\cdot\}$ denotes the expected value over the distribution of data, $|c_k|^2 = 1$ for unit amplitude constellation such as PSK. As in (2.36), we can approximate (5.5) to

$$\text{ICR} \approx \frac{(\pi\epsilon)^2}{3}. \quad (5.6)$$

Hence, average ICR does not vary with k and not depend on the data frame. However, it does not provide any insight of the ICI effects in a OFDM block basis. Therefore, it is much useful to define a parameter that specifies the ICI effects on a block by block basis. This is further enhanced by the fact that ICI on each subcarrier (i.e. I_k) depends on the data frame in each OFDM block.

5.2.2 PICR Definition

We define the Peak Interference-to-Carrier Ratio (PICR) as

$$\text{PICR}(\mathbf{c}) = \max_{0 \leq k \leq N-1} \left\{ \frac{|I_k|^2}{|S_0 c_k|^2} \right\} \quad (5.7)$$

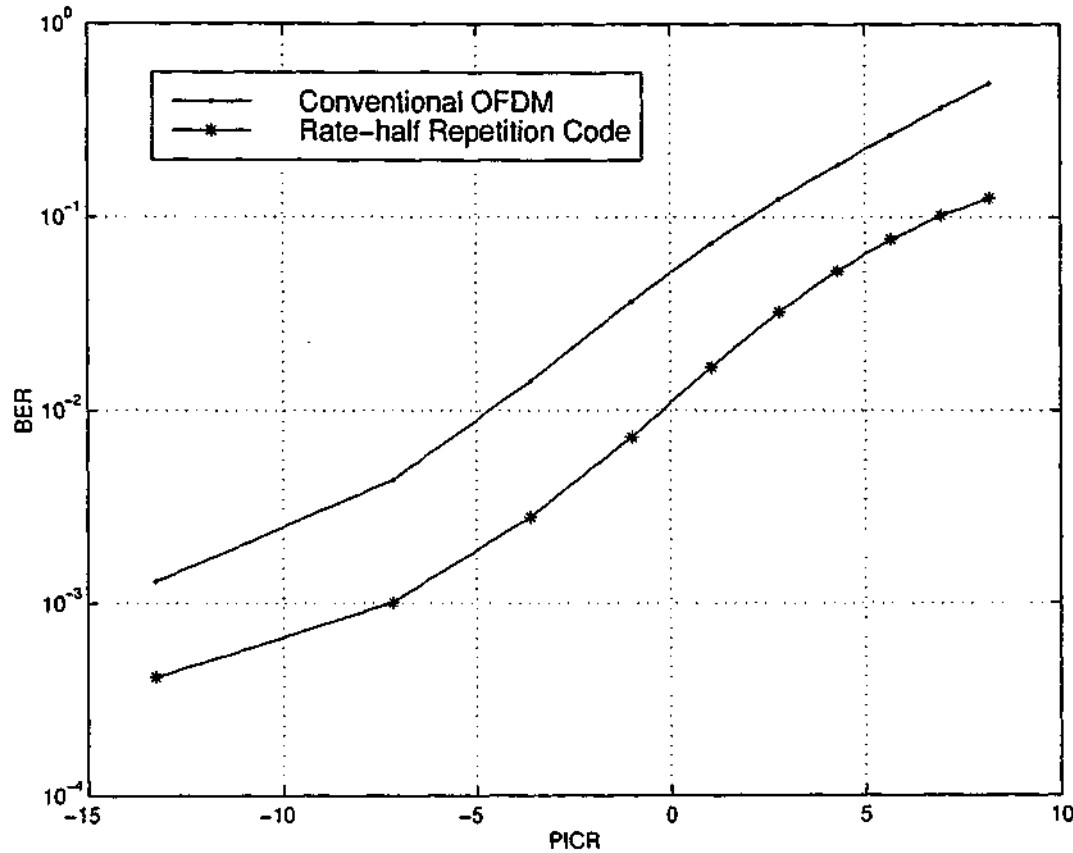


Figure 5.4: Variation of BER with average PICR for an OFDM system with $N = 128$.

CFO (ϵ_{wc}), it should be robust to any low CFO ($|\epsilon| < \epsilon_{wc}$).

5.3.1 Independence in PICR Performance on Frequency Offset

The key motivation for PICR definition is to illustrate the ICI effects on block by block basis. That is to exploit the fact that ICI depends on the data frame \mathbf{c} . Note that the exact value of ϵ is not known a priori. Therefore, the performance of a PICR reduction scheme should be independent of ϵ . For example, the rate-half repetition codes [66, 68] perform independent of ϵ .

To show this independent property of the PICR, assume the maximum PICR on a codeword \mathbf{c}_m occurs at the k_{max} -th subcarrier, where $k_{max} \in \{0, 1, \dots, N-1\}$. Without loss of generality, we can also assume $|c_k|^2 = 1$ (for $k = 0, \dots, N-1$). Therefore the PICR of codeword \mathbf{c}_m can be expressed as

$$\text{PICR}(\mathbf{c}_m) = \frac{\left| \sum_{l=0, l \neq k_{max}}^{N-1} S_{l-k_{max}} c_l \right|^2}{|S_0|^2}. \quad (5.21)$$

This can be expanded as

$$\text{PICR}(\mathbf{c}_m) = |w_0 c_0 + w_1 c_1 + \dots + w_{N-1} c_{N-1}|^2 \quad (5.22)$$

where w_l is given by

$$w_l = \frac{S_{l-k_{max}}}{|S_0|}. \quad (5.23)$$

Therefore, the $\text{PICR}(\mathbf{c}_m)$ is the linear combinations of w_l 's (for $l = 0, \dots, N-1$), where w_l s are function of ε . Moreover, k_{max} does not depend on ε for a particular codeword. Therefore, the same subcarrier k_{max} always exposes to maximum $\text{PICR}(\mathbf{c}_m)$ for any ε , despite its PICR value. In other words, for a particular codeword, the relative ICI effects are always same among the subcarriers in spite of ε .

Now consider the code \mathcal{C} , consisting of all codewords (say L) of length N . For ε_1 , the PICR of the code can be arranged as

$$\text{PICR}(\mathbf{c}_1) > \text{PICR}(\mathbf{c}_2) > \dots > \text{PICR}(\mathbf{c}_L) \quad (5.24)$$

where $\mathbf{c}_m \in \mathcal{C}$ for $m = 1, 2, \dots, L$. Since the maximum $\text{PICR}(\mathbf{c}_m)$ is always on the same subcarrier, the PICR of the code for ε_2 also satisfies (5.24). Therefore, (5.24) holds for any ε . Thus, the relative PICR performance of a code is independent of ε . Further, this independence property holds as long as all the codewords are under same change. For instance, if all the codewords are phase rotated, then (5.24) will still hold true.

5.3.2 PICR Reduction by Block Coding

Since PICR is a function of \mathbf{c} , coding to select only those data frames with low PICR as valid codewords can reduce PICR. To the best of our knowledge, such an approach for ICI reduction has not been proposed or studied before. Here we show the existence of such PICR-reduction codes by computer simulation.

The achievable code rate of the PICR-reduction codes for a threshold value, PICR_0 can be expressed as

$$R(\text{PICR}_0) = \frac{\log_2[q^N \Pr\{\text{PICR}(\mathbf{c}) < \text{PICR}_0\}]}{\log_2 q^N} \quad (5.25)$$

where q is the signal constellation size.

Figure 5.5 shows how the achievable code rate varies with PICR_0 corresponding to the CCDF in Figure 5.1. For example, the PICR (for $N = 64$) can be limited to -7 dB

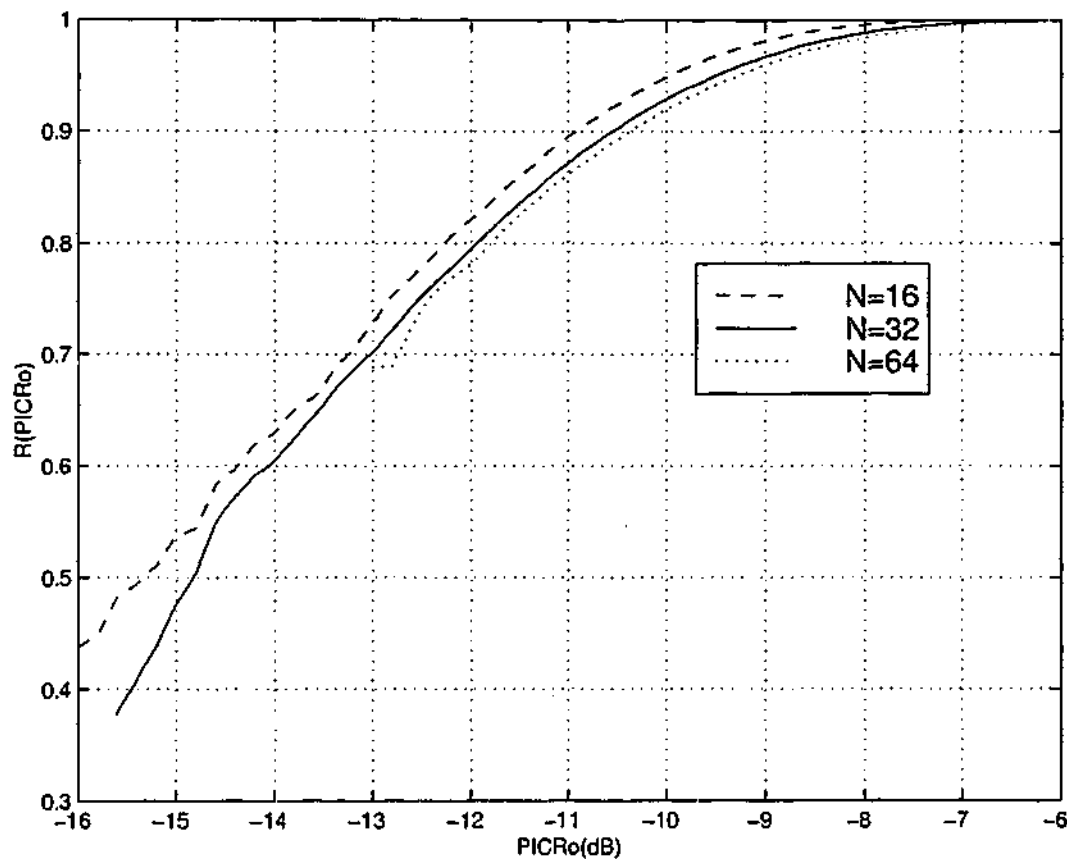


Figure 5.5: Variation of code rate with PICR_0 .

with almost unity code rate whereas in the uncoded case, the PICR is less than -7 dB with a probability of 0.9. Thus, avoiding codewords with high PICR will improve the statistical properties of ICI. This will significantly reduce the overall ICI effects.

To illustrate the existence of PICR-reduction codes, consider an OFDM system with $N = 4$ and BPSK-modulated subcarriers. The PICR for all data frames is given in Table 5.1 in ascending order. Note that 10 data frames result in the maximum PICR of -18.56 dB for $\epsilon = 0.05$. Clearly, we can reduce the PICR by avoiding transmitting these frames. This can be done by block coding the data such that 2 bits of data are mapped on to 4 best data frames. Such a block code would reduce the PICR by about 2 dB for any offset ϵ . The reason is that the complete rank-ordering of all codewords is independent of the frequency offset. This also proves our previous analytical derivation of independent PICR performance over ϵ .

The rate-half repetition codes exhibits the lowest PICR. However, there are six codewords with low PICR for $N = 4$, while the number of rate half repetition codewords is 4. Clearly, we can select more codewords with low PICR than that of rate half repetition codes, particularly for large N . This approach will improve the efficiency of

Table 5.1: PICR for $N = 4$ and BPSK modulation

d_1	d_2	d_3	d_4	PICR (dB) $\epsilon = 0.05$	PICR (dB) $\epsilon = 0.1$
0	1	0	1	-28.06	-21.87
1	0	1	0	-28.06	-21.87
0	0	1	1	-20.97	-14.76
0	1	1	0	-20.97	-14.76
1	0	0	1	-20.97	-14.76
1	1	0	0	-20.97	-14.76
0	0	0	0	-18.56	-12.49
0	0	0	1	-18.56	-12.49
0	0	1	0	-18.56	-12.49
0	1	0	0	-18.56	-12.49
0	1	1	1	-18.56	-12.49
1	0	0	0	-18.56	-12.49
1	0	1	1	-18.56	-12.49
1	1	0	1	-18.56	-12.49
1	1	1	0	-18.56	-12.49
1	1	1	1	-18.56	-12.49

the coded scheme.

5.3.3 Construction of PICR-reduction Codes

The rate-half repetition coding [66, 68, 69, 71, 72] reduces the PICR effectively despite the loss of 50% data throughput. Interestingly, this rate-half repetition codes, $C_{\frac{1}{2}}$, can be used as a base for constructing higher-rate PICR-reduction codes, C_α . Suppose we are able to construct C_α around $C_{\frac{1}{2}}$, then C_α might have low PICR. Thus, C_α includes all codewords of $C_{\frac{1}{2}}$ and any sequence with Hamming distance W_{max} from $C_{\frac{1}{2}}$. Mathematically,

$$C_\alpha = \left\{ c \mid d_H(c, c') \leq W_{max} \text{ for any } c' \in C_{\frac{1}{2}} \right\} \quad (5.26)$$

where $d_H(x, y)$ denote the number of positions where x and y differ.

The number of q -ary codewords in C_α is $|C_\alpha| \leq q^{N/2} \times \sum_{m=1}^{W_{max}} \binom{N}{m}$. Therefore, the code rate R of C_α can be bounded as

$$\frac{1}{2} \leq R \leq \frac{1}{2} + \frac{1}{N \log_2 q} \log_2 \left[\sum_{m=1}^{W_{max}} \binom{N}{m} \right]. \quad (5.27)$$

For the binary case with $W_{max} = 1$, the code rate will be

$$R = \frac{1}{2} + \frac{\log_2 N}{N}. \quad (5.28)$$

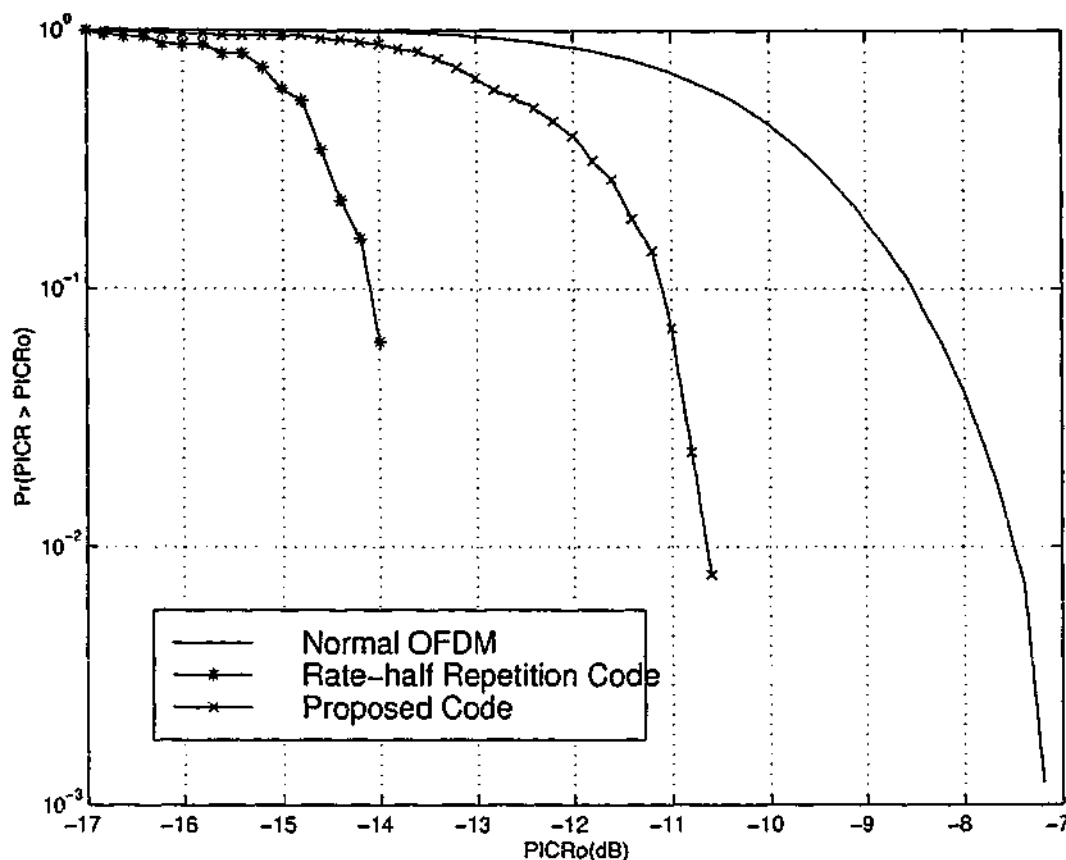


Figure 5.6: CCDF of PICR for a coded OFDM system with $N = 16$ and $\varepsilon = 0.1$.

The improvement in code rate over the rate-half repetition codes is significant for small N .

Figure 5.6 shows the CCDF of the PICR of $C_{\frac{1}{2}}$ and C_{α} with $W_{max} = 1$ for $N = 16$ and $\varepsilon = 0.1$. The PICR performance of C_{α} is between that of the conventional OFDM and the $C_{\frac{1}{2}}$ codes. However, C_{α} offers 25% gain in data throughput over $C_{\frac{1}{2}}$. Note that the above construction of high-rate PICR reduction codes shows the existence of PICR-reduction codes. However, this is not an efficient way to construct such codes in code design point of view.

It is also worthwhile to see the PICR characteristics of the rate 2/3 and 3/4 codes proposed in Chapter 4 (Section 4.3). Note that these codes were also constructed based on rate-half repetitive structures. Their BER performance and average CIR are comparable to rate-half repetition codes, while they significantly improves the data throughput. Figure 5.7 shows the CCDF of the PICR of rate 2/3 and 3/4 codes. Their PICR performances are better than uncoded scheme but rate-half repetition code exhibits superior performance. Again, it is a trade-off between PICR performance and gain in data throughput.

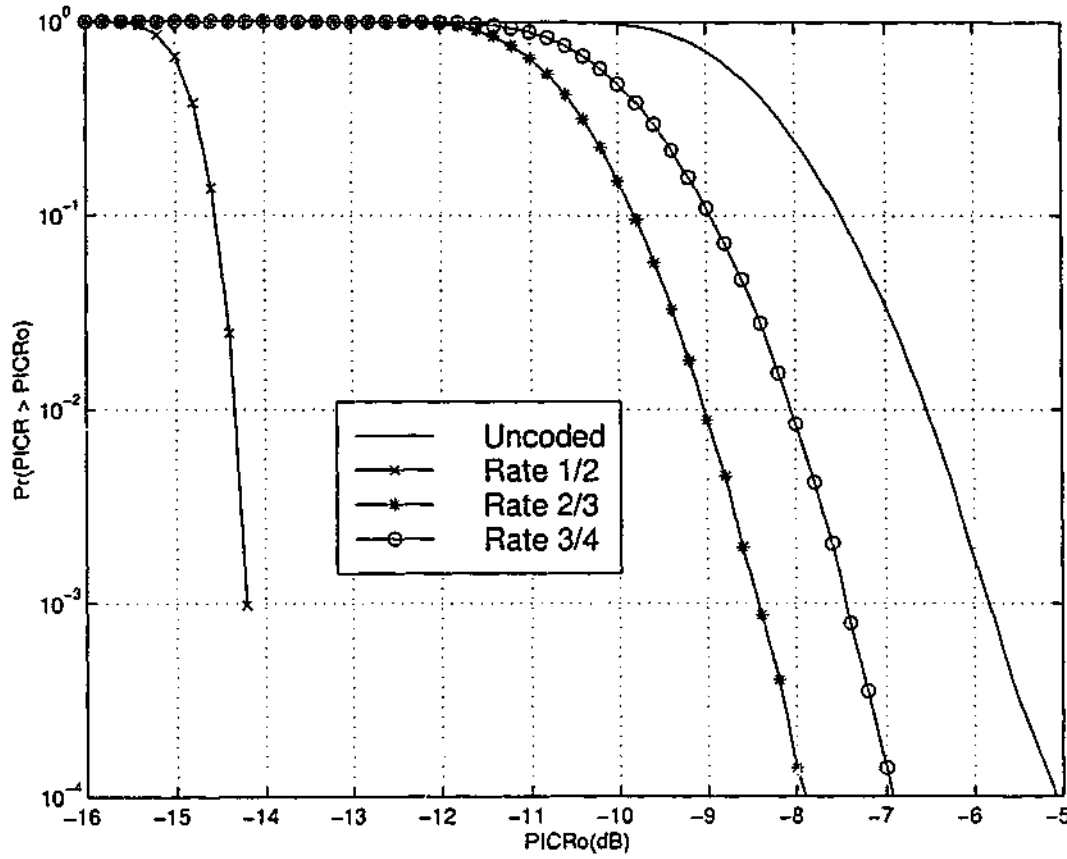


Figure 5.7: CCDF of PICR for rate rate $\frac{2}{3}$ and $\frac{3}{4}$ codes with $N = 128$ and $\epsilon = 0.1$.

5.4 PICR Reduction by Tone Reservation

Tone reservation approach has been proposed for the reduction of PAR of OFDM signals [189,195]. In this method, the transmitter does not send data on a small subset of carriers, which are used to insert the optimized tones. The complex baseband signal may now be represented as

$$s(t) = \sum_{k \in I_{info}}^{N-1} c_k e^{j2\pi k \Delta f t} + \sum_{k \in I_{tones}}^{N-1} c_k e^{j2\pi k \Delta f t}, 0 \leq t \leq T \quad (5.29)$$

where I_{info} and I_{tones} are two disjoint sets such that

$$I_{info} \cup I_{tones} = \{0, 1, \dots, N-1\}.$$

These tones can be computed at the transmitter and can be easily stripped off at the receiver.

Consider the ICI on k -th subcarrier (2.30)

$$I_k = \sum_{l=0, l \neq k}^{N-1} S_{l-k} c_l. \quad (5.30)$$

Therefore, ICI terms on all subcarriers can be denoted in vector form as

$$\mathbf{I} = \mathbf{S}_I \mathbf{c} \quad (5.31)$$

where \mathbf{S}_I is $N \times N$ matrix with $S_{ij} = S_{j-i}$ and $S_{ii} = 0$ and $\mathbf{I} = [I_0 I_1 \dots I_{N-1}]^T$.

Note that I_k should be zero for all k to completely eliminate ICI. To achieve that, we set $I_{tones} = \{0, m, 2m, \dots, (p-1)m\}$ ($m = \lfloor \frac{N}{P} \rfloor$) and let $\mathbf{c}_p = [c_0, c_m, c_{2m}, \dots, c_{(p-1)m}]$. Therefore, I_k needs to be zero for only $(N - P)$ subset of k , that belongs to the data. Thus, for ICI free channel, \mathbf{c}_p should satisfy the following condition.

$$\mathbf{S}_o \mathbf{c} = \mathbf{0} \quad (5.32)$$

where \mathbf{S}_o results from eliminating P rows, corresponding to pilot tone positions, from \mathbf{S}_I and $\mathbf{c} = \mathbf{c}_d \cup \mathbf{c}_p$ is the IFFT input consisting data ($\mathbf{c}_d = (c_0, \dots)_{1 \times (N-P)}$) and pilots (\mathbf{c}_p). Now, the computation of \mathbf{c}_p from (5.32) requires an optimization technique and we will consider two different approaches. Moreover, CFO should be known at the transmitter for the computation of \mathbf{S}_o . However, worst case CFO can be assumed for the computation. The simulation results show that any CFO less than the worst case perform same as if the computation is done with that CFO. That means computation of pilot tones is independent of CFO if those CFO are less than the worst case scenario.

5.4.1 Least Square Error Optimization

This is a simple near optimization technique that minimizes the error. (5.32) can be written as

$$\mathbf{S}_1 \mathbf{c}_p = -\mathbf{S}_2 \mathbf{c}_d \quad (5.33)$$

where \mathbf{S}_1 is P columns of \mathbf{S}_o for index set $\{0, m, 2m, \dots, (p-1)m\}$ and \mathbf{S}_2 is the remaining $(N - P)$ columns of \mathbf{S}_o . Thus, the least square error solution to (5.33) is [237]

$$\mathbf{c}_p = -(\mathbf{S}_1^T \mathbf{S}_1)^{-1} \mathbf{S}_1^T \mathbf{S}_2 \mathbf{c}_d \quad (5.34)$$

where A^T denotes the conjugate transpose of A .

5.4.2 Standard Linear Programming Approach

In the least square error approach, we have focused on eliminating all ICI terms. This is a rather difficult optimization criterion and less ICI effects are tolerable. Hence,

our optimization criterion is to minimize the maximum ICI. i.e., maximum of $|\mathbf{S}_o \mathbf{c}|$ should be minimized. However, this is a non-linear optimization problem. Therefore, we optimize t , where $|\mathbf{S}_o \mathbf{c}| \leq t$ subject to following constraints.

$$\begin{aligned} |\Re\{S_1 \mathbf{c}_p + S_2 \mathbf{c}_d\}| &\leq tU \\ |\Im\{S_1 \mathbf{c}_p + S_2 \mathbf{c}_d\}| &\leq tU \end{aligned} \quad (5.35)$$

where $\mathbf{U} = [1, 1, \dots]_{(N-P) \times 1}^T$ and $\Re\{x\}$ and $\Im\{x\}$ denote the real part of x and imaginary part of x respectively. Then (5.35) can be expanded as

$$\begin{aligned} \Re\{S_1 \mathbf{c}_p\} - tU &\leq \Re\{S_2 \mathbf{c}_d\} \\ -\Re\{S_1 \mathbf{c}_p\} - tU &\leq -\Re\{S_2 \mathbf{c}_d\} \\ \Im\{S_1 \mathbf{c}_p\} - tU &\leq \Im\{S_2 \mathbf{c}_d\} \\ -\Im\{S_1 \mathbf{c}_p\} - tU &\leq -\Im\{S_2 \mathbf{c}_d\} \end{aligned} \quad (5.36)$$

Let us define

$$\hat{\mathbf{c}} = \begin{pmatrix} \Re\{\mathbf{c}_p\} \\ \Im\{\mathbf{c}_p\} \end{pmatrix}, \quad S_{1r} = \begin{pmatrix} \Re\{S_1\} & -\Im\{S_1\} \end{pmatrix} \text{ and } S_{1i} = \begin{pmatrix} \Im\{S_1\} & \Re\{S_1\} \end{pmatrix}$$

and then (5.36) can be expressed as

$$\begin{pmatrix} S_{1r} & -U \\ -S_{1r} & -U \\ S_{1i} & -U \\ -S_{1i} & -U \end{pmatrix} \times \begin{pmatrix} \hat{\mathbf{c}} \\ t \end{pmatrix} \leq \begin{pmatrix} -\Re\{S_2 \mathbf{c}_d\} \\ \Re\{S_2 \mathbf{c}_d\} \\ -\Im\{S_2 \mathbf{c}_d\} \\ \Im\{S_2 \mathbf{c}_d\} \end{pmatrix} \quad (5.37)$$

Now, (5.37) is a standard linear programming problem with $(2P + 1)$ unknowns subject to $4(N - P)$ constraints [237]. Hence, pilot tones \mathbf{c}_p can be computed.

5.4.3 Simulation Results

Figure 5.8 shows the CCDF of PICR for $N = 128$, $P = 32$ and $\epsilon = 0.1$ with BPSK modulation scheme. This illustrates how ICI effects can be reduced by inserting pilot tones in the data frame. There is 5 to 6 dB reduction in PICR for $P = 32$ and this is a sort of rate $\frac{3}{4}$ coding. In fact, ICI can be completely eliminated if half of the subcarriers are assigned for pilot tones, that becomes half-rate coding. Note that in the computation of \mathbf{c}_p , P unknowns were solved from $(N - P)$ equations ($P < N$) and exact solution is possible if $P = \frac{N}{2}$. Note that the linear programming (LP) approach

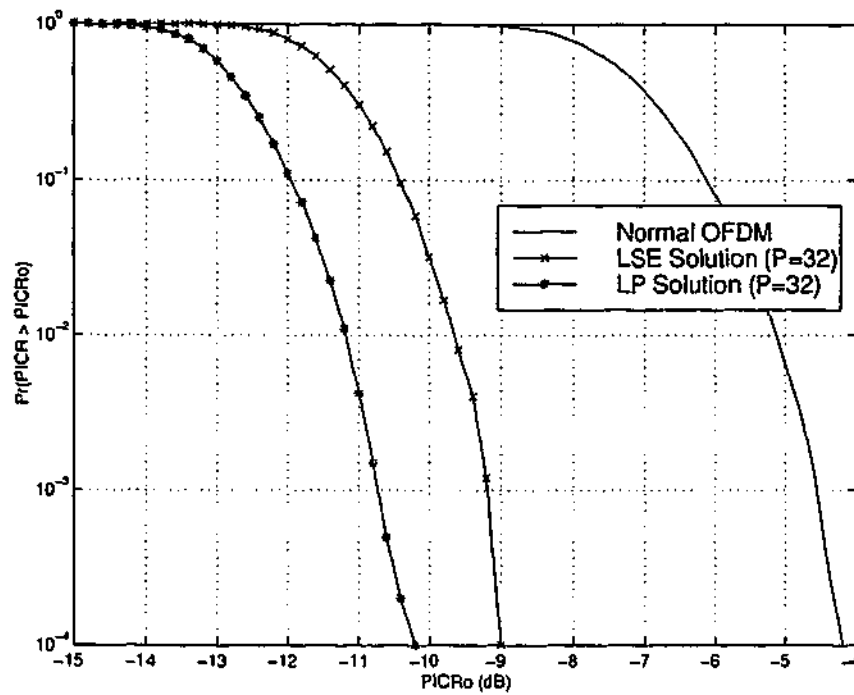


Figure 5.8: CCDF of PICR for an OFDM System with $N = 128$ and $\epsilon = 0.1$.

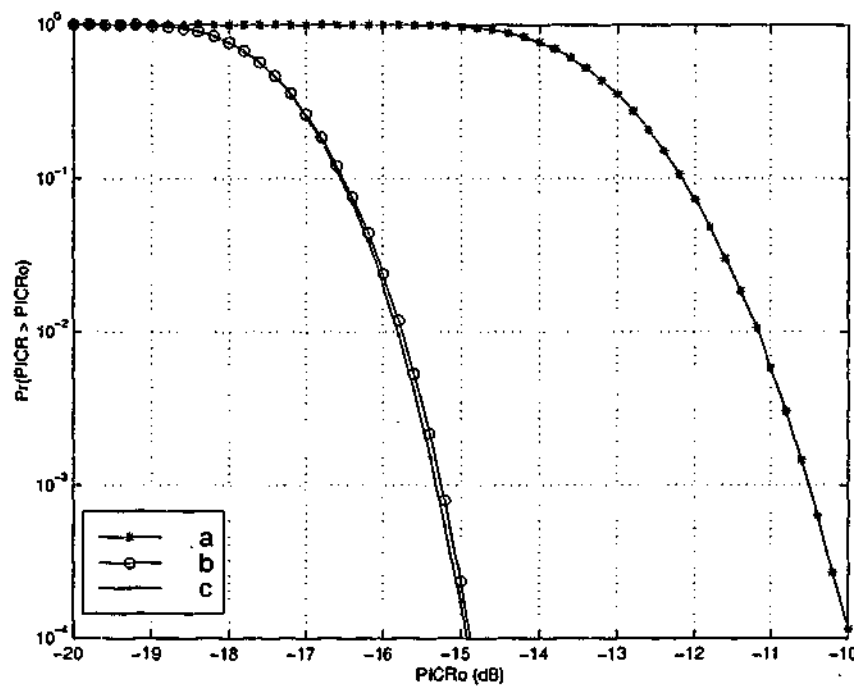


Figure 5.9: CCDF of PICR for an OFDM system with $N = 128$; a: Conventional OFDM ($\epsilon = 0.05$), b: $\epsilon = 0.05$ and $\epsilon_{wc} = 0.05$, c: $\epsilon = 0.05$ and $\epsilon_{wc} = 0.05$.

performs better than least square error (LSE) solution method. However, the latter is faster computation.

Figure 5.9 shows the CDF of PICR as a function of ε with LSE solution. It can be seen from Figure 5.9 that c_p can be computed by assuming worst case ε_{wc} and the optimization will not be affected if $|\varepsilon| < \varepsilon_{wc}$.

5.5 PICR Reduction by SLM and PTS Schemes

Generating several statistically different OFDM frames for a data frame and selecting the one with the lowest PAR is a common approach for PAR reduction. [172, 180, 183, 185] This approach improves the statistics of the PAR at the expense of additional complexity. Motivated by their success in reducing the PAR, we apply SLM [172, 180] and PTS [172, 183, 185] to reduce the PICR. It is worthwhile to note that PAR and PICR exhibit somewhat similar statistical distributions. Since SLM and PTS exploit the statistical property to reduce the PAR, they will also be effective in reducing PICR.

5.5.1 Selected Mapping (SLM)

U statistically different alternative transmit sequences $\mathbf{a}^{(u)}$ represent the same information. The sequence with lowest PICR is selected for transmission. To generate $\mathbf{a}^{(u)}$, we define U distinct fixed vectors $\mathbf{P}^{(u)} = [P_0^{(u)}, \dots, P_{N-1}^{(u)}]$ with $P_v^{(u)} = e^{j\varphi_v^{(u)}}$, $\varphi_v^{(u)} \in [0, 2\pi]$, $0 \leq v < N$, $1 \leq u \leq U$. Then, each modulated symbol $\mathbf{c} = [c_0, c_1, \dots, c_{N-1}]$ is multiplied carrierwise with the U vectors $\mathbf{P}^{(u)}$, resulting in a set of U different modulated symbols $\mathbf{c}^{(u)}$ with components

$$c_v^{(u)} = c_v P_v^{(u)} \text{ for } 0 \leq v < N \text{ and } 1 \leq u \leq U. \quad (5.38)$$

For simple implementation, we select $P_v^{(u)} \in [\pm 1, \pm j]$ for $0 \leq v < N$, $1 \leq u \leq U$. Using Eqs. (2.30) and (5.38), the resulting ICI on the k -th subcarrier can be expressed as

$$I_{k,SLM} = \sum_{l=0, l \neq k}^{N-1} P_l^{(u)} c_l S_{l-k} \quad (5.39)$$

which is a function of the weighting sequence $\mathbf{P}^{(u)}$. Finally, the optimal PICR can be found as

$$\text{PICR}_{\text{optimal}} = \min_{\mathbf{P}^{(1)}, \dots, \mathbf{P}^{(U)}} \left[\frac{\max_{0 \leq k \leq N-1} |I_{k,SLM}|^2}{|S_0 c_k|^2} \right]. \quad (5.40)$$

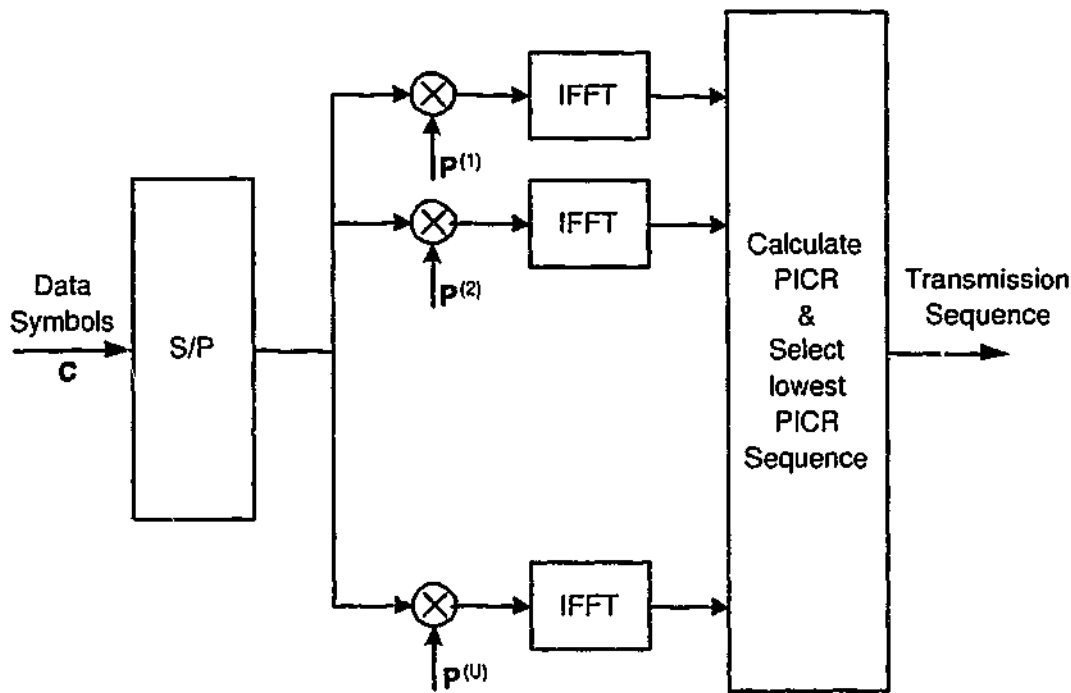


Figure 5.10: Simplified block diagram of SLM for PICR reduction.

Figure 5.10 shows the simplified block diagram of SLM for PICR reductions. The computation of PICR at the transmitter requires ϵ . However, a worst-case ϵ can be assumed for the computation. Simulation results show that optimized phase factors for ϵ_{wc} are effective for another ϵ provided $|\epsilon| < \epsilon_{wc}$. That is, any mismatch between the actual CFO and the worst-case CFO can be handled under this condition.

In order to recover the data, a pointer to the multiplied sequence has to be transmitted to the receiver as side information (SI). However, an interesting idea is reported in [181] to get rid of the explicit SI in SLM.

Simulation Results

The simulation results for SLM and PTS were obtained for an OFDM system with $N = 128$. The subcarriers are modulated with QPSK and an AWGN channel is assumed throughout this study. Further, a worst-case ϵ of 0.1 is assumed. For brevity, results for higher-order modulations such as M-ary Phase Shift Keying (M-PSK where $M > 4$) are not provided here. However, comparable performance gains have been observed for both QPSK and other modulation schemes.

Figure 5.11 shows the CCDF of PICR per OFDM block as a function of U for $\epsilon = 0.1$. In SLM approach with $U = 8$, only 1 out of 10^4 of all OFDM blocks exceeds the PICR of -8.5 dB whereas in conventional OFDM, 1 out of 10^4 of all OFDM blocks

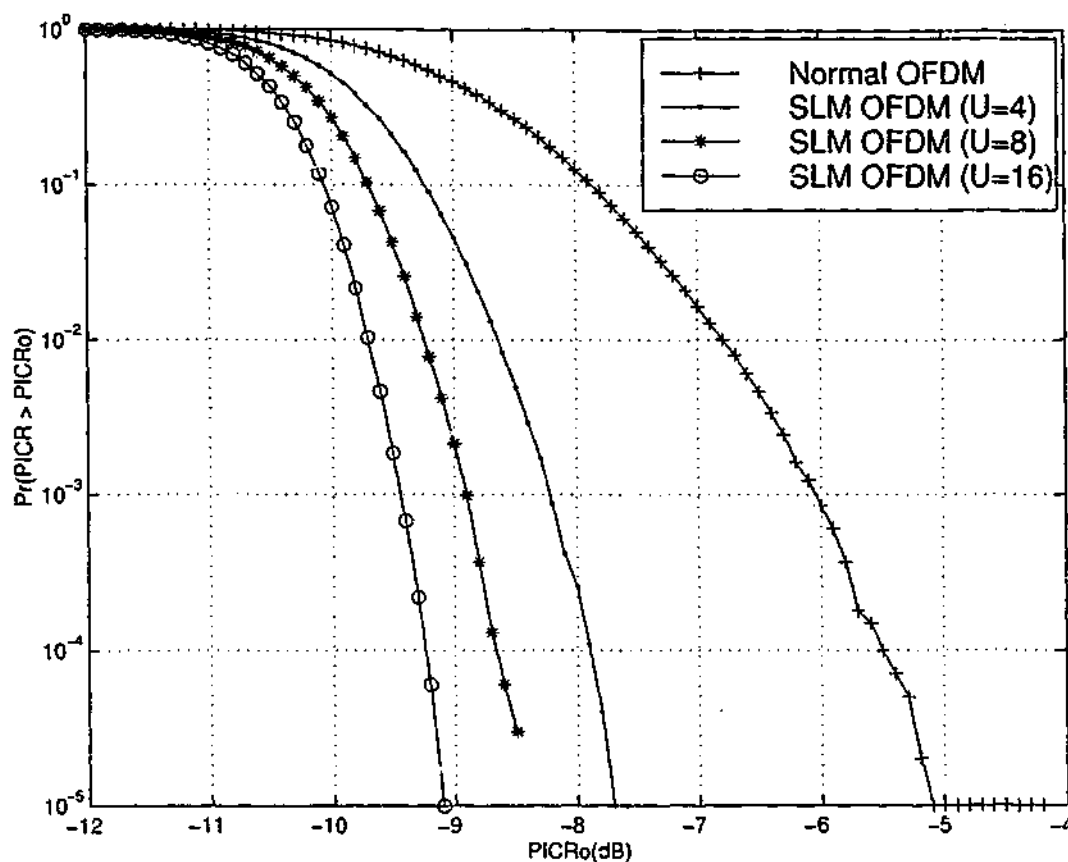


Figure 5.11: CCDF of PICR of SLM OFDM system with $\epsilon = 0.1$.

exceeds the PICR of -5.5 dB. That amounts to a 3.0 dB reduction in PICR. Moreover, PICR reduction increases with increasing U . However, the computational complexity also increases with U . Thus, the performance can be traded off against complexity.

Figure 5.12 shows the BER performance of QPSK modulated SLM OFDM System in an AWGN channel. Exact knowledge of SI is assumed at the receiver. For $U = 16$, an SNR gain of 3 dB is obtained at 10^{-4} BER over conventional OFDM. In fact, SLM OFDM removes the error floor caused by ICI. Moreover, the SNR gain is large when M is large.

5.5.2 Partial Transmit Sequences (PTS)

In PTS, the input data block is partitioned into disjoint subblocks or clusters which are combined to minimize the peaks. We partition the data frame \mathbf{c} into M disjoint subblocks, represented by the vectors $\{\mathbf{c}_m, m = 1, 2, \dots, M\}$, such that $\mathbf{c} = [\mathbf{c}_1, \mathbf{c}_2, \dots, \mathbf{c}_M]$. It is assumed that each subblock consists of a contiguous set of subcarriers and the subblocks are of equal size. Then, each subblock is zero padded to make its length N and is multiplied by a weighting factor b_m ($m = 1, 2, \dots, M$). Thus, the ICI on the k -th

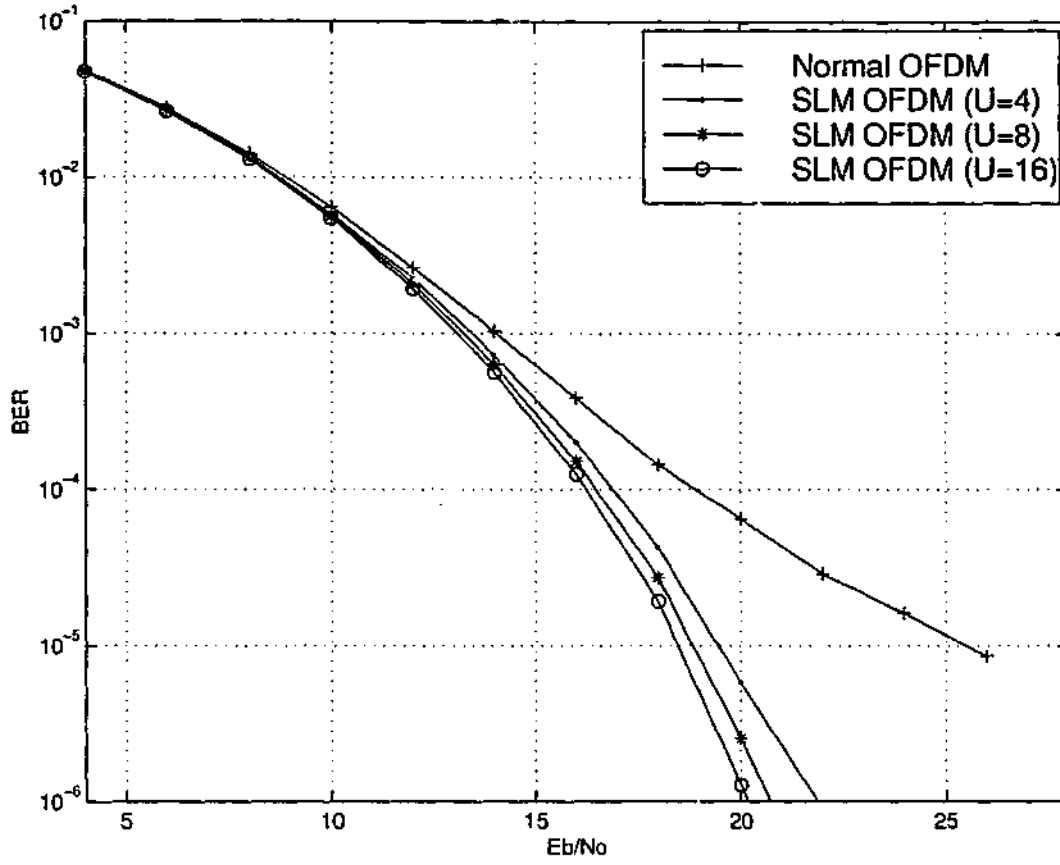


Figure 5.12: BER Performance of SLM OFDM system in AWGN channel with $\epsilon = 0.1$.

subcarrier can be expressed as

$$I_{k,PTS} = \sum_{m=1}^M \sum_{l=0, l \neq k}^{N-1} b_m c_l^m S_{l-k} \quad (5.41)$$

where c_l^m is the data symbol in the newly formed m -th subblock.

We can write (5.41) as

$$I_{k,PTS} = \sum_{m=1}^M b_m I_k^m \quad (5.42)$$

where I_k^m is the interference on k -th subcarrier of block m . Thus, the total ICI is the weighted sum of ICI from each subblock and the total ICI and PICR can be reduced by optimizing the phase sequence $\mathbf{b} = [b_1, b_2, \dots, b_M]$.

A drawback in the PTS approach is the complexity of the optimization of phase factors. To reduce this complexity, we only consider binary phase factors (i.e., $b_m = \pm 1$). Without loss of generality, we can set $b_1 = 1$ and observe that there are $(M - 1)$ binary variables to be optimized. Finally, the optimal PICR can be found as

$$\text{PICR}_{\text{optimal}} = \min_{b_1, \dots, b_M} \left[\frac{\max_{0 \leq k \leq N-1} |I_{k,PTS}|^2}{|S_{0Ck}|^2} \right]. \quad (5.43)$$

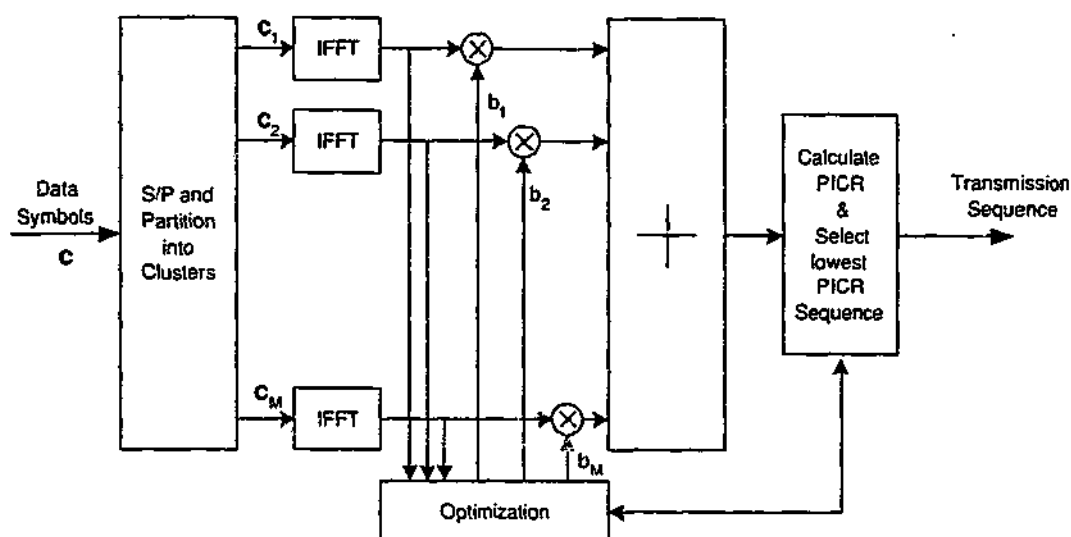


Figure 5.13: Simplified block diagram of PTS for PICR reduction.

Figure 5.13 shows the simplified block diagram of PTS for PICR reductions. The worst-case ε can be assumed for the computation of PICR, as in SLM. Moreover, the receiver must know the generation process of the transmitted OFDM signal. The phase factors must then be transmitted to the receiver as SI. However, with differential modulation schemes, SI need not be transmitted.

Simulation Results

Figure 5.14 shows the CCDF of PICR per OFDM for $N = 128$, $\varepsilon = 0.1$ and $M = 4, 8$ and 16. In the PTS approach, the PICR exceeds -7 dB for only 1 out 10^4 of all OFDM blocks whereas that of conventional OFDM is for only 1 out 100. There is 3 dB reduction in PICR over normal OFDM with $M = 8$.

Figure 5.14 also shows how the performance varies with M . When M is large, PICR reduction is large. However, the computational complexity depends on M . Thus, it is a trade off between the performance and complexity. Moreover, optimized phase sequence requires 2^{M-1} computations of PICR. Note that an N -point IFFT and an N -point FFT are required at the transmitter to compute PICR. Thus, computation of optimized phase sequence is difficult. Instead, several selections of \mathbf{b} can be generated randomly until PICR is reduced. Even 100 trials achieve a performance level that is nearly optimal for $M = 8$.

Figure 5.15 shows the CCDF of PICR per OFDM block as a function of ε for both PTS and SLM. The PICR can be computed by assuming worst-case CFO and the

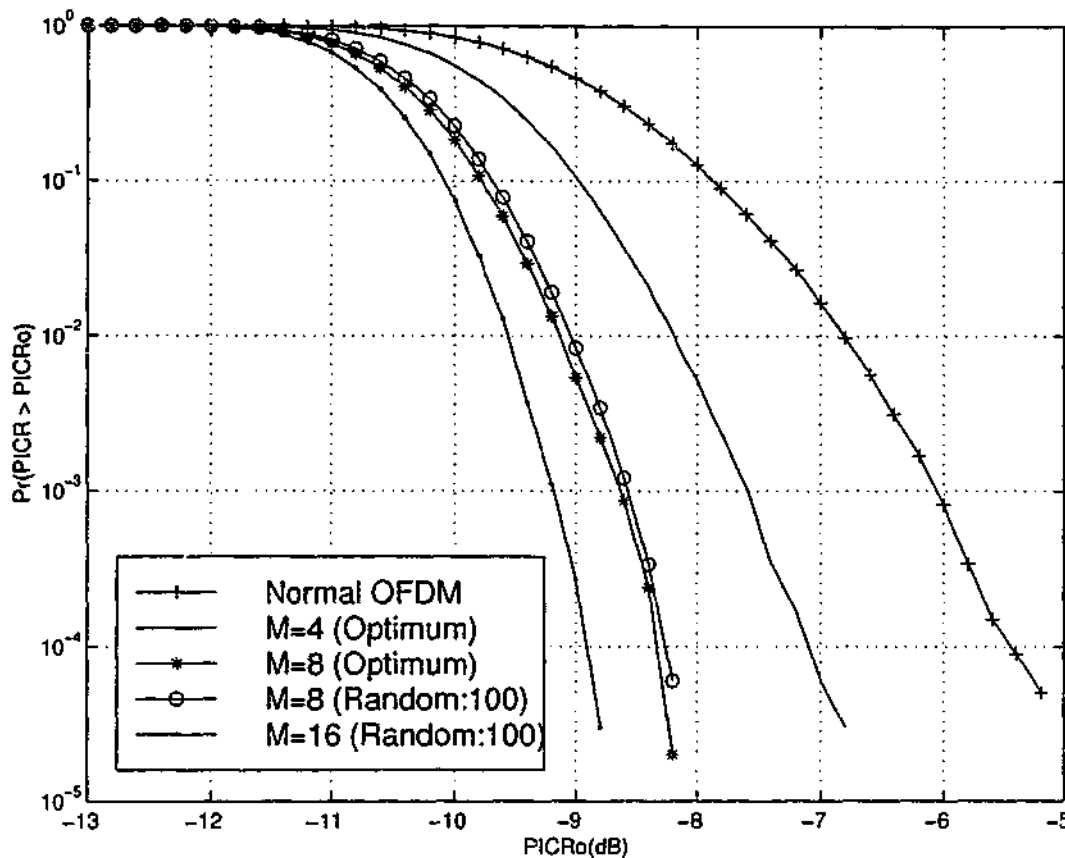


Figure 5.14: CCDF of PICR of PTS OFDM system with $\epsilon = 0.1$.

performance of SLM and PTS will not be affected by CFO less than the worst-case CFO.

5.6 Both PAR and PICR Reduction by Coding

In Chapter 2, we have explored the two limitations, the high PAR and the ICI due to CFO, of OFDM systems and their consequent solutions. However, proposed techniques in the literature treat these limitations as two separate problems. The introduction of PICR have motivated us to use PAR reduction schemes for PICR reduction. Interestingly, there is a possibility that the both PAR and PICR can be reduced simultaneously. Motivated by this observation, we investigate the coding scheme to reduce both PAR and PICR.

To the best of our knowledge, a coding technique that limits PAR and PICR together has not been reported before. For a code \mathcal{C} , we define

$$\text{PAR}(\mathcal{C}) = \max_{\mathbf{c} \in \mathcal{C}} \text{PAR}(\mathbf{c}) \text{ and } \text{PICR}(\mathcal{C}) = \max_{\mathbf{c} \in \mathcal{C}} \text{PICR}(\mathbf{c}, \epsilon). \quad (5.44)$$

We next state the main problem arising from these definitions. For length N , what

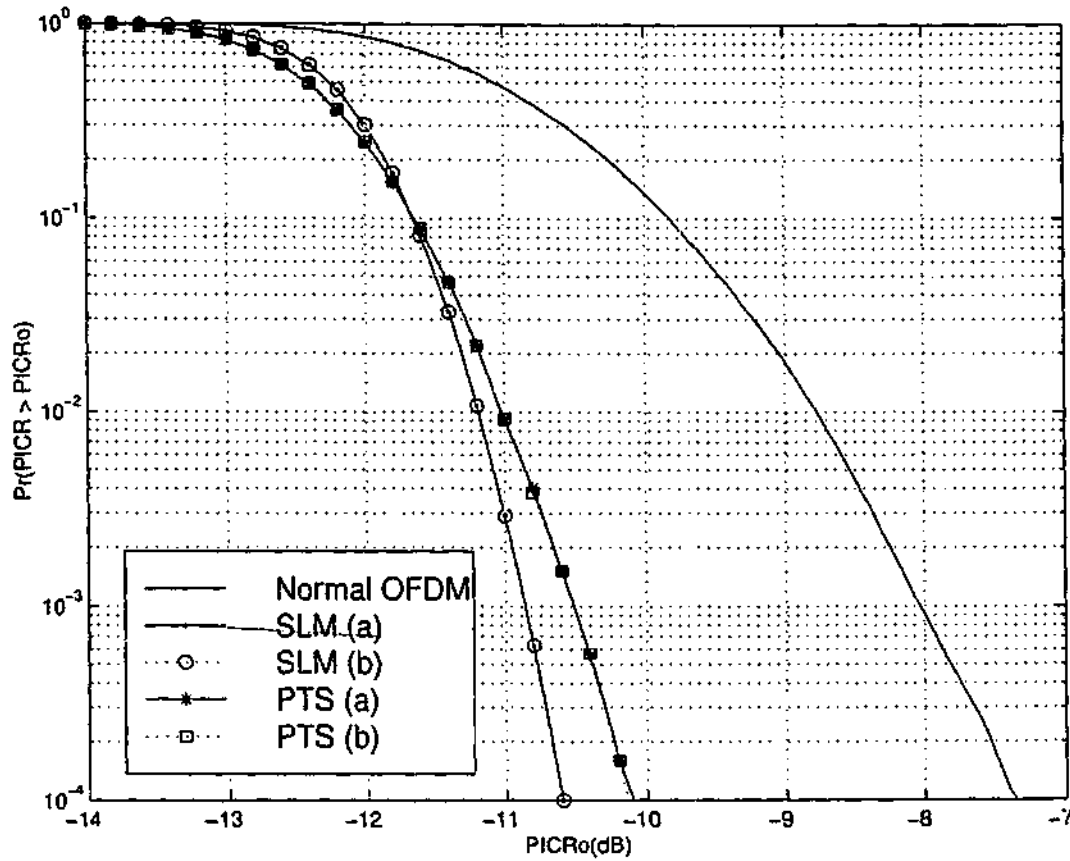


Figure 5.15: CCDF of PICR of an OFDM system with a: ($\epsilon = 0.08, \epsilon_{wc} = 0.08$) and b: ($\epsilon = 0.08, \epsilon_{wc} = 0.1$).

is the achievable region of quadruple $(R, d, \text{PAR}(\mathcal{C}), \text{PICR}(\mathcal{C}))$? where R is the code rate and d is the minimum Euclidean distance of \mathcal{C} . So the problem at hand is to find out all the codewords in \mathcal{C} that minimize both PAR and PICR for a fixed ϵ_{wc} and having error correcting capability with a high code rate.

The achievable code rate (R) of the PAR-PICR-reduction codes for threshold values, PAR_{th} and PICR_{th} can be expressed as

$$R = \frac{\log_2 [q^N \text{Pr}\{\text{PAR}(c) < \text{PAR}_{th}, \text{PICR}(c) < \text{PICR}_{th}\}]}{\log_2 q^N} \quad (5.45)$$

where q is the signal constellation size. R is a function of both PAR_{th} and PICR_{th} .

5.6.1 Block Coding for both PAR and PICR Reduction

Since PAR and PICR are function of c , coding to select only those data frames with low PAR and PICR as valid codewords can reduce both PAR and PICR. This block coding idea was first suggested in [151] to reduce PAR and we have applied to reduce PICR.

Table 5.2: PICR and PAR for $N = 4$ and BPSK modulation

d_1	d_2	d_3	d_4	PICR (dB) $\epsilon = 0.05$	PICR (dB) $\epsilon = 0.1$	PAR (dB)
0	1	0	1	-28.06	-21.87	6.02
1	0	1	0	-28.06	-21.87	6.02
0	0	1	1	-20.97	-14.76	3.73
0	1	1	0	-20.97	-14.76	3.73
1	0	0	1	-20.97	-14.76	3.73
1	1	0	0	-20.97	-14.76	3.73
0	0	0	0	-18.56	-12.49	6.02
0	0	0	1	-18.56	-12.49	2.32
0	0	1	0	-18.56	-12.49	2.32
0	1	0	0	-18.56	-12.49	2.32
0	1	1	1	-18.56	-12.49	2.32
1	0	0	0	-18.56	-12.49	2.32
1	0	1	1	-18.56	-12.49	2.32
1	1	0	1	-18.56	-12.49	2.32
1	1	1	0	-18.56	-12.49	2.32
1	1	1	1	-18.56	-12.49	6.02

To show that PAR-PICR-reduction codes exist, we consider an OFDM system with $N = 4$ and BPSK modulated subcarriers. The PICR for all data frames is given in Table 5.2 in ascending order. Corresponding PAR is also tabulated. Ten data frames have a PICR of -12.49 dB for $\epsilon = 0.1$. Four data frames have a PAR of 6.02 dB. Some data frames have both moderate PAR and PICR. Clearly, we can choose only these data frames for transmission in order to reduce both PAR and PICR simultaneously.

In Table 5.2, codewords 0011, 0110, 1001, and 1100 have a PAR of 3.73 dB and a PICR of 14.76 dB. Thus, by transmitting only these data frames, PAR can be reduced by 2.3 dB and PICR can be reduced by 2.3 dB for $\epsilon = 0.1$. This can be done by block coding the data such that 2 bits of data are mapped on to 4 best data frames. Thus, this code halves the data throughput. Note that these codes are different from rate-half repetition codes.

5.6.2 Golay Complementary Repetition Codes

A simple approach to construct codes to reduce both PAR and PICR simultaneously is to use repetitive coding of Golay complementary sequence of length $N/2$. Davis and Jedwab [162] explicitly determine a large class of Golay complementary sequences over

Z_{2^h} of length 2^m . The i -th element of a Golay sequence of length 2^m for any $b, b_k \in Z_{2^h}$ can be expressed as

$$f_i = 2^{h-1} \sum_{k=1}^{m-1} x_{\pi(k)} x_{\pi(k+1)} + \sum_{k=1}^m b_k x_k + b \quad (5.46)$$

where $x = (x_1, x_2, \dots, x_m)$ is the binary representation of the integer $i = \sum_{j=1}^m x_j 2^{m-j}$, h is the number of bits per symbol and π is the any permutation of the symbols $\{1, 2, \dots, m\}$. Moreover, (5.46) determines $2^{h(m+1)} m! / 2$ number of Golay sequences over Z_{2^h} .

Now, consider the 2^h -PSK codeword given by

$$c_{gr} = (\alpha^{f_0}, -\alpha^{f_0}, \alpha^{f_1}, -\alpha^{f_1}, \dots, \alpha^{f_{N/2-1}}, -\alpha^{f_{N/2-1}}) \quad (5.47)$$

where $\alpha = e^{j\frac{2\pi}{2^h}}$. It can be easily proved that the PAR of c_{gr} is no greater than 6 dB while its PICR is equal to that of repetition codes. The code rate of a binary Golay complementary repetition code can be expressed as

$$R = \frac{\log_2(2^{(m+1)} m! / 2)}{N} \quad (5.48)$$

where $m = \log_2(N/2)$. For large N , the code rate decreases rapidly.

5.6.3 Simulation Results

The simulation results were obtained for an OFDM system with $N = 16$. Note that we choose small N and BPSK in this study so that all possible (2^N) sequences can be investigated. For large N and higher order modulation formats, only a small subset of all possible sequences can be investigated. Further, we assume an AWGN channel and a worst case ϵ of 0.1.

Figure 5.16 shows the code rate as a function of PAR_{th} and PICR_{th} . All codewords (2^{16}) of length 16 are generated to find the code rate. The block coding principle offers the flexibility to choose the amount of both PAR and PICR reduction and the code rate. For example, for a code rate of 1/2, PAR and PICR can be limited to 4 dB and -12 dB respectively. Thus, an 8 dB reduction in maximum PAR and 5 dB reduction in maximum PICR. In fact, the code rate reduces rapidly for large PAR and PICR reductions.

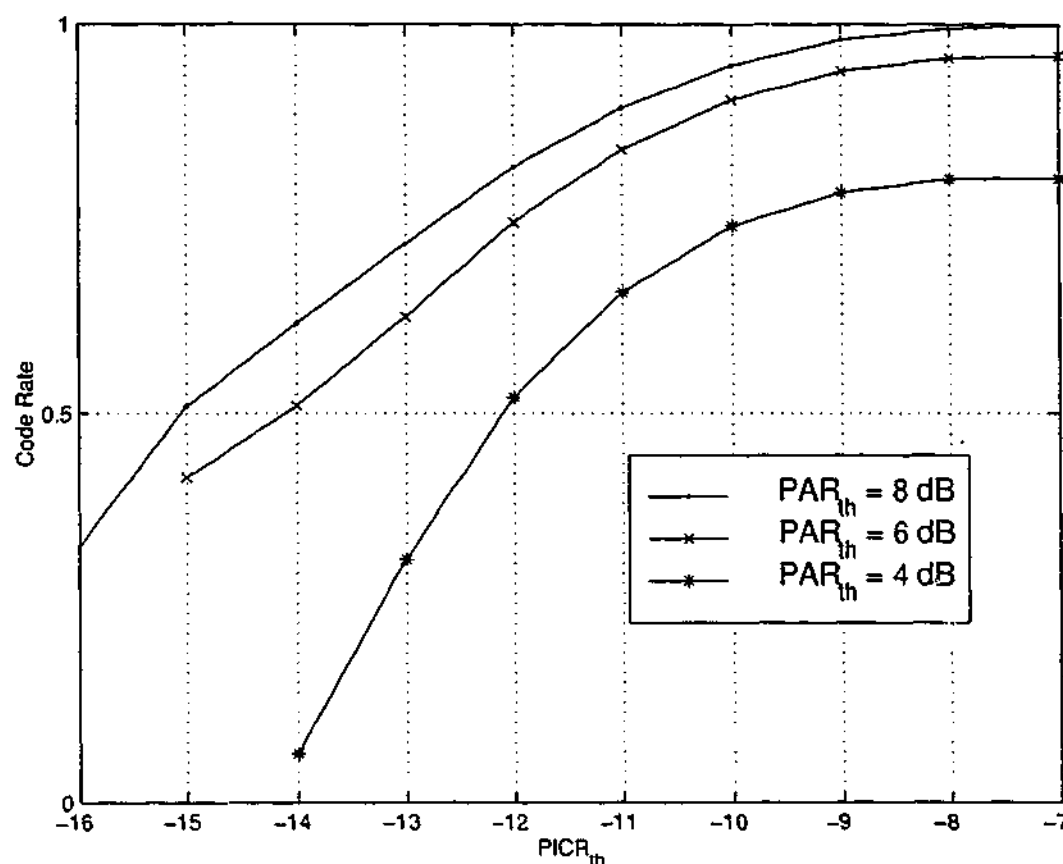


Figure 5.16: Variation of code rate with PAR and PICR for $N = 16$ and $\epsilon = 0.1$.

Figure 5.17 and Figure 5.18 shows the CCDF of PAR and PICR respectively. Note that the PAR characteristics of the rate-half repetition codes are worse than conventional OFDM while the PICR characteristics of Golay complementary sequences are almost same as conventional OFDM. The Golay complementary repetition codes show better PAR and PICR characteristics due to their code-structure. Its maximum PAR is limited to 6 dB while its PICR is almost same as rate-half repetition codes. However, the price for these benefits is low data throughput of 0.35. However, data throughput of these codes are even low for large N . Algebraic constructions for high-rate PAR-PICR reduction codes would therefore be very useful. This study paves the way for further research on this direction.

5.7 Conclusions

In this chapter, we have presented the distribution for PICR to study ICI effects and devise ICI reduction schemes. Our studies show that there exists code sets offering less ICI effects different of frequency offset errors. However, construction of good codes is

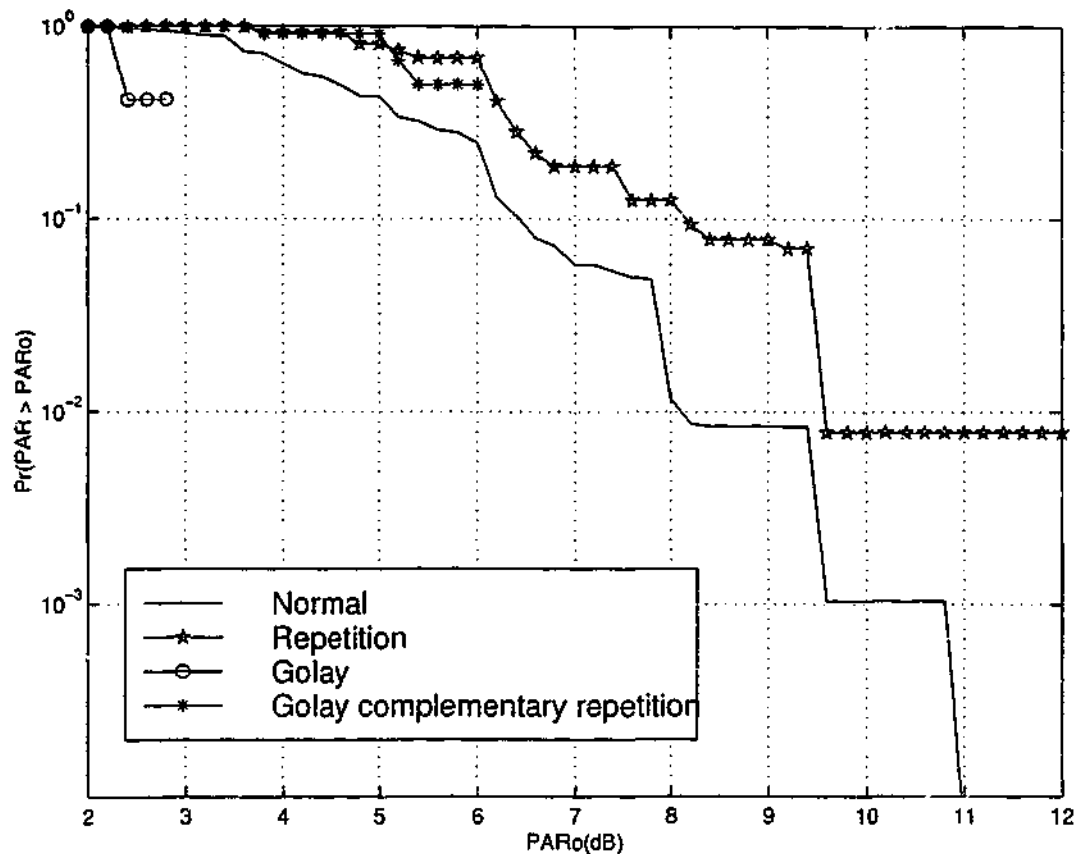


Figure 5.17: CCDF of PAR of an OFDM System.

a challenging task and it is an open research problem.

We have also proposed the tone reservation method to reduce ICI effects. This scheme offers 5 to 6 dB gain in PICR over conventional OFDM with 75% of data throughput. The price for this scheme is complex computation at the transmitter, which may not be an issue as faster computational devices are readily available. We have also investigated the SLM and PTS methods to reduce PICR. They improve the PICR statistics of an OFDM signal at the expense of additional complexity, but with little loss in efficiency. For an OFDM system with $N = 128$ and $\epsilon = 0.1$, SLM with $U = 3$ and PTS with $M = 8$ reduce PICR by 3 dB. Moreover, both schemes work independently of ϵ , provided $|\epsilon| < \epsilon_{wc}$. Finally, we stress that our proposed scheme has been applied to an AWGN or a frequency non-selective fading channel. If the fading channel is dispersive, the transmitter requires knowledge of the channel in order to perform the PICR optimization.

We have also discussed the existence of PAR-PICR-reduction codes. The proposed block coding scheme offers the flexibility to trade code rates against both PAR and PICR reductions. As an example, we constructed Golay complementary repetition

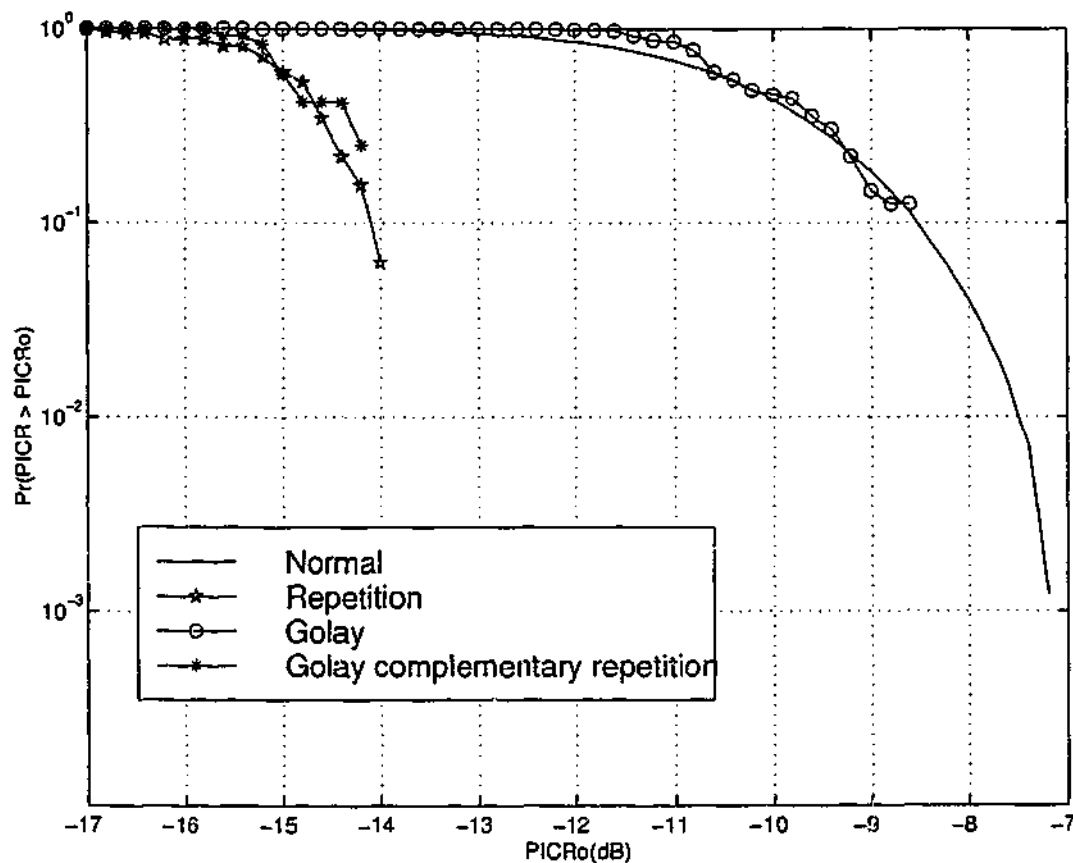


Figure 5.18: CCDF of PICR of an OFDM system with $\epsilon = 0.1$.

codes. The PAR of these codes is limited to 6 dB while their PICR is almost the same as that of rate-half repetition codes. However, data throughput of these codes is low, particularly for large N . Algebraic constructions for high-rate PAR-PICR reduction codes would therefore be very useful. This study paves the way for further research in this direction. Alternatively, we introduce a new adaptive mapping scheme in the next chapter to reduce both PAR and ICI simultaneously.

Chapter 6

Adaptive Zero-padded PSK for both PAR and ICI Reduction

This chapter shows that a simple adaptive mapping scheme is effective in reducing both PAR and ICI simultaneously. This is achieved by using M -point zero-padded phase shift keying (M-ZPSK), which includes a signal point of zero amplitude. The performance of the proposed scheme is evaluated by the statistical distribution of PAR, out of band radiation and the BER. The performance of the proposed scheme with SLM [171, 172] and its complexities with other approaches [175, 176] of this nature are discussed. Analytical expressions for the error rates of M-ZPSK on AWGN, Rayleigh, Nakagami- m and Ricean fading channels are also derived. Performance in wide band fading channels is also evaluated. The reliable transmission of side information (SI) is another issue in the proposed scheme. Explicit and implicit methods for the transmission of SI are investigated.

6.1 Introduction

The key idea for the PAR reduction technique in [238, 239] is to expand the M-PSK constellation with an extra, zero amplitude point. Thus, some subcarriers have zero amplitude and their presence reduces the peaks of an OFDM signal. However, these subcarriers are not fixed and they should be selected by considering the entire OFDM block in such a way as to reduce PAR. In [238], a bit mapping procedure using a Johnson association is proposed to select those zero amplitude subcarriers. In [239], the signal space is expanded by varying the non-modulated subcarrier set and the symbol pattern with low PAR is selected for transmission. This approach is suitable for small N as

both transmitter and receiver need to maintain a lookup table. Interestingly, these two approaches offer higher bandwidth efficiency over conventional OFDM with increased complexity as non-modulated subcarrier positions are also used to carry information bits.

Motivated by these two successful approaches [238, 239], an M-ZPSK modulation scheme, which includes a signal point of zero amplitude, is proposed. Both M-ZPSK and M-PSK have the same number of signal points. The main innovation is a simple adaptive version of M-ZPSK that reduces both PAR and ICI simultaneously. One of the M bit patterns of $\log_2 M$ bits is mapped to a signal point of zero amplitude. This mapping leads to M different OFDM frames representing the same information. Then, the OFDM frame with the lowest PAR is selected for transmission. The mapping pattern used at the transmitter is sent to the receiver as side information (SI). M-ZPSK reduces the ICI as the signal point of zero amplitude does not contribute to overall ICI. Thus, the adaptive M-ZPSK also reduces the ICI. Other techniques proposed in the literature treat the PAR and ICI problems as two separate issues. To the best of our knowledge, however over [240], a technique that limits PAR and ICI together has not been reported before. Although [238, 239] are proposed to reduce PAR, they may also reduce ICI because of some null subcarriers.

6.2 PAR Reduction by Adaptive Mapping

6.2.1 M-ZPSK Modulation Scheme

The signal constellation of M-ZPSK can be expressed as

$$F_M = [0, \alpha, \alpha\xi, \dots, \alpha\xi^{M-2}] \quad (6.1)$$

where $\alpha = \sqrt{\frac{M}{M-1}}$ and $\xi = e^{j\frac{2\pi}{M-1}}$. Figure 6.1 shows this constellation for $M = 2, 4, 8$ and 8 . The average power of these signal points is one. Further, this new mapping does not require any redundant subcarriers to deliberately introduce zero amplitude symbol in an OFDM block. Thus, the bandwidth efficiency and the complexity of this mapping is the same as conventional OFDM system, unlike in [238, 239].

However, M-ZPSK incurs a penalty over conventional M-PSK in signal-to-noise ratio (SNR) as signal points are closer in M-ZPSK. Note that the minimum Euclidean distance of M-ZPSK is $\min\{2\sqrt{\frac{M}{M-1}} \sin\{\frac{\pi}{M-1}\}, \sqrt{\frac{M}{M-1}}\}$ whereas that of M-PSK

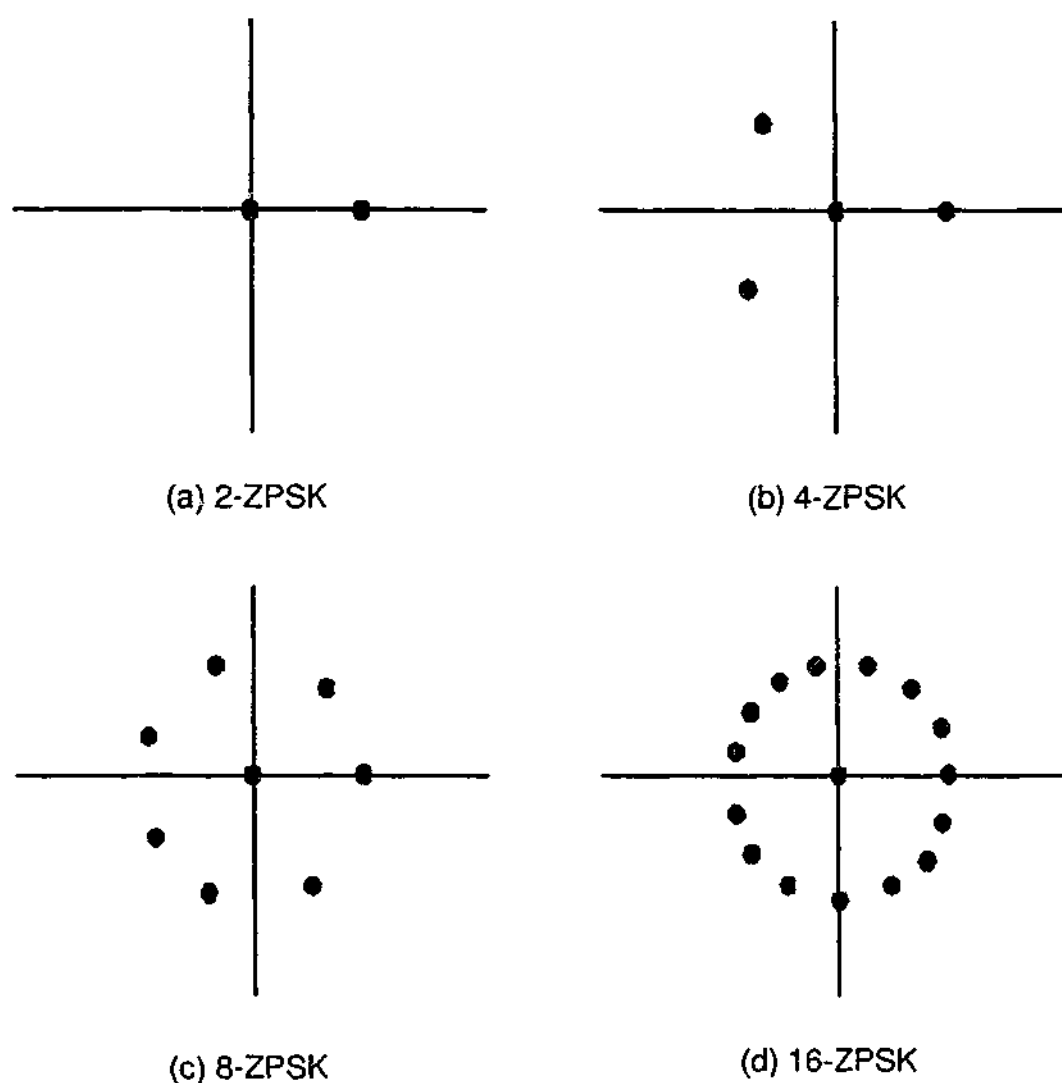


Figure 6.1: Signal constellation for M-ZPSK modulation scheme.

is $2 \sin\{\frac{\pi}{M}\}$. For example, the minimum Euclidean distance is 1.4142 for 4-PSK and 1.1547 for 4-ZPSK. This loss is more than compensated for by the advantages of PAR and ICI reduction.

6.2.2 Adaptive Approach for PAR Reduction

The maximum PAR of a baseband OFDM signal with M-ZPSK can be expressed as

$$\max \text{PAR}(c) = N - N_z \quad (6.2)$$

where N_z is the number of zero amplitude signal points in the OFDM block. Note that N_z is random and it determines the PAR reduction capability of the M-ZPSK mapping. Thus, PAR reduction is insignificant for small N_z .

If all the signal points in M-ZPSK have the same a priori probability, then N_z is equal to $\frac{N}{M}$ on average. For $N = 128$ and $M=4$, the maximum PAR is 19.8 dB whereas

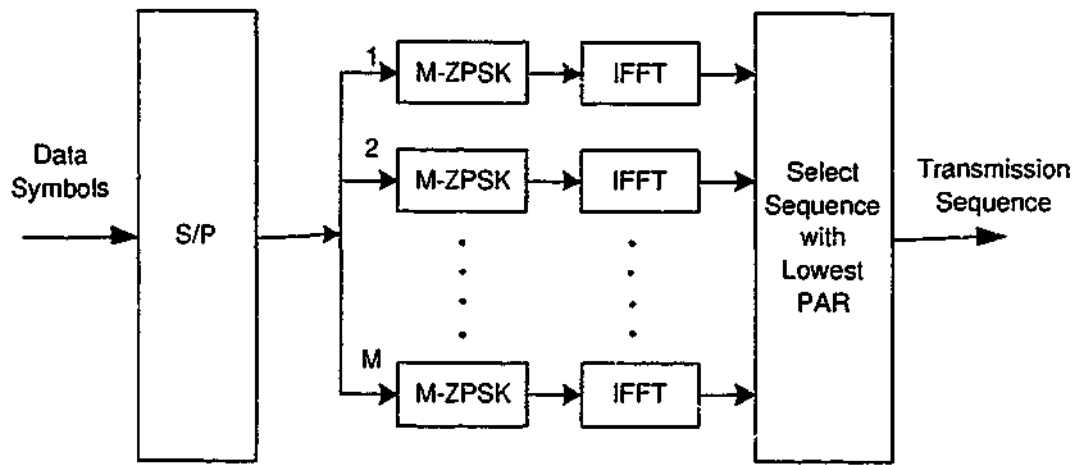


Figure 6.2: Block diagram for an adaptive OFDM scheme.

that of conventional MPSK is 21 dB. However, the PAR reduction of 1.2 dB due to M-ZPSK mapping may not be realized as maximum PAR occurs very rarely in practice.

To exploit the characteristics of the M-ZPSK mapping, we propose an adaptive scheme to reduce PAR for any random data. Let $F_{M_0} = [\theta_0, \theta_1, \dots, \theta_{M-1}]$ where $\theta_0 = 0$ and $\theta_k = \alpha \xi^{k-1}$ for $k = 1, \dots, M-1$. We generate additional $M-1$ constellations which are cyclic shifts of F_{M_0} . That is, $F_{M_1} = [\theta_1, \theta_2, \dots, \theta_{M-1}, \theta_0]$ and $F_{M_2} = [\theta_2, \theta_3, \dots, \theta_{M-1}, \theta_0, \theta_1]$ and so on. Now $N \log_2 M$ bits of data can be modulated into M different frames using the M constellations. The frame with the lowest PAR is selected for transmission. Figure 6.2 shows the simplified block diagram for this adaptive M-ZPSK scheme and Figure 6.3 shows the signal constellation mapping for $M = 4$.

The approximate CCDF of the PAR of this scheme can be expressed as [130]

$$\Pr\{\text{PAR} > \text{PAR}_0\} \approx \left\{ 1 - \exp \left[-\sqrt{\frac{\pi}{3}} N \sqrt{\text{PAR}_0} e^{-\text{PAR}_0} \right] \right\}^M. \quad (6.3)$$

Figure 6.4 shows the CCDF of the PAR of an OFDM signal with $N = 128$. The PAR of an adaptive 4-ZPSK scheme exceeds 9 dB for only 1 out of 10^3 whereas that of QPSK OFDM is 1 out of 10. Further, the simulation results are also close to approximate theoretical results from (2.72) and (6.3).

To recover the data, the receiver has to know which mapping has actually been used in the transmitter. This can be achieved by transmitting $\log_2 M$ bits as SI. As these bits are most important, they should be protected by channel coding. The proposed scheme requires M number of data mapping blocks and IFFT blocks in the transmitter. Moreover, this approach applies to an arbitrary number of subcarriers. Note that this

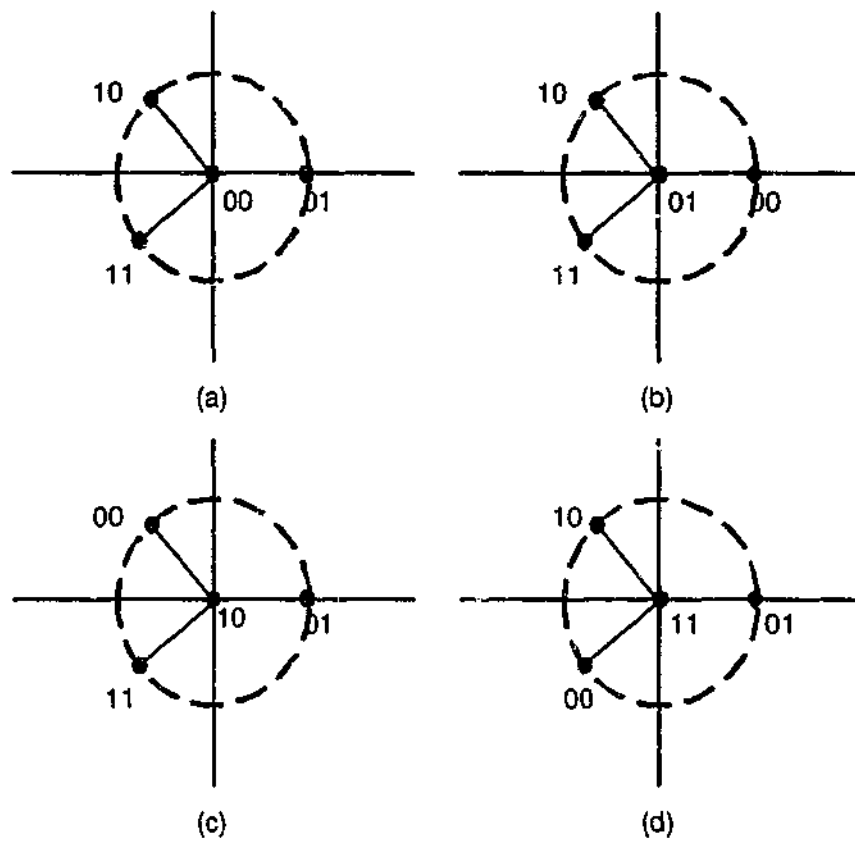


Figure 6.3: Mapping signal constellation for an adaptive OFDM system for $M = 4$.

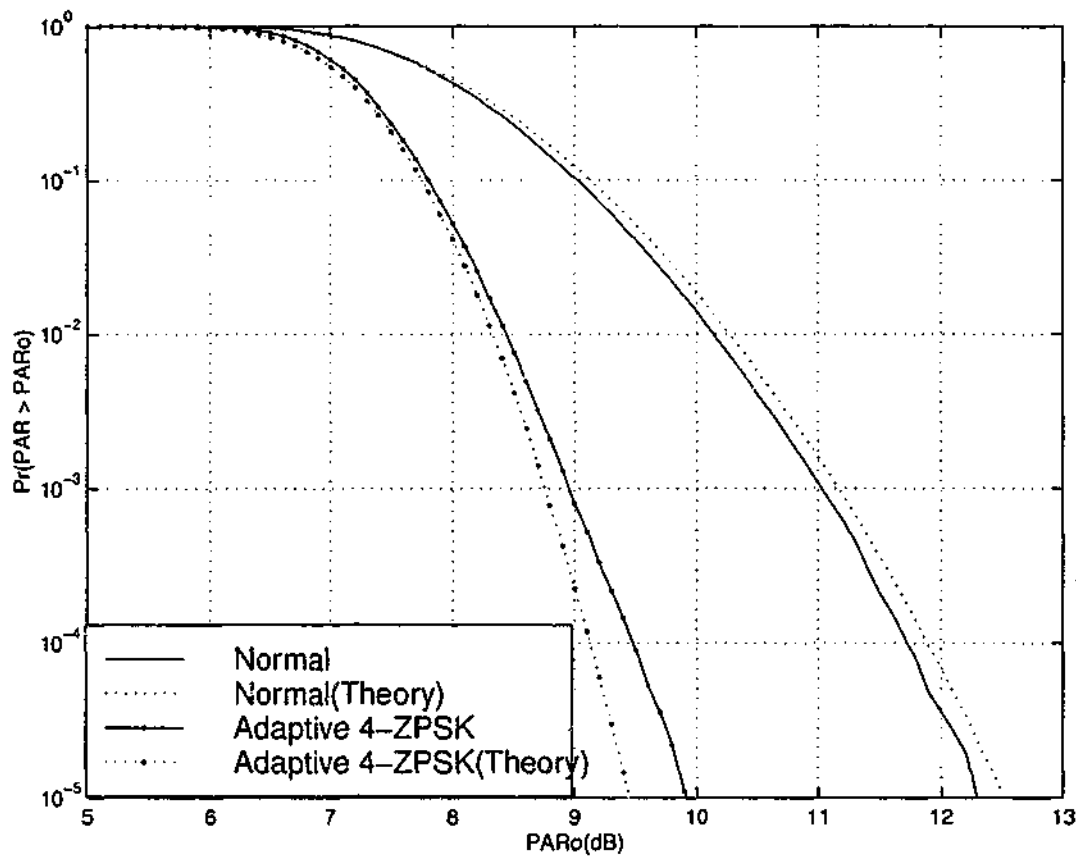


Figure 6.4: CCDF of the PAR of a conventional and adaptive OFDM signal for $M = 4$.

scheme does not require any multiplication and/or complicated optimization as in [172]. Mapping of bits to constellation symbols is a rather simple operation comparing with multiplication. A comparison of complexities of similar schemes for M number of different OFDM blocks is presented in Table 6.1.

Table 6.1: Comparison of the complexity

	Mapping	IFFTs	PAR comparisons	Multiplications
Adaptive OFDM	M	M	M	-
SLM [241]	-	M	M	$N \times M$
PTS [172]	-	M	2^{M-1}	$\frac{2^{M-1} \times N \times (M-1)}{M}$
Interleaving [242]	-	M	M	-

The reduction capability of the proposed scheme is restricted by modulation scheme as M determines the number of different OFDM frames representing the same information. Yet, this is not an issue as high peaks occur infrequently and it is desirable to keep the complexity minimum. Another important advantage of this scheme is reduced sensitivity to frequency offset errors. We will elaborate this in the sequel.

6.2.3 Selected Mapping (SLM)

It is worthwhile to compare the performance of the adaptive M-ZPSK with SLM. In fact, the proposed adaptive M-ZPSK, SLM and other PAR reduction techniques in [130, 172, 183, 241, 242] are based on selecting the OFDM block with lowest PAR among the different OFDM blocks representing the same information. However, they all differ from each other in how different OFDM blocks are generated.

In SLM, U statistically different alternative transmit sequences $\mathbf{a}^{(u)}$ represent the same information. The sequence with the lowest PAR is selected for transmission. To generate $\mathbf{a}^{(u)}$, we define U distinct fixed vectors $\mathbf{P}^{(u)} = [P_0^{(u)}, \dots, P_{N-1}^{(u)}]$ with $P_v^{(u)} = e^{j\varphi_v^{(u)}}$, $\varphi_v^{(u)} \in [0, 2\pi]$, $0 \leq v < N$, $1 \leq u \leq U$. Then, each modulated symbol $\mathbf{c} = [c_0, c_1, \dots, c_{N-1}]$ is multiplied carrierwise with the U vectors $\mathbf{P}^{(u)}$, resulting in a set of U different modulated symbols $\mathbf{c}^{(u)}$ with components

$$c_v^{(u)} = c_v P_v^{(u)} \text{ for } 0 \leq v < N \text{ and } 1 \leq u \leq U. \quad (6.4)$$

For simple implementation, we select $P_v^{(u)} \in [\pm 1, \pm j]$ for $0 \leq v < N$, $1 \leq u \leq U$. All U distinct modulated symbols are passed through IFFT process to get the transmit

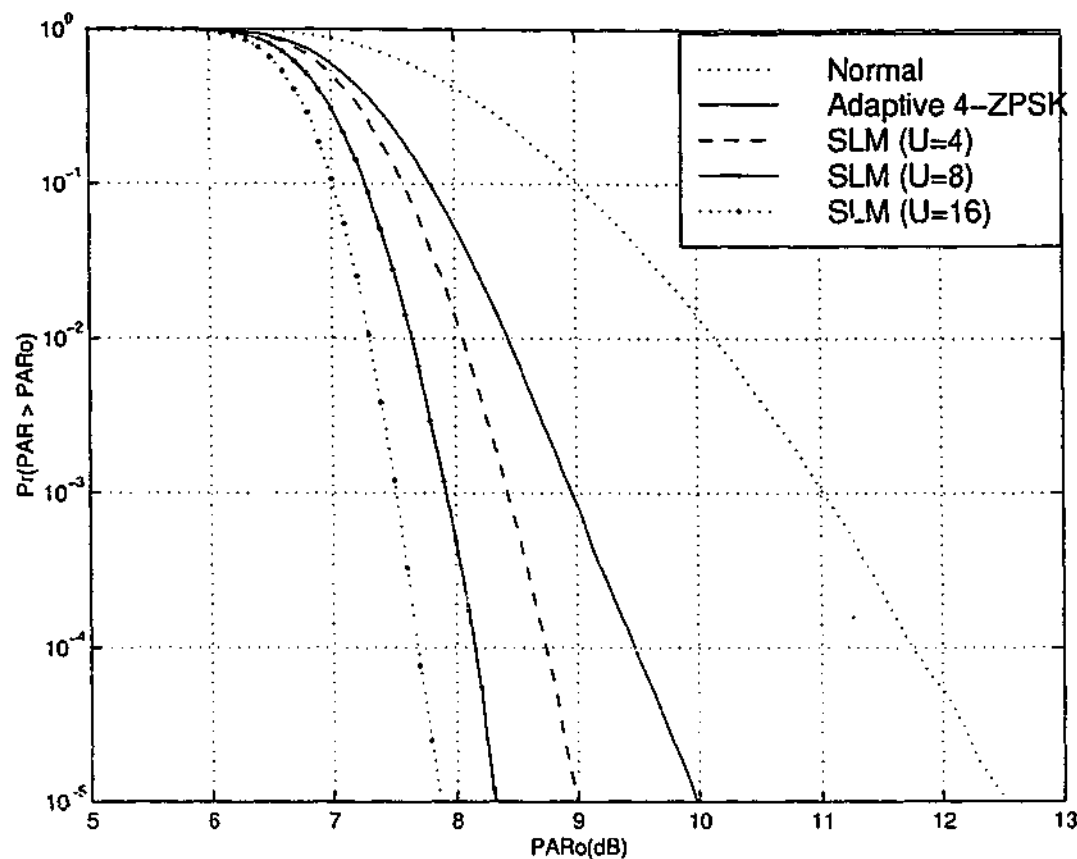


Figure 6.5: CCDF of the PAR of an adaptive OFDM and SLM scheme.

sequences $\mathbf{a}^{(u)} = \text{IFFT}\{\mathbf{c}^{(u)}\}$ and the sequence with the lowest PAR is selected for transmission. In order to recover the data, a pointer to the multiplied sequence has to be transmitted to the receiver as side information [172].

Figure 6.5 shows the CCDF of the PAR of our adaptive OFDM and the SLM scheme for $N = 128$. The PAR of an adaptive 4-ZPSK exceeds 9 dB for only 1 out of 10^3 whereas that of SLM scheme with $U = 4$ is 1 out of 10^5 . With the same number of different OFDM blocks ($M = U = 4$), SLM performs better than the adaptive scheme. Moreover, PAR reduction can be increased in SLM by increasing U whereas the adaptive scheme is limited by M . However, the price for these benefits in SLM is the expensive multiplicative operation.

6.2.4 BER Analysis

We use an analytical method due to Craig [243] to derive the BER for arbitrary 2-D M-ary constellation with polygonal decision boundaries. The conditional symbol error

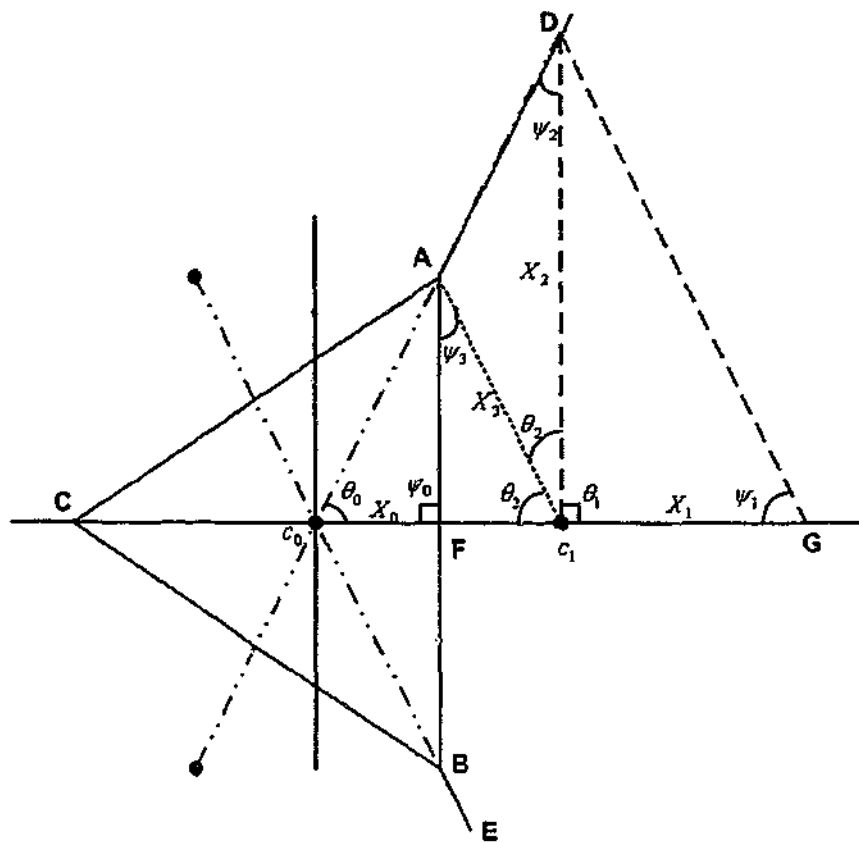


Figure 6.6: Typical 4-ZPSK signal constellation and approximate decision boundaries.

probability (CSEP) given symbol c transmitted is expressed as [243]

$$\Pr_c\{\text{error}/\gamma\} = \frac{1}{\pi} \sum_{k=1}^K W_k \int_0^{\theta_k} \exp \left[\frac{-\gamma X_k \sin^2(\psi_k)}{\sin^2(\theta + \psi_k)} \right] d\theta \quad (6.5)$$

where K is the total number of signal points or decision regions, W_k is the apriori probability of the symbol to which subregion k corresponds, X_k , θ_k and ψ_k are parameters related to decision subregion k and they are independent of the instantaneous SNR denoted by γ .

In M-ZPSK, the zero amplitude symbol, c_0 , has a decision boundary of a polygon with $M - 1$ sides. The minimum distance from c_0 to each side is a where a is equal to $\frac{1}{2} \sqrt{\frac{M-1}{M}}$. The other $(M - 1)$ signal points $(c_1, c_2, \dots, c_{M-1})$ are evenly placed on a circle with radius $2a$. Therefore, the decision region is symmetric for those $(M - 1)$ signal points and $\Pr_{c_n}\{\text{error}/\gamma\}$'s are equal for $n = 1, 2, \dots, M - 1$.

Figure 6.6 shows the signal constellation and decision boundaries for 4-ZPSK. c_0 has a decision boundary of equal triangle (ABC) and other three symbols have a symmetric infinite decision region. Since their conditional probabilities are equal, we consider the symbol c_1 and approximate its infinite decision region as a polygon (DABGE) with five

sides, as shown in Figure 6.6. This approximation can be justified if the distance (say X_1) from the symbol c_1 to the side on the infinite region is large enough.

The conditional symbol error probability given symbol c_1 transmitted is expressed as (6.5)

$$\Pr_{c_1}\{\text{error}/\gamma\} = \frac{2}{M\pi} \sum_{k=1}^3 \int_0^{\theta_k} \exp\left[\frac{-\gamma X_k \sin^2(\psi_k)}{\sin^2(\theta + \psi_k)}\right] d\theta. \quad (6.6)$$

The corresponding angles and lengths are marked on Figure 6.6 and can be calculated by trigonometric manipulations. We also assume equal apriori probabilities for all symbols and neglect the effect of bit mapping.

The conditional symbol error probability given symbol c_0 transmitted is expressed as (6.5)

$$\Pr_{c_0}\{\text{error}/\gamma\} = \frac{2(M-1)}{M\pi} \int_0^{\theta_0} \exp\left[\frac{-\gamma X_0 \sin^2(\psi_0)}{\sin^2(\theta + \psi_0)}\right] d\theta. \quad (6.7)$$

The CSEP can be expressed as

$$\Pr_c\{\text{error}/\gamma\} = \Pr_{c_0}\{\text{error}/\gamma\} + (M-1) \times \Pr_{c_1}\{\text{error}/\gamma\}. \quad (6.8)$$

Using the relationship between symbol error rate and bit error rate [15], the conditional bit error probability (CBEP) becomes

$$P_b\{\text{error}/\gamma\} = \frac{2(M-1)}{M\pi \log_2 M} \sum_{k=0}^3 \int_0^{\theta_k} \exp\left[\frac{-\gamma X_k \sin^2(\psi_k)}{\sin^2(\theta + \psi_k)}\right] d\theta. \quad (6.9)$$

To obtain the average BER on a fading channel, we average (6.9) over the probability density function of the received SNR.

Rayleigh Fading

In a Rayleigh fading channel, the average Symbol Error Probability(SEP) can be expressed as

$$\bar{P}_S = \int_0^\infty \Pr_c\{\text{error}/\gamma\} f(\gamma) d\gamma \quad (6.10)$$

where $f(\gamma)$ is the Rayleigh distributed probability density function (PDF) given by [15]

$$f(\gamma) = \frac{1}{\bar{\gamma}} \exp\{-\gamma/\bar{\gamma}\} \quad (6.11)$$

where $\bar{\gamma}$ is the average SNR. The integral in (6.10) evaluates to

$$\bar{P}_S = \frac{2(M-1)}{M\pi} \sum_{k=0}^3 \int_0^{\theta_k} \left[\frac{\sin^2(\theta + \psi_k)}{\sin^2(\theta + \psi_k) + \bar{\gamma} X_k \sin^2(\psi_k)} \right] d\theta. \quad (6.12)$$

This type of trigonometric integrals can be evaluated in exact closed-form. Using [244, Eq. (6)], (6.12) reduces to

$$\bar{P}_S = \frac{2(M-1)}{M\pi} \sum_{k=0}^3 I_S(\psi_k, \psi_k + \theta_k, \bar{\gamma}X_k \sin^2(\psi_k), 1) \quad (6.13)$$

where

$$\begin{aligned} I_S(\theta_L, \theta_U, a, b) &= \int_{\theta_L}^{\theta_U} \left[\frac{\sin^2 \theta}{a + \sin^2 \theta} \right]^b d\theta \\ &= (\theta_L - \theta_U) + \sum_{n=1}^b (-1)^n \sum_{r=0}^{n-1} \frac{a^{n-r-1/2}}{(1+a)^{n-1/2}} \binom{b}{n} \binom{n-1}{r} \\ &\quad \times P \left(\sqrt{\frac{1+a}{a}} \tan \theta_L, \sqrt{\frac{1+a}{a}} \tan \theta_U, 1+r \right) \end{aligned} \quad (6.14)$$

and

$$\begin{aligned} P(a, b, n) &= \int_a^b \frac{dx}{(1+x^2)^n} \\ &= \frac{(2n-3)!!}{2^{n-1}(n-1)!} (\tan^{-1} b - \tan^{-1} a) + \frac{(2n-3)!!}{(n-1)!} \sum_{k=1}^{n-1} \frac{(n-k-1)!}{2^k (2n-2k-1)!!} \\ &\quad \times \left[\frac{b}{(1+b^2)^{n-k}} - \frac{a}{(1+a^2)^{n-k}} \right]. \end{aligned} \quad (6.15)$$

Therefore, the average BER (6.13) becomes

$$\bar{P}_b = \frac{2(M-1)}{M\pi \log_2 M} \sum_{k=0}^3 \theta_k - \lambda_k \left[\tan^{-1} \{ \lambda_k \tan(\theta_k + \psi_k) \} - \tan^{-1} \{ \lambda_k \tan \psi_k \} \right] \quad (6.16)$$

where

$$\lambda_k = \sqrt{\frac{\bar{\gamma}X_k \sin^2 \psi_k}{1 + \bar{\gamma}X_k \sin^2 \psi_k}} \quad (6.17)$$

(6.16) is a closed-form expression for the error rate.

Nakagami-m Fading

In a Nakagami-m fading channel, the average SER is given by (6.10), where $f(\gamma)$ is the Nakagami-m distributed PDF [15]

$$f(\gamma) = \frac{1}{\Gamma(m)} \left(\frac{m}{\bar{\gamma}} \right)^m \gamma^{m-1} e^{-m\gamma/\bar{\gamma}} \quad (6.18)$$

where m is a parameter specifying the severity of fading.

Using [244, Eq. (29)], the average BER of M-ZPSK in the Nakagami- m fading channel can be expressed as

$$\bar{P}_b = \frac{2(M-1)}{M\pi \log_2 M} \sum_{k=0}^3 I_S(\psi_k, \psi_k + \theta_k, (\bar{\gamma}/m) X_k \sin^2 \psi_k, m). \quad (6.19)$$

Ricean Fading

In a Ricean fading channel, the average SER is given by (6.10), where $f(\gamma)$ is the Ricean distributed PDF given by [245]

$$f(\gamma) = \frac{1+K}{\bar{\gamma}} \exp\left(-K - \frac{(1+K)\gamma}{\bar{\gamma}}\right) I_0\left(2\sqrt{\frac{K(K+1)\gamma}{\bar{\gamma}}}\right) \quad (6.20)$$

where $K(\geq 0)$ is the Rice factor and I_0 is the zero-order Bessel function of the first kind.

Using [246, Eq. (6.631.1)], we can simplify (6.10) to

$$\bar{P}_s = \frac{2\lambda(M-1)e^{-K}}{M\pi} \sum_{k=0}^3 \int_{\psi_k}^{\psi_k+\theta_k} \frac{\sin^2 \theta}{X_k \sin^2 \psi_k + \lambda \sin^2 \theta} \exp\left\{\frac{K\lambda \sin^2 \theta}{X_k \sin^2 \psi_k + \lambda \sin^2 \theta}\right\} d\theta \quad (6.21)$$

where $\lambda = \frac{1+K}{\bar{\gamma}}$.

AWGN Channel

To compute the BER of the 4-ZPSK in AWGN channel, (6.9) can be used directly. Moreover, the average BER of QPSK for AWGN channel is expressed as [15]

$$P_b = Q\left(\sqrt{\frac{2E_b}{N_0}}\right) \quad (6.22)$$

where $Q(x) = \int_x^\infty \frac{e^{-t^2/2}}{\sqrt{2\pi}}$.

Figure 6.7 shows the BER of the adaptive 4-ZPSK modulated OFDM signal and QPSK modulated OFDM signal in AWGN channel. We assume coherent symbol detection and perfect SI at the receiver. The simulation results and the theoretical results for 4-ZPSK are not close as they differ at low SNR. This is due to the approximate decision region used in the analysis. The BER may also depend on the bit mapping as these constellations are not according to Gray mapping. However, we assume the same

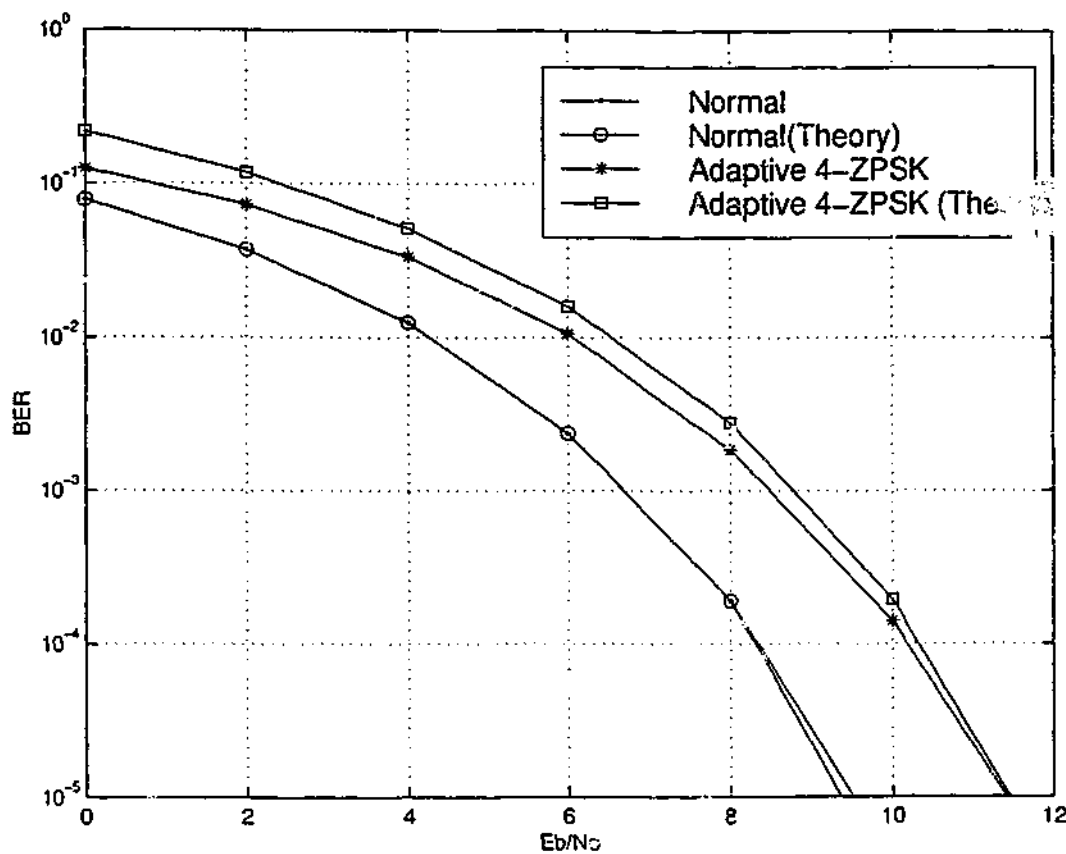


Figure 6.7: BER of an adaptive OFDM scheme in AWGN channel for $M = 4$.

probability of error for all mappings. Further, QPSK performs better than 4-ZPSK with an SNR gain of 1 dB at any BER. This is due to larger minimum Euclidean distance in QPSK over 4-ZPSK. Note however that this is more than compensated for by ICI and PAR reduction.

Multipath Fading Channel

The fading channel next considered in this paper is a multipath fading channel with coherence bandwidth smaller than the total bandwidth of the OFDM system and thus seen as frequency selective fading. The fading process is assumed to be stationary and slowly varying compared with the symbol duration of the OFDM signal, such that it is approximately constant during one OFDM symbol length T_o . We assume that the use of a cyclic prefix (CP) both preserves the orthogonality of the tones and eliminates the ISI between consecutive OFDM symbols.

The impulse response of the multipath channel model can be written as [15]

$$g(\tau) = \sum_{l=0}^{L-1} \alpha_l \delta(\tau - \tau_l T_s) \quad (6.23)$$

where α_l are zero mean complex Gaussian random variables with a power-delay profile $\theta(\tau_l)$ and L is the total number of resolvable paths. We assume an exponentially decaying power-delay profile $\theta(\tau_l) = Ce^{-\tau_l/\tau_{rms}}$ where C is a constant. We also assume that the delays $\tau_l T_s$ are uniformly and independently distributed over the guard length of the OFDM symbol.

The received sequence can be expressed as [15]

$$\hat{c}_k = H_k c_k + n_k \text{ for } k = 0, 1, \dots, N - 1 \tag{6.24}$$

where H_k is the attenuation on each tone given by [15]

$$H_k = G\left(\frac{k}{NT_s}\right) \tag{6.25}$$

where $G(\cdot)$ is the frequency response of the channel $g(\tau)$. Since H_k is complex Gaussian random variable, each subchannel can be considered as Rayleigh fading. Therefore, the average BER of QPSK can be expressed as [15]

$$P_b = \frac{1}{2} \left(1 - \sqrt{\frac{\bar{\gamma}}{1 + \bar{\gamma}}} \right) \tag{6.26}$$

and the average BER of 4-ZPSK can be calculated from (6.16).

Figure 6.8 shows the BER of an adaptive 4-ZPSK modulated OFDM signal and QPSK modulated OFDM signal in a multipath fading channel with $L = 6$ and $\tau_{rms} = 1\mu s$. Maximum Likelihood (ML) coherent symbol detection and exact knowledge of channel are assumed. Further, we assume perfect SI. QPSK performs better than 4-ZPSK with an SNR gain of 2 dB at any BER. This degradation is due to small minimum Euclidean distance in 4-ZPSK over QPSK. Further, the simulation and analytical results for 4-ZPSK do not agree closely as approximate decision regions are used for deriving the BER of 4-ZPSK.

6.3 ICI Reduction

The average Carrier-to-Interference Ratio (CIR) is defined as [65, 66, 68, 69]

$$\text{CIR}(k) = \frac{|c_k S_0|^2}{E\left\{ \left| \sum_{l=0, l \neq k}^{N-1} S_{l-k} c_l \right|^2 \right\}} \tag{6.27}$$

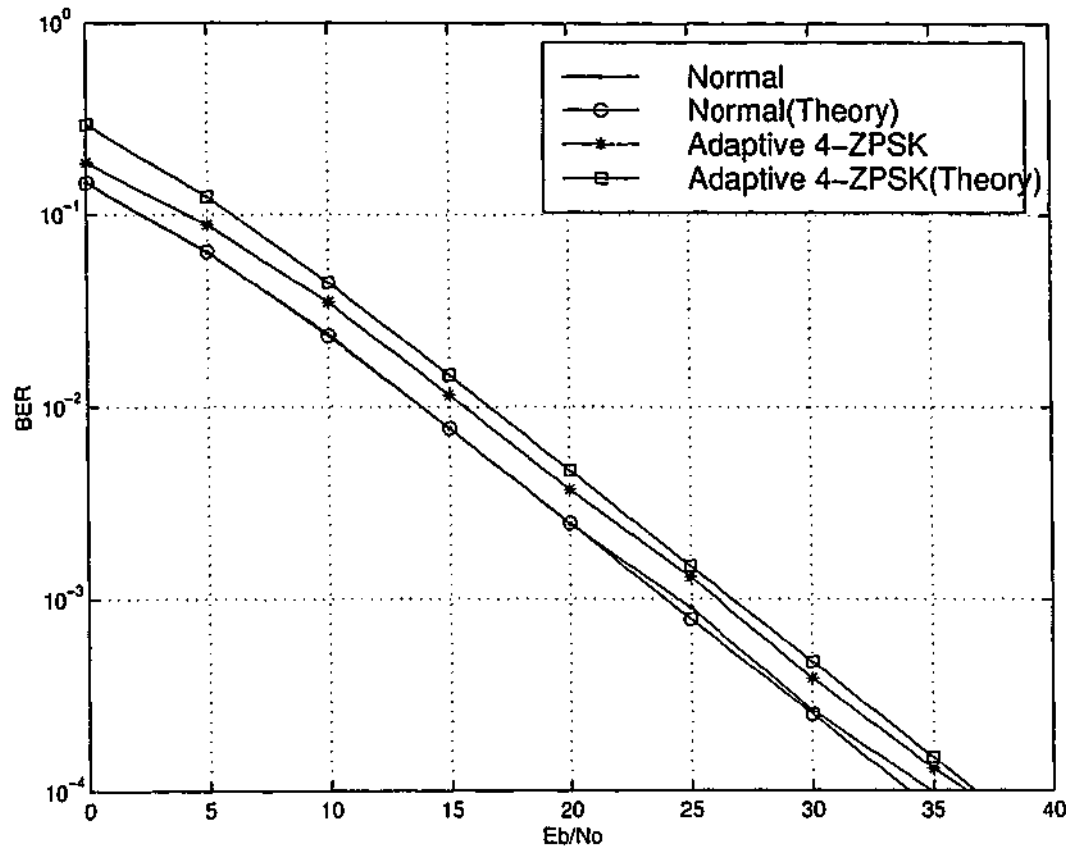


Figure 6.8: BER of an adaptive OFDM scheme in multipath fading channel for $M = 4$.

where $E\{\cdot\}$ denotes the expected value over the distribution of data. This average CIR has previously been used by many authors to study the effects of ICI. This measure readily gives an indication of system performance. Alternatively, an exact calculation of BER in the presence of ICI can be done using the CHF method [247]. However, the average CIR is inappropriate for M-ZPSK, as a CIR of zero does not provide any insight of the ICI effects. Thus, we use BER as a prime measure to study ICI effects of the proposed system. However, the average CIR of nonzero symbol carrying subcarrier can be used to study the ICI reduction capability of the proposed scheme. Figure 6.9 shows the variation of average CIR of 0-th subcarrier with ϵ . A nonzero symbol is fixed on the 0-th subcarrier of the adaptive scheme. The adaptive scheme offers an average CIR gain of 1.5 dB over the conventional QPSK scheme independent of ϵ .

Moreover, the average CIR of a nonzero symbol carrying subcarrier can be derived approximately to compare the performance of M-PSK and M-ZPSK schemes. The average CIR for an OFDM system with M-PSK can be expressed as (2.34)

$$\text{CIR}(k) = \frac{|S_0|^2}{\sum_{(N-1) \text{ terms}} |S_{l-k}|^2} \quad (6.28)$$

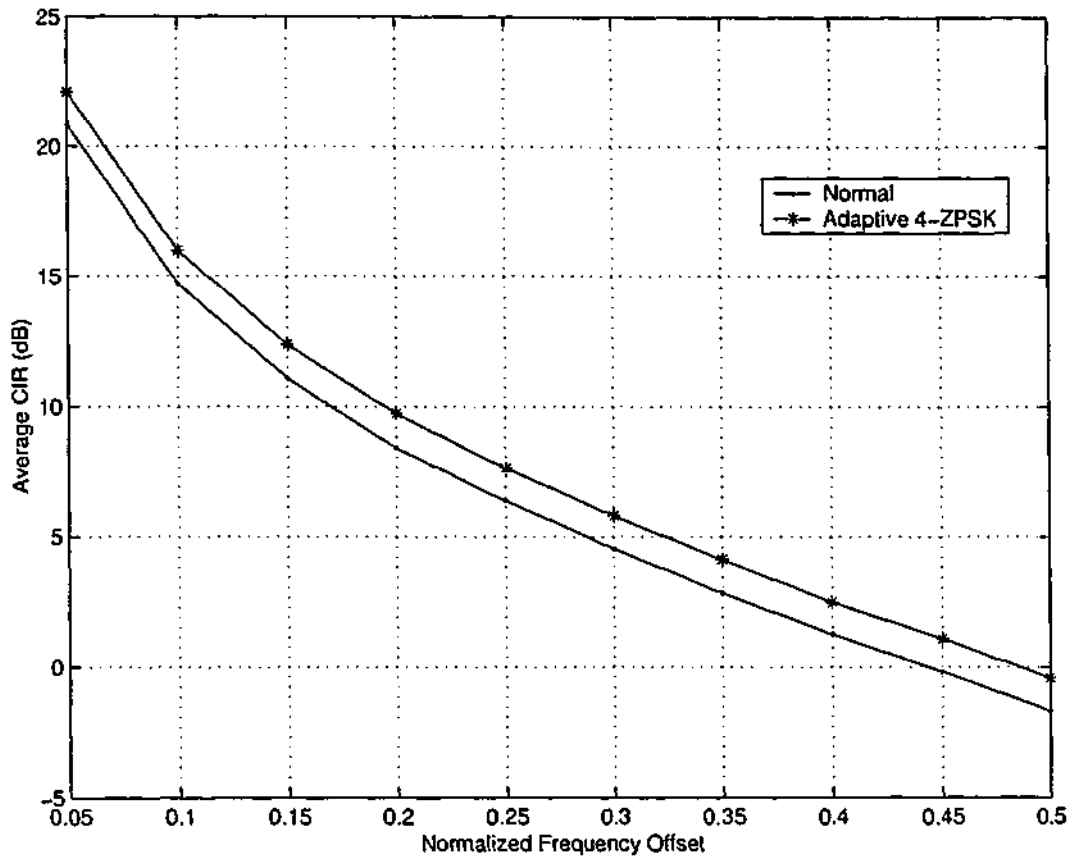


Figure 6.9: Variation of average CIR of non zero symbol with ϵ .

and that of M-ZPSK for nonzero symbol carrying subcarrier is

$$\text{CIR}(k) = \frac{|S_0|^2}{\sum_{(N-N_z-1) \text{ terms}} |S_{l-k}|^2} \quad (6.29)$$

Thus, the average CIR in M-ZPSK is higher than that of M-PSK as the number of terms in the summation in denominator is low in M-ZPSK. Therefore, the M-ZPSK modulated OFDM signal is less sensitive to ICI than the conventional schemes. The following simulation results of BER also confirm this behavior.

Figure 6.10 shows the BER of an adaptive 4-ZPSK modulated OFDM signal for $\epsilon = 0.05$ and 0.1. The adaptive scheme out performs the conventional QPSK scheme at high SNR and large ϵ . For instance, QPSK scheme performs better than adaptive scheme with $\epsilon = 0.05$. The adaptive scheme offers an SNR gain of 3 dB over conventional QPSK scheme at the BER of 10^{-4} and $\epsilon = 0.1$. Figure 6.11 also shows the BER performance as a function of $\epsilon = 0.1$. Clearly, the adaptive scheme is less sensitive to frequency errors than the conventional scheme but its benefits over the conventional scheme depend on ϵ and SNR.

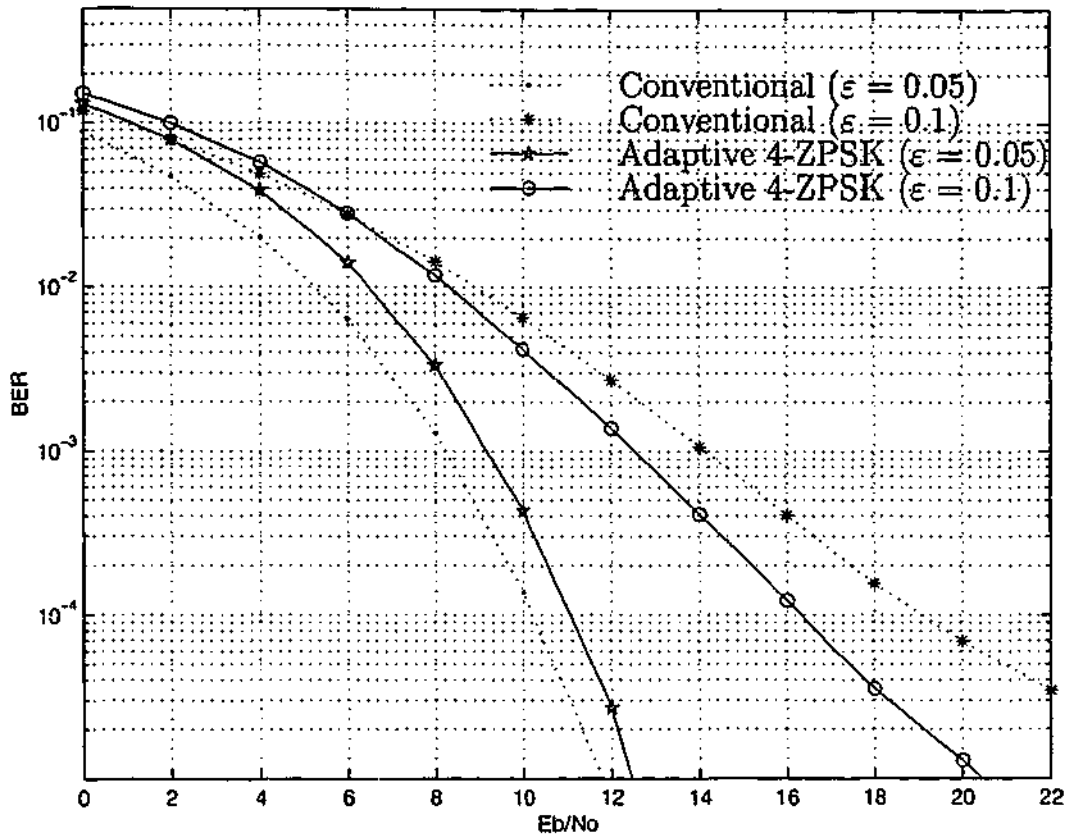


Figure 6.10: BER Performance in AWGN channel for $M = 4$.

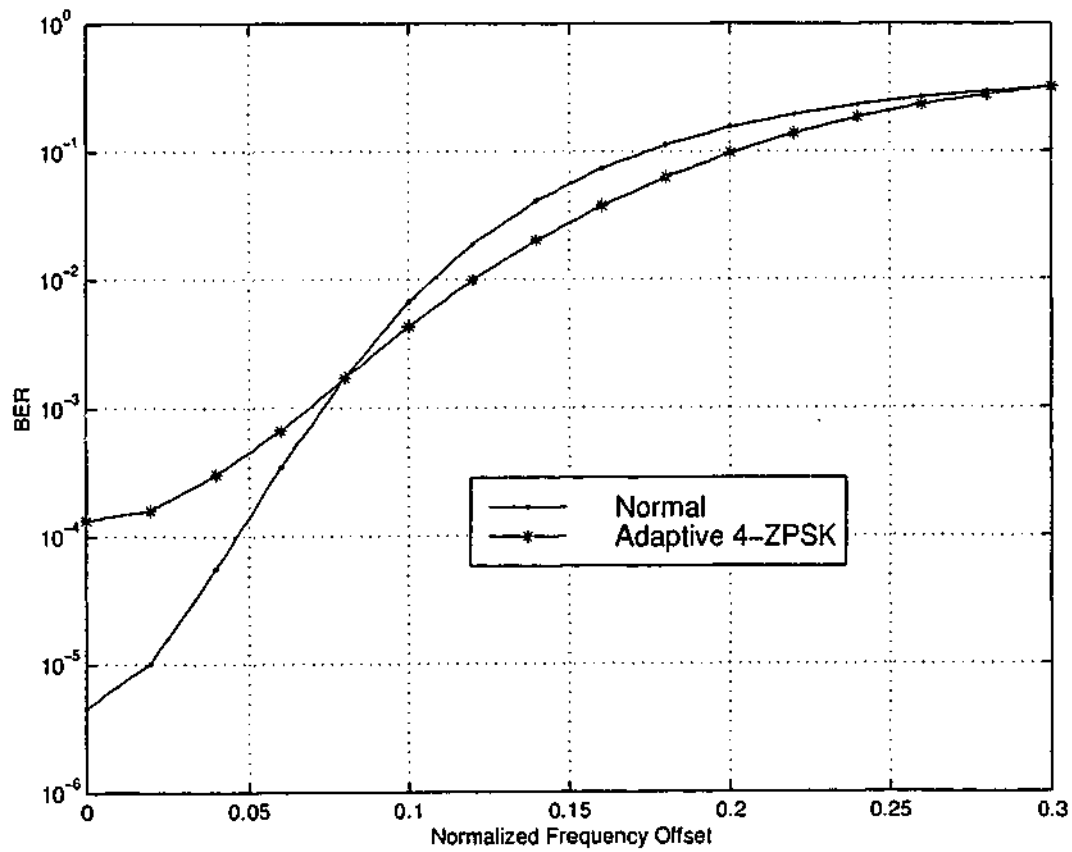


Figure 6.11: Variation of BER with ϵ in AWGN channel for $M = 4$ and $E_b/N_o = 10dB$.

Interestingly, a simplified adaptive M-ZPSK mapping could be used for ICI reduction if PAR reduction is not taken into account. In this case, the frequency of the bit pattern of $\log_2 M$ bits in an input data frame is counted. The most likely bit pattern is mapped to a signal point of zero amplitude. This increases the vanishing terms in the summation in (6.29) and thus reduces the ICI effects. Therefore, we need only one mapping and one IFFT calculation, as in the conventional system. A simple counter circuit can be used to select a mapping scheme based on the input data sequence. However, transmission of SI is necessary as in PAR reduction criteria. Note that this approach will not maximize the PAR reduction. Therefore, we do not consider this simplified approach further as we are only interested in a single solution for PAR and ICI issues.

6.4 Out-of-band Radiation

Out of band radiation are caused by non-linearities. The PSD of the OFDM signal and the proposed adaptive OFDM signal are estimated via simulations. The PSD is estimated using Welch's averaged periodogram method specified in Matlab. The OFDM signal is oversampled by a factor of eight and these samples (total of $8N$) are windowed by a Hanning window of length $8N$.

Figure 6.12 and Figure 6.13 depict the PSD in the presence of SL and SSPA non-linear devices respectively. Curves 1 to 4 represent the different back-off values of the amplifier. For example, for a back-off of 8 dB, to provide -60 dB adjacent channel separation requires a channel spacing of about two times the symbol rate for conventional OFDM, with adaptive OFDM the channel spacing is nearly the symbol rate. Thus, the adaptive OFDM provides a spectrally-efficient solution for the adjacent channel interference problem, which can arise in portable cellular applications. Comparison of performances in Figure 6.12 and Figure 6.13 reveals that depending on the permissible out of band radiation level, the amplifier back-off can be reduced by 2 to 3 dB when adaptive OFDM is used instead of conventional OFDM. When the back-off of the amplifier is decreased, out of band radiation level is increased and both schemes show the same out of band radiation level.

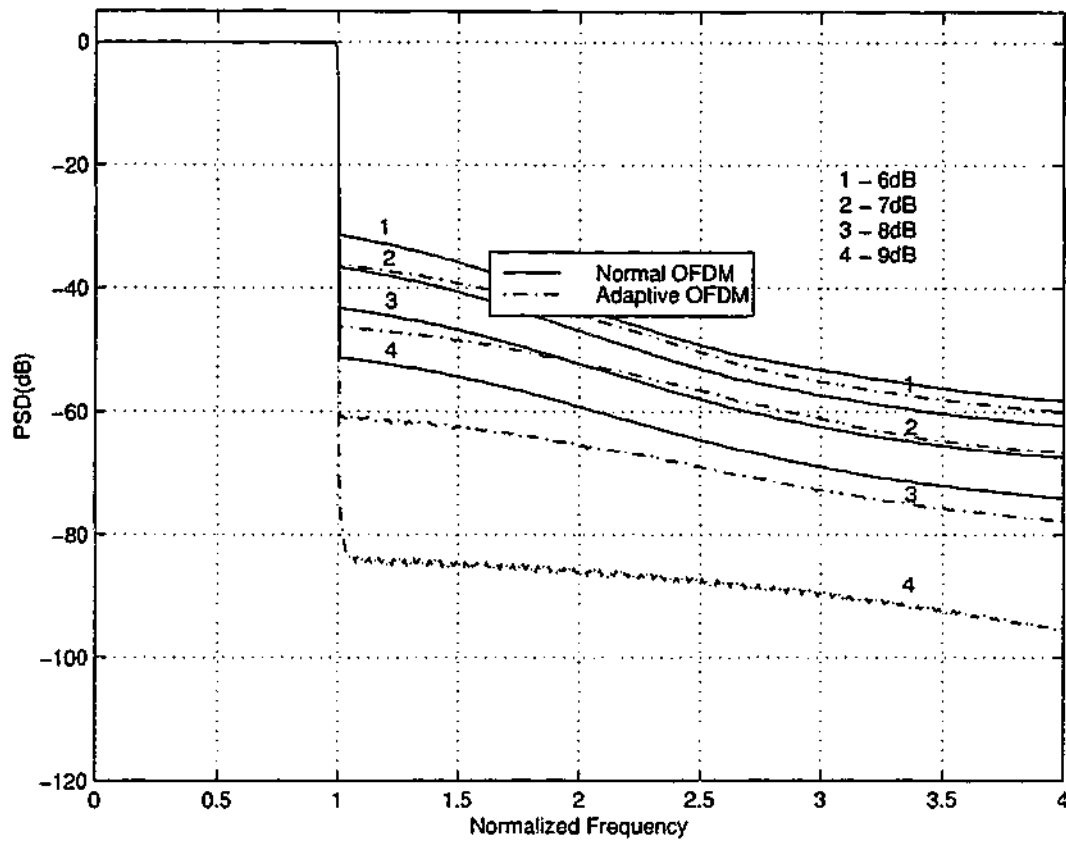


Figure 6.12: Spectrum of an OFDM signal after passing through a SL.

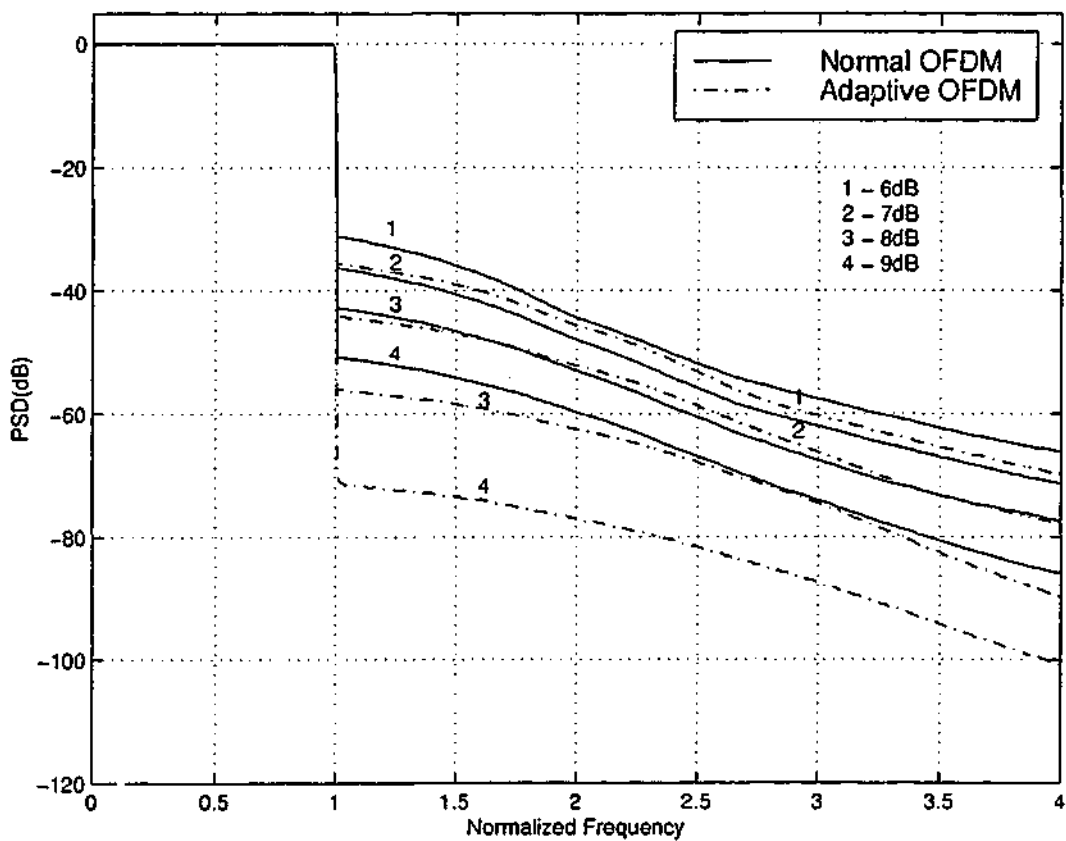


Figure 6.13: Spectrum of an OFDM signal after passing through a SSPA.

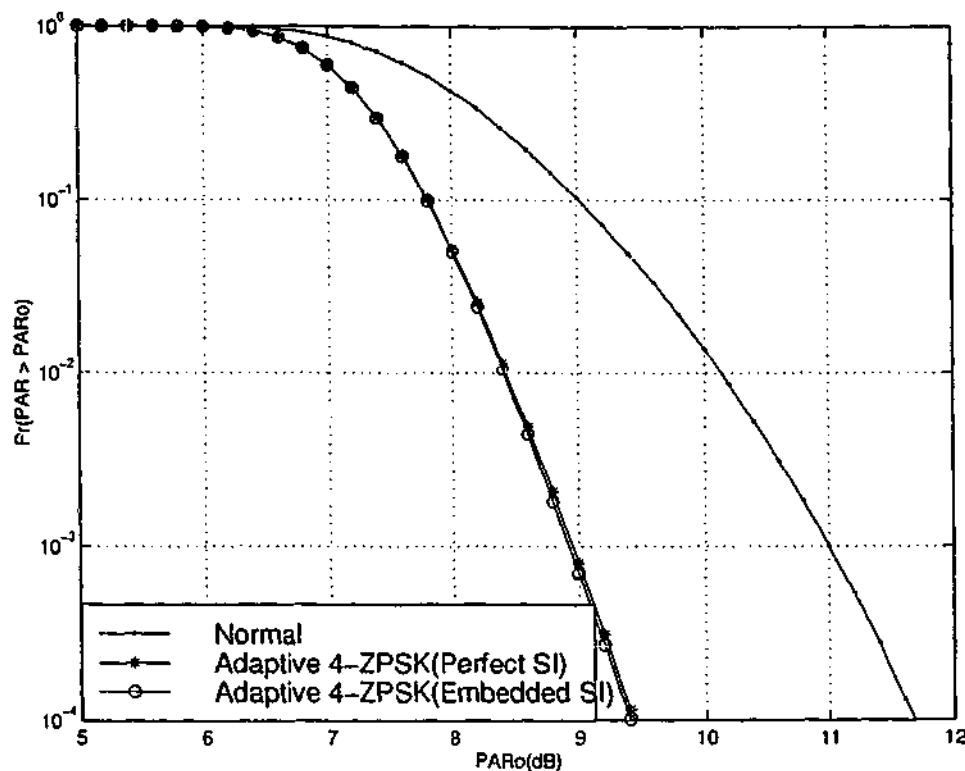


Figure 6.14: CCDF of the PAR of an adaptive OFDM for $M = 4$ with embedded SI.

6.5 Side Information (SI)

SI to the receiver is a critical issue as unreliable SI will increase the bit error rate. We propose two techniques to recover the transmitted data frame at the receiver. First approach is to use some subcarriers to transmit SI explicitly and the other is to use error correction codes.

6.5.1 Explicit SI

We propose to embed the SI at the beginning of the data frame. Thus, we explicitly allocate some subcarriers to carry SI bits. The uncoded SI requires a minimum of $\log_2 M$ bits. However, a simple forward error correction (FEC) code can be used to increase the reliability of the SI. The SI bits are modulated using a conventional modulation scheme and the modulated symbols are placed onto the N_{SI} subcarriers. The data symbols, which are adaptive M-ZPSK symbols, are on the remaining $(N - N_{SI})$ subcarriers. Now the PAR optimization process is done with the embedded SI. This is one advantage of using an adaptive modulation scheme. The receiver first decodes the bits in the first N_{SI} subcarriers to receive the SI. However, the data throughput is now slightly reduced.

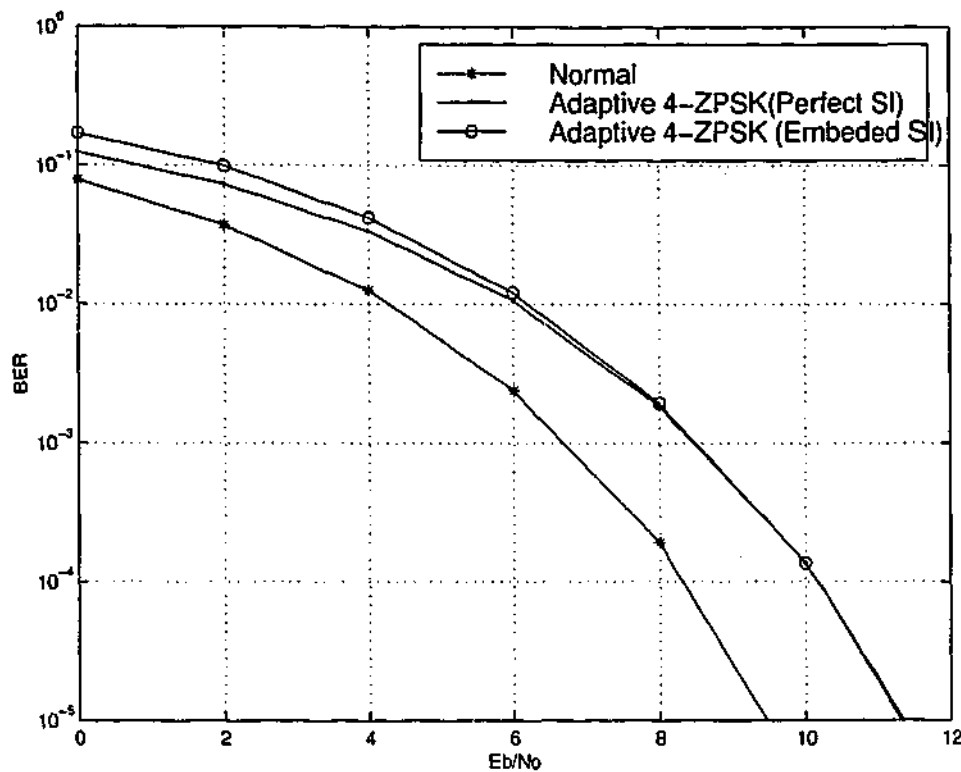


Figure 6.15: BER of an adaptive OFDM in AWGN channel for $M = 4$ with embedded SI.

Figure 6.14 shows the CCDF of the PAR of an OFDM signal with embedded SI for $N = 128$ and $M = 4$. We use a (7,4) Hamming code with single error-correcting capability. For the above system parameters, we now need to allocate 4 subcarriers (0, 1, ..., 3) for the coded SI. Figure 6.14 shows an insignificant degradation in the CCDF as SI is inserted in the data frame before the PAR optimization process. Figure 6.15 shows the corresponding BER performance in AWGN channel. Again, we observe a negligible degradation in BER performance at high SNR.

6.5.2 Implicit SI

The perfect SI is necessary to correctly identify the mapping used in the transmitter. However, we have only M possible de-mappings at the receiver and one out of M is correct one. If there are no transmission errors in the channel, only one out of M de-mapping will give an error free data frame. Therefore, we propose to use a coding scheme to correctly identify the transmitted data frame.

We consider a block code $[n, k, d]$ with t error correcting capability. The receiver makes upto M decoding attempts using the M signal constellations. Suppose F_{Mk} ($0 \leq k \leq M - 1$) be the constellation used by the transmitter. In the first attempt,

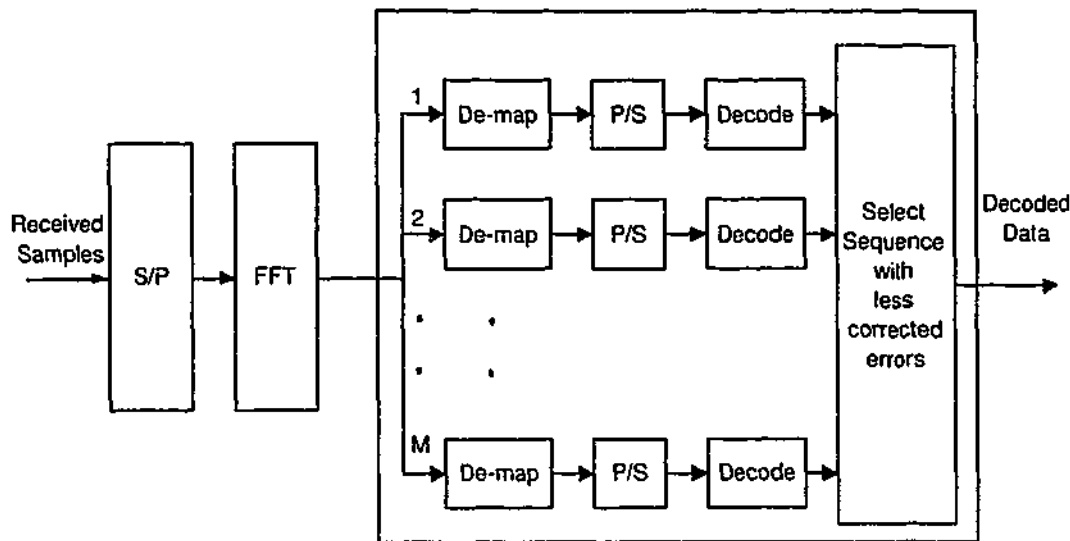


Figure 6.16: Receiver block diagram for an adaptive OFDM with implicit SI.

the receiver uses F_{M_0} and hard decision decoding to decode the data and counts the number of errors it has corrected. Likewise, the number of errors are counted to other $(M - 1)$ constellations $(F_{M_1}, \dots, F_{M_{M-1}})$. The receiver chooses the frame with low number of corrected errors as a transmitted data frame. Therefore, we do not need any SI explicitly to identify the transmitted data frame. However, loss in data throughput due to coding and the moderate complexity in the receiver incurs in this scheme. Yet, the channel coding is vital to improve the error performance and this proposed scheme serves this purpose as well. The block diagram of the receiver for the proposed scheme is shown in Figure 6.16.

Figure 6.17 shows the CCDF of the PAR of a $(255,191,8)$ BCH coded OFDM signal for $N = 128$ and $M = 4$. The correlation introduced by the coding does not influence the CCDF of PAR. Figure 6.18 shows the corresponding BER performance in AWGN channel. We use hard decision decoding. At low SNR, we observe a significant degradation in BER performance of the proposed approach over that of perfect SI. This is due to the inability of the code to correct errors at low SNR. That means noise dominates at low SNR and the coding is ineffective. However, the proposed approach improves the BER performance at high SNR. Adaptive coded 4-ZPSK with perfect SI is also shown in Figure 6.18 to realize the efficiency of the used codes. The coding gain will be high if soft decision decoding is used. However, it is difficult to extend the proposed implicit SI method with soft decision decoding, thus limiting the use of powerful convolutional codes.

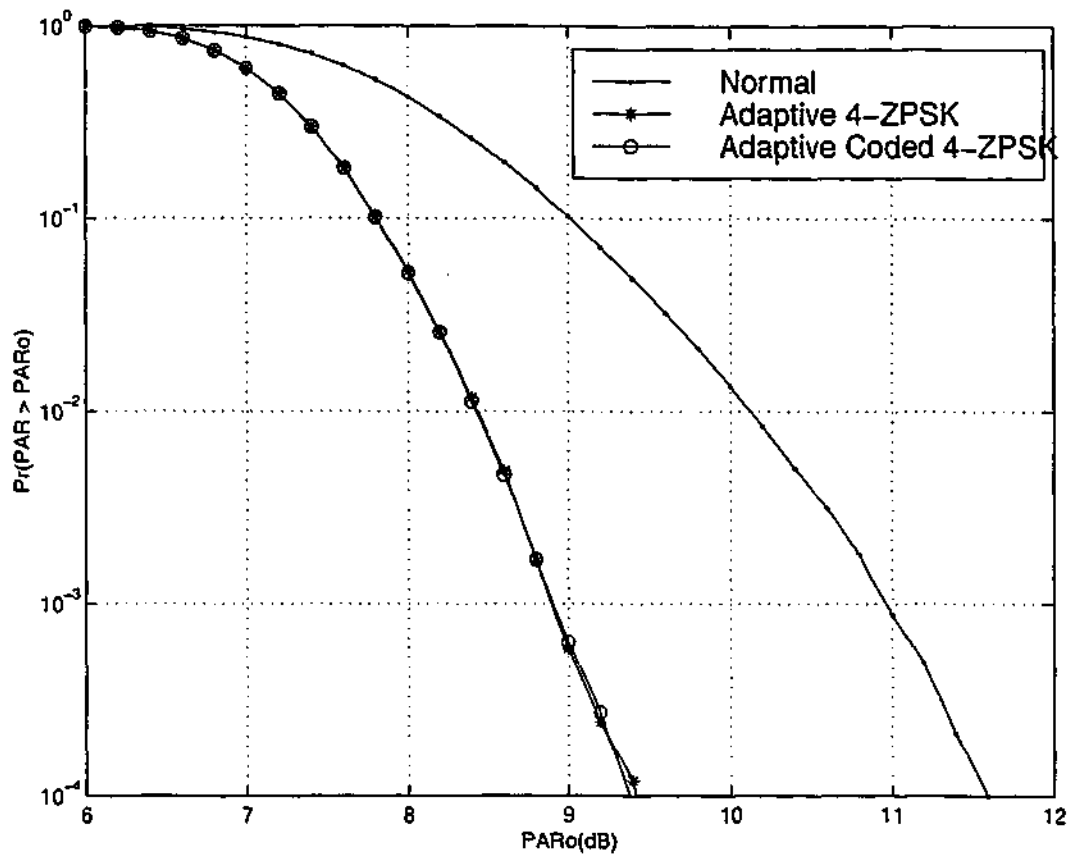


Figure 6.17: CCDF of the PAR of an adaptive coded OFDM for $M = 4$.

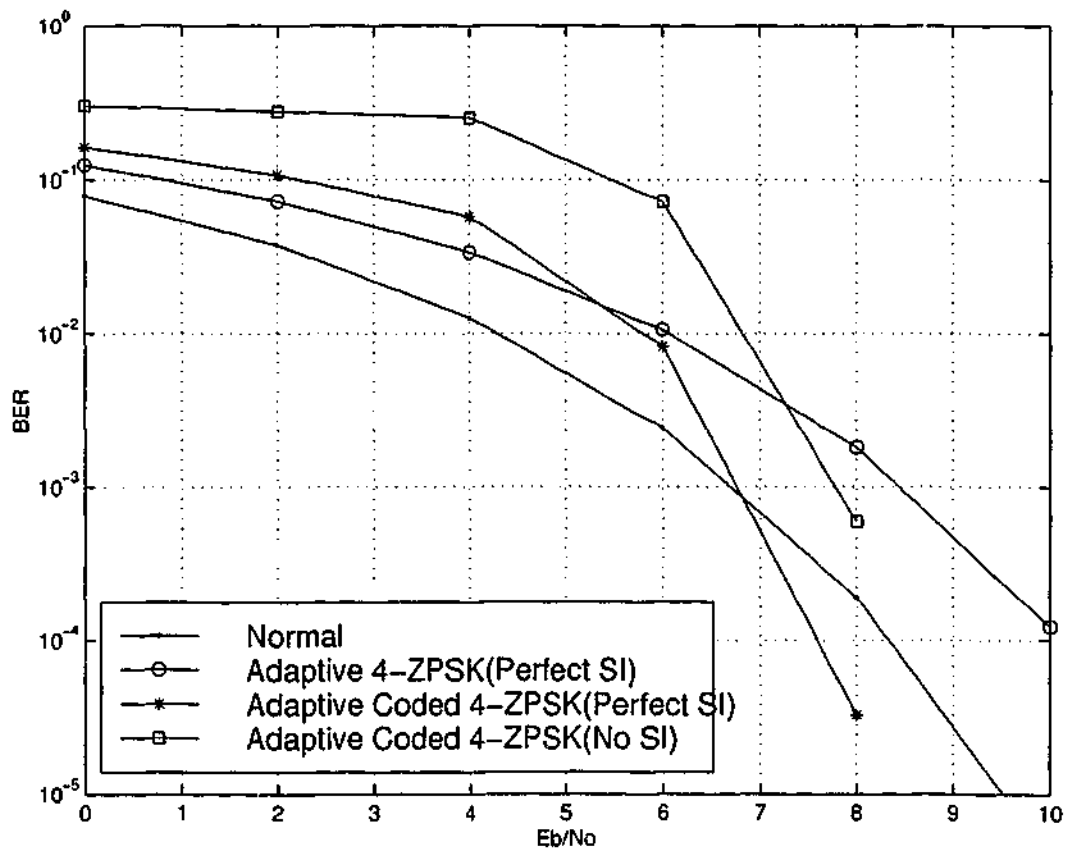


Figure 6.18: BER of an adaptive coded OFDM in AWGN channel for $M = 4$.

6.6 Conclusions

This chapter has presented the adaptive M-ZPSK to reduce both PAR and ICI of an OFDM signal simultaneously. The PAR improvement of the proposed scheme is comparable with other well known approaches [172, 183, 241, 242] with almost the same or less complexity. Simulation and analytical results show that adaptive 4-ZPSK modulated OFDM system with 128 subcarriers improves the PAR by 2.5 dB at the expense of 2 dB loss in SNR over conventional QPSK system. However, in a channel with normalized frequency offset of 0.1, it offers a 3 dB gain in SNR at BER of 10^{-4} over conventional QPSK. Moreover, for a back-off of 8 dB, to provide -60 dB adjacent channel separation requires a channel spacing of about two times the symbol rate for conventional OFDM; with adaptive OFDM the channel spacing is nearly the symbol rate, which is a 50% saving in bandwidth. The price for these benefits is increased complexity over conventional OFDM systems. The simulation results show that the transmission of embedded SI in an OFDM block does not degrade the PAR characteristics of the proposed scheme and the BER performance. The proposed coded adaptive scheme, which does not require any explicit SI, performs better than an uncoded adaptive scheme at high SNR but with increased complexity.

Chapter 7

PAR Reduction for Multi-Code CDMA

This chapter presents the analysis of peak-to-average power ratio (PAR) problem in multi-code code division multiple access (multi-code CDMA) systems. The statistical distribution of PAR is derived and the achievable PAR reduction for a given code rate is estimated. We show that the PAR in multi-code CDMA communications systems can be reduced by the PTS and SLM approaches. In PTS, the subblocks are multiplied by a set of phase factors that are optimized to minimize PAR. In SLM, several different data frames are generated and the data frame with the lowest PAR is selected for transmission. We also show that BER performance improves when the PAR-reduced multi-code CDMA signal is passed through a nonlinear amplifier.

7.1 Introduction

Mobile communications services are penetrating into our society at an explosive growth rate. The major services offered by the second generation mobile systems are limited to basic services such as voice and low bit-rate data applications. The demand for a variety of wideband services, high speed internet access and high quality video transmission, will continue to increase. The physical limitations and impairments on radio channels, such as bandwidth constraints, multipath fading, noise and interference, present a technical challenge to reliable high data rate communications. The third generation (3G) wireless systems, called IMT-2000, are being designed to support such wideband services and to provide universal access and global roaming. Introduction of wideband packet data services for wireless a Internet up to 2 Mb/s will probably be the main

attribute of 3G systems [248–250]. Wideband direct sequence code division multiple access (Wideband CDMA or WCDMA) is emerging as the predominant wireless access technology for the 3G systems and is being developed by a number of vendors.

Recently, multi-code CDMA has been introduced as a new transmission scheme for high speed and flexible data rate communications over wireless channels [251]. The basic idea of multi-code CDMA is to split the high speed traffic source data into a number of low speed streams, each occupying the same bandwidth. These low speed data streams are modulated using parallel orthogonal codes such as a Walsh code to achieve simultaneous transmission. Depending on the user's data rate, the number of codes are allocated by a central control unit. That is, the user who wishes to transmit at a higher data rate is simply assigned additional orthogonal transmission channels and appears to the base station as multiple users. Incidentally, the abbreviation MC-CDMA has been widely used in the literature for both multicarrier CDMA, where characteristic of OFDM and CDMA systems are combined, and multi-code CDMA. To avoid confusion and ambiguity, we refrain from using the abbreviation MC-CDMA to denote multi-code CDMA. Instead, we always refer to it as "multi-code CDMA".

In the recent ETSI and ARIB standard WCDMA, variable spreading factors and multi-code transmission are used to obtain multiple data rates [252, 253]. Variable spreading factors are used for the low and medium data rates and it is combined with multi-code for high data rates. For high data rates, spreading gain in the variable spreading scheme will be very small and thus the performance will significantly degrade due to intersymbol interference. Thus, multi-code CDMA can effectively deal with various multimedia data of various bit rates by suitable multiplexing. Like CDMA, the multi-code CDMA systems utilize Rake receivers to cope with multipath fading and maintain several advantages of the CDMA systems, such as soft handoff and frequency reuse. Moreover, the multi-code CDMA requires no major alteration of the radio frequency circuitry. However, high peak-to-average power ratio (PAR) is considered as a critical problem in multi-code CDMA systems [253–265]. This is discussed in detail in the following sections.

7.2 Multi-code CDMA Systems

The conventional CDMA systems have very limited user throughput and are not well suited to varying data rate applications. The multi-code CDMA is proposed to support variable rate users and provide high data rate applications in CDMA systems. In the multi-code system, when a user needs n times the basic source rate, it converts its signal stream into n basic rate streams by a serial-to-parallel conversion, encodes each with a different orthogonal code, and superimpose them before upconverting for radio transmission. Walsh-Hadamard codes are used as orthogonal codes and typically n is equal to 2^m with m between 0 and 6 [260, 261]. In fact, n is a variable that denotes the source rate a user is transmitting. For instance, $n = 1$ means that the user is transmitting at the basic rate. Since multi-code CDMA is used for high speed data transmission with high transmit power, the number of active users supported by the system is small. Therefore, for simple analysis, we will consider single user utilizing full capacity.

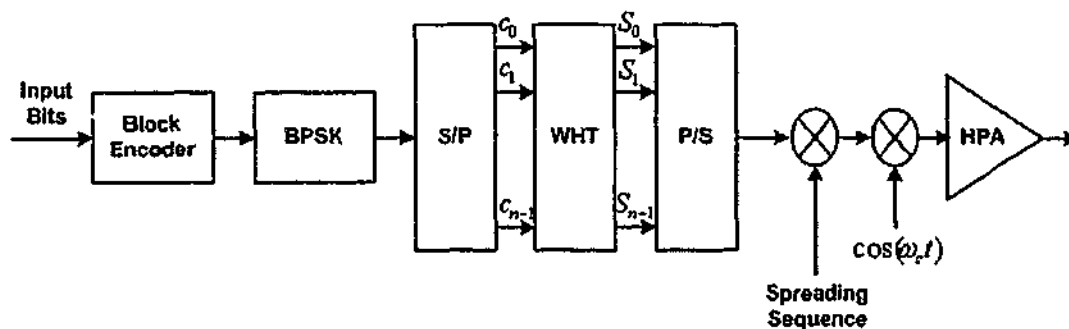


Figure 7.1: Simplified block diagram of the transmitter in multi-code CDMA system.

Figure 7.1 shows the simplified block diagram of the transmitter in multi-code CDMA systems. The high rate data stream is first converted into n parallel streams and then it is coded and superimposed by a Walsh-Hadamard transform (WHT). The resulting parallel-to-serial converted sequence is multiplied by a spreading sequence, which is used to identify the base station a user is communicating with. Thus, all the users in a cell will have the same base station code. This sequence is then transmitted as a form of BPSK signal after the upconversion and amplification process. At the receiver, the received signal is downconverted by the local oscillator and despread by the spreading sequence. The despread signal is then serial-to-parallel converted to pass through the inverse Walsh-Hadamard transform (IWHT). The resulting sequence is

converted back to serial for detecting the transmitted sequence. A simplified block diagram of the receiver in multi-code CDMA systems is shown in Figure 7.2. Since we are interested in PAR problem, we assume an AWGN channel. Thus, we ignore the Rake receiver structure at the receiver.

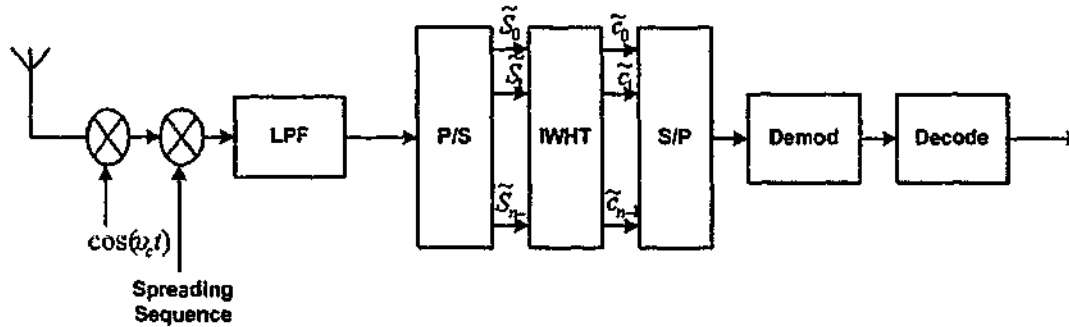


Figure 7.2: Simplified block diagram of the receiver in multi-code CDMA system.

7.3 PAR Analysis

The transmitted signal in the multi-code CDMA systems has large amplitude fluctuation since the multi-code signal is the sum of each parallel code channel signal. This large amplitude fluctuation causes nonlinear distortions in the presence of nonlinear devices, such as HPA. The power efficiency of the HPA is an important factor as it determines the size, weight and the battery recharging time of mobile hand sets. The HPA exhibits high power efficiency when it operates near the saturation point. However, the HPA is very nonlinear in the saturation region and this nonlinearity causes out-of-band radiation and in-band distortion. This results in bit error performance degradation and spectral spreading to adjacent bands. The degree of these effects depends on the envelope variation of the signal. The PAR is used to quantify these envelope fluctuations. To avoid signal distortion, the HPA can be operated in the linear region by providing large back-off to the HPA. This results in lower power efficiency. Otherwise, signal distortion is inevitable if HPA is operated near saturation point to have high power efficiency. Therefore, reducing the PAR of the multi-code signal is an efficient way to tackle this problem.

Several techniques have been proposed in the open literature to reduce the PAR of the multi-code signal. In fact, this problem is clearly parallel to that of OFDM systems. Both OFDM and multi-code CDMA involve signals that are the sums of some number

of basic signals from an orthogonal set. That means the resulting signal is an orthogonal transform of the data to be transmitted. In OFDM, the signal is related to a Fourier transform where as it is Walsh-Hadamard transform in multi-code signal. Thus, OFDM results in continuous-time sinusoidal signals and multi-code CDMA results in discrete-time Walsh-Hadamard sequences. Because of linear combinations of basic signals, both systems can suffer from high PAR. It is worthwhile to note that the multi-code signal does not require oversampling to find true PAR, unlike in OFDM. In fact, the possible PAR values can be calculated in advance. Because of this discrete PAR, the statistical distribution of PAR becomes discrete. Moreover, the resemblance of PAR problem in both leads to the use of PAR reduction techniques in OFDM to multi-code CDMA systems.

It is worthwhile to mention that the block coding approach for PAR reduction in OFDM was first proposed in [151, 152]. The basic idea is not to transmit OFDM symbols with large PAR values. This requires that both the transmitter and the receiver keep a list of "allowed" data frames (ie. a codebook). Unfortunately, this implementation fails for large n . However, this failure motivates algebraic encoding/decoding for such block codes. To this end, progress has been made on several fronts. First, PAR reduction codes using Golay complementary sequences and second-order Reed-Muller codes have been developed [162, 163]. This method ensures PAR at most 3 dB while allowing simple encoding and decoding for binary, quaternary or higher-phase signalling together with good error correction. However, these codes suffer from vanishing code rate as n increases.

This block coding principle is extended to multi-code CDMA signal to reduce its PAR. In [253–255] precoding techniques to reduce the signal envelope variations are developed, with precoder designs based on simulated annealing and analytical expressions. Constant amplitude coding techniques are also developed in [256–259], but these are ad-hoc and valid for short lengths only. In [260, 261], PAR reduction codes are systematically studied. Codes which are distant (Hamming sense) from the first-order Reed-Muller code will have small PAR. Bounds on the trade-off between rate, PAR and error-correcting capability of codes for multi-code CDMA are also derived. The connections between the code design problem, bent functions and algebraic coding theory are exploited to construct code families.

In [262,263] the impact of an amplifier nonlinearity is investigated for various multi-code systems. The use of a few parallel transmitted sequences, in conjunction with quasi-ML (maximum likelihood) detection, is proposed in [262,263] as an effective way to combat nonlinear effects in multi-code systems. A predistortion technique to reduce nonlinear effects are reported in [264,265]. This data predistorter, which rests upon the fixed point approach associated with the contraction mapping theorem, employs an iterative method for effective and simple implementation.

We add to the above contributions by proposing the use of PTS [172,183,185] and SLM [172] to reduce the PAR in multi-code CDMA systems. Generating several statistically different OFDM frames for a data frame and selecting the one with the lowest PAR is a common approach in [172,183,185]. This approach improves the statistics of the PAR at the expense of additional complexity. However, an advantage is that this approach does not require much redundancy compared to that of coding. That is to say, PAR-reduced coding can lead to very low code rates.

7.3.1 PAR Definition

The output of the WHT can be represented as

$$\mathbf{S} = H_n(c_0, c_1, \dots, c_{n-1})^T \quad (7.1)$$

where n is the size of the WHT and $c_k \in \{+1, -1\}$ is a data symbol. The $n \times n$ Hadamard matrix H_n is a matrix whose entries are limited to ± 1 and can be defined recursively by $H_1 = (1)$ and

$$H_n = \begin{pmatrix} H_{n/2} & H_{n/2} \\ H_{n/2} & -H_{n/2} \end{pmatrix}.$$

We shall write ordered n -tuples $\mathbf{c} = (c_0, c_1, \dots, c_{n-1})$ and $\mathbf{S} = (S_0, S_1, \dots, S_{n-1})$. The sequence $\{S_k\}$ is a multilevel sequence, with levels varying from $-n$ to $+n$. The transmitted signal is obtained by multiplying S_k by a spreading sequence, filtering and frequency up conversion. Details of these operations are omitted, as they do not greatly affect the PAR.

The peak-to-average-power ratio (PAR) is defined as

$$\text{PAR}(\mathbf{c}) = \frac{1}{n} \max_{0 \leq k \leq n-1} |S_k|^2. \quad (7.2)$$

The PAR is a function of the data frame and recall that there are 2^n distinct data frames. For any input data frame, we have

$$1 < \text{PAR}(\mathbf{c}) \leq n. \quad (7.3)$$

For example, for $n = 64$ the PAR can be as high as 18 dB ($10 \log_{10}(64)$). Very high PAR values are very rare though. If $n = 2^m$, all sequences that achieve $\text{PAR}(\mathbf{c}) = n$ must be codewords of RM(1, m) (first order Reed-Muller code of length 2^m). There are 2^{m+1} such codewords. For randomly distributed data, the probability of an occurrence of the highest peak is $2^{m+1}/2^n = 2^{m+1-n}$. This probability is negligible when n is large - as is the case in practice.

7.3.2 CCDF of the PAR

Since the input data is randomly distributed in many applications (if not, it can be made so by the use of a suitable scrambling operation), $\text{PAR}(\mathbf{c})$ itself is a random variable. The complementary cumulative distribution function (CCDF), the probability that the PAR of an OFDM symbol exceeds a certain threshold, is useful for many purposes. The CCDF is defined as

$$F(\zeta) = \Pr(\text{PAR}(\mathbf{c}) \geq \zeta). \quad (7.4)$$

In order to determine this distribution, we first evaluate the statistical distribution of S_k . The data symbols c_k are discrete random variables with $\Pr(c_k = 1) = \Pr(c_k = -1) = \frac{1}{2}$. Since each row of H_n consists of $+1$ and -1 , S_k can be modelled by the binomial distribution. For example, the first row of H_n is $[1, 1, \dots, 1]$ and thus $S_0 = \sum_{k=0}^{n-1} c_k$. The magnitude of S_0 is equal to $2l$ if $n/2 + l$ c_k 's are $+1$ and $n/2 - l$ c_k 's are -1 . The probability of this occurrence can be readily evaluated. Similar considerations apply to other S_k as well. Consequently, the distribution of the magnitude of S_k ($0 \leq k < n$) is given by

$$\Pr(|S_k| = 2l) = \begin{cases} \frac{1}{2^n} \binom{n}{n/2}, & l = 0 \\ \frac{1}{2^{n-1}} \binom{n}{\frac{n+2l}{2}}, & 0 < l \leq n/2. \end{cases} \quad (7.5)$$

The corresponding cumulative distribution function (cd) of $|S_k|$ ($0 \leq k < n$) is a staircase function and is given by

$$F_1(\zeta) = \begin{cases} \sum_{l=0}^m \Pr(|S_k| = 2l), & 2m \leq \zeta < 2m + 2 \\ 1, & n < \zeta. \end{cases} \quad (7.6)$$

The distribution of the PAR relates to the distribution of $\max(|S_0|, |S_1|, \dots, |S_{n-1}|)$, which is simply the above raised to the power n provided $|S_k|$ ($0 \leq k < n$) *independently* distributed. We assume that they are different. As shown below using simulation results, this assumption leads to an accurate expression for the distribution. The CCDF of the PAR is then given by

$$F(\zeta) = 1 + [F_1(\zeta)]^n. \quad (7.7)$$

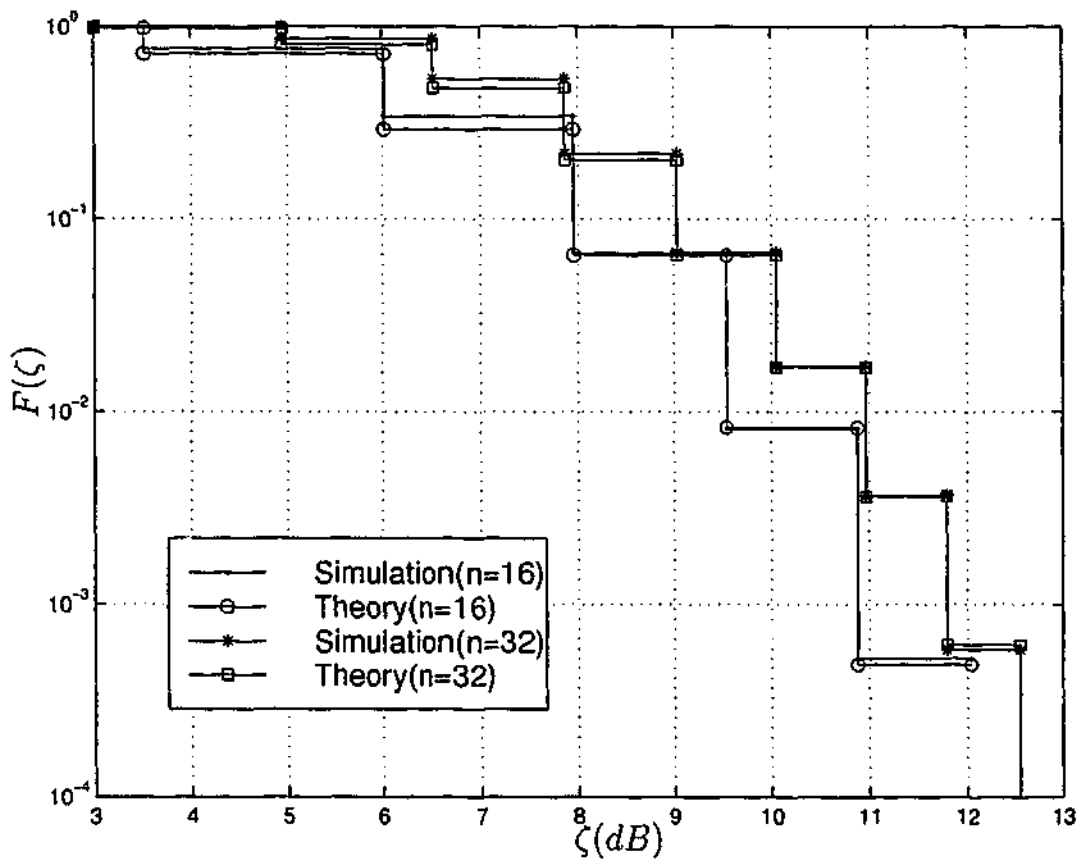


Figure 7.3: CCDF of PAR of conventional multi-code CDMA system.

Figure 7.3 shows the CCDF of the PAR as a function of n . For $n = 64$, the PAR exceeds 13.5 dB for only 1 out of 10^4 of all data blocks and for 90% of all data blocks, the PAR is below 9.5 dB. Moreover, the theoretical results for CCDF agree with simulation results.

The above CDF is an approximation, albeit a good one. In fact, some probabilities can be computed exactly. Paterson has shown that for any word \mathbf{c} of length n [260],

$$\text{PAR}(\mathbf{c}) = n \left(1 - \frac{2d_*(\mathbf{c})}{n} \right)^2 \quad (7.8)$$

where $d_*(\mathbf{c}) := \min\{d_H(\mathbf{c}, \mathbf{w}) : \mathbf{w} \in \text{RM}(1, m)\}$ denotes the minimum Hamming distance between \mathbf{c} and the first-order Reed-Muller(RM) code of length 2^m .

For each $\text{RM}(1, m)$ codeword, we can find $\binom{n}{l}$ binary sequences at a Hamming distance l from it. Provided $l \leq 2^{m-2}$, two sequences at distance l from two distinct $\text{RM}(1, m)$ codewords cannot be the same. Based on this observation, we have

$$\Pr \left\{ \text{PAR}(\mathbf{c}) = \frac{(n-2l)^2}{n} \right\} = \binom{n}{l} \frac{2^{m+1}}{2^n} \text{ for } 0 \leq l \leq 2^{m-2}. \quad (7.9)$$

This exact probabilities may also be used to evaluate upper tails of the PAR distribution.

7.3.3 Achievable Coding Rate

Consider block coding to reduce the PAR to ζ . This can in principle be achieved by excluding all sequences with PAR over ζ . From (7.7), the achievable coding rate is

$$R(\zeta) = \frac{\log_2 [2^n \Pr(\text{PAR}(\mathbf{c}) \leq \zeta)]}{n} = 1 - \log_2 [F_1(\zeta)]. \quad (7.10)$$

Figure 7.4 shows the variation of code rate as a function of PAR. For $n = 32$, PAR can be reduced below 3 dB with a code rate of 0.7. However, finding low PAR codes are difficult for large n .

7.4 Reducing PAR Using Multiple Signal Generation

The basic idea behind this approach is to generate multiple, different symbols to represent an input data frame and select the minimum PAR symbol for transmission. There are several techniques based on this idea and these primarily differ in the way they generate the multiple symbols. Another issue with this approach is the need for side information to tell the receiver which one of the signals has been used. Suppose $M \geq 1$

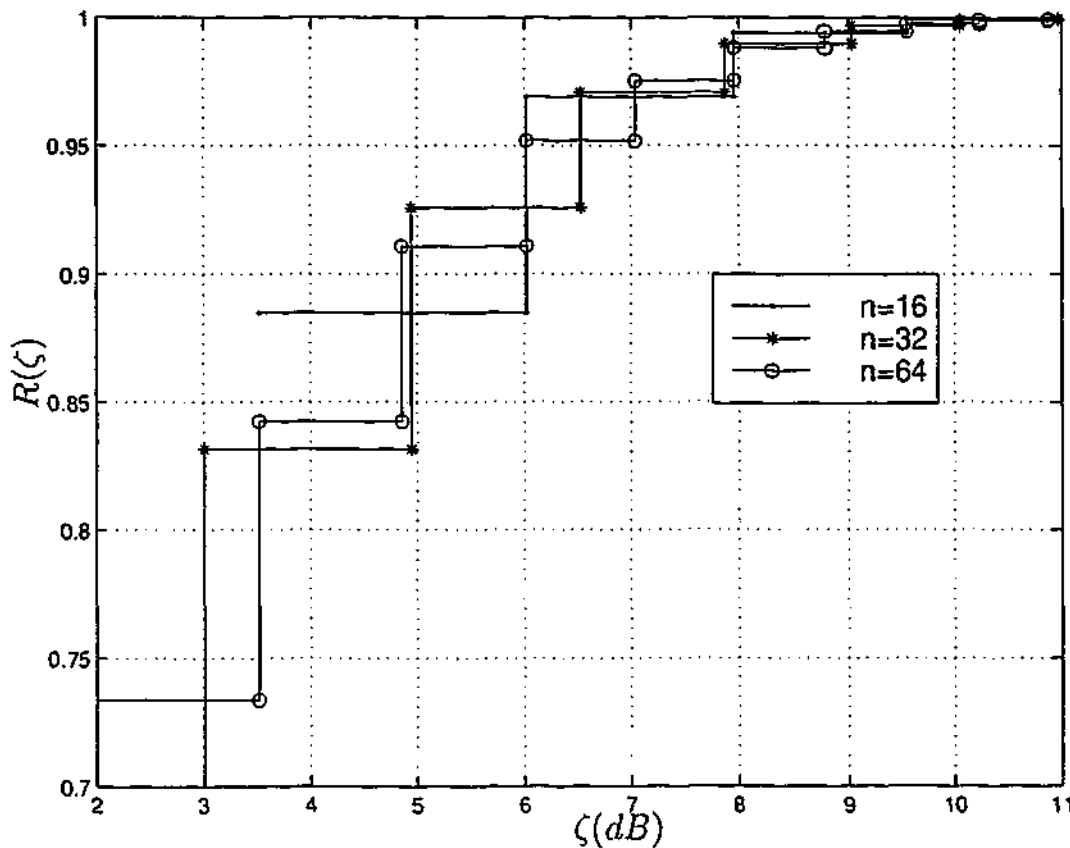


Figure 7.4: Variation of code rate with PAR.

"different" multi-code CDMA symbols are generated for an information sequence. The CCDF of the minimum of these is given by

$$\Pr(\text{PAR}_{\min} \geq \zeta) = [F_c(\zeta)]^M. \quad (7.11)$$

Figure 7.5 shows the CCDF of the multiple signal generation method as a function of M for $n = 32$. Both PAR reduction and complexity increase with M .

7.4.1 Partial Transmit Sequences (PTS)

In PTS, the input data block is partitioned into disjoint subblocks or clusters which are combined to minimize the peaks. We partition the data block \mathbf{c} into M disjoint subblocks, represented by the vectors $\{\mathbf{c}_m, m = 1, 2, \dots, M\}$, such that $\mathbf{c} = [\mathbf{c}_1, \mathbf{c}_2, \dots, \mathbf{c}_M]$. It is assumed that each subblock consists of a contiguous set of data symbols and the subblocks are of equal size. Then, each subblock is multiplied by a weighting factor b_m ($m = 1, 2, \dots, M$). PAR can be reduced by optimizing the weighting factor $\mathbf{b} = [b_1, b_2, \dots, b_M]$. Finally, the optimal PAR can be found as

$$\text{PAR}_{\text{optimal}} = \frac{1}{n} \min_{b_1, \dots, b_M} \left[\max |H_n (\mathbf{c}_m \mathbf{b}^T)^T|^2 \right]. \quad (7.12)$$

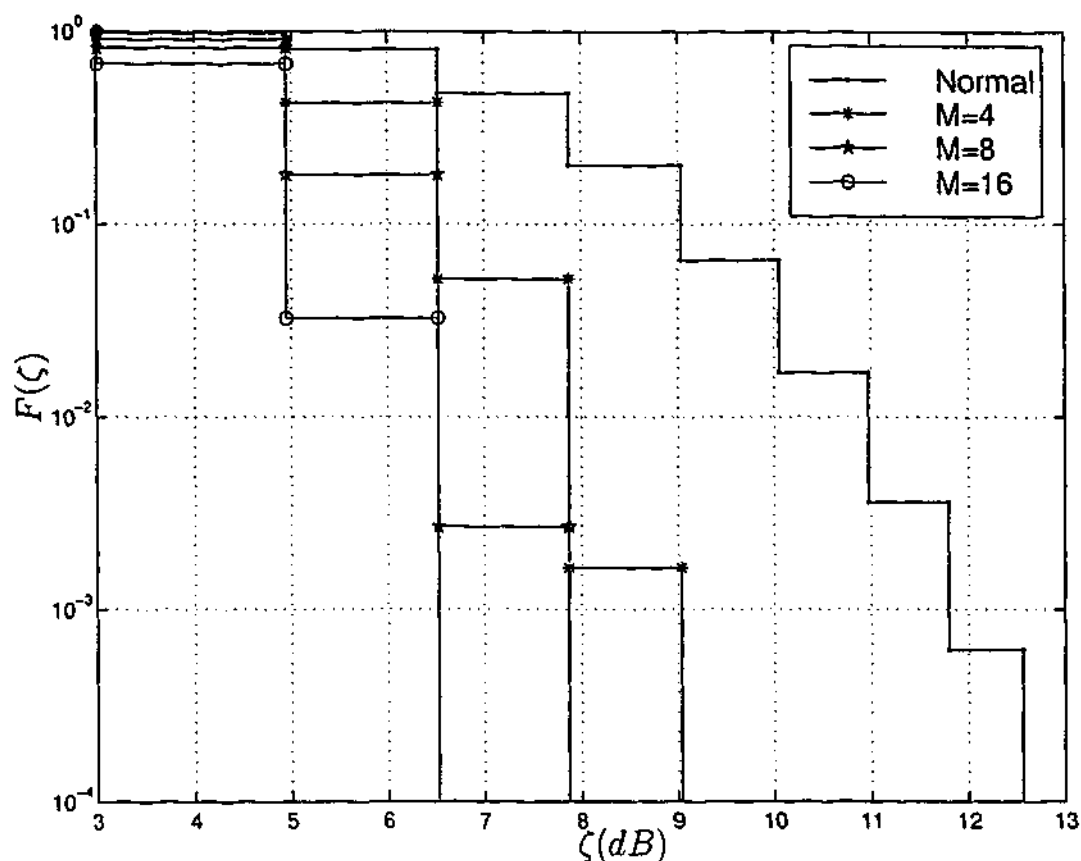


Figure 7.5: CCDF of PAR of multiple signal generated multi-code CDMA system for $n = 32$.

Figure 7.6 shows the simplified block diagram for the PTS scheme. For simplicity, we select $b_m \in \{+1, -1\}$. Therefore, total of 2^M sequences are searched to find the optimum \mathbf{b} . For $M = 8$, we need to examine 256 sequences. However, certain number of random sequences of length M performs close to optimum solution [183]. This approach reduces the extensive search for the optimum weighting factor.

Moreover, the receiver must know the multiplexed sequence \mathbf{b} to recover the data. Thus, a pointer to the phase factors must then be transmitted to the receiver as side information [172, 183, 185]. This requires at least $\log_2 M$ bits to be transmitted as side information. If these bits are embedded in the OFDM data block, the loss in efficiency is $\frac{\log_2 M}{n}$. This is negligible for large n . However, with differential modulation schemes, side information need not be transmitted.

Figure 7.7 shows the CCDF of PTS for $n = 32$. For $M = 8$, the PAR exceeds 10 dB for only 1 out of 10^4 of all data blocks whereas that of conventional case is for only 1 out of 10. There is about a 3 dB reduction in PAR in PTS with $M = 8$ over a conventional system. This causes a negligible code rate loss of 0.05. This agrees with

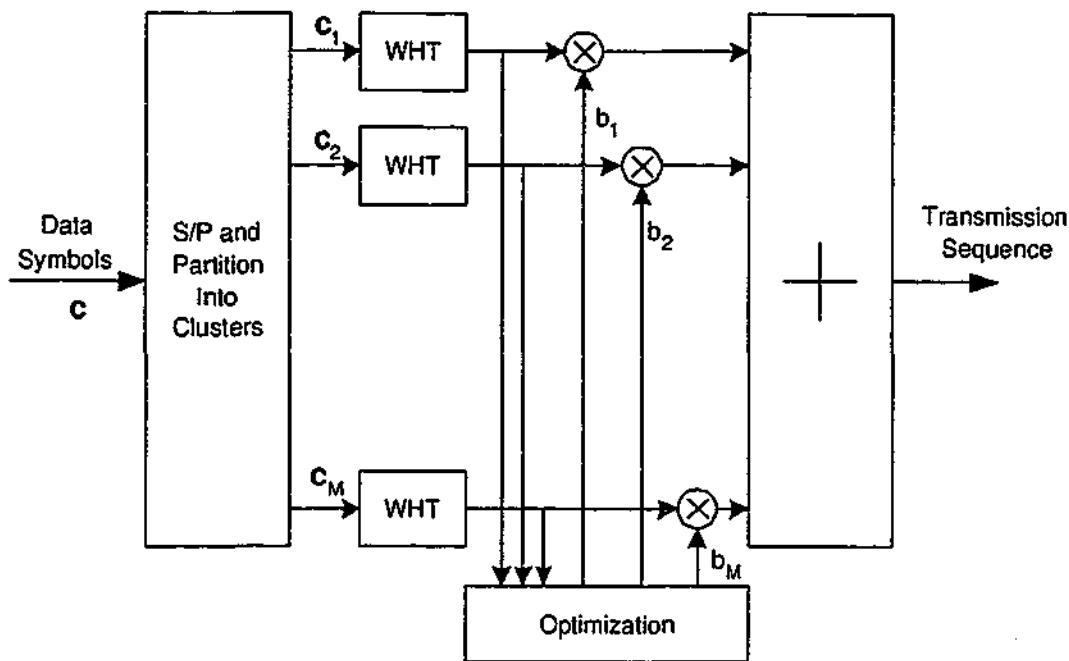


Figure 7.6: Simplified block diagram for the PTS scheme.

the results in Fig. 7.4, where PAR can be reduced below 10 dB with almost unity code rate.

Figure 7.7 also shows how the performance varies with M . When M is large, the PAR reduction is large. However, the computational complexity also increases with M (the optimized phase sequence requires 2^{M-1} computations of PAR). Thus, performance can be traded off against complexity. For $M \geq 8$, the full search of all possible \mathbf{b} is not implemented here. As suggested in [183], we randomly generate a number of phase sequences and choose the best in reducing PAR.

7.4.2 Selected Mapping (SLM)

M statistically different alternative transmit sequences $\mathbf{a}^{(m)}$ represent the same information. The sequence with lowest PAR is selected for transmission. To generate $\mathbf{a}^{(m)}$, we define M distinct fixed vectors $\mathbf{b}^{(m)} = [b_0^{(m)}, \dots, b_{n-1}^{(m)}]$ with $b_k^{(m)} \in \{+1, -1\}$ $0 \leq k < n$, $1 \leq m \leq M$. Then, each data symbol $\mathbf{c} = [c_0, c_1, \dots, c_{n-1}]$ is multiplied symbol-wise with the M vectors $\mathbf{b}^{(m)}$, resulting in a set of M different data symbols $\mathbf{c}^{(m)}$ with components

$$c_k^{(m)} = c_k \times b_k^{(m)} \text{ for } 0 \leq k < n \text{ and } 1 \leq m \leq M. \quad (7.13)$$

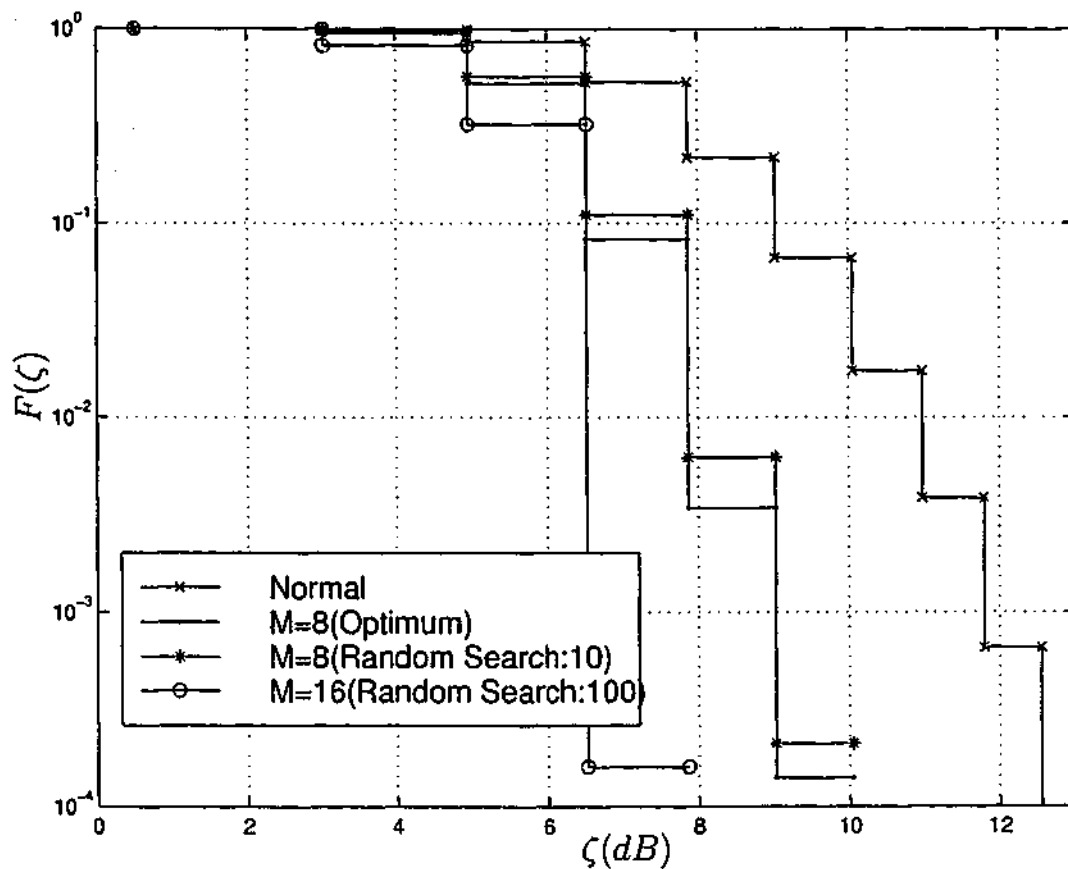


Figure 7.7: CCDF of PAR of PTS multi-code CDMA system with $n = 32$.

Finally, the optimal PAR can be found as

$$\text{PAR}_{\text{optimal}} = \frac{1}{n} \min_{b^{(1)}, \dots, b^{(M)}} \left[\max |H_n (\mathbf{c}^{(m)})^T|^2 \right]. \quad (7.14)$$

In order to recover the data, a pointer to the multiplied sequence has to be transmitted to the receiver as side information [172]. Figure 7.8 shows the simplified block diagram for the SLM scheme.

Figure 7.9 shows the CCDF of the PAR as a function of M for $N = 32$. For $M = 4$, only 1 out of 10^5 of data frame exceeds a PAR of 10 dB whereas in the conventional case, 1 out of 10 of data frame exceeds a PAR of 10 dB. That amounts to a 4 dB reduction in PAR, which is better than that of the PTS approach. However, both the PAR reduction and computational complexity increase with M . Consequently, as with PTS, performance can be traded off against complexity.

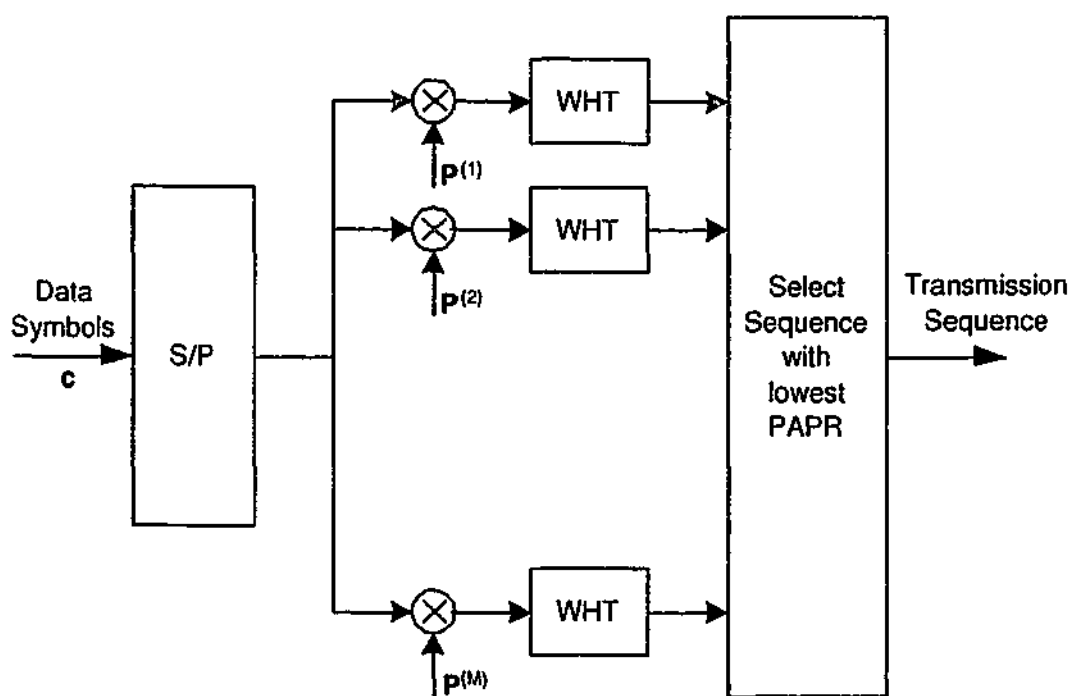


Figure 7.8: Simplified block diagram for the SLM scheme.

7.4.3 Impairments in the Presence of Nonlinearities

The Multi-code CDMA signal is passed through a HPA to obtain a sufficient power level required for transmission. As mentioned previously, the HPA introduces nonlinear distortion because of operating at or close to saturation region. The nonlinear distortion causes out-of-band radiation and BER degradation. However, out-of-band radiation is not a significant problem since the multi-code CDMA signal occupies a wider bandwidth. Thus, BER degradation is of interest in this nonlinear studies [256–259, 262, 263]. The nonlinear distortion of multi-code CDMA signal increases, when amplified with nonlinear power amplifiers operating at lower back-offs. Thus, high PAR of multi-code CDMA signal requires high back-offs at the amplifiers, which is inefficient.

Simulation Results

Figure 7.10 and Figure 7.11 show the BER of the multi-code CDMA signal subject to amplifier nonlinearities, SL and SSPA respectively. We assume coherent symbol detection in AWGN channel and perfect SI at the receiver. As discussed in Chapter 6, SI can be embedded into the data frame. The loss in data throughput due to embedded SI is negligible. In both SL and SSPA amplifiers with an input back-off of 3 dB, SLM offers an SNR gain of 2 dB at 10^{-4} BER. When the back-off of the amplifier

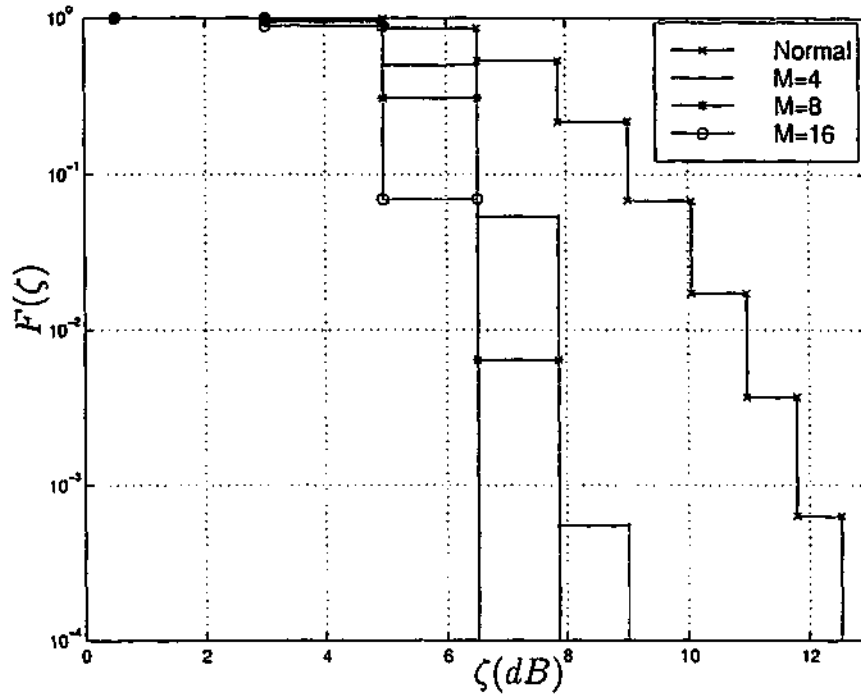


Figure 7.9: CCDF of PAR of SLM multi-code CDMA system with $n = 32$.

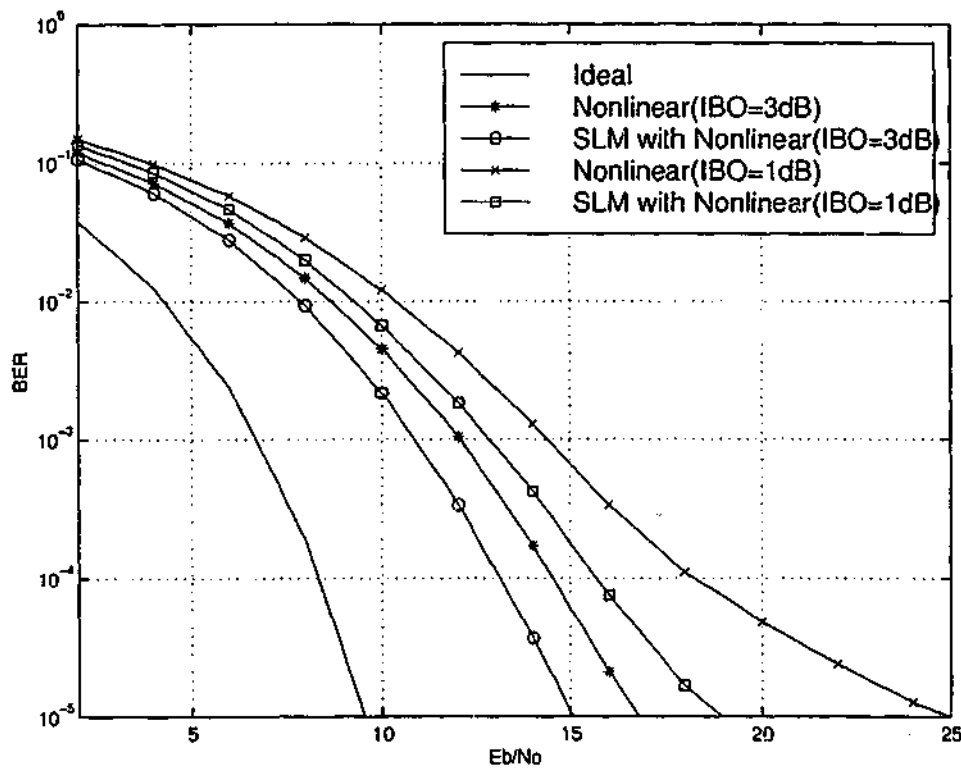


Figure 7.10: BER of multi-code CDMA signal passed through SL ($n = 32$ and $M = 8$).

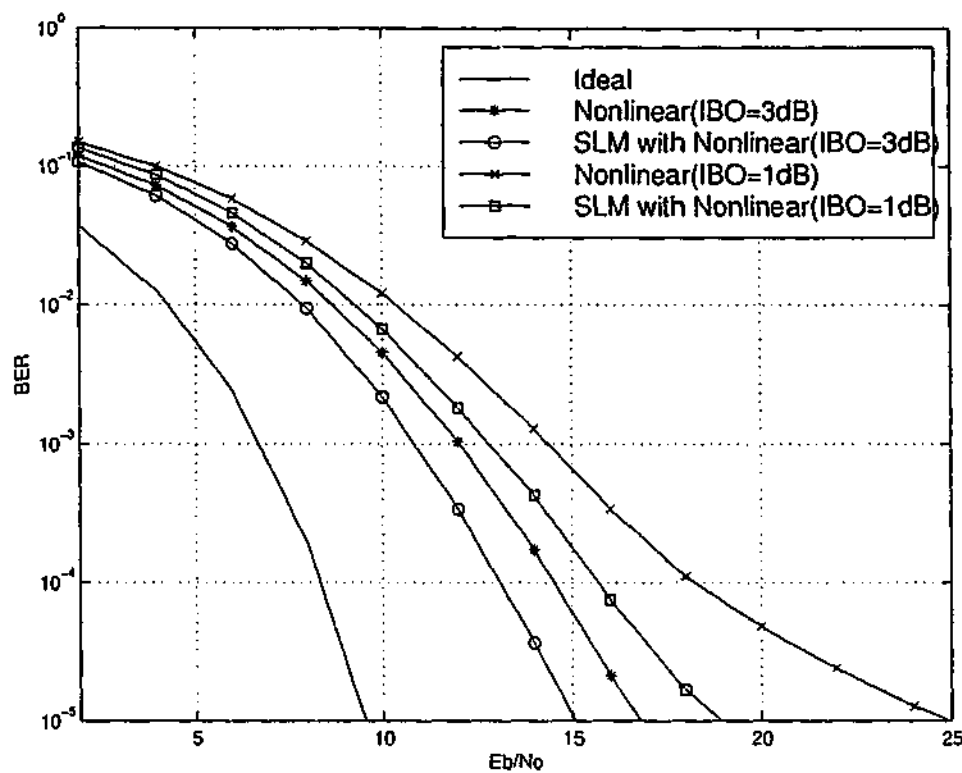


Figure 7.11: BER of multi-code CDMA signal passed through SSPA ($n = 32$ and $M = 8$).

is decreased, BER degradation is increased and resulting in error floor. However, SLM reduces this error floor and offers an SNR gain of 5dB at 10^{-4} BER with input back-off of 0dB.

We have used SLM to show that PAR reduction will translate into BER improvement. Similar BER performance improvement can be obtained for PTS as well. Figure 7.12 compares the BER performance of SLM and PTS in the presence of SSPA with back-off of 1 dB. For fair comparison, $M = 8$ is used in both SLM and PTS and 2^7 sequences are searched in PTS to find the optimum weighting factor. In fact, both shows almost same BER performance. As discussed in Chapter 6, the issue in these schemes is the complexity.

7.5 Conclusions

This chapter has presented the PAR problem in multi-code CDMA systems. Theoretical expressions for the CCDF of PAR and achievable code rates are derived. PTS and SLM methods have been used to reduce PAR. They improve the PAR statistics of the multi-code CDMA signal at the expense of additional complexity, but with little

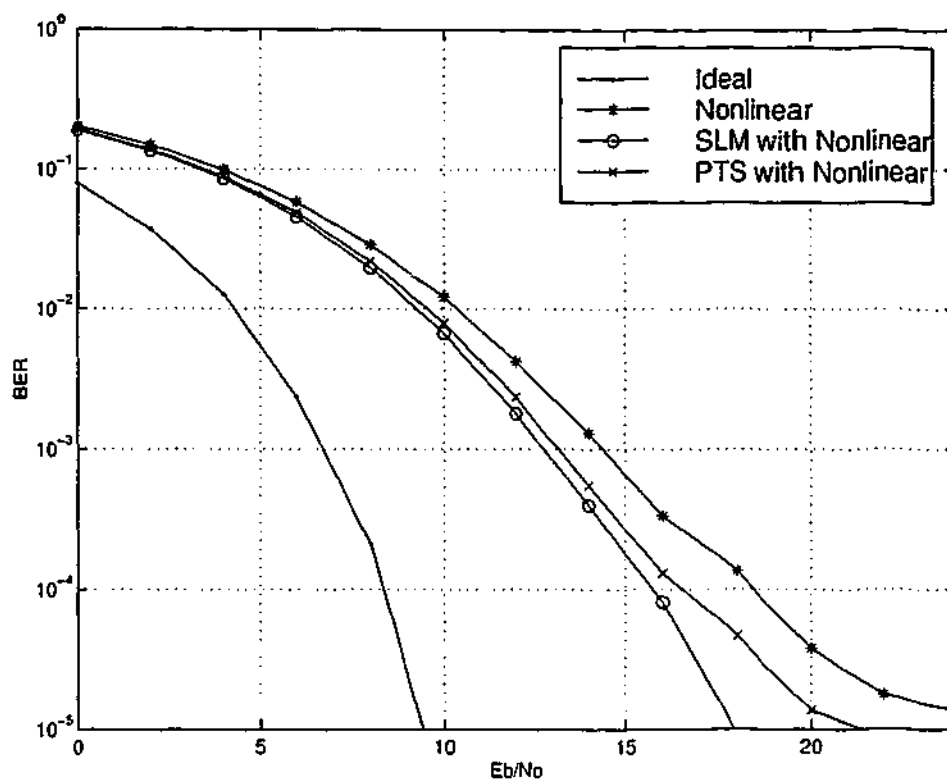


Figure 7.12: BER of multi-code CDMA signal passed through SSPA ($n = 32$, $M = 8$, IBO=1 dB).

loss in data rate. For $n = 32$ and $M = 4$, PTS reduces PAR by 3 dB whereas that of SLM is 4 dB. We have also shown the BER performance improvement by SLM. SLM reduces the error floor caused by amplifier nonlinearities and offers an SNR gain of 5 dB at 10^{-4} BER with an input back-off of 1 dB.

Chapter 8

Conclusions and Future Work

8.1 Thesis Conclusions

In this thesis, we have analyzed the problems in OFDM and multi-code CDMA systems and developed some new techniques to improve their performance. In the case of OFDM, two major problems, high PAR and sensitivity to frequency offset errors, have been considered while multi-code CDMA has been studied in relation to the former problem. Based on our theoretical analysis and simulation results, we draw the following conclusions.

The proposed analytical tool for determining the error performance of OFDM systems with ICI is very precise and independent of any parameter. Its readily available error performance results are useful from the system design point of view in contrast to time consuming simulations. To demonstrate this, an error performance of rate-half repetition codes are evaluated. The proposed $2/3$ and $3/4$ rate codes by symbol mapping offer a comparable error performance to that of rate-half repetition codes while their bandwidth efficiency is improved over the latter codes. Alternatively, RCPC codes can be used to reduce ICI. As it is, RCPC codes or the proposed high rate codes can be used with rate adaptation based on ICI effects in the channel with the same receiver. There is potential for the same benefits to be realized in OFDM based automatic repeat request (ARQ) systems such as wireless LANs.

The introduction of PICR to quantify ICI effects is also shown to be very useful in designing ICI reduction schemes at the transmitter. The analytical and simulation results show that the PICR reduction at the transmitter effectively translates into improvement in error performance. Based on this PICR measure, block coding, tone

reservation, SLM and PTS methods are developed to reduce ICI effects in OFDM systems. We have also introduced the concept of PAR-PICR-reduction codes to reduce both PAR and PICR simultaneously. Previous coding schemes have been effective in reducing only one impairment, PAR or PICR. We demonstrate the existence of PAR-PICR-reduction codes analytically and by simulation.

As single technique to reduce both PAR and ICI simultaneously, we have proposed the adaptive mapping scheme. This is based on M-ZPSK modulation. This scheme improves PAR statistics at the expense of 1 dB degradation in SNR gain over conventional M-PSK schemes in non-frequency offset channels. However, this adaptive M-ZPSK is less sensitive to frequency offset errors. We also derive analytical expressions for the error performance of this scheme.

The derivation of PAR statistics in multi-code CDMA is very useful in analyzing the PAR issue. For example, the PAR statistics can be used to identify the code rate of the PAR-reduction codes. We also demonstrate that the multiple signal generation method can reduce PAR effectively. In this instance, SLM and PTS demonstrate the improvement in PAR statistics.

8.2 Recommendations for Future Work

Some of the concepts and results presented in this thesis suggest that further research can be beneficially undertaken to improve the performance and efficiency of the OFDM and multi-code systems.

At the present time, the proposed precise error rate calculation techniques only consider the BPSK, QPSK and 16QAM modulation schemes, which are widely used in OFDM. However, it would be worthwhile to extend this technique to M-PSK and M-QAM modulation formats. Moreover, channel fading effects can also be considered in deriving closed form solutions for error performance. Another potential applications of this technique would be for use in multicarrier CDMA (MC-CDMA) systems to evaluate their performance. Another recommendation is the investigation of channel coding schemes with adaptive M-ZPSK. Since this adaptive mapping is effective in reducing both PAR and ICI, performance analysis with error control codes in a practical channel would be of value.

PICR is effectively used to design several ICI reduction schemes. However, an

AWGN channel is assumed in these studies. Since rate-half repetition codes are effective in any channel, one can expect a similar performance with PICR-based ICI reduction schemes. However, it would also be worthwhile to investigate their performance with fading channels. Moreover, the derived PICR-BER relationship and the statistical distribution of PICR are at this stage only approximate; therefore, precise derivations would be useful. As well, the proposed method for the construction of PICR-reduction codes is not optimum from the coding point of view. Therefore, an efficient code construction method needs to be developed. This is also true for PAR-PICR-reduction codes. Therefore, optimum code construction for the proposed concepts would be both an interesting and useful research direction.

Bibliography

- [1] R. R. Moiser and R. G. Clabaugh, "Kineplex, a bandwidth efficient binary transmission system," *AIEE Trans.*, vol. 76, pp. 723-728, Jan. 1958.
- [2] R. W. Chang, *Orthogonal frequency division multiplexing*. U. S. Patent 3 488 445, filed Nov. 14, 1966, issued Jan. 6, 1970.
- [3] S. B. Weinstein and P. M. Ebert, "Data transmission by frequency division multiplexing using the discrete Fourier transform," *IEEE Trans. Commun.*, vol. 19, pp. 628-634, Oct. 1971.
- [4] J. A. C. Bingham, "Multicarrier modulation for data transmission: An idea whose time has come," *IEEE Commun. Mag.*, vol. 28, pp. 5-14, May 1990.
- [5] W. Y. Zou and Y. Wu, "COFDM: An overview," *IEEE Trans. Broadcast.*, vol. 41, pp. 1-8, March 1995.
- [6] L. J. Cimini, "Analysis and simulation of a digital mobile channel using orthogonal frequency division multiplexing," *IEEE Trans. Commun.*, vol. COM-33, pp. 665-675, July 1985.
- [7] H. Rohling and V. Engels, "Differential amplitude phase shift keying (DAPSK)-a new modulation method for DTVB," in *International Broadcasting Convention*, pp. 102-108, 1995.
- [8] A. Peled and A. Ruiz, "Frequency domain data transmission using reduced computational complexity algorithms," in *IEEE Int. Conf. on Acoust., Speech, Signal Processing*, pp. 964-967, IEEE, Apr. 1980.

- [9] J. M. C. A. Ruiz and S. Kasturia, "Discrete multiple tone modulation with coset coding for the spectrally shaped channel," *IEEE Trans. Commun.*, vol. 40, pp. 1012-1029, June 1992.
- [10] A. Vahlin, H. N., and R. L. Frank, "Use of a guard interval in OFDM on multipath channels," *IEE Elect. Lett.*, vol. 30, pp. 2015-2016, Nov. 1994.
- [11] P. Shelswell, "The COFDM modulation system: the heart of digital audio broadcasting," *Elec. Commun. Eng. J.*, pp. 127-136, June 1995.
- [12] R. Nee and R. Prasad, *OFDM for wireless multimedia communications*. Artech House Publishers, Mar. 2000.
- [13] W. W. L. Hanzo and T. Keller, *Single- and Multi-carrier Quadrature Amplitude Modulation*. England: John Wiley & Sons, Ltd, 1st ed., 2000.
- [14] H. Ochiai, *Analysis and Reduction of Peak-to-average power ratio in OFDM systems*. PhD thesis, The graduate school of engineering, The university of Tokyo, Mar. 2001.
- [15] J. G. Proakis, *Digital communications*. McGraw-Hill series in electrical engineering. Communications and signal processing, New York: McGraw-Hill, 3rd ed., 1995.
- [16] P. Moose, "A technique for orthogonal frequency division multiplexing frequency offset correction," *IEEE Trans. Commun.*, vol. 42, pp. 2908-2914, Oct. 1994.
- [17] T. Pollet, Mark Van Bladel and Marc Moeneclaey, "The BER performance of OFDM systems using non-synchronized sampling," in *IEEE GLOBECOM*, pp. 253-257, IEEE, 1994.
- [18] T. Pollet, Mark Van Bladel and Marc Moeneclaey, "BER sensitivity of OFDM systems to carrier frequency offset and wiener phase noise," *IEEE Trans. Commun.*, vol. 43, pp. 191-193, February/March/April 1995.
- [19] A. A. Hutter, R. Hasholzner, and J. S. Hammerschmidt, "Channel estimation for mobile OFDM systems," in *IEEE Vehicular Technology Conference*, vol. 1, pp. 305-309, IEEE, 1999.

- [20] F. Classen and M. Meyr, "Frequency synchronization algorithms for OFDM systems suitable for communications over frequency selective fading channels," in *IEEE Vehicular Technology Conference*, pp. 1655-1659, IEEE, 1994.
- [21] H. Nogami and T. Nagashima, "A frequency and timing period acquisition technique for OFDM systems," in *IEEE PIMRC*, pp. 1010-1015, IEEE, Sept. 1995.
- [22] T. M. Schmidl and D. C. Cox, "Robust frequency and timing synchronization for OFDM," *IEEE Trans. Commun.*, vol. 45, pp. 1613-1621, Dec. 1997.
- [23] M. Morellis and U. Mengali, "An improved frequency offset estimator for OFDM applications," *IEEE Commun. Lett.*, vol. 3, pp. 75-77, Mar. 1999.
- [24] Z. Sayeed, "Fast, accurate and simple carrier acquisition algorithm for OFDM systems," in *IEEE GLOBECOM*, vol. 4, pp. 2274-2278, IEEE, 1999.
- [25] B. Y. Prasetyo, F. Said, and A. H. Aghvami, "On the guard band-based coarse frequency offset estimation technique for burst OFDM systems," in *IEEE Vehicular Technology Conference*, pp. 220-224, IEEE, May 2000.
- [26] M. Morelli, A. N. D'Andrea, and U. Mengali, "Frequency ambiguity resolution in OFDM systems," *IEEE Commun. Lett.*, vol. 4, pp. 134-136, Apr. 2000.
- [27] K. Bang, N. Cho, J. Cho, K. Kim, H. Park, and D. Hong, "A coarse frequency offset estimation in an OFDM system using the concept of the coherence phase bandwidth," in *IEEE ICC*, pp. 1135-1139, IEEE, June 2000.
- [28] M. Ghogho, A. Swami, and G. B. Giannakis, "Optimized null-subcarrier selection for CFO estimation in OFDM over frequency-selective fading channels," in *IEEE GLOBECOM*, pp. 202-206, IEEE, Nov. 2001.
- [29] T. Keller, L. Piazzo, P. Mandarini, and L. Hanzo, "Orthogonal frequency division multiplex synchronization techniques for frequency-selective fading channels," *IEEE J. Select. Areas. Commun.*, vol. 19, pp. 999-1008, June 2001.
- [30] S. Patel, L. J. Cimini Jr., and B. McNair, "Comparison of frequency offset estimation techniques for burst OFDM," in *IEEE Vehicular Technology Conference*, pp. 772-776, IEEE, May 2002.

- [31] C. Tellambura, I. R. Johnson, Y. J. Guo, and S. K. Barton, "Equalization and frequency offset corrections for HIPERLAN," in *IEEE PIMRC*, pp. 796–800, IEEE, Sept. 1997.
- [32] C. Tellambura, "Frequency-offset estimation for HIPERLAN," *IEEE Trans. Commun.*, vol. 47, pp. 1137–1139, Aug. 1999.
- [33] J. Li, G. Liu, and G. Giannakis, "Carrier frequency offset estimation for OFDM-based WLANs," *IEEE Signal Processing Lett.*, vol. 8, pp. 80–82, Mar. 2001.
- [34] F. Daffara and O. Adami, "A new frequency detector for orthogonal multicarrier transmission techniques," in *IEEE Vehicular Technology Conference*, pp. 804–809, IEEE, July 1995.
- [35] J. S. Oh, Y. M. Chung, and S. U. Lee, "A carrier synchronization technique for OFDM on the frequency-selective fading environment," in *IEEE Vehicular Technology Conference*, pp. 1574–1578, IEEE, May 1996.
- [36] J. J. v. d. Beek, M. Sandell, and P. O. Borjesson, "ML estimation of timing and frequency offset in OFDM systems," *IEEE Trans. Signal Processing*, vol. 45, pp. 1800–1805, July 1997.
- [37] N. Lashkarian and S. Kiaei, "Minimum variance unbiased estimation of frequency offset in OFDM systems, a blind synchronization approach," in *IEEE International Conference on Acoustics, Speech, and Signal Processing, ICASSP '00.*, pp. 2945–2948, IEEE, June 2000.
- [38] N. Lashkarian and S. Kiaei, "Class of cyclic-based estimators for frequency-offset estimation of OFDM systems," *IEEE Trans. Commun.*, vol. 48, pp. 2139–2149, Dec. 2000.
- [39] N. Lashkarian and S. Kiaei, "Globally optimum ML estimation of timing and frequency offset in OFDM systems," in *IEEE ICC*, pp. 1044–1048, IEEE, June 2000.
- [40] U. Tureli, H. Liu, and M. Zoltowski, "OFDM blind carrier offset estimation: ESPRIT," *IEEE Trans. Commun.*, vol. 48, pp. 1459–1461, Sept. 2000.

- [41] U. Tureli, D. Kivanc, and H. Liu, "Experimental and analytical studies on a high-resolution OFDM carrier frequency offset estimator," *IEEE Trans. Veh. Technol.*, vol. 50, pp. 629-643, Mar. 2001.
- [42] H. Liu and U. Tureli, "A high-efficiency carrier estimator for OFDM communications," *IEEE Commun. Lett.*, vol. 2, pp. 104-106, April 1998.
- [43] M. A. Visser, P. Zong, and Y. Bar-Ness, "A novel method for blind frequency offset correction in an OFDM system," in *IEEE PIMRC*, pp. 816-820, IEEE, 1998.
- [44] B. McNair, L. J. Cimini, Jr., and N. Sollenberger, "A robust timing and frequency offset estimation scheme for orthogonal frequency division multiplexing (OFDM) systems," in *IEEE Vehicular Technology Conference*, pp. 690-694, IEEE, 1999.
- [45] I. Hwang, H. Lee, and K. Kang, "Frequency and timing period offset estimation technique for OFDM systems," *IEE Elect. Lett.*, vol. 34, pp. 520-521, Mar. 1998.
- [46] V. B. S. Simoens and M. D. Courville, "A new method for joint cancellation of clock and carrier frequency offsets in OFDM receivers over frequency selective channels," in *IEEE Vehicular Technology Conference*, pp. 390-394, IEEE, May 2000.
- [47] E. Serpedin, A. Chevreuil, G. B. Giannakis, and P. Loubaton, "Blind channel and carrier frequency offset estimation using periodic modulation precoders," *IEEE Trans. Signal Process.*, vol. 48, pp. 2389-2405, Aug. 2000.
- [48] B. C. H. Wang, "Blind OFDM carrier frequency offset estimation via oversampling," in *Thirty-Fifth Asilomar Conference on Signals, Systems and Computers*, pp. 1465-1469, IEEE, Nov. 2001.
- [49] B. Chen, "Maximum likelihood estimation of OFDM carrier frequency offset," *IEEE Signal Processing Lett.*, vol. 9, pp. 123-126, Apr. 2002.
- [50] B. Chen and L. Wang, "Maximum likelihood estimation of OFDM carrier frequency offset," in *IEEE ICC*, pp. 49-53, IEEE, Apr. 2002.

- [51] H. Bolcskei, "Blind estimation of symbol timing and carrier frequency offset in wireless OFDM systems," *IEEE Trans. Commun.*, vol. 49, pp. 988-998, June 2001.
- [52] X. Ma, C. Tepedelenlioglu, and G. Giannakis, "Consistent blind synchronization of OFDM transmissions using null sub-carriers with distinct spacings," in *Third Workshop on Signal Processing Advances in Wireless Communications (SPAWC'01)*, pp. 146-149, IEEE, Mar. 2001.
- [53] D. Landstrom, J. M. Arenas, J. J. v. d. Beek, P. O. Borjesson, M.-L. Boucheret, and P. Oldling, "Time and frequency offset in OFDM systems employing pulse shaping," in *IEEE ICUPC*, pp. 279-283, IEEE, 1997.
- [54] V. B. Manimohan and W. J. Fitzgerald, "Blind frequency synchronisation for OFDM systems with pulse shaping," in *IEEE ICC*, pp. 178-181, IEEE, 1999.
- [55] M. Morelli and U. Mengali, "Feedforward frequency estimation for PSK: a tutorial review," *Euro. Trans. Telecommun.*, vol. 9, no. 2, pp. 103-116, 1998.
- [56] C. Muschallik, "Improving an OFDM reception using an adaptive nyquist windowing," *IEEE Trans. Consumer Electron.*, vol. 42, pp. 259-269, Aug. 1996.
- [57] S. H. Muller-Weinfurtner and J. B. Huber, "Robust OFDM reception with near-optimum Nyquist window," in *IEEE Vehicular Technology Conference*, pp. 289-293, IEEE, Sept. 1999.
- [58] S. H. Muller-Weinfurtner and J. B. Huber, "Optimum Nyquist windowing for improved OFDM receivers," in *IEEE GLOBECOM*, pp. 711-715, IEEE, Nov. 2000.
- [59] S. H. Muller-Weinfurtner, "Optimum Nyquist windowing in OFDM receivers," *IEEE Trans. Commun.*, vol. 49, pp. 417-420, Mar. 2001.
- [60] M. Russell and G. L. Stuber, "Interchannel interference analysis of OFDM in a mobile environment," in *IEEE Vehicular Technology Conference*, pp. 820-824, IEEE, 1995.

- [61] D. Kim and G. L. Stuber, "Performance of multiresolution OFDM on frequency-selective fading channels," *IEEE Trans. Veh. Technol.*, vol. 48, pp. 1740-1746, Sept. 1999.
- [62] K. Sathananthan and C. Tellambura, "Carrier frequency offset effect on OFDM systems: analysis and solutions," in *International Symposium on Wireless Personal Multimedia Communications*, vol. 2, pp. 688-692, Nov. 2000.
- [63] K. Sathananthan and C. Tellambura, "Forward error correction codes to reduce intercarrier interference in OFDM," in *IEEE ISCAS 2001*, pp. 566-569, IEEE, May 2001.
- [64] Y. Zhao, J.-D. Leclercq, and S. G. Häggman, "Intercarrier interference compression in OFDM communication systems by using correlative coding," *IEEE Commun. Lett.*, vol. 2, pp. 214-216, Aug. 1998.
- [65] Y. Zhao and S. G. Häggman, "Sensitivity to Doppler shift and carrier frequency errors in OFDM systems - the consequences and solutions," in *IEEE Vehicular Technology Conference*, pp. 1564-1568, IEEE, Apr. 1996.
- [66] Y. Zhao and S. G. Häggman, "Intercarrier interference self-cancellation scheme for OFDM mobile communication systems," *IEEE Trans. Commun.*, vol. 49, pp. 1185-1191, July 2001.
- [67] J. Armstrong, P. M. Grant, and G. Povey, "Polynomial cancellation coding of OFDM to reduce intercarrier interference due to Doppler spread," in *IEEE GLOBECOM*, pp. 2771 -2776, IEEE, Nov. 1998.
- [68] J. Armstrong, "Analysis of new and existing methods of reducing intercarrier interference due to carrier frequency offset in OFDM," *IEEE Trans. Commun.*, vol. 47, pp. 365-369, Mar. 1999.
- [69] K. Sathananthan, R. M. A. P. Rajatheva, and S. B. Slimane, "Analysis of OFDM in the presence of frequency offset and a method to reduce performance degradation," in *IEEE GLOBECOM*, vol. 1, pp. 72 - 76, IEEE, Nov. 2000.

- [70] K. Sathananthan, R. M. A. P. Rajatheva, and S. B. Slimane, "Cancellation technique to reduce intercarrier interference in OFDM," *IEE Elect. Lett.*, vol. 36, pp. 2078–2079, Dec. 2000.
- [71] K. A. Seaton and J. Armstrong, "Polynomial cancellation coding and finite differences," *IEEE Trans. Inform. Theory*, vol. 46, pp. 311–313, Jan. 2000.
- [72] J. Armstrong and C. Tellambura, "Multicarrier CDMA systems using PCC OFDM," in *IEEE VTC 2000*, vol. 2, pp. 1475–1479, IEEE, 2000.
- [73] J. Armstrong, T. Gill, and C. Tellambura, "Performance of PCC-OFDM with overlapping symbol periods in a multipath channel," in *IEEE GLOBECOM*, pp. 87–91, IEEE, 2000.
- [74] P. K. Remvik and H. Holte, "Carrier frequency offset robustness for OFDM systems with different pulse shaping filters," in *IEEE GLOBECOM*, pp. 11–15, IEEE, 1997.
- [75] P. Remvik, N. Holte, and A. Vahlin, "Fading and carrier frequency offset robustness for different pulse shaping filters in OFDM," in *IEEE Vehicular Technology Conference*, pp. 777–781, IEEE, May 1998.
- [76] S. Chang and E. J. Powers, "Cancellation of inter-carrier interference in OFDM systems using a nonlinear adaptive filter," in *IEEE ICC*, pp. 1039–1043, IEEE, 2000.
- [77] J. Rinne and M. Renfors, "An equalization method for orthogonal frequency division multiplexing systems in channels with multipath propagation, frequency offset and phase noise," in *IEEE GLOBECOM*, pp. 1442–1446, IEEE, Nov. 1996.
- [78] I. T. Monroy and G. Hooghiemstra, "On a recursive formula for the moments of phase noise," *IEEE Trans. Commun.*, vol. 48, pp. 917–920, June 2000.
- [79] T. Pollet, M. V. Bladel, and M. Moeneclaey, "BER sensitivity of OFDM systems to carrier frequency offset and Wiener phase noise," *IEEE Trans. Commun.*, vol. 43, pp. 191–193, 1995.

- [80] L. Tomba and W. A. Krzymien, "Effect of carrier phase noise and frequency offset on the performance of multicarrier CDMA systems," in *IEEE ICC*, pp. 1513-1517, IEEE, June 1996.
- [81] L. Tomba, "On the effect of Wiener phase noise in OFDM systems.," *IEEE Trans. Commun.*, vol. 46, pp. 580-583, May 1998.
- [82] G. J. Foschini and G. Vannucci, "Characterizing filtered light waves corrupted by phase noise," *IEEE Trans. Inform. Theory*, vol. 34, pp. 1437-1448, Nov. 1988.
- [83] G. L. Pierobon and L. Tomba, "Moment characterization of phase noise in coherent optical systems," *Journal of Lightwave Technology*, vol. 9, pp. 996-1005, Aug. 1991.
- [84] M. S. El-Tanany and Y. Wu, "Impact of phase noise on the performance of OFDM systems over frequency selective channels," in *IEEE Vehicular Technology Conference*, pp. 1802-1806, IEEE, May 1997.
- [85] R. Howald, S. Kesler, and M. Kam, "BER performance of M-QAM using OFDM with RF carrier phase noise," in *Thirtieth Southeastern Symposium on System Theory*, pp. 419-423, IEEE, Mar. 1998.
- [86] N. Benvenuto, G. Cherubini, and L. Tomba, "Achievable bit rates of DMT and FMT systems in the presence of phase noise and multipath," in *IEEE Vehicular Technology Conference*, pp. 2108-2112, IEEE, May 2000.
- [87] M. S. El-Tanany, Y. Wu, and L. Hazy, "Analytical modeling and simulation of phase noise interference in OFDM-based digital television terrestrial broadcasting systems," *IEEE Trans. Broadcast.*, vol. 47, pp. 20-31, Mar. 2001.
- [88] A. G. Armada and M. Calvo, "Phase noise and sub-carrier spacing effects on the performance of an OFDM communication system," *IEEE Commun. Lett.*, vol. 2, pp. 11-13., Jan. 1998.
- [89] P. Robertson and S. Kaiser, "Analysis of the effect of phase-noise in orthogonal frequency division multiplex (OFDM) systems," in *IEEE ICC*, pp. 1652-1657, IEEE, 1995.

- [90] N. Benvenuto, G. Cherubini, and L. Tomba, "A novel phase noise suppression technique in OFDM receiver," in *International Conference on Consumer Electronics (ICCE)*, pp. 388-389, IEEE, June 1998.
- [91] A. Yamamoto and K. Nishimura, "Low phase noise and low intermodulation analog front-end for an OFDM system," *IEEE Trans. Consumer Electron.*, vol. 44, pp. 1001-1011, Aug. 1998.
- [92] A. G. Armada, "Understanding the effect of phase noise in orthogonal frequency division multiplexing (OFDM)," *IEEE Trans. Broadcast.*, vol. 47, pp. 153-159, June 2001.
- [93] G. Santella, "Bit error rate performances of M-QAM orthogonal multicarrier modulation in presence of time-selective multipath fading," in *IEEE ICC*, pp. 1683-1688, IEEE, 1995.
- [94] Y. H. Kim, I. Song, H. G. Kim, T. Chang, and H. Myung, "Performance analysis of a coded OFDM system in time-varying multipath Rayleigh fading channels," *IEEE Trans. Veh. Technol.*, vol. 48, pp. 1610-1615, Sept. 1999.
- [95] H. Steendam and M. Moeneclaey, "Analysis and optimization of the performance of OFDM on frequency-selective time-selective fading channels," *IEEE Trans. Commun.*, vol. 47, pp. 1811-1819, Dec. 1999.
- [96] J. Li and M. Kavehrad, "Effects of time selective multipath fading on OFDM systems for broadband mobile applications," *IEEE Commun. Lett.*, vol. 3, pp. 332-334, Dec. 1999.
- [97] L. Wan and V. K. Dubey, "Bit error probability of OFDM system over frequency nonselective fast Rayleigh fading channels," *IEE Elect. Lett.*, vol. 36, pp. 1306-1307, July 2000.
- [98] L. Wan and V. K. Dubey, "BER performance of OFDM system over frequency nonselective fast Ricean fading channels," *IEEE Commun. Lett.*, vol. 5, pp. 19-21, Jan. 2001.

- [99] E. Chiavaccini and G. M. Vitetta, "Performance analysis of OFDM signalling over doubly-selective fading channels," in *IEEE GLOBECOM*, pp. 975-979, IEEE, 2000.
- [100] J. Ahn and H. S. Lee, "Frequency domain equalization of OFDM signals over frequency non selective Rayleigh fading channels," *IEE Elect. Lett.*, vol. 29, pp. 1476-1477, Aug. 1993.
- [101] W. G. Jeon, K. H. Chang, and Y. S. Cho, "An equalization technique for orthogonal frequency-division multiplexing systems in time-variant multipath channels," *IEEE Trans. Commun.*, vol. 47, pp. 27-32, Jan. 1999.
- [102] Y. H. Kim, H. G. Kim, I. Song, M. J. Lee, and S. H. Yoon, "A coded OFDM system for time-varying multipath Rayleigh fading environment," in *IEEE MILCOM*, pp. 867-871, IEEE, 1997.
- [103] M. Toeltsch and A. F. Molisch, "Equalization of OFDM-systems by interference cancellation techniques," in *IEEE ICC*, pp. 1950-1954, IEEE, June 2001.
- [104] C. Tellambura, "Use of m-sequences for OFDM peak-to-average power ratio reduction," *IEE Elect. Lett.*, vol. 33, pp. 1300-1301, July 1997.
- [105] C. Tellambura, "Upper bound on the peak factor of N-multiple carriers," *IEE Elect. Lett.*, vol. 33, pp. 1608-1609, Sept. 1997.
- [106] M. Park, H. Jun, N. Cho, N. Cho, D. Hong, and C. Kang, "PAPR reduction in OFDM transmission using Hadamard transform," in *IEEE ICC*, pp. 430-433, IEEE, June 2000.
- [107] S. Shepherd, J. Orriss, and S. Barton, "Asymptotic limits in peak envelope power reduction by redundant coding in orthogonal frequency-division multiplex modulation," *IEEE Trans. Commun.*, vol. 46, pp. 5-10, Jan. 1998.
- [108] R. van Nee and A. D. Wild, "Reducing the peak-to-average power ratio of OFDM," in *IEEE Vehicular Technology Conference*, pp. 2072-2076, IEEE, 1998.

- [109] M. Friese, "On the achievable information rate with peak-power-limited orthogonal frequency-division multiplexing," *IEEE Trans. Inform. Theory*, vol. 46, pp. 2579-2587, Nov. 2000.
- [110] H. Ochiai and H. Imai, "On the distribution of the peak-to-average power ratio in OFDM signals," *IEEE Trans. Commun.*, vol. 49, no. 2, pp. 282-289, 2001.
- [111] N. Dinur and D. Wulich, "Peak-to-average power ratio in high order OFDM," *IEEE Trans. Commun.*, vol. 49, pp. 1063-1072, June 2001.
- [112] C. Tellambura, "Computation of the continuous-time PAR of an OFDM signal with BPSK subcarriers," *IEEE Commun. Lett.*, vol. 5, pp. 185-187, May 2001.
- [113] H. Minn, C. Tellambura, and V. K. Bhargava, "On the peak factors of sampled and continuous signals," *IEEE Commun. Lett.*, vol. 5, pp. 129-131, Apr. 2001.
- [114] H. E. Rowe, "Memoryless nonlinearities with gaussian inputs: Elementary results," *BELL Systems Technical Journal*, vol. 61, pp. 1519-1525, Sept. 1982.
- [115] G. Santella and F. Mazzenga, "A hybrid analytical simulation procedure for performance evaluation in M-QAM-OFDM schemes in presence of nonlinear distortions," *IEEE Trans. Veh. Technol.*, vol. 47, pp. 142-151, Feb. 1998.
- [116] J. Tellado, *Peak to Average Power Reduction for Multicarrier Modulation*. PhD Dissertation, Stanford University, Sept. 1999.
- [117] Q. Shi, "OFDM bandpass nonlinearity," *IEEE Trans. Consumer Electron.*, vol. 42, no. 3, pp. 253-258, 1996.
- [118] M. Friese, "On the degradation of OFDM-signals due to peak-clipping in optimally predistorted power amplifiers," in *IEEE GLOBECOM*, pp. 936-944, IEEE, Nov. 1998.
- [119] C.-L. Liu, "The effect of nonlinearity on a QPSK-OFDM-QAM signal," *IEEE Trans. Consumer Electron.*, vol. 43, pp. 443-447, Aug. 1997.
- [120] S. Merchan, A. G. Armada, and J. L. Garcia, "OFDM performance in amplifier nonlinearity," *IEEE Trans. Broadcast.*, vol. 44, pp. 106-114, Mar. 1998.

- [121] C. van den Bos, M. H. L. Kouwenhoven, and W. A. Serdijn, "Effect of smooth nonlinear distortion on OFDM symbol error rate," *IEEE Trans. Commun.*, vol. 49, pp. 1510–1514, Sept. 2001.
- [122] D. Dardari, V. Tralli, and A. Vaccari, "A theoretical characterization of nonlinear distortion effects in OFDM systems," *IEEE Trans. Commun.*, vol. 48, pp. 1755–1764, Oct. 2000.
- [123] N. Ermolova, "Analysis of nonlinear effects in OFDM communications systems," in *IEEE Vehicular Technology Conference*, pp. 737–740, IEEE, May 2001.
- [124] P. Banelli, G. Baruffa, and S. Cacopardi, "Effects of HPA non linearity on frequency multiplexed OFDM signals," *IEEE Trans. Broadcast.*, vol. 47, pp. 123–136, June 2001.
- [125] E. Costa and S. Pupolin, "M-QAM-OFDM system performance in the presence of a nonlinear amplifier and phase noise," *IEEE Trans. Commun.*, vol. 50, pp. 462–472, Mar. 2002.
- [126] R. O'Neill and L. B. Lopes, "Envelope variation and spectral splatter in clipped multicarrier signals," in *IEEE PIMRC*, pp. 71–75, IEEE, Sept. 1995.
- [127] D. W. Bennett, P. B. Kenington, and R. J. Wilkinson, "Distortion effects of multicarrier envelope limiting," *IEE Proc. Commun.*, vol. 144, pp. 349–356, Oct. 1997.
- [128] X. Li and L. J. Cimini, "Effects of clipping and filtering on the performance of OFDM," in *IEEE Vehicular Technology Conference*, vol. 2, pp. 1634–1638, IEEE, 1997.
- [129] X. Li and L. J. Cimini, "Effects of clipping and filtering on the performance of OFDM," *IEEE Commun. Lett.*, vol. 2, pp. 131–133, May 1998.
- [130] H. Ochiai and H. Imai, "Performance of the deliberate clipping with adaptive symbol selection for strictly band-limited OFDM systems," *IEEE J. Select. Areas. Commun.*, vol. 18, pp. 2270–2277, Nov. 2000.

- [131] H. Ochiai and H. Imai, "On the clipping for peak power reduction of OFDM signals," in *IEEE GLOBECOM*, pp. 731-735, IEEE, Nov. 2000.
- [132] D. Wulich and L. Goldfeld, "Reduction of peak factor in orthogonal multicarrier modulation by amplitude limiting and coding," *IEEE Trans. Commun.*, vol. 47, pp. 18-21, Jan. 1999.
- [133] D. Kim and G. L. Stuber, "Clipping noise mitigation for OFDM by decision-aided reconstruction," *IEEE Commun. Lett.*, vol. 3, pp. 4-6, Jan. 1999.
- [134] H. Saeedi, M. Sharif, and F. Marvasti, "Clipping noise cancellation in OFDM systems using oversampled signal reconstruction," *IEEE Commun. Lett.*, vol. 6, pp. 73-75, Feb. 2002.
- [135] J. Armstrong, "New OFDM peak-to-average power reduction scheme," in *IEEE Vehicular Technology Conference*, vol. 2, pp. 756-760, IEEE, 2001.
- [136] M. Faulkner, "The effect of filtering on the performance of OFDM systems," *IEEE Trans. Veh. Technol.*, vol. 49, pp. 1877-1884, Sept. 2000.
- [137] M. Pauli and H.-P. Kuchenbecker, "Minimization of the intermodulation distortion of a nonlinearly amplified OFDM signal," *Wireless Personal Communications*, vol. 4, pp. 93-101, Jan. 1997.
- [138] K. Sathananthan, R. M. A. P. Rajatheva, and K. M. Ahmed, "Reduction of peak-to-average power ratio by limiting the dynamic range of an OFDM signal," in *Third International Symposium on Wireless Personal Multimedia Communications*, pp. 33-34, IEEE, 2000.
- [139] X. Wang, T. T. Tjhung, and C. S. Ng, "Reduction of peak-to-average power ratio of OFDM system using a companding technique," *IEEE Trans. Broadcast.*, vol. 45, pp. 303-307, Sept. 1999.
- [140] A. Mattsson, G. Mendenhall, and T. Dittmer, "Comments on : Reduction of peak-to-average power ratio of OFDM system using a companding technique, *IEEE Transactions on Broadcasting*, vol. 45, no. 3, September 1999.," *IEEE Trans. Broadcast.*, vol. 45, pp. 418-419, Dec. 1999.

- [141] X. Wang, T. T. Tjhung, and C. S. Ng, "Reply to the comments on: Reduction of peak-to-average power ratio of OFDM system using a companding technique, *IEEE Transactions on Broadcasting* vol. 45, no.3, September 1999," *IEEE Trans. Broadcast.*, vol. 45, pp. 420-422, Dec. 1999.
- [142] X. Wang, T. T. Tjhung, C. S. Ng, and A. A. Kassim, "On the SER analysis of A-law companded OFDM system," in *IEEE GLOBECOM*, pp. 756-760, IEEE, Nov. 2000.
- [143] X. Huang, J. Lu, J. Chuang, and J. Zheng, "Companding transform for the reduction of peak-to-average power ratio of OFDM signals," in *IEEE Vehicular Technology Conference*, pp. 835 -839, IEEE, 2001.
- [144] X. Huang, J. Lu, J. Zheng, J. Chuang, and J. Gu, "Reduction of peak-to-average power ratio of OFDM signals with companding transform," *IEE Elect. Lett.*, vol. 37, pp. 506-507, Apr. 2001.
- [145] M.-G. Di Benedetto and P. Mandarini, "An application of MMSE predistortion to OFDM systems.," *IEEE Trans. Commun.*, vol. 44, pp. 1417-1420, Nov. 1996.
- [146] M.-G. Di Benedetto and P. Mandarini, "A new analog predistortion criterion with application to high efficiency digital radio links," *IEEE Trans. Commun.*, vol. 43, pp. 2966-2974, Nov. 1995.
- [147] A. Brajal and A. Chouly, "Compensation of nonlinear distortions for orthogonal multicarrier schemes using predistortion," in *IEEE GLOBECOM*, pp. 1909-1914, IEEE, Nov. 1994.
- [148] H. W. Kang, Y. S. Cho, and D. H. Youn, "On compensating nonlinear distortions of an OFDM system using an efficient adaptive predistorter," *IEEE Trans. Commun.*, vol. 47, pp. 522-526, Apr. 1999.
- [149] S. Chang and E. J. Powers, "A simplified predistorter for compensation of nonlinear distortion in OFDM systems," in *IEEE GLOBECOM*, pp. 3080-3084, IEEE, Nov. 2001.

- [150] A. N. D'Andrea, V. Lottici, and R. Reggiannini, "An amplitude and phase pre-distortion to OFDM systems," in *IEEE GLOBECOM*, pp. 1417–1421, IEEE, Nov. 2000.
- [151] E. A. Jones, T. Wilkinson, and S. Barton, "Block coding scheme for reduction of peak-to-mean envelope power ratio of multicarrier transmission schemes," *IEE Elect. Lett.*, vol. 30, pp. 2098–2099, Dec. 1994.
- [152] A. E. Jones and T. A. Wilkinson, "Combined coding for error control and increased robustness to system nonlinearities in OFDM," in *IEEE Vehicular Technology Conference*, pp. 904–907, IEEE, 1996.
- [153] S. J. Shepherd, P. W. J. Van Eetvelt, C. W. Wyatt-Millington, and S. K. Barton, "Simple coding scheme to reduce peak factor in QPSK multicarrier modulation," *IEE Elect. Lett.*, vol. 31, pp. 1131–1132, July 1995.
- [154] S. Fragiaco, C. Matrakidis, and J. J. O'Reilly, "Multicarrier transmission peak-to-average power reduction using simple block code," *IEE Elect. Lett.*, vol. 34, pp. 953–954, May 1998.
- [155] Y. Zhang, A. Yongacoglu, J.-Y. Chouinard, and L. Zhang, "OFDM peak power reduction by sub-block coding and its extended versions," in *IEEE Vehicular Technology Conference*, pp. 695–699, IEEE, 1999.
- [156] P. Fan and X.-G. Xia, "Block coded modulation for the reduction of the peak to average power ratio in OFDM systems," in *Wireless and Networks*, pp. 1095–1099, IEEE, 1999.
- [157] X. Li and J. A. Ritcey, "M-sequences for OFDM peak-to-average power ratio reduction and error correction," *IEE Elect. Lett.*, vol. 33, pp. 554–555, Mar. 1997.
- [158] J. Jedwab, "M-Sequences for OFDM peak-to-average power ratio reduction and error correction," *IEE Elect. Lett.*, vol. 33, pp. 1293–1294, July 1997.
- [159] R. D. J. van Nee, "OFDM codes for peak-to-average power reduction and error correction," in *IEEE GLOBECOM*, pp. 740–744, IEEE, 1996.

- [160] J. A. Davis and J. Jedwab, "Peak-to-mean power control and error correction for OFDM transmission using Golay sequences and Reed-Muller codes," *IEE Elect. Lett.*, vol. 33, pp. 267-268, Feb. 1997.
- [161] A. J. Grant and R. van Nee, "Efficient maximum likelihood decoding of peak power limiting codes for OFDM," in *IEEE Vehicular Technology Conference*, pp. 2081-2084, IEEE, 1998.
- [162] J. A. Davis and J. Jedwab, "Peak-to-mean power control in OFDM, Golay complementary sequences, and Reed-Muller codes," *IEEE Trans. Inform. Theory.*, vol. 45, pp. 2397-2417, Nov. 1999.
- [163] K. G. Paterson, "Generalised Reed-Muller codes and power control in OFDM modulation," *IEEE Trans. Inform. Theory.*, vol. 46, Jan. 1998.
- [164] K. G. Paterson and V. Tarokh, "On the existence and construction of good codes with low peak-to-average power ratio," *IEEE Trans. Inform. Theory.*, vol. 46, pp. 1974-1987, Sept. 2000.
- [165] V. Tarokh and H. Jafarkhani, "On the computation and reduction of the peak-to-average power ratio in multicarrier communications," *IEEE Trans. Commun.*, vol. 48, pp. 37-44, Jan. 2000.
- [166] H. Ochiai and H. Imai, "Performance of block codes with peak power reduction for indoor multicarrier systems," in *IEEE Vehicular Technology Conference*, (New York, NY, USA), pp. 338-342, IEEE, 1998.
- [167] H. Ochiai and H. Imai, "Block codes for frequency diversity and peak power reduction in multicarrier systems," in *Proc. of International Symposium on Information Theory'98*, p. 192, IEEE, 1998.
- [168] C. V. Chong and V. Tarokh, "A simple encodable/decodable OFDM QPSK code with low peak-to-mean envelope power ratio," *IEEE Trans. Inform. Theory.*, vol. 47, pp. 3025-3029, Nov. 2001. Nov.
- [169] C. Robing and V. Tarokh, "A construction of OFDM 16-QAM sequences having low peak powers," *IEEE Trans. Inform. Theory.*, vol. 47, pp. 2091-4, July 2001.

- [170] W. Henkel, "Analog codes for peak-to-average power ratio reduction," in *VDE-Verlag. Itg-Fachbericht*, pp. 151–155, VDE-Verlag, 2000.
- [171] R. W. Bäuml, R. F. H. Fischer and J. B. Huber, "Reducing the peak-to-average power ratio of multicarrier modulation by selected mapping," *IEE Elect. Lett.*, vol. 32, pp. 2056–2057, Oct. 1996.
- [172] S. H. Müller, R. W. Bäuml, R. F. H. Fisher and J. B. Huber, "OFDM with reduced peak-to-average power ratio by multiple signal representation," *Annals of Telecommunications*, vol. 52, pp. 58–67, Feb. 1997.
- [173] S. H. Müller and J. B. Huber, "A novel peak power reduction scheme for OFDM," in *IEEE PIMRC*, pp. 1090–1094, IEEE, 1997.
- [174] S. H. Müller and J. B. Huber, "A comparison of peak power reduction schemes for OFDM," in *IEEE GLOBECOM*, vol. 1, pp. 1–5, IEEE, Nov. 1997.
- [175] S. H. Müller and J. B. Huber, "OFDM with reduced peak-to-average power ratio by optimum combination of partial transmit sequences," *IEE Elect. Lett.*, vol. 33, pp. 368–369, Feb. 1997.
- [176] A. D. S. Jayalath and C. Tellambura, "Reducing the peak-to-average power ratio of an OFDM signal through bit or symbol interleaving," *IEE Elect. Lett.*, vol. 36, pp. 1161–1163, June 2000.
- [177] A. D. S. Jayalath, K. Sathanandan, and C. Tellambura, "OFDM with reduced peak-to-average power ratio by interleaving," in *IEEE Pacific-Rim Conference on Multimedia*, pp. 120–123, IEEE, 2000.
- [178] K. Sathananthan and C. Tellambura, "Novel adaptive modulation scheme to reduce both PAR and ICI of an OFDM signal," in *6th International Symposium on DSP for Communication Systems*, pp. 229–233, Jan. 2002.
- [179] M. Breiling, S. H. Müller-Weinfurtner, and J. B. Huber, "Distortionless reduction of peak power without explicit side information," in *IEEE GLOBECOM*, pp. 1494–1498, IEEE, Nov. 2000.

- [180] M. Breiling, S. H. Müller-Weinfurtner, and J. B. Huber, "SLM peak-power reduction without explicit side information," *IEEE Commun. Lett.*, vol. 5, no. 6, pp. 239–241, 2001.
- [181] A. D. S. Jayalath, *OFDM for Wireless Broadband Communications (Peak Power Reduction, Spectrum and Coding)*. PhD Dissertation, Monash University, 2002.
- [182] L. J. Cimini and N. R. Sollenberger, "Peak-to-average power ratio reduction of an OFDM signal using partial transmit sequences," in *IEEE ICC*, pp. 511–515, IEEE, 1999.
- [183] L. J. Cimini and N. R. Sollenberger, "Peak-to-average power ratio reduction of an OFDM signal using partial transmit sequences," *IEEE Commun. Lett.*, vol. 4, pp. 511–515, Mar. 1999.
- [184] C. Tellambura, "Phase optimisation criterion for reducing peak-to-average power ratio in OFDM," *IEE Elect. Lett.*, vol. 34, pp. 169–170, Jan. 1998.
- [185] C. Tellambura, "Improved phase factor computation for the PAR reduction of an OFDM signal using PTS," *IEEE Commun. Lett.*, vol. 5, no. 4, 2001.
- [186] G. R. Hill, M. Faulkner, and J. Singh, "Reducing the peak-to-average power ratio in OFDM by cyclically shifting partial transmit sequences," *IEE Elect. Lett.*, vol. 36, pp. 560–561, Mar. 2000.
- [187] H. Chen and G. J. Pottie, "An orthogonal projection-based approach for PAR reduction in OFDM," *IEEE Commun. Lett.*, vol. 6, pp. 169–171, May 2002.
- [188] L. J. Cimini and N. R. Sollenberger, "Peak-to-average power ratio reduction of an OFDM signal using partial transmit sequences with embedded side information," in *IEEE GLOBECOM*, IEEE, Mar. 2000.
- [189] J. Tellado and J. M. Coiffi, "Peak power reduction for multicarrier transmission," in *IEEE GLOBECOM*, pp. 219–224, IEEE, 1998.
- [190] C.-S. Hwang, "Peak power reduction method for multicarrier transmission," *IEE Elect. Lett.*, vol. 37, pp. 1075–1077, Aug. 2001.

- [191] H. Kwok and D. Jones, "Par reduction via constellation shaping," in *International Symposium on Information Theory*, p. 166, IEEE, 2000.
- [192] D. L. Jones, "Peak power reduction in OFDM and DMT via active channel modification," in *Thirty-Third Asilomar Conference on Signals, Systems, and Computers*, pp. 1076–1079, IEEE, 1999.
- [193] D. A. Wiegandt, C. R. Nassar, and W. Zhiqiang, "Overcoming peak-to-average power ratio issues in OFDM via carrier-interferometry codes," in *IEEE Vehicular Technology Conference*, vol. 2, pp. 660–663, IEEE, 2001.
- [194] D. A. Wiegandt, C. R. Nassar, and W. Zhiqiang, "Peak-to-average power reduction in high-performance, high-throughput OFDM via pseudo-orthogonal carrier-interferometry coding," in *IEEE Pacific Rim Conference on Communications, Computers and signal Processing*, vol. 2, pp. 453–456, IEEE, 2001.
- [195] J. Tellado and J. M. Coiffi, "Efficient algorithms for reducing PAR in multicarrier systems," in *IEEE ISIT*, p. 191, IEEE, 1998.
- [196] B. S. Krongold, *New Techniques for Multicarrier Communication Systems*. PhD Dissertation, University of Illinois, 2001.
- [197] B. S. Krongold and D. L. Jones, "A new method for PAR reduction in baseband DMT systems," in *Thirty-Fifth Asilomar Conference on Signals, Systems and Computers*, pp. 502–506, IEEE, Nov. 2001.
- [198] B. S. Krongold and D. L. Jones, "A new tone reservation method for complex-baseband PAR reduction in OFDM systems," in *International Conference on Acoustics, Speech, and Signal Processing*, pp. 2321–2324, IEEE, May 2002.
- [199] H. Schmidt and K. D. Kamneyer, "Reducing the peak to average power ratio of multicarrier signals by adaptive subcarrier selection," in *IEEE ICUPC*, pp. 933–937, IEEE, 1998.
- [200] E. Lawrey and J. Kikkert, "Peak to average power ratio reduction of OFDM signals using peak reduction carriers," in *ISSPA*, pp. 737–740, IEEE, 1999.

- [201] M. Fernandez-Getino Garcia, J. Paez-Borrillo, and O. Edfors, "Orthogonal pilot sequences for peak-to-average power reduction in OFDM," in *IEEE Vehicular Technology Conference*, vol. 2, pp. 650–654, IEEE, 2001.
- [202] M. Fernandez-Getino Garcia, O. Edfors, and J. Paez-Borrillo, "Joint channel estimation and peak-to-average power reduction in coherent OFDM :A novel approach," in *IEEE Vehicular Technology Conference*, pp. 815 –819, IEEE, 2001.
- [203] O. Muta and Y. Akaiwa, "A peak power reduction scheme with adaptive transmit power control for multicarrier transmission," in *IEEE Vehicular Technology Conference*, pp. 2144–2148, IEEE, 1999.
- [204] O. Muta and Y. Akaiwa, "A peak power reduction scheme with adaptive transmit power control for multicarrier transmission," *Transactions of the Institute of Electronics & Communication Engineers of Japan*, vol. J83-B, pp. 289–296, Mar. 2000.
- [205] W. Henkel and B. Wagner, "Another application of trellis shaping: PAR reduction for DMT (OFDM)," *IEEE Trans. Commun.*, vol. 48, pp. 1471–1476, Sept. 2000.
- [206] W. Henkel and B. Wagner, "Trellis shaping for reducing the peak-to-average ratio of multitone signals," in *Proc. of International Symposium on Information Theory'97*, p. 519, IEEE, 1997.
- [207] S. B. Slimane, "Peak-to-average power ratio reduction of OFDM signals using pulse shaping," in *IEEE GLOBECOM*, pp. 1412 –1416, IEEE, Nov. 2000.
- [208] R. Prasad and S. Hara, "An overview of multi-carrier CDMA," in *International Symposium on Spread Spectrum Techniques and Applications Proceedings*, pp. 1510–1514, IEEE, Sept. 1996.
- [209] T. F. Ho and V. K. Wei, "Synthesis of low-crest waveforms for multicarrier CDMA system," in *IEEE GLOBECOM*, pp. 131–135, IEEE, Nov. 1995.
- [210] L. Freiberg, A. Annamalai, and V. K. Bhargava, "Crest factor reduction using orthogonal spreading codes in multi-carrier CDMA systems," in *IEEE PIMRC*, pp. 120–124, IEEE, Sept. 1997.

- [211] H. Ochiai and H. Imai, "OFDM-CDMA with peak power reduction based on the spreading sequences," in *IEEE ICC*, pp. 1299–1303, IEEE, 1998.
- [212] B. Natarajan and C. R. Nassar, "Crest factor considerations in MC-CDMA with carrier interferometry codes," in *Pacific Rim Conference on Communications, Computers and signal Processing*, pp. 445–448, IEEE, Aug. 2001.
- [213] T. Ginige, N. Rajatheva, and K. M. Ahmed, "Dynamic spreading code selection method for PAPR reduction in OFDM-CDMA systems with 4-QAM modulation," *IEEE Commun. Lett.*, vol. 5, pp. 39–43, Oct. 2001.
- [214] Y. Kim, K. Bang, S. Choi, C. You, and D. Hong, "Effect of carrier frequency offset on performance of MC-CDMA systems," *IEE Elect. Lett.*, vol. 35, pp. 378–379, Mar. 1999.
- [215] J. Jang and K. B. Lee, "Effects of frequency offset on MC/CDMA system performance," *IEEE Commun. Lett.*, vol. 3, pp. 196–198, July 1999.
- [216] H. Steendam and M. Moeneclaey, "The effect of synchronisation errors on MC-CDMA performance," in *IEEE ICC*, pp. 1510–1514, IEEE, June 1999.
- [217] G. J. Foschini and M. J. Gans, "On the limits of wireless channels," *Wireless Personal Communications*, vol. 6, pp. 311–335, 1998.
- [218] C. Garnier, M. Loosvelt, V. Le Thuc, Y. Delignon, and L. Clavier, "Performance of an OFDM-SDMA based system in a time-varying multi-path channel," in *IEEE Vehicular Technology Conference*, pp. 1686–1690, IEEE, Oct. 2001.
- [219] P. Vandenameele, L. Van Der Perre, M. G. E. Engels, B. Gyselinckx, and H. J. De Man, "A combined OFDM/SDMA approach," *IEEE J. Select. Areas. Commun.*, vol. 18, pp. 2312–2321, Nov. 2000.
- [220] A. van Zelst, R. van Nee, and G. A. Awater, "Space division multiplexing (SDM) for OFDM systems," in *IEEE Vehicular Technology Conference*, pp. 1686–1690, IEEE, Oct. 2000.

- [221] Y. Li, N. Seshadri, and S. Ariyavisitakul, "Channel estimation for OFDM systems with transmitter diversity in mobile wireless channels," *IEEE J. Select. Areas. Commun.*, vol. 17, pp. 461-471, Mar. 1999.
- [222] Y. G. Li, J. Chuang, and N. R. Sollenberger, "Transmitter diversity for OFDM systems and its impacts on high-rate wireless networks," in *IEEE ICC*, pp. 534-538, IEEE, 1999.
- [223] L. J. Cimini and N. R. Sollenberger, "OFDM with diversity and coding for advanced cellular internet service," in *IEEE GLOBECOM*, pp. 305-309, IEEE, 1997.
- [224] V. Tarokh, N. Seshadri and A. R. Calderbank, "Space-time codes for high data rate wireless communication: Performance analysis and code construction," *IEEE Trans. Inform. Theory.*, vol. 44, pp. 744-765, Mar. 1998.
- [225] S. Diggavi, N. Al-Dhahir, and A. Stamoulis, "Intercarrier interference in MIMO OFDM," in *icc*, pp. 485-489, IEEE, Apr. 2002.
- [226] R. Narasimhan, "Performance of diversity schemes for OFDM systems with frequency offset, phase noise and channel estimation errors," in *IEEE ICC*, pp. 1551-1557, IEEE, Apr. 2002.
- [227] A. N. Mody and G. L. Stüber, "Synchronization for MIMO OFDM systems," in *IEEE GLOBECOM*, pp. 509-513, IEEE, Nov. 2001.
- [228] T. Pollet and M. Moeneclaey, "The effect of carrier frequency offset on the performance of band limited single carrier and OFDM signals," in *IEEE GLOBECOM*, pp. 719-723, IEEE, 1996.
- [229] H. Nikookar and R. Prasad, "On the sensitivity of multicarrier transmission over multipath channels to phase noise and frequency offset," in *IEEE PIMRC*, pp. 68-72, IEEE, 1996.
- [230] Y. Zhao and S. G. Häggman, "BER analysis of OFDM communication systems with intercarrier interference," in *International Conference on Communication Technology*, IEEE, Oct. 1998.

- [231] J. Hasson and B. Z. Bobrovsky, "BER calculation for MQAM-OFDM with ICI caused by carrier frequency fluctuations," in *IEEE Vehicular Technology Conference*, pp. 1194-1196, IEEE, May 2001.
- [232] N. C. Beaulieu, "An infinite series for the computation of the complementary probability distribution function of a sum of independent random variables and its application to the sum of Rayleigh random variables," *IEEE Trans. Commun.*, vol. 38, pp. 1463-1474, Sept. 1990.
- [233] C. Tellambura and A. Annamalai, "Further results on the Beaulieu series," *IEEE Trans. Commun.*, vol. 48, pp. 1774-1777, Nov. 2000.
- [234] N. C. Beaulieu, "The evaluation of error probabilities for intersymbol and cochannel interference," *IEEE Trans. Commun.*, vol. 39, pp. 1740-1749, Dec. 1991.
- [235] S. B. Wicker, *Error control systems for digital communication and storage*. Englewood Cliffs, NJ: Prentice Hall, 1995.
- [236] J. Hagenauer, "Rate-compatible punctured convolutional codes (RCPC Codes) and their applications," *IEEE Trans. Commun.*, vol. 36, pp. 389-400, Apr. 1988.
- [237] E. K. P. Chong and S. H. Zak, *An Introduction to Optimization*. A Wiley-Interscience Publication, 1996.
- [238] P. K. Frenger and N. A. B. Svensson, "Parallel combinatorial OFDM signalling," *IEEE Trans. Commun.*, vol. 47, pp. 558-567, Apr. 1999.
- [239] A. Sumasu, T. Ue, M. Usesugi, O. Kato, and K. Homma, "A method to reduce the peak power with signal space expansion (ESPAR) for OFDM system," in *IEEE Vehicular Technology Conference*, pp. 405-409, IEEE, 2000.
- [240] K. Sathanathan and C. Tellambura, "Coding to reduce both PAR and PICR of an OFDM signal," *IEEE Commun. Lett.*, vol. 6, pp. 316-318, Aug. 2002.
- [241] R. W. Bauml, R. F. H. Fischer, and J. B. Huber, "Reducing the peak-to-average power ratio of multicarrier modulation by selected mapping," *IEE Elect. Lett.*, vol. 32, pp. 2056-2057, Oct. 1996.

- [242] A. D. S. Jayalath and C. Tellambura, "Reducing the peak-to-average power ratio of an OFDM signal through bit or symbol interleaving," *IEE Elect. Lett.*, vol. 36, pp. 1161-1163, June 2000.
- [243] J. W. Craig, "A new, simple, and exact result for calculating the probability of error for two-dimension signal constellations,," in *IEEE MILCOM*, pp. 571-575, IEEE, Oct. 1991.
- [244] A. Annamalai and C. Tellambura, "Error rates for Nakagami-m fading multi-channel reception of binary and M-ary signals," *IEEE Trans. Commun.*, vol. 49, pp. 58-68, Jan. 2001.
- [245] A. Annamalai and C. Tellambura, "A new approach to performance evaluation of generalized selection diversity receivers in wireless channels," in *IEEE Vehicular Technology Conference*, pp. 2309-2313, IEEE, 2001.
- [246] I. S. Gradshteyn and I. M. Ryzhik, *Table of integrals, series, and products*. Academic Press, Inc., 5th ed., 1994.
- [247] K. Sathananthan and C. Tellambura, "Probability of error calculation of OFDM systems with frequency offset," *IEEE Trans. Commun.*, vol. 49, pp. 1884-1888, Nov. 2001.
- [248] F. Adachi, M. Sawahashi, and H. Suda, "Wideband DS-CDMA for next-generation mobile communications systems," *IEEE Commun. Mag.*, vol. 36, pp. 56-69, Sept. 1998.
- [249] M. Zeng, A. Annamalai and V. K. Bhargava, "Harmonization of global third generation mobile systems," *IEEE Commun. Mag.*, vol. 38, pp. 94-104, Dec. 2000.
- [250] M. Zeng, A. Annamalai and V. K. Bhargava, "Recent advances in cellular wireless communications," *IEEE Commun. Mag.*, vol. 37, pp. 128-138, Sept. 1999.
- [251] C.-L. I and R. D. Gitlin, "Multi-code CDMA wireless personal communications networks," in *IEEE ICC*, pp. 1060-1064, IEEE, 1995.

- [252] M. Fan, T. Minn, and K.-Y. Siu, "Performance of multirate techniques in W-CDMA," in *IEEE Vehicular Technology Conference*, pp. 2262–2266, IEEE, Oct. 2001.
- [253] T. Ottosson and T. Palenius, "The impact of using multicode transmission in the WCDMA system," in *IEEE Vehicular Technology Conference*, pp. 1550–1554, IEEE, 1999.
- [254] T. Ottosson, "Precoding in multicode DS-CDMA systems," in *Int. Symp. Info. Thy.*, p. 351, IEEE, June 1997.
- [255] T. Ottosson, "Precoding for minimization of envelope variations in multicode DS-CDMA systems," *Wireless Personal Communications*, vol. 13, pp. 57–58, May 2000.
- [256] T. Wada, T. Yamazato, M. Katayama, and A. Ogawa, "A constant amplitude coding for orthogonal multi-code CDMA systems," *IEICE Trans. Fundamentals*, vol. E80-A, pp. 2477–2484, Dec. 1997.
- [257] T. Wada, T. Yamazato, M. Katayama, and A. Ogawa, "Error correcting capability of constant amplitude coding for orthogonal multi-code CDMA systems," *IEICE Trans. Fundamentals*, vol. E81-A, pp. 2166–2169, Oct. 1998.
- [258] T. Wada, "Characteristic of bit sequence applicable to constant amplitude orthogonal multicode systems," *IEICE Trans. Fundamentals*, vol. E83-A, pp. 2160–2164, Nov. 2000.
- [259] S. I. Kim, G. Y. Jung, S. Y. Yoon, and H. S. Lee, "Enhancement of constant amplitude coding for multicode wideband CDMA systems," *IEICE Trans. Commun.*, vol. E83-B, pp. 2550–2555, Nov. 2000.
- [260] K. Paterson, "On codes with low peak-to-average power ratio for multi-code CDMA." Tech. Rep. HPL-2002-115, HP Laboratories, Bristol, UK, 2001.
- [261] K. Paterson, "On codes with low peak-to-average power ratio for multi-code CDMA." Tech. Rep. HPL-2002-146, HP Laboratories, Bristol, UK, 2001.

- [262] N. Guo and L. B. Milstein, "Uplink performance evaluation of multicode DS-CDMA systems in the presence of nonlinear distortions," *IEEE J. Select. Areas. Commun.*, vol. 18, pp. 1418-1428, Aug. 2000.
- [263] N. Guo and L. B. Milstein, "The impact of nonlinear amplification on multi-code CDMA systems," in *IEEE ICC*, pp. 1034-1038, IEEE, 2000.
- [264] K.-S. Jin, Y. Shin, and S. Im, "A predistorter for nonlinear distortion in multi-code CDMA systems," in *IEEE PIMRC*, pp. 1481-1485, IEEE, Sept. 1998.
- [265] K.-S. Jin, Y. Shin, and S. Im, "Compensation of nonlinear distortion with memory in multi-code CDMA systems," in *IEEE ICC*, pp. 565-569, IEEE, June 1999.